THE UNIVERSITY OF HULL

Antiferroelectric Liquid Crystals: Hosts and Binary Mixtures

being a Thesis submitted for the Degree of PhD

in the University of Hull

by

Deven D. Parghi BSc MSc

April 2000

Text close to edge of page in original.

Some text is cut off.

CONTENTS

ACKNOWLEDGEMENTS

I would like to dedicate this thesis to my mother.

SUMMARY

This thesis details the work carried out towards a doctoral degree in the synthesis, characterisation and evaluation of liquid-crystalline materials possessing antiferroelectric smectic C* (SmC_A*) and non-chiral anticlinic smectic C (SmC_{alt}) phases. The effects of structural modifications of the materials on the occurrence and stability of the alternating-tilt smectic phases are described. The work was designed to evaluate the potential use of chiral-dopant antiferroelectric mixtures for antiferroelectric liquid crystal display devices (AFLCDs), analogous to the chiral-dopant ferroelectric mixtures used currently in ferroelectric liquid crystal display devices (FLCDs), for fast-switching display device applications. The most suitable materials from those prepared, including both optically active (chiral) dopants and achiral or racemic hosts, were selected and their applications in this novel mixture concept investigated. The switching characteristics of some model chiral-dopant binary mixtures were also studied, and the practical applicabilities of the mixtures developed are discussed.

ABBREVIATIONS

The following abbreviations are used in this thesis;-

P_s – Spontaneous polarisation

DCM - dichloromethane

THF - tetrahydrofuran

n-BuLi - *n*-butyllithium

DCC – (*N,N'*-dicyclohexylcarbodiimide

DMAP - 4-(*N,N*-dimethylamino)pyridine

DEAD – diethyl azodicarboxylate

d-DMSO - deuterated dimethylsulphoxide

MS - Mass Spectrum

HPLC – High Performance Liquid Chromatography

^{1}H-NMR – Proton Nuclear Magnetic Resonance Spectrum;

  singlet (s), doublet (d), triplet (t), quartet (q), quintet (p), sextet (sx),

  septet (sp), doublet-of-doublets (dd), multiplet (m).

IR – Infra-red spectrum

TT – Transition temperatures

The abbreviations used to denote the various liquid-crystalline phases discussed in this thesis are based on the nomenclature recommended in the Handbook of Liquid Crystals (1998 edition, ed. Demus, D.) Weinheim: Wiley-VCH.

References are numbered in square brackets, [] in the text; appendices are superscripted (Eg. [App.X]).

# Introduction

INTRODUCTION

i.   Liquid Crystals

The "Fourth State of Matter"

Of the many novel synthetic organic compounds synthesised to date, those which constitute the group of materials termed "liquid crystals" have proven to be of great value both scientifically and commercially. The liquid-crystalline state, or "mesomorphic state", is sometimes referred to as the "fourth state of matter" [1, 2] due to the inherent nature of the materials to possess a degree of structural ordering not present in isotropic liquids allied to a degree of fluidity not associated with solids.

Liquid-crystalline phases, in the first instance, can be categorised as being formed either by the effect of changes in temperature, termed *thermotropic* liquid crystals, or by the addition of solvents, termed *lyotropic* liquid crystals. There exist, of course, materials that exhibit both thermotropic and lyotropic liquid crystal phases (sometimes called *amphotrophic* liquid crystals). Only purely thermotropic liquid crystals will be discussed in this thesis.

The thermotropic liquid-crystalline state was originally observed in 1888 in the benzoate and acetate derivatives of cholesterol [3] (*figure 1*). For the first material the solid seemed to exhibit two distinct melting points; for the second material the solidified melt, when reheated, first melted to give an opaque liquid, which appeared to melt again to form a clear isotropic liquid at a much higher temperature.
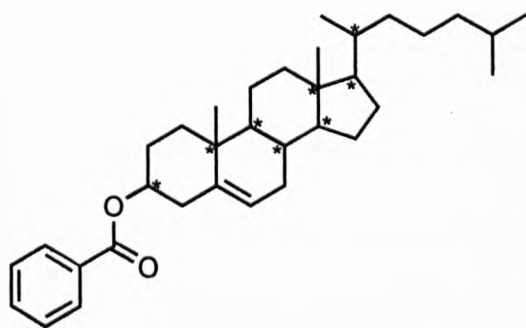
Cholesteryl benzoate   Cholesteryl acetate

Solid – "Opaque Liquid" – Liquid   *Solid – ("Opaque Liquid") – Liquid*

{145.5 °C |————————| 178.5 °C}   *{116.5 °C (|————————| 94.5 °C)}*

"E n a n t i o t r o p i c"   "M o n o t r o p i c"

Figure 1:- The first reported thermotropic liquid crystals.

Microscopic investigations revealed highly birefringent patterns observed between crossed polarisers for this opaque liquid, between the two "melting points" [4]. These observed "textures", due to the effect of changes in birefringence as a function of thickness of the material, were not unlike those observed in solid crystals, yet these materials flowed like liquids. The apparent paradoxical nature of the materials, principally the coexistence of both solid and liquid characteristics over a stable temperature range, suggested that the materials may be fluids which possess a unique form of organisation. This observation led to the classification of these materials as "fliessende Kristalle", or "liquid crystals".

Although little work was carried out immediately after the initial discovery of these novel materials, the subject of liquid crystals was revived later in the first half of the 20th century [5]. The unusual melting phenomenon was also observed in some Schiff's Bases (*figure 2*).

2

C_5H_{11}—⟨benzene⟩—$\overset{H}{C}$=N—⟨benzene⟩—C_5H_{11}
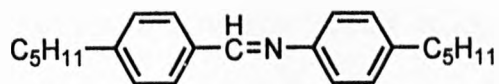
Solid – (*Mesophase 2* (Crystal B)) – *Mesophase 1* (Nematic) – Liquid

(*34.5 °C* |————————| (*32 °C*) |————————| *43.7 °C*)

Figure 2:- An example of a liquid-crystalline Schiff's Base [6].

The investigation of these compounds led to the conclusion that the materials formed a unique "phase" which, although possessing many of the characteristics of both solids and liquids, was in fact distinctly different in nature from both of these two states. The anisotropic nature of liquid crystals, manifested in their ability to be physically reoriented in the liquid-crystalline state by an electric field, eventually led to their utilisation in electrooptic display devices in the second half of the 20th century [7]. This prompted a surge of interest in the subject in the late 1960s, particularly with a view to the use of materials for electrooptic display device applications, and this interest continues to be the principal driving force for the sustained interest in liquid-crystalline materials today.

Liquid crystal phases are believed to be formed by the combined effect of the shape of the constituent molecules and partial microphase separation, that is, the partial association between the *like*-parts of the molecules in the bulk material. During the melting of a liquid crystal-forming, or "mesogenic" solid, thermal energy is sufficient to break down the *positional* order of the molecules relative to the solid crystal, but is not sufficient to completely disrupt all the *orientational* order of the molecules relative to the isotropic liquid. This is manifested in liquid crystals as the tendency of the constituent molecules to align in a "domain", with their long molecular axes on average parallel to one another. This direction is termed the "director". By

3

comparison, during the melting of a non-mesogenic solid, both the positional and orientational order of the component molecules are destroyed completely to generate the isotropic liquid directly.

The degree of loss of order of the solid crystal lattice during a liquid crystal melt can lead to the formation of different liquid-crystalline phases at different temperatures for the same material. These mesophases differ by what may tentatively describe as "degrees of breakdown" of the molecular ordering of the crystal lattice. In the most common type of liquid crystal, the calamitic mesophases, the molecules are *rod-like* in appearance (*figure 3*). The most common mesophases formed from these molecules are the smectic and nematic phases (*figure 4*).
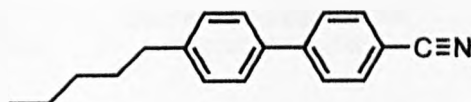

Figure 3:- An example of a calamitic liquid crystal;
4-cyano-4'-pentylbiphenyl ("5CB")

Solid Crystal
Long range positional and
orientational order

n̂

n̂

Smectic
Orientational order present,
varying degrees of positional order

Nematic
Orientational order present,
no positional order

Isotropic Liquid
No orientational
or positional order
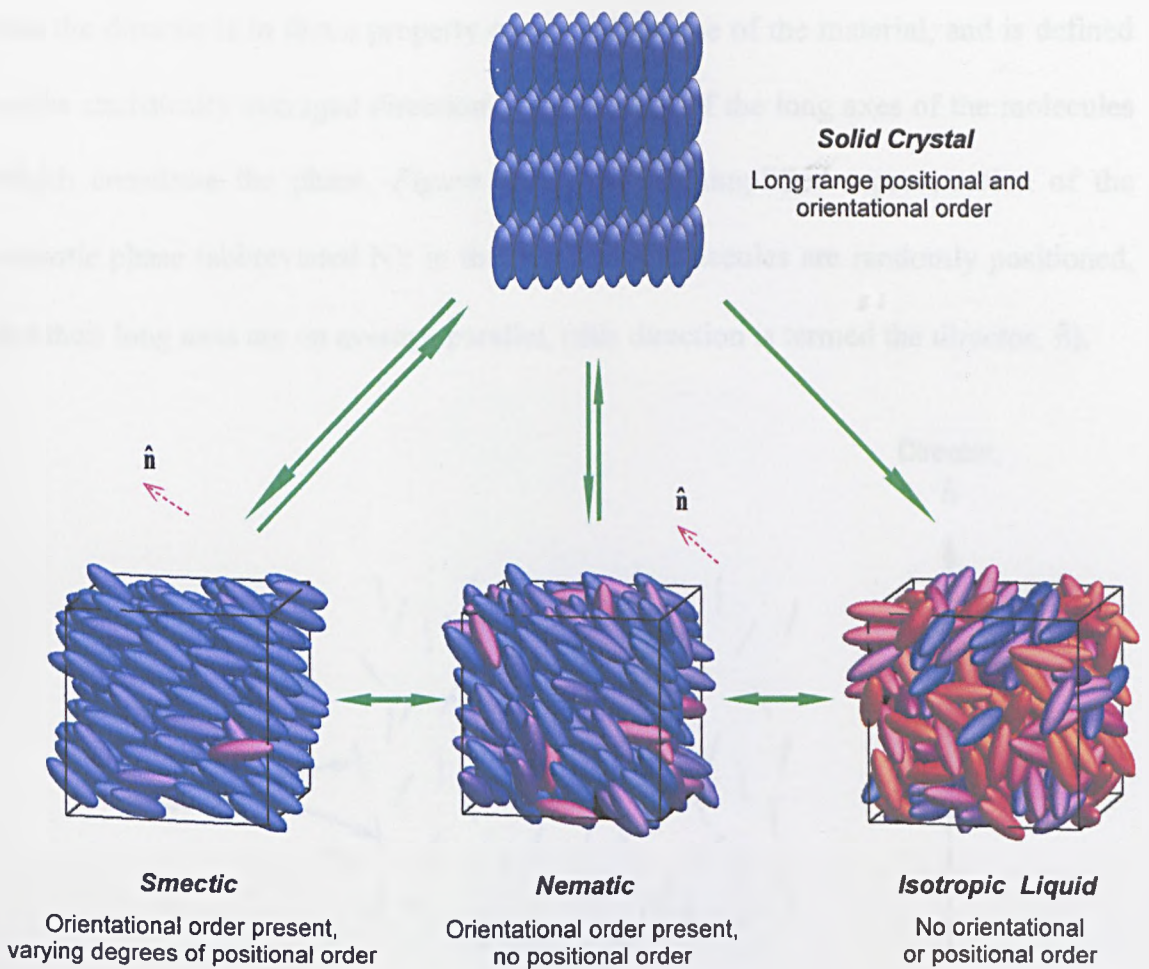
Figure 4:- Melting order of a calamitic liquid-crystalline solid showing the
generalised structures of the common phases and degrees of ordering (relative to the
solid crystal). The director (the average direction of orientation of the molecules, "n̂")
is shown by the dashed arrows for the nematic and smectic mesophases.
(courtesy of the Molecular Simulations Group, University of Bristol, UK)

Classification of Liquid Crystals

1. The Nematic Phase

Thermotropic liquid crystals can be classified into several categories according to the

organisation and orientation of molecules. Although the director is a convenient way

to describe the average orientation of the molecules in the material, it should be noted

that the director is in fact a property of the bulk phase of the material, and is defined as the statistically averaged direction of orientation of the long axes of the molecules which constitute the phase. *Figure 5* below is a simplified representation of the *nematic* phase (abbreviated N); in this phase the molecules are randomly positioned, but their long axes are on average parallel, (this direction is termed the director, ñ).

Figure 5:- Simplified representation of the nematic phase showing the director, ñ.

In the situation where the bulk phase is composed of molecules of which some or all are optically active there exist in the phase some significant macroscopic modifications to the nature of the nematic phase. In the chiral nematic (N*, also called the *cholesteric*) phase, the molecules pack in such a manner, that there exists a further organisation of the molecules: the director rotates in a particular direction through an angle of 360° over a distance called the *pitch* of the helical structure formed. The helical axis and the local director are orthogonal to each other (see *figure 6*). This *helix* is able to selectively reflect light of wavelengths related to the pitch length of the *helix*. The selective reflection of wavelengths of light in the visible region of the spectrum often gives chiral nematic liquid crystals their characteristic iridescent

appearance. Changes in temperature alter the length of the pitch and consequently the wavelength of reflected light. A spectrum of reflected colours may often be observed during the heating or cooling of a chiral nematic liquid crystal.
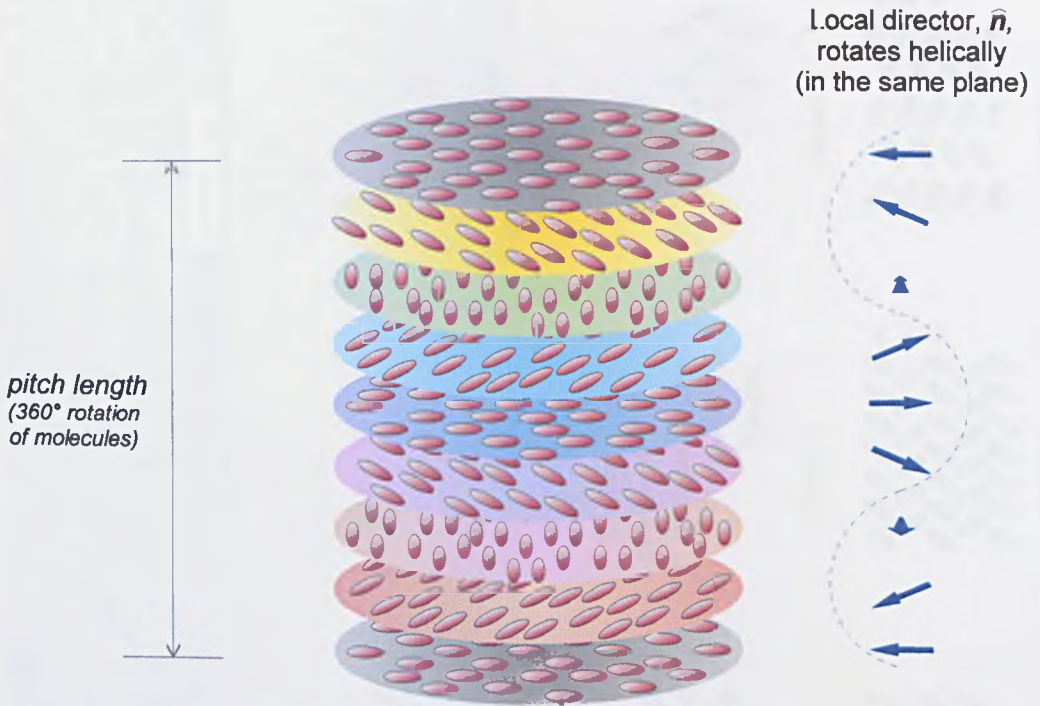
Figure 6:- Simplified representation of the Chiral Nematic (N*) phase showing the formation of a "helix" by rotation of the local director in the same plane through 360°.

2. *The Smectic Phases*

The *smectic* phases (abbreviated Sm) have a greater degree of layer ordering in comparison to the nematic phase. This is reflected in the arrangement of the molecules in "layers" in which the axes of the molecules lie approximately perpendicular, or tilted, to the planes of the layers (see *figure 7*). Differences in both the degree and type of organisation within these layers, the degree of correlation between them and the angle the director is tilted with respect to the layer normal, lead to the occurrence of various smectic phases.

Figure 7:- Side and plan views of the different smectic phases.
(The triangles and arrows represent the direction of tilt of the molecules).

8
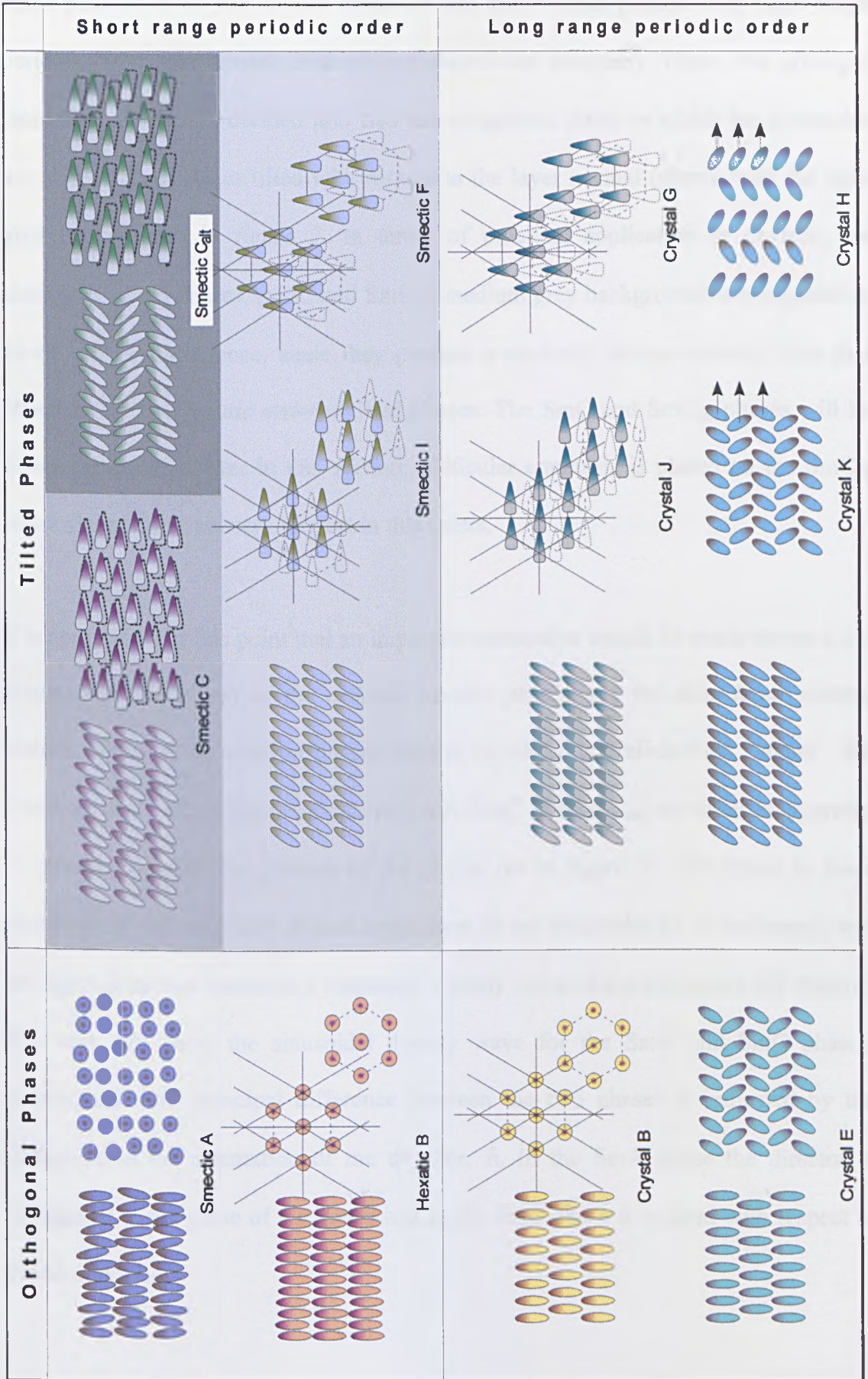
Smectic phases can be divided into two principal types: those which possess long range periodic order (the *crystal smectics*) and those which possess only short range periodic order (the *hexatic ordered* and *disordered smectics*). These two principal categories are further divided into two sub-categories: those in which the molecules are either orthogonal or tilted with respect to the layer normal (shown with the light grey background) in *figure 7*. In terms of practical application in devices, the *disordered* tilted phases, (SmC and SmC$_{alt}$, medium grey background) are regarded to be of greater importance, since they possess a markedly lower viscosity than that observed for the *hexatic ordered* tilted phases. The SmC and SmC$_{alt}$ phases will be discussed in detail later in this section; particular emphasis is placed on the SmC$_{alt}$ phase since it is of primary interest in this thesis.

It is appropriate at this point that an important distinction should be made between the macroscopic structures of the *ordered* smectic phases and the *disordered* smectic phases. Whereas the *ordered* phases consist of relatively well-defined "layers", the layers present in the disordered phases (SmA, SmC and SmC$_{alt}$) are often exaggerated in order to simplify the pictures of the phases (as in *figure 7*). The layers in these phases are in fact relatively diffuse (regardless of any molecular tilt in the layers), and are approximations based on a sinusoidal density wave of the molecules [8]. *Figures 8(a)* and *8(b)* show the sinusoidal density wave for the SmA and SmC phases, respectively. The principal difference between the two phases is indicated by the difference in the orientation of the director, n̂. In the SmA phase the director is orthogonal to the plane of the layers and in the SmC phase it is tilted with respect to the layer normal.

The orthogonal and tilted hexatic smectic phases (SmB, SmI and SmF respectively) are also composed of relatively diffuse layers, but exhibit increased ordering within the layers in comparison with the disordered phases.

As is the case for chiral nematic liquid crystals, when the component molecules are tilted with respect to the layer normal and are optically active, there also exists a number of macroscopic modifications to the structure of the smectic phases. These modifications will be the focus of the following sections (sections (ii.) and (iii.)) of this introduction, particularly the optically active forms of the SmC and SmC$_{alt}$ phases (the SmC* and SmC$_A$* phases respectively).
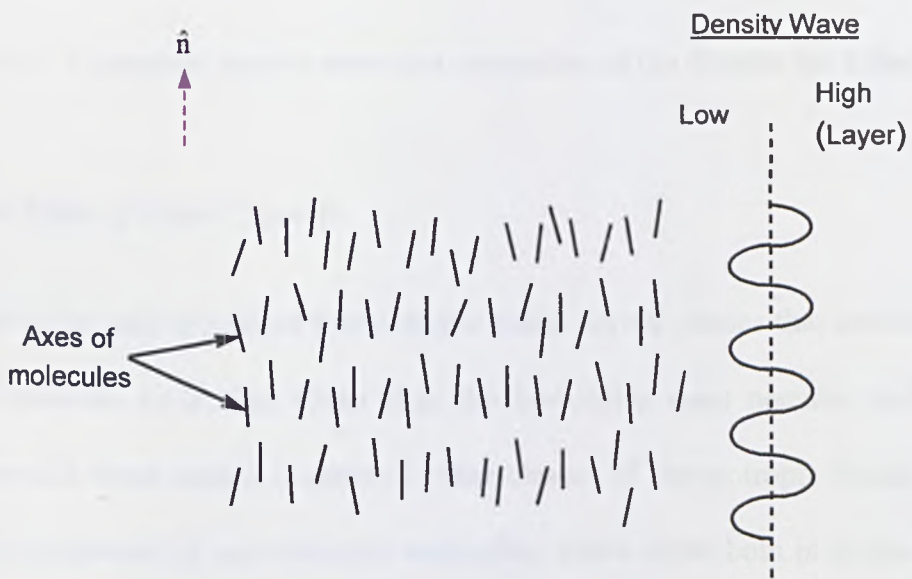
Figure 8(a):- Sinusoidal density wave and orientation of the director for a SmA phase.
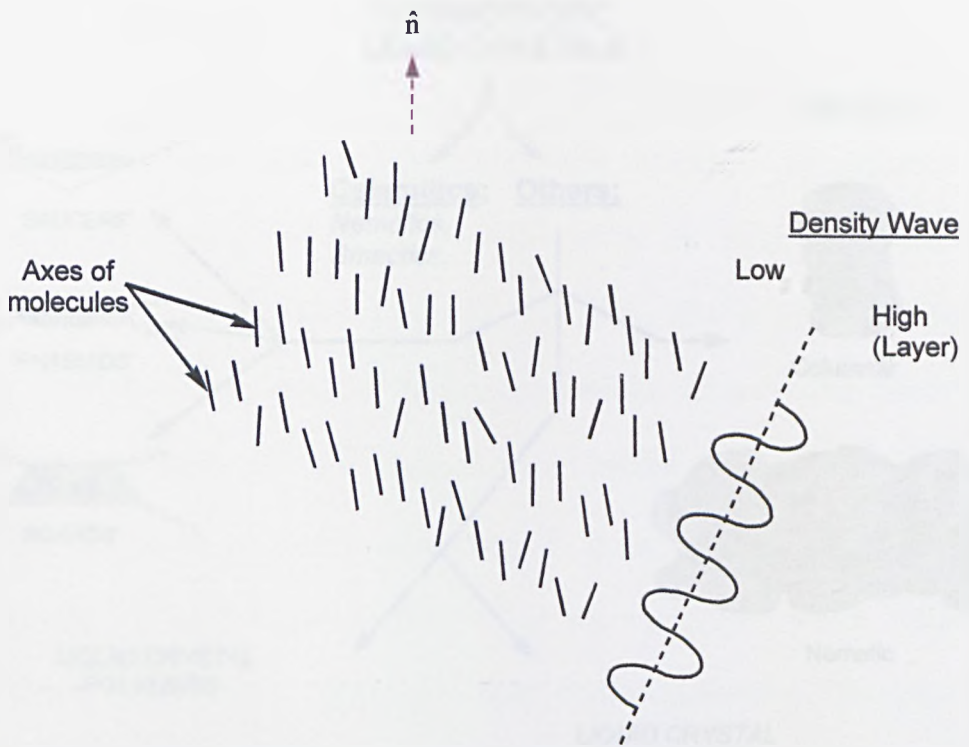
Figure 8b:- Sinusoidal density wave and orientation of the director for a SmC phase.

3. Other Types of Liquid Crystals

We have so far only discussed thermotropic liquid crystal phases that consist of rod-like or *calamitic* molecules. Other than the low-molar mass nematic and smectic liquid crystals there exist a number of other classes of thermotropic liquid crystals. These are composed of *non-calamitic* molecules, which differ both in shape and size, and range from the disc-shaped *discotic* liquid crystals [9] to the high-molar mass *polymeric* systems [10] *Figure 9* summarises some of these types of liquid crystals. Both the discotics and liquid crystal polymers can exhibit nematic and smectic phases. Since none of these types of liquid crystals feature in this thesis, they will not be described in greater detail.

THERMOTROPIC
LIQUID CRYSTALS

'SAUCERS'

'PHASMIDS'

'BOARDS'

Calamitics:
Nematics,
Smectics.

Others:

DISCOTIC

Columnar

Nematic

LIQUID CRYSTAL
POLYMERS

Main Chain

Side Chain

LIQUID CRYSTAL
ELASTOMERS

Figure 9:- Examples of other thermotropic liquid crystal systems

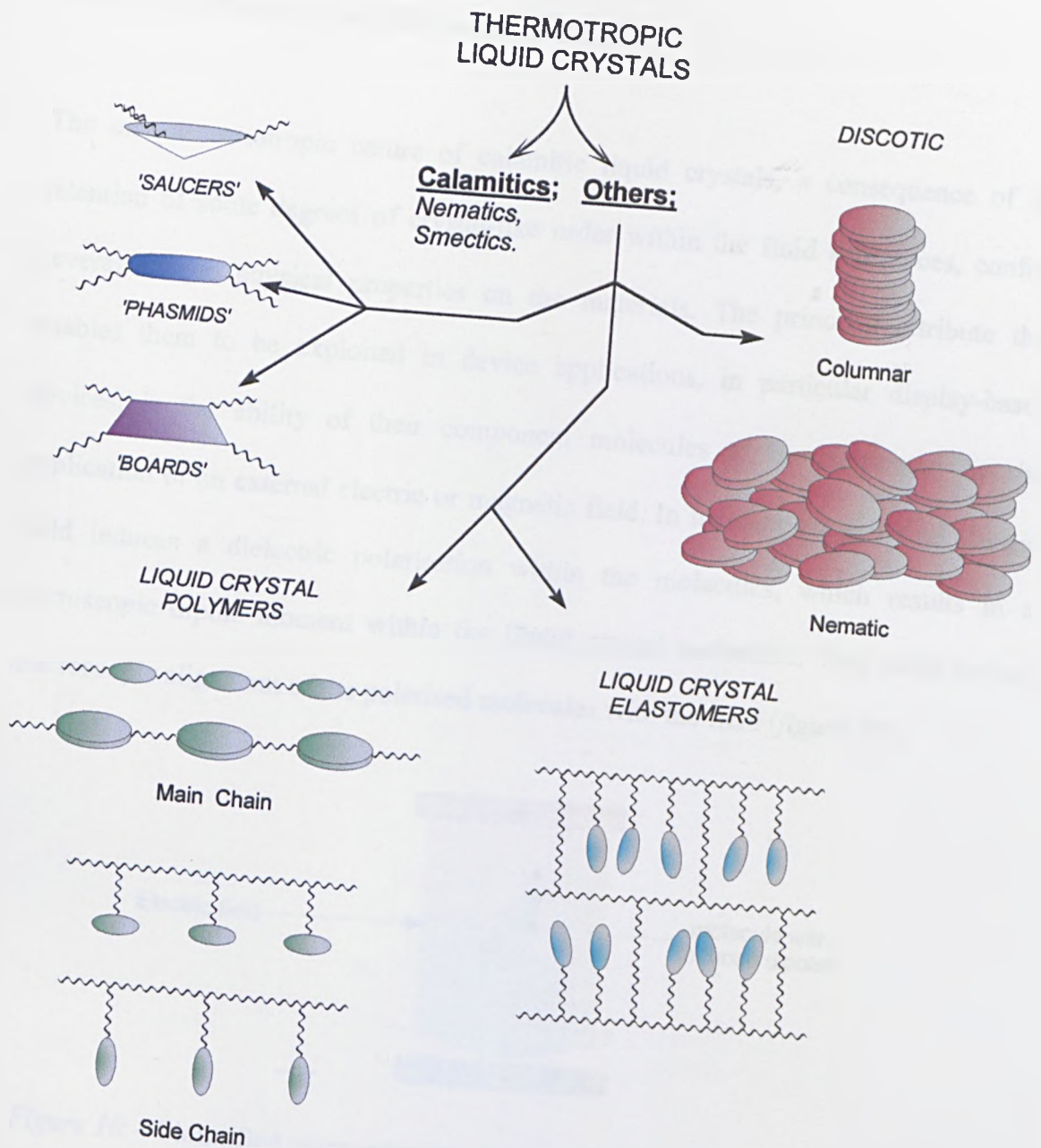The unique anisotropic nature of calamitic liquid crystals, a consequence of the retention of some degrees of crystal-like order within the fluid substances, confers several unique physical properties on the materials. The principal attribute that enables them to be exploited in device applications, in particular display-based devices, is the ability of their component molecules to be re-oriented by the application of an external electric or magnetic field. In the simplest sense an electric field induces a dielectric polarisation within the molecules, which results in a microscopic dipole moment within the liquid crystal molecules. This leads to the macroscopic alignment of the polarised molecules with the field (*figure 10*).
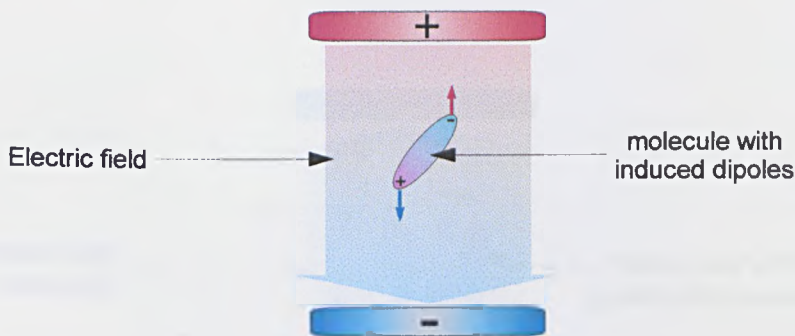
Figure 10:- Simplified representation of an individual molecule with an induced dipole moment in an electric field.

In the case of a nematic liquid crystal, such as 5CB (*figure 3* above), the component molecules already possess a permanent electric dipole along their long axes (*figure 11*). The alignment of the molecules constituting the nematic phase is, however, such that these dipoles couple in an inter-digitated (head-to-head and tail-to-tail) fashion even under the influence of a weak external electric field [11] (*figure 12(a)*). On reversing the direction of application of the electric field the overall direction of the *induced* dipole moment across the molecules also reverses (*figure 12(b)*).
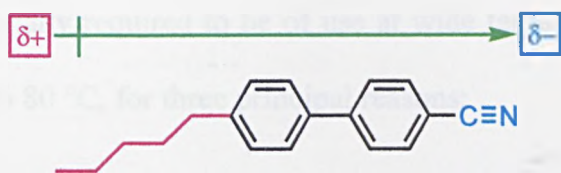
Figure 11:- Direction of the permanent dipole moment in 5CB
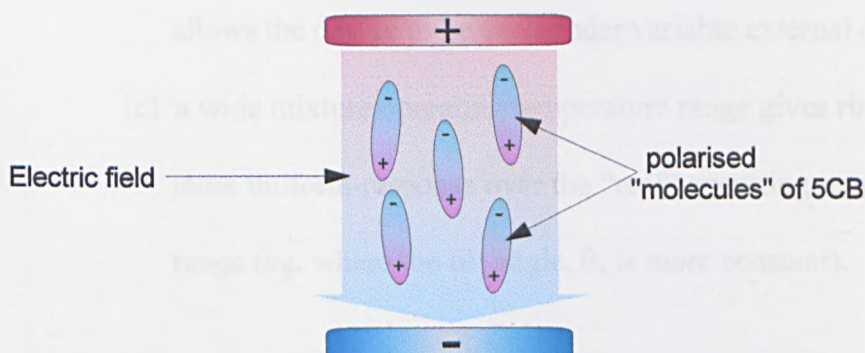
Figure 12(a):- Polarisation of 5CB molecules in an electric field
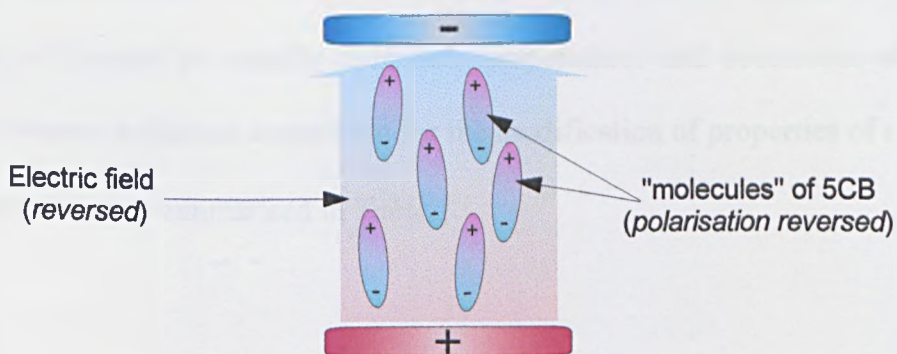
Figure 12(b):- Orientation of 5CB molecules in a reversed electric field
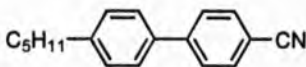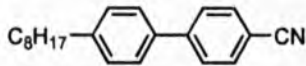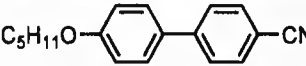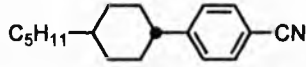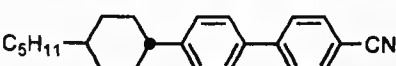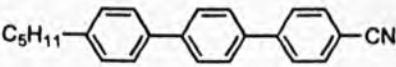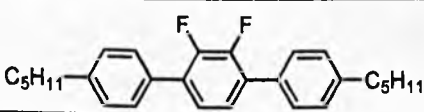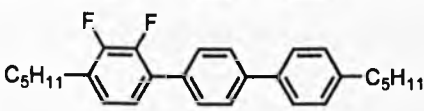
It is the ability of liquid crystals to be easily reoriented by the application of relatively weak external forces, such as electric fields, that makes them useful for electrooptic applications, especially display devices. Since all display devices operate principally at room temperature, a pre-requisite for any liquid-crystalline material to be used in a practical device is that it must exhibit the desired phase at room temperature. In fact

the materials are generally required to be of use at wide temperature ranges, usually from around –20 °C to 80 °C, for three principal reasons;

(a) "room temperatures" vary world-wide, and

(b) extending the operating temperatures of the device allows the device to be used under variable external conditions.

(c) a wide mixture operating temperature range gives rise to a more uniform response over the "real" operating temperature range (eg. where the tilt angle, θ, is more constant).

Mixing components with different chemical structures, and transition temperatures, is the standard method of tailoring the physical properties of liquid crystals, in order to meet the specifications of individual display types. At the simplest level, the properties of interest are usually transition temperatures and occurrence of desired phases. Common variations carried out for the modification of properties of a series of related materials are summarised in *Table 1*.

Table 1:- Effects on transition temperatures of variations in the structures of some calamitic liquid crystals.

Liquid Crystal	Transition Temperatures / °C
C_5H_{11}—⬡—⬡—CN	Cr 24 N 35.3 I
C_8H_{17}—⬡—⬡—CN	Cr 21.5 SmA 33.5 N 40.5 I
$C_5H_{11}O$—⬡—⬡—CN	Cr 48 N 68 I
C_5H_{11}—⬡—⬡—CN	Cr 30 N 55 I
C_5H_{11}—⬡—≡—⬡—CN	Cr 55 N 70.7 I
$C_5H_{11}O$—⬡—≡—≡—⬡—CN	Cr 164 N (150) I
C_5H_{11}—⬡—⬡—⬡—CN	Cr 96 N 222 I
C_5H_{11}—⬡—⬡—⬡—CN	Cr 131.5 N 240 I
C_5H_{11}—⬡(F,F)—⬡—C_5H_{11}	Cr 60 N 120 I
C_5H_{11}—⬡(F,F)—⬡—⬡—C_5H_{11}	Cr 81 SmC 115.5 SmA 131.5 N 142 I

The chemical structures of the vast majority of both calamitic and non-calamitic liquid crystals correspond to the general template shown in *figure 13(a)* [12]. Some examples illustrating the diverse range of materials that form liquid crystal phases are shown in *figure 13(b)-(e)*; all the materials correspond to the structure-template.

Figure 13:- Some examples of liquid crystal structures;-
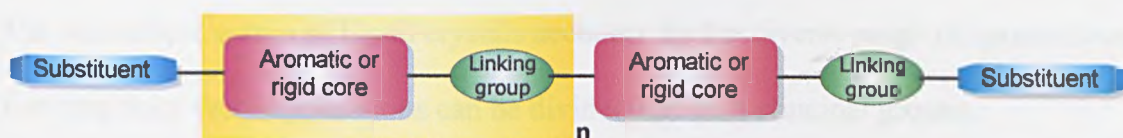
(a) General structure-template for a liquid crystal (*n = 0, 1, 2 etc.*)

(b) Representative "common" liquid crystal (*n = 0*)
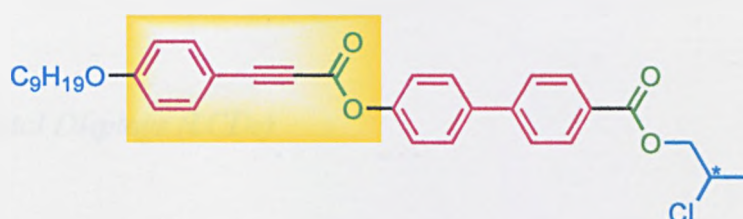
(b) Example of an optically-active (chiral) liquid crystal (*n=1*) [13]
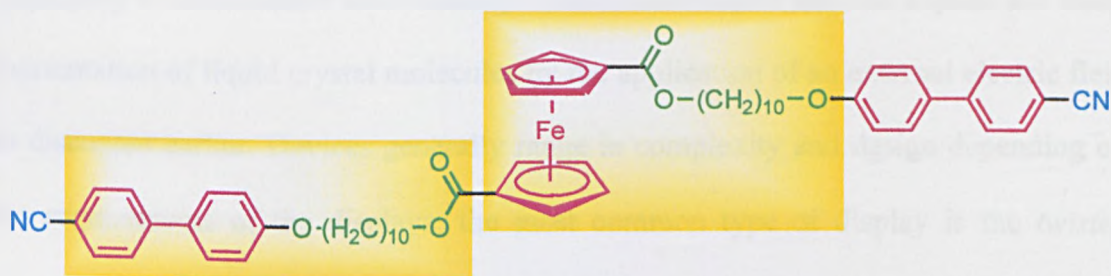
(d) Liquid crystal possessing a metallo-organic ferrocene core (*n=2*) [14]
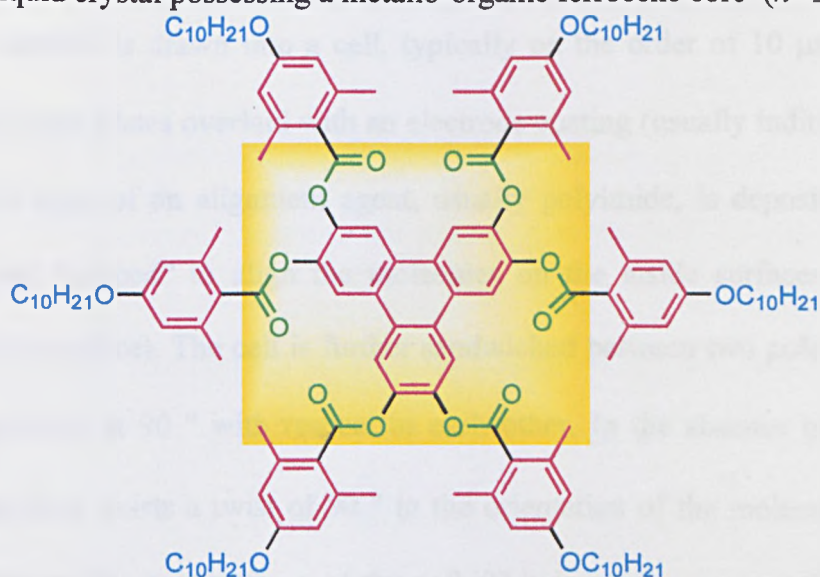
(e) Triphenylene-centred discotic liquid crystal (*n=1*) [15]

Applications of Liquid Crystals

The anisotropic nature of liquid crystals accounts for the diverse range of applications. For simplicity these applications can be divided into two principal groups;

(1) liquid crystal displays

(2) non-display applications

1. Liquid Crystal Displays (LCDs)

By far the most widespread use of thermotropic liquid crystals today is in the displaying of information electronically. These _electrooptic_ devices exploit the facile reorientation of liquid crystal molecules by the application of an external electric field as discussed earlier. Devices generally range in complexity and design depending on the requirements of the displays; the most common type of display is the _twisted nematic_ liquid crystal display (TN-LCD) (_figure 14_). In this display a nematic liquid-crystalline material is drawn into a cell, typically on the order of 10 μm thickness, consisting of glass plates overlaid with an electrode coating (usually indium tin oxide, ITO). A thin layer of an alignment agent, usually polyimide, is deposited onto the electrodes and "rubbed" to align the molecules on the inside surfaces of the cell (parallel to the surface). The cell is further sandwiched between two polarising filters which are crossed at 90 ° with respect to each other. In the absence of an applied electric field there exists a twist of 90 ° in the orientation of the molecules (and the director) between the two surfaces of the cell. This is a consequence of mechanical constraints ("anchoring") imposed by alignment of the molecules with the alignment

layers on the surfaces, which are also perpendicular to each other. Interaction of the molecules with incident light, plane-polarised by the first filter, causes the light to be directed through a twist of 90° allowing it to pass through the second (crossed) polariser. The cell, as a result of the so-called "wave-guiding" action of the liquid crystal, appears transparent or "light" (*figure. 14(a)*).
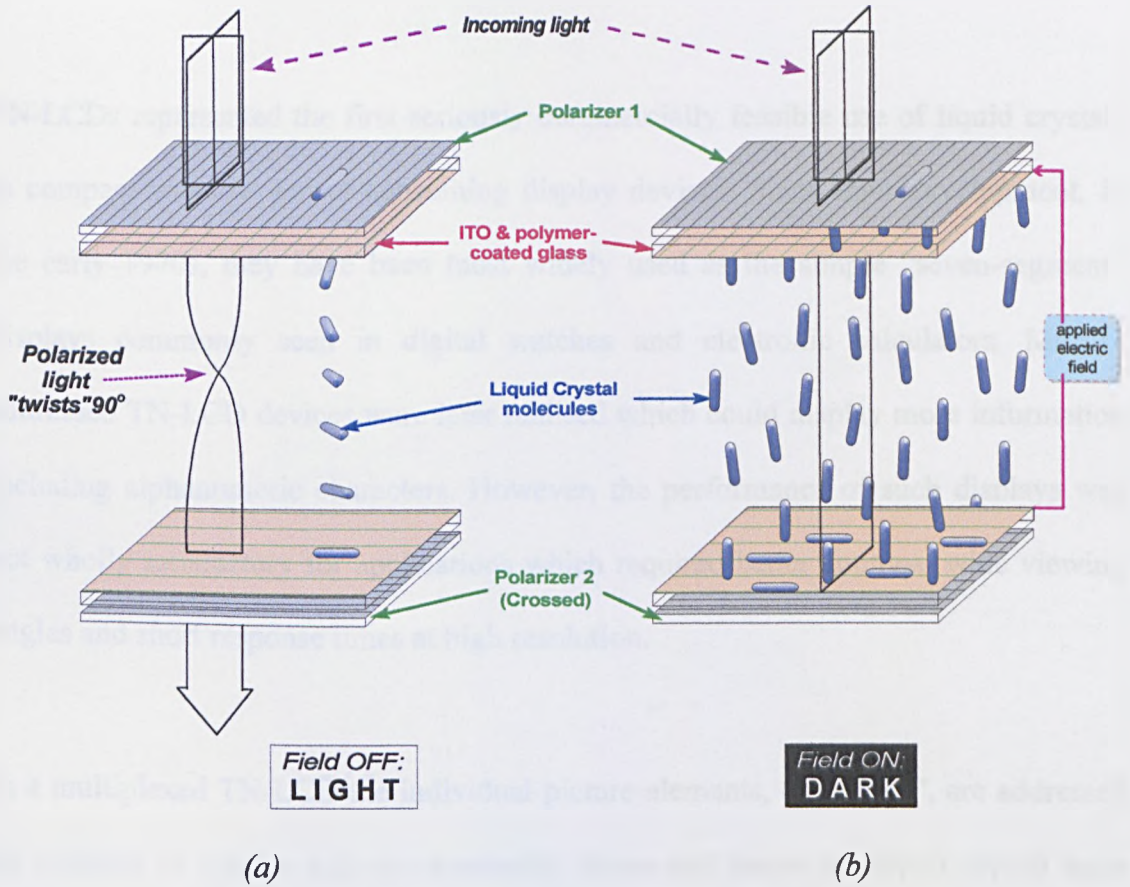
Figure 14:- The twisted nematic liquid crystal display device (TN-LCD); field off ("light") state, (b) field on ("dark") state. The molecules at the surfaces remain anchored parallel to the glass even in the field ON state.

On application of an electric field between the cell electrodes an induced polarisation is generated within the molecules. This causes them to align with the field, degenerating the twisted state of the liquid crystal, so that light polarised by the first filter is no longer "guided" through the second polariser. The cell then appears "dark" (*figure 14(b)*).

Two modes of operation are generally used in these and the vast majority of all other liquid crystal devices. In the *transmissive* mode light is directed from behind the cell towards the observer (using a "backlight"); in the *reflective* mode a mirror placed behind the second polariser reflects ambient light back to the observer through the cell. A "transflector" allows the combination of both modes for intermediate light conditions.

TN-LCDs represented the first seriously commercially feasible use of liquid crystals in compact and low power-consuming display devices. Since their development, in the early 1970s, they have been most widely used as the simple "seven-segment" displays commonly seen in digital watches and electronic calculators. Matrix-addressed TN-LCD devices were later realised which could display more information including alphanumeric characters. However, the performance of such displays was not wholly satisfactory for applications which required better contrast, wide viewing angles and short response times at high resolution.

In a multiplexed TN-LCD the individual picture elements, or "pixels", are addressed by a matrix of column and row electrodes above and below the liquid crystal layer (*figure 15*). This form of *passive* addressing allows a large number of pixels to be switched by the minimum number of electrodes. A variation of the simple multiplexed twisted-nematic device is the super-twisted nematic display device, the STN-LCD, developed in the mid-1980s. In this device the liquid crystal in the cell is twisted through an angle of 240 ° to 270 ° instead of 90 ° (*figure 16*). Advantages of these devices over TN-LCDs include the ability to realise displays with higher resolution, improved contrast ratio, and wider viewing angles.
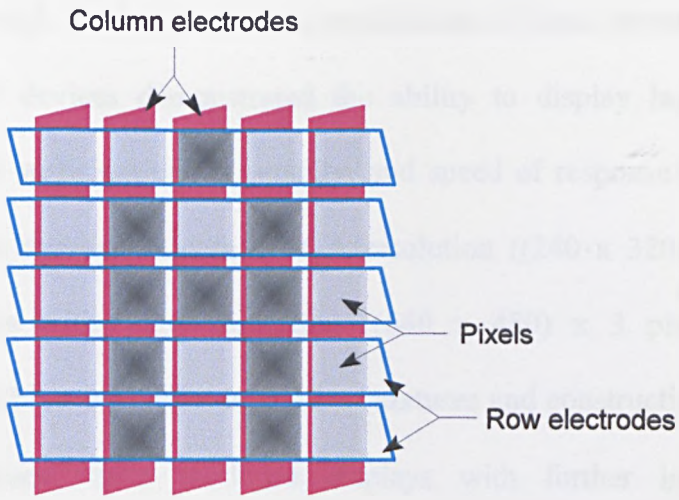
Figure 15:- Multiplex addressing in a TN-LCD or STN-LCD.
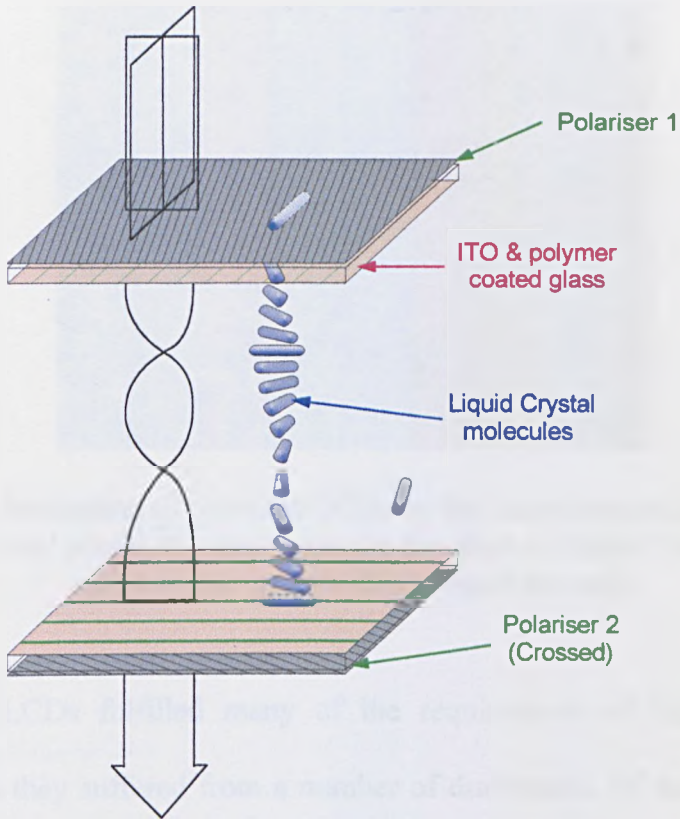
Figure 16:- The super-twisted nematic liquid crystal display device (STN-LCD).
(The director twists through 240 ° to 270°).

The incorporation of colour into these devices, by the integration of red, green and blue colour filters during the manufacturing process of the cell (*figure 17*), presented a

further breakthrough for the commercial exploitation of liquid crystal displays. By the late 1980s STN devices demonstrated the ability to display larger quantities of information with sufficient clarity, quality, and speed of response for application in hand-held colour televisions with QVGA resolution ((240 x 320) x 3 pixels) and laptop computers with VGA resolution ((640 x 480) x 3 pixels). Subsequent enhancements in both the liquid-crystalline mixtures and construction of STN-LCDs, during this decade, have produced displays with further improved viewing characteristics (the Dual Scan-STN-LCDs, Fast Response-STN-LCDs, etc.).
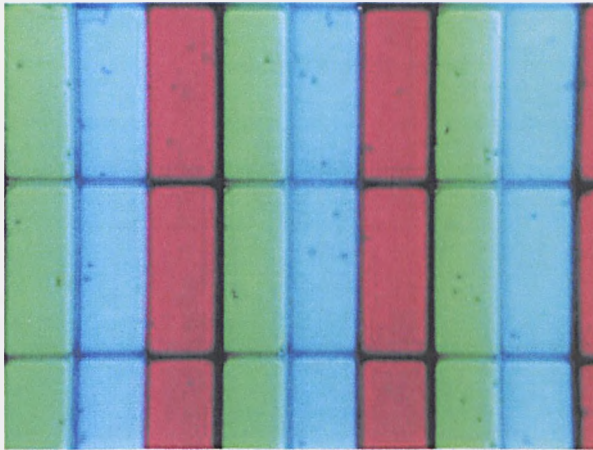
Figure 17:- Production of colour in LCDs by the incorporation of colour filters in the individual pixels (the dark spots are the glass or plastic "spacers" which maintain the uniform thickness of the cell).

Although STN-LCDs fulfilled many of the requirements of higher information-content displays they suffered from a number of drawbacks. Of these drawbacks the relatively narrow viewing angles, and problems associated with "cross-talk" (due to the partial switching of pixels adjacent to the selected pixels), were amongst the most severe. As the demands for wider viewing angles and the ability to display information closer to video frame rate (for multimedia applications) increased, the solution was to isolate individual pixels from each other and to *actively* drive the

device. This was achieved by incorporating a switch, in the form of a thin-film transistor (TFT) within the glass substrate, into every pixel to form an "active matrix" (*figure 18*). This device, often referred to as a TFT-TN-LCD, is based on a TN-LCD since the angle of twist of the liquid crystal in the cell is 90°. Faster response times, wider viewing angles and elimination of cross-talk were the obvious advantages of TFT-TN-LCDs over STN-LCDs. These displays also demonstrated the suitability of devices based on liquid crystals for more demanding applications, such as larger-area XGA ((1024 x 768) x 3) and SXGA ((1280 x 1024) x 3) desktop monitors, and also high resolution miniature displays for projection-based displays [16].
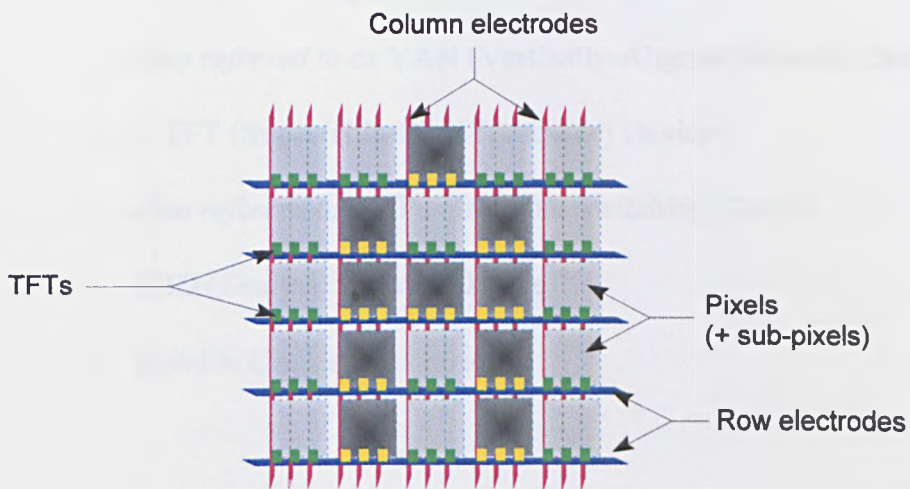
Figure 18:- Addressing in a TFT-LCD.

The complex manufacturing processes of TFT-TN-LCDs, together with much higher construction costs in comparison with TN- and STN-LCDs, are the main disadvantages of TFT-TN-LCDs. This fact accounts for the greater popularity of TN- and STN-LCDs for the majority of medium-area (eg. mobile telephones, electronic organisers etc.) and large-area (eg. notebook computers) "flat panel displays" respectively, even today.

There exist a number of other types of nematic-based display devices in addition to the three principal types described above. These exploit alternative methods of switching liquid crystals and possess both advantages and disadvantages over the above types. Since the passively addressed (multiplexed) TN-LCD and STN-LCD, as well as the actively addressed TFT-TN-LCD, have proved to be the most prolific for the development of LCDs, over the last three decades, these alternative devices will not be discussed here. For the interests of general awareness, however, some examples of these peripheral devices [17, 18] are listed below;-

- ECB (Electrically-Controlled Birefringence) Device

  Also referred to as VAN (Vertically-Aligned Nematic) Device

- S-TFT (Super Thin-Film Transistor) Device

  Also referred to as IPS (In-Plane Switching) Device

- ZBD (Zenithal Bistable Device)

- Bistable Cholesteric Device

2. Non-Display Applications

Although thermotropic liquid crystals have mostly found uses in displays, a number of novel non-display applications, both potential and realised, are recognised, and are discussed briefly in this sub-section.

Liquid Crystal Thermometers

As mentioned earlier the length of the helical pitch, and consequently the wavelength

of selectively reflected visible light, of a chiral nematic liquid crystal is dependent on the temperature of the material. A change in temperature alters the pitch length, resulting in the reflection of a different wavelength of light, hence the "colour" of the bulk material changes. By placing materials which display colour at different temperatures adjacent to one another it is possible to produce temperature sensors which are responsive across a range of different temperatures. Such sensors have found uses as thermometers in both medical and engineering environments.

Information storage

Liquid-crystalline materials have been demonstrated as suitable media for the storage of information, ranging from re-writeable optical computer discs [2] to optical imaging media such as holograms, on account of their semi-mobile nature. Prototype re-writeable compact discs are "written" by the reorientation of liquid crystals embedded onto the surface of a plastic-coated disc by local heating of the material within the "tracks" on the disc, using a high-intensity miniature laser. "Reading" of the data is enabled by decoding the recorded patterns reflected from the surface of the disc by a standard optical laser.

Holographic images are formed by changes in molecular conformation (from *cis* to *trans*), of liquid-crystalline materials related to the stilbenes, by the absorption of coherent (laser) light.

A recent novel application for liquid crystals is as the media for "instant photographic transparencies" [19]. A liquid-crystalline material placed in a cell between two layers of photoconducting material becomes reorganised on exposure to light as an electric

25

field develops within the cell. As the field is proportional to the intensity of light the patterns of reorganisation are transmitted allowing an image to be recorded "electronically".

(ii)   Ferroelectric Liquid Crystals

The term "pyroelectric" is used to describe any substance in which the electrical properties change with temperature. Within this classification there exists a group of substances which possess what are referred to as "ferroelectric" properties [20-23]. The phenomenon of ferroelectricity was originally discovered in 1920, in crystals of an inorganic tartrate commonly known as Rochelle salt, by Valasek. The principal characteristic of the bulk solid was that it displayed a measurable net electrical polarisation (which we shall soon define as the *spontaneous polarisation*, P_s), the direction of which could be reversed on application of an external electric field, below a certain temperature. This critical point, the "Curie temperature", marked the onset of polar electrical order in the low-symmetry crystalline structure of the material. In 1974 Meyer [24] proposed that a liquid-crystalline substance consisting of molecules with low symmetry (ie. those that possess chirality), in a smectic C* phase, should also display ferroelectric properties when confined in a thin cell with the appropriate surface treatment. By 1975 this was experimentally confirmed in the first recognised ferroelectric liquid crystal, DOBAMBC (*figure 19*) [25]. As with the inorganic crystalline ferroelectrics, ferroelectric liquid crystals (FLCs) also possess a spontaneous polarisation, the direction of which can be reversed by application of an external electric field of a suitable size. The existence of the spontaneous polarisation

26

in certain smectic phases is recognised as being a consequence of the combination of a uniform macromolecular order and the *reduced symmetry* of the molecules in the smectic layers. It is the symmetry aspect of FLCs that we shall now focus upon.
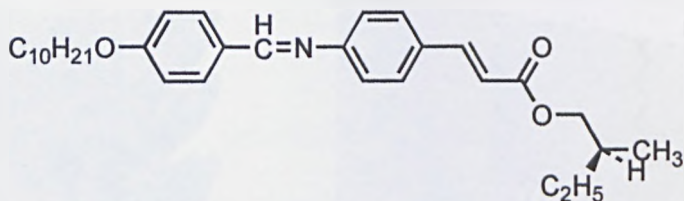
Figure 19:- DOBAMBC, the first reported ferroelectric SmC* material.

Origin of Spontaneous Polarisation

In the case of the SmA phase the molecules lie, on average, approximately perpendicular to the plane of the layers (*figure 20*). The phase possesses a space symmetry of $D_{\infty h}$.
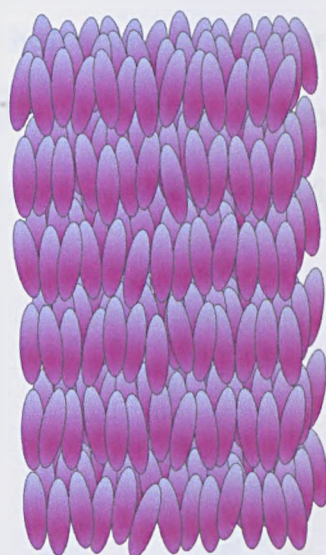
Figure 20:- Structure of the SmA phase ($D_{\infty}h$ symmetry)

When the molecules in the layers are tilted (at an angle θ) and are not optically active, as in the SmC phase (*figure 21a*), the space symmetry changes to C_{2h}. The symmetry elements of this group are (in relation to the phase); a two-fold axis of rotation

(parallel to the plane of the layers), a centre of inversion, and a mirror plane (perpendicular to the axis of rotation) (*figure 21b*).
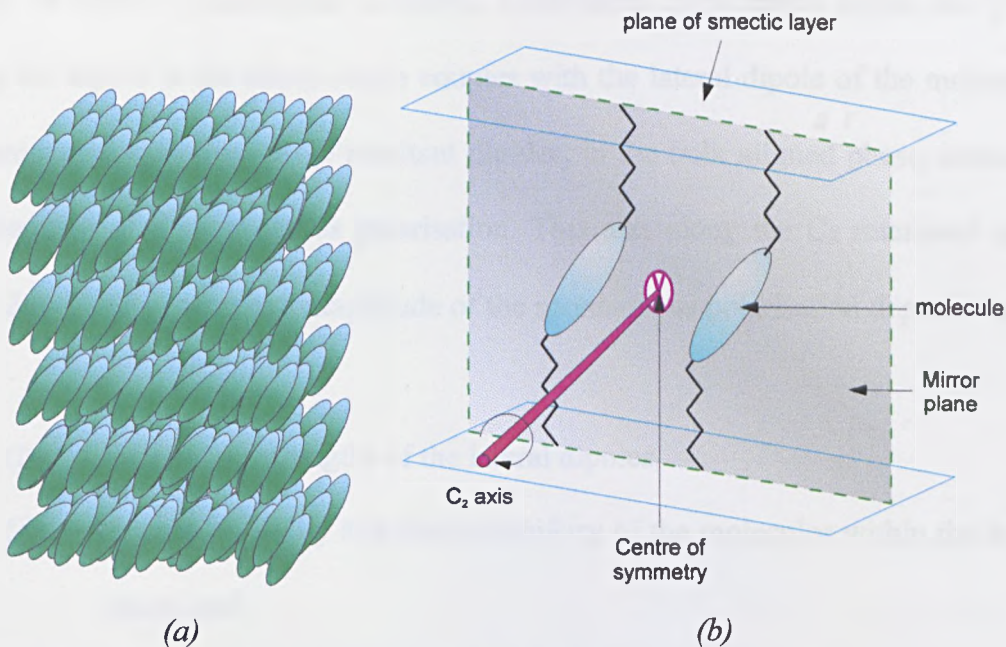
Figure 21:- The achiral Smectic C phase; general structure, *(a)* and symmetry elements *(b)*.

In the situation where the tilted phase is composed of optically active (chiral) molecules, the symmetry of the SmC* phase is reduced to C_2, the only symmetry element present in this case is the C_2 axis of rotation (*figure 22*).
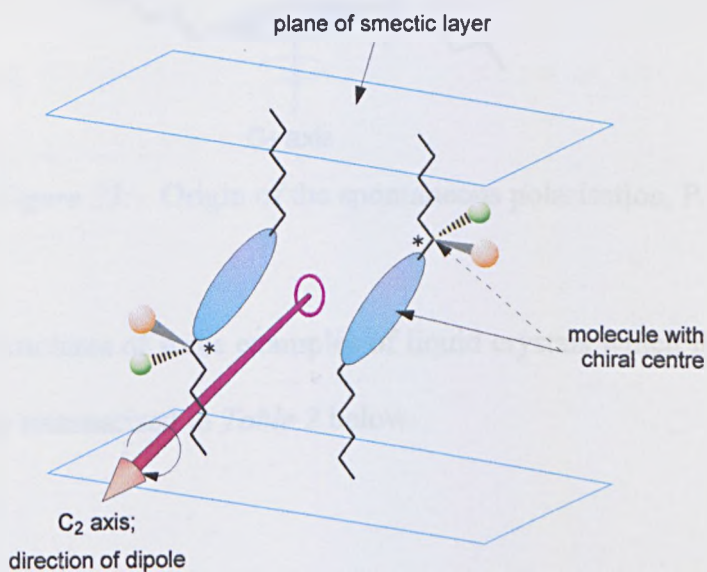
Figure 22:- Reduced space symmetry of the SmC* phase.

This "breaking of symmetry" of the SmC* phase results in a coupling of the lateral dipole which acts *along* the layers. The magnitudes of the dipoles depend on their freedom of rotation, quadrupolar coupling, substituents at the chiral centre etc. [26-28]. As the dipole at the chiral centre couples with the lateral dipole of the molecule the spontaneous coupling of the resultant dipoles, in the bulk aligned phase, leads to the generation of a spontaneous polarisation. This acts along the C_2 rotational axis (*figure 23*). The direction and magnitude of the spontaneous polarisation depends on:

(i)   the relative strengths of the lateral dipoles,

(ii)   the optical purity and stereochemistry of the molecules within the bulk phase, and

(iii)   the "parity" of the chiral centre [27].
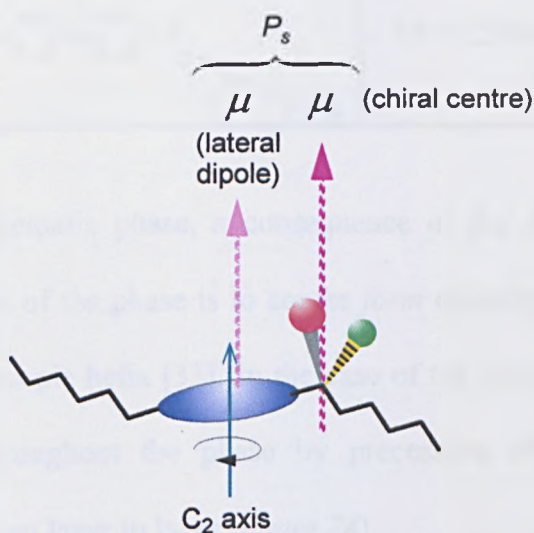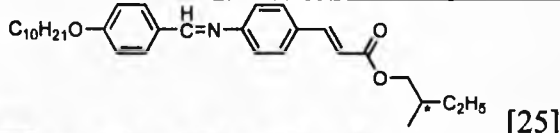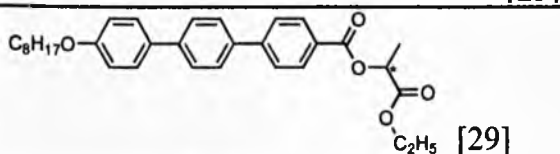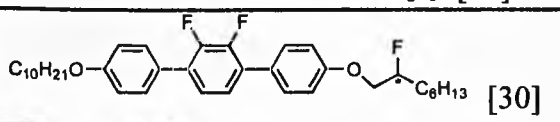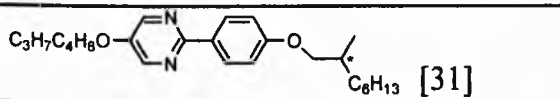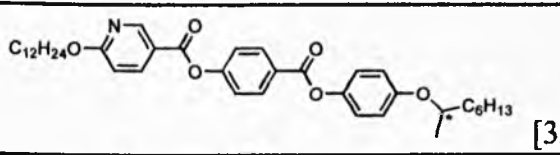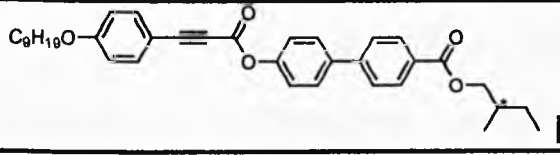
Figure 23:- Origin of the spontaneous polarisation, P_s.

The molecular structures of some examples of liquid crystals which form ferroelectric SmC* phases are summarised in *Table 2* below.

Table 2:- Structures and transition temperatures of some examples of liquid crystals which form ferroelectric SmC* phases.

Ferroelectric Liquid Crystal	Transition Temperatures / °C
$C_{10}H_{21}O$—〇—$\overset{H}{C}$=N—〇—〇 ... O ... O—C_2H_5 [25]	Cr 76 (SmH* 63) SmC* 95 SmA* 117 I
$C_8H_{17}O$—〇—〇—〇 ... O ... O—C_2H_5 [29]	Cr 127 SmC* 158.5 SmA* 180.2 I
$C_{10}H_{21}O$—〇—〇(F,F)—〇—O ... F—C_6H_{13} [30]	Cr 88.6 SmC* 144.1 SmA* 154.9 N* 157.3 BPI 157.8 I
$C_3H_7C_4H_8O$—〇(N,N)—〇—O ... C_6H_{13} [31]	Cr 80.7 SmC* 109.9 SmA* 113.3 I
$C_{12}H_{24}O$—〇(N)—O—〇—O—〇—O—C_6H_{13} [32]	Cr 65.8 SmC* 94 SmA* 100.5 I
$C_9H_{19}O$—〇—≡—O—〇—〇—O [13]	Cr 72.2 SmC* 80.5 SmA* 116.6 N* 144.2 I

As with the chiral nematic phase, a consequence of the intrinsic chirality of the component molecules of the phase is to confer *form* chirality on the bulk sample, in the form of a macroscopic helix [33]. In the case of the chiral smectic C* phase this helix perpetuates throughout the phase by precession of the molecules around hypothetical cones from layer to layer (*figure 24*).

(a)   (b)
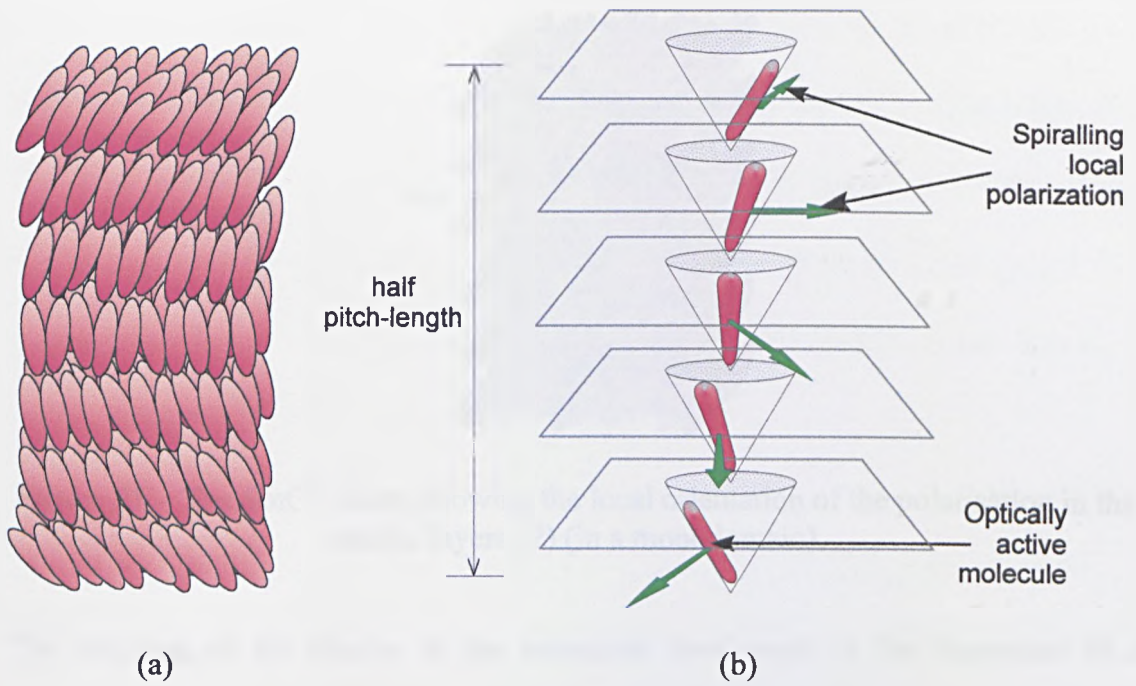
Figure 24:- (a) helical pitch of the SmC* phase (half-pitch length);
(b) precession of the chiral molecules around a "cone" between adjacent smectic
layers and spiralling local polarisation.

On application of an external electric field normal to the helical axis the spiralling

local spontaneous polarisations align with the direction of the field to the unwound

ferroelectric states. In this form the SmC* phase is referred to as being *helielectric*. In

order to truly exploit the bistable character of the ferroelectric SmC* phase for

applications in devices, however, it is necessary to prevent the formation of this helix

in the first instance. It was postulated that this could be achieved by confining the

SmC* phase in a thin cell, the gap of which must be considerably smaller than the

pitch of the phase [24] (usually on the order of 2 µm thickness), and imposing surface

constraints (in the form of alignment layers) on the material. The resulting SmC*

"monodomain" would then exhibit a spontaneous polarisation which can be reversed,

in a bistable manner, by an external electric field applied parallel to the smectic layers

(*figure 25*).
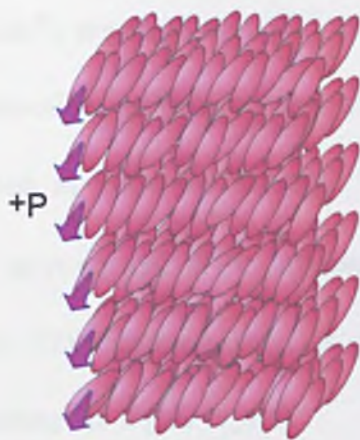
Figure 25:- The SmC* phase, showing the local orientation of the polarisation in the smectic layers (P) (in a monodomain).

The coupling of the dipoles at the molecular level leads to the formation of a spontaneous polarisation, which is transmitted through the bulk material, and it is here that ferroelectricity in the SmC* phase is actually observed. An unaligned sample of a material in the SmC* phase has a macroscopic spontaneous polarisation of zero. This is due, firstly, to the presence of the helix; and secondly, the "cancelling-out" effect of adjacent domains in which the spontaneous polarisation lies in opposite directions (since there is no field present to align it in a common direction). In a sample aligned by an external electric field a monodomain structure is formed which exhibits a net ferroelectric polarisation. On removal of the field this structure "relaxes" back into the helical structure, described above, and the value of the polarisation is reduced to zero.

In the helical state the orientation of the molecules around the "cone" is said to be "degenerate" since they are able to adopt any position, around the cone, in order to perpetuate the helical ordering throughout the material (*figure 26a*). By placing the material in a thin cell, with the inside surfaces coated with alignment layers (such as rubbed polyimide), the helix can be permanently unwound [34]. By removing the helix, the degeneracy of the molecules on the cone is reduced so that there are now

only two degenerate (or "stable") states (*figure 26b*). In each of the states the local

polarisation lies in opposite directions perpendicular to the long axis of the molecules.

The cone angle, 2θ, is defined as twice the average "tilt angle" of the molecules,

θ, with respect to the smectic layer normal. If the cell (described above) is coated with

a conducting material (such as ITO), between the glass walls and alignment layers, an

electric field can be applied across the liquid crystal.

(a)   (b)
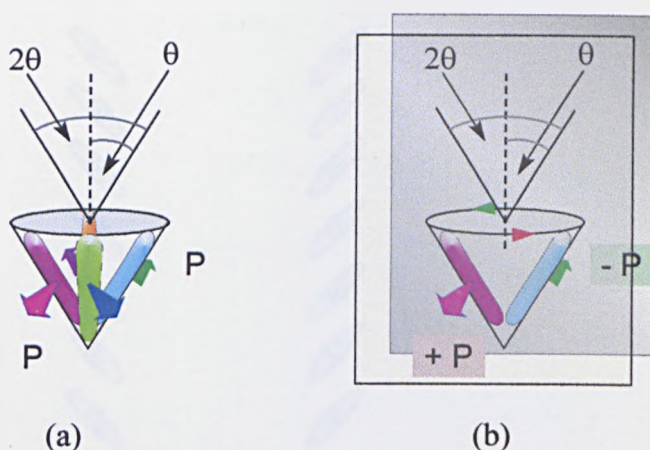
Figure 26:- Degeneracy in the "cone" of an FLC molecule; in the unaligned SmC*
phase (all positions are equally stable), (a); and aligned phase, (b). By placing the
phase in a thin cell and imposing surface interactions on the material only two
possible degenerate states of the molecules can exist; (-P) and (+P)[App.A] are the
directions of the polarisation in each orientation.

As with the inorganic crystalline ferroelectrics the direction of the spontaneous

polarisation (P) in this "unwound" state can be reversed, by application of an external

electric field, *via* a threshold and polarisation hysteresis (*figure 27a*). In doing so (this

very fact of course defines ferroelectricity itself) the molecules in the mesophase

undergo re-alignment from one of the degenerate "ferroelectric SmC*" states to the

other (*figure 27b*). The direction of re-orientation of the molecules is dependent on the

direction of the applied field, between the cell, since the spontaneous polarisation in

effect "follows" the field.
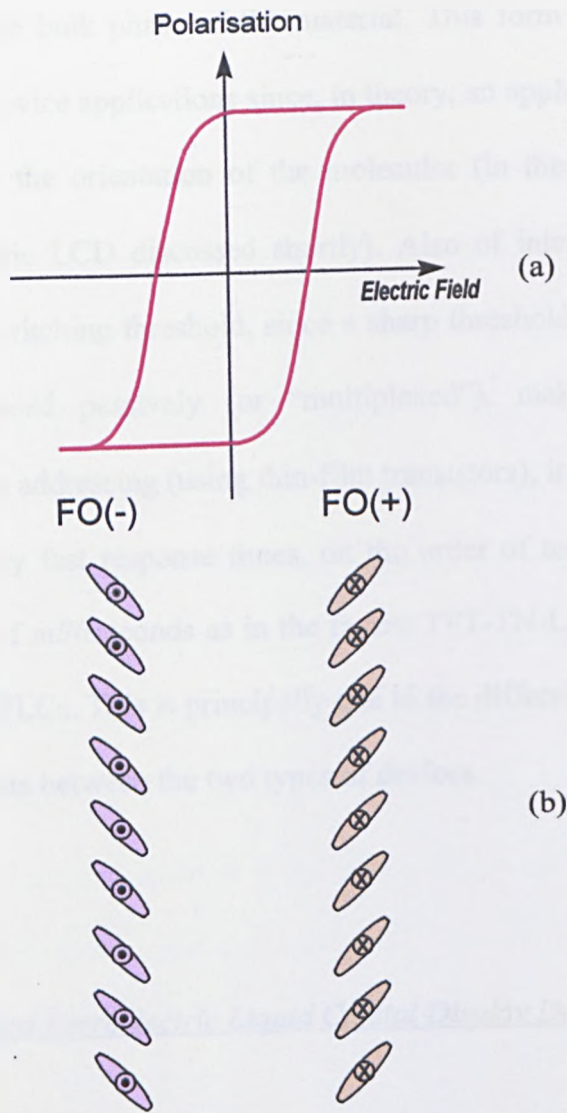
Figure 27:- Ferroelectric threshold and polarisation hysteresis of an unwound / aligned SmC* phase, (a); corresponding directions of orientation of the molecules, (b). The directions of polarisation are represented by the dots (going "into" the page) and crosses ("coming out" of the page).

The reversal of the direction of spontaneous polarisation is facilitated by reorientation of the molecules constituting the phase around the "cone" described above (the "Goldstone" mode).

On removal of the applied field a net polarisation, facilitated by preservation of the direction of orientation of the molecules (as a consequence of the alignment layers in

the cell), exists in the bulk phase of the material. This form of "bistability" is of primary interest for device applications since, in theory, an applied electric field is not required to maintain the orientation of the molecules (in the case of the Surface-Stabilised Ferroelectric LCD discussed shortly). Also of interest is the incline, or "steepness", of the switching threshold, since a sharp threshold confers the ability of FLCs to be addressed passively (or "multiplexed"), making unnecessary the requirement of *active* addressing (using thin-film transistors), in order to produce high quality displays. Very fast response times, on the order of tens of *micro*seconds in comparison to tens of *milli*seconds as in the fastest TFT-TN-LCDs, can be conferred on devices utilising FLCs. This is principally due to the difference in the nature of the switching mechanisms between the two types of devices.

The Surface-Stabilised Ferroelectric Liquid Crystal Display Device

In 1980, the Surface Stabilised Ferroelectric Liquid Crystal (SS-FLC) Device, the first practical device application of the ferroelectric SmC* phase, was demonstrated by Clark and Lagerwall [34]. By carefully varying the thickness of a cell, containing an unwound and aligned SmC* phase, the optical retardation of plane-polarised light could be modified. This enabled the transmission of light directed through the cell, sandwiched between crossed polarisers, to be controlled so that "light" and "dark" states could exist in the two ferroelectric SmC* states. In order to maintain the unwound character of the SmC* phase the cell gap had to be less than a quarter of the helical pitch of the material. A description of the SS-FLC device now follows.

35

Unlike the TN- and STN-based devices, an SSFLC device functions as a light-valve based on a switchable *half-wave (λ/2) optical retardation plate*. At one of the ferroelectric positions the component of incident plane-polarised light (from behind the device), *perpendicular* to the optic axes of the molecules (ie. the "extraordinary ray"), is shifted in phase by 180 ° (π radians) relative to the other component (the "ordinary ray") *(figure 28a)*. The polarised light is in effect then rotated by 90 ° (π/2 radians), enabling it to pass through the second polariser (the "analyser"), to produce the "light" state. In the opposite ferroelectric state the light is not rotated, since the direction of polarisation of light is parallel to the optic axis, hence there is no shift in phase and the device (ie. the light-valve) appears dark *(figure 28b)*. For optimum transmission in the "light" and "dark" states, ie. to effect a phase shift of 180 ° (π radians), the molecules must undergo reorientation of the optic axis by exactly 45 ° between the two ferroelectric states. Consequently the tilt angle of the molecules normal to the plane of the smectic layers is required to be 22.5 °.
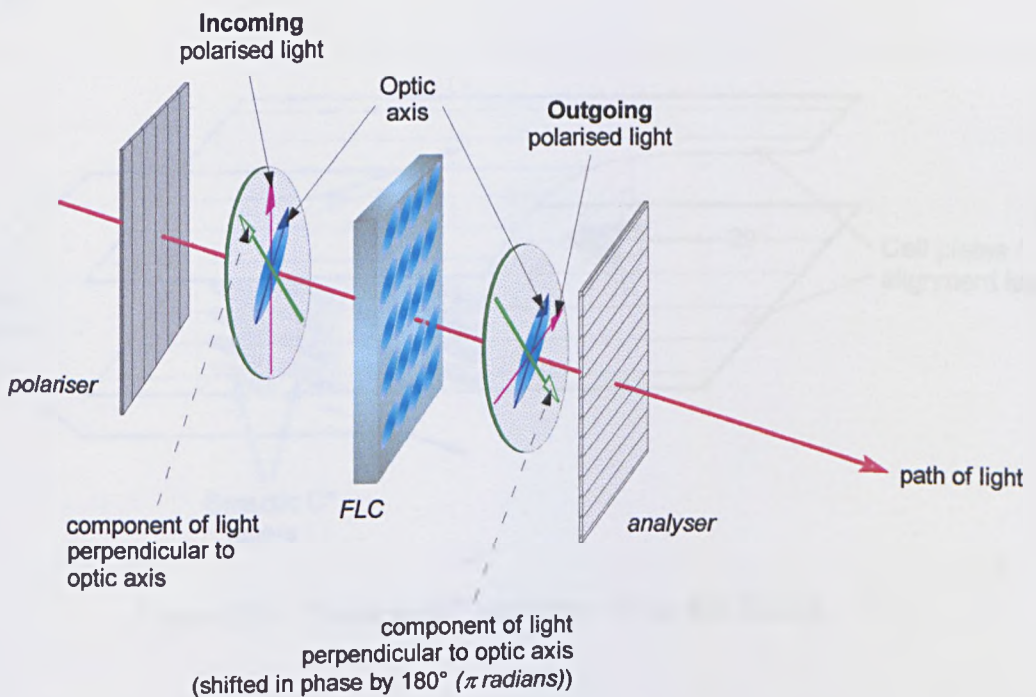
Figure 28a:- Optical retardation of light after passing through the FLC in the "light" state of an SS-FLC device.
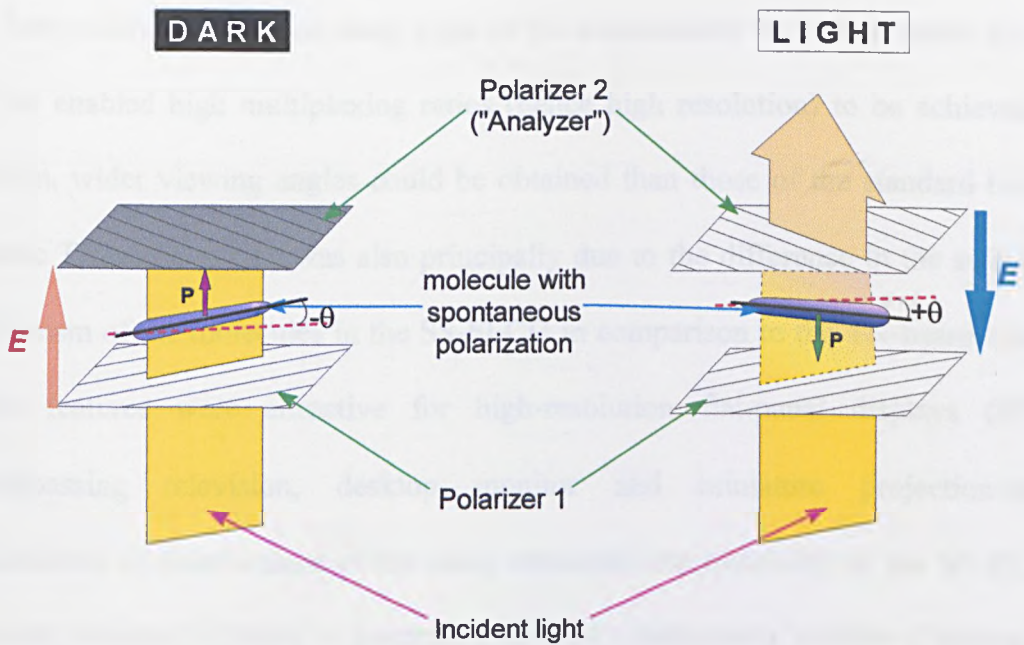
Figure 28b:- Ferroelectric light-valve based on a switchable half-wave plate.

The SS-FLCD can be regarded as a composite of these light valves in which the picture elements ("pixels") act as individual light valves. The "bookshelf" geometry of the SS-FLCD, so-called due to the arrangement of the SmC* layers, is shown in figure 29.
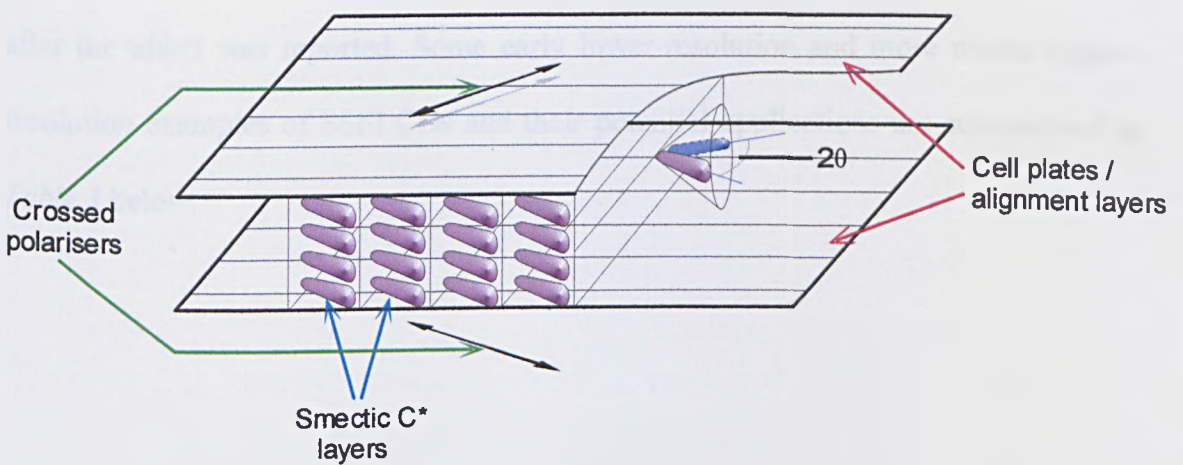
Figure 29:- "Bookshelf" geometry of the SS-FLCD.

The fast switching times and steep slope of the transmission vs. voltage curve for SS-FLCDs enabled high multiplexing ratios (hence high resolution) to be achieved. In addition, wider viewing angles could be obtained than those of the standard twisted nematic TFT-LCDs. This was also principally due to the difference in the switching mechanism of the molecules in the SS-FLCD in comparison to the TN-based device. These features were attractive for high-resolution flat-panel displays (FPDs) encompassing television, desktop monitor and miniature projection-based applications. A disadvantage of the sharp threshold and bistability of the SS-FLCD, however, was the difficulty in generating suitable continuously variable ("analogue") greyscale. Spatial and/or temporal "dithering" techniques are currently employed to emulate greyscale. Both these techniques are more effectively controlled by *actively* driving the FLC devices using thin-film transistors in a manner analogous to those used in twisted nematic TFT-LCDs. This inevitably increases both the costs and complexity in manufacturing these devices.

The first examples of display devices utilising the SS-FLC effect were presented soon after the effect was reported. Some early lower-resolution and more recent higher-resolution examples of SSFLCDs and their potential applications are summarised in *Table 3* below.

Table 3:- Examples of both early and more recent SSFLCDs and their potential applications [35, 36].

Group	Year	Size / Resolution	Potential Application
Seiko Instruments & Electronics	1985	• 12" diagonal, • 640 x 400 (monochrome)	Portable computer screen
Joers/Alvey ProjectGroup	1986	• 12" diagonal • 720 x 400 • Video frame-rate (monochrome)	Television
Canon	1989	• 14" diagonal • 1280 x 1120 (monochrome)	Desktop monitor
Canon	1992	• 15" diagonal • 1280 x 1024 • Colour	Desktop monitor
Displaytech [37]	1998	• 0.85" diagonal • 1280 x 1024 • Video frame-rate • Colour	Miniature / Projection display (SLM)

Despite the obvious attractive properties of SSFLCDs, commercial exploitation of the technology has been rather limited. The reasons for this are believed to be principally two-fold;-

(i) The inherent sensitivity of the smectic C* layers to shock [38]: deformation of the bookshelf geometry due to mechanical stress (such as dropping or shaking the device) can only be corrected by the application of large AC fields [39] or by re-alignment *via* heating of the material to the isotropic liquid and cooling back into the SmC* phase.

(ii) The problems of "image sticking": the shadow of a previous image remnant after a new one is written, due to the build-up of space charge in the device.

A number of variations of devices exist which have attempted to exploit alternative methods of manipulating FLC molecules for display applications particularly for the purpose of generating analogue greyscale. Principal examples of these are the Deformed Helix Ferroelectric LCD (DHF-LCD) [40-42], the Short-Pitch Bistable Ferroelectric LCD (SBF-LCD) [43, 44], and the Ferroelectric Twisted Structure (FTS) device [45]. The bistable SSFLCD configuration described above has however remained the most popular area of research, with respect to FLCs to date, in terms of the development of materials and devices.

A more recent and promising alternative for achieving many of the attractive properties offered by SSFLCDs, along with some additional advantages, is the SS-*A*FLCD. This device uses the *anti*ferroelectric effect, a modification of the ferroelectric liquid-crystalline effect, and is described in the following section.

(iii)   Antiferroelectric Liquid Crystals

The early SSFLCDs demonstrated a novel and effective method of manipulating liquid crystal molecules; in chiral ferroelectric (SmC*) systems the spontaneous polarisation acts as a "handle" with which an external electric field can effectively "switch" the direction of orientation of the molecules. In order to a build a better understanding of the correlation between molecular structure and the formation of SmC* phases with wide-temperature ranges [26, 46-48], with the desired values of other physical properties (eg. tilt angle, contrast ratio, and response time), a vast number of ferroelectric liquid crystals have been prepared to date. Over two decades of research has yielded SmC* materials, and above all mixtures, with broad phase temperature ranges (*figure 30a*) and fast switching times (*figure 30b*), meeting two of the necessary criteria for practical device applications [49].
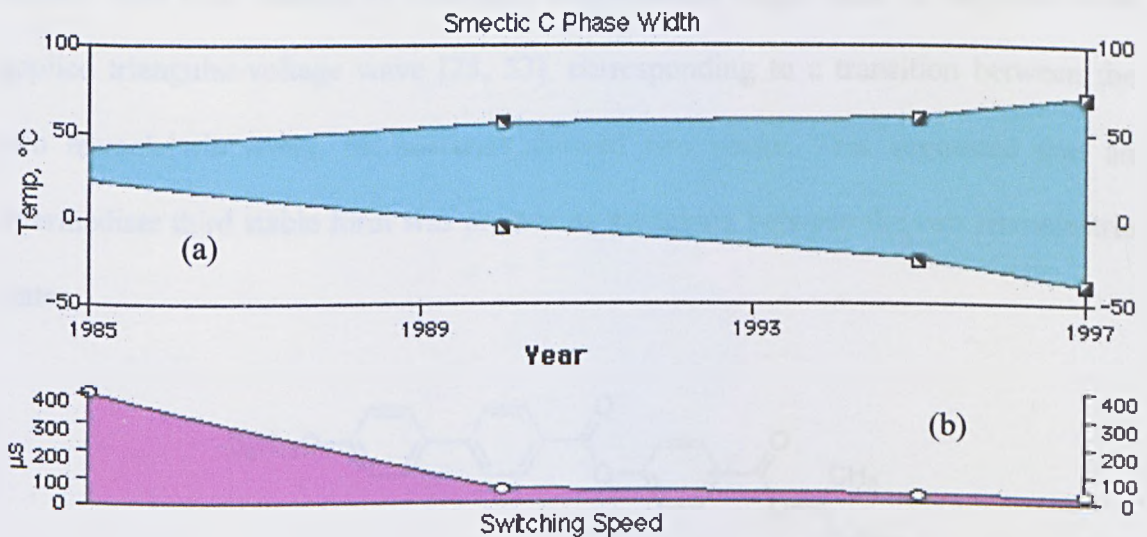
Figure 30:- (a) Increase in width of the SmC* phase (1985-1997);
(b) Decrease in the switching time of ferroelectric SmC* materials (1985-1997).
(courtesy of Displaytech)

41

The combination of large lateral or "transverse" dipole moments, and steric factors related to the shapes of the molecules, is generally accepted to play a key role in the formation of the ferroelectric smectic C* phase. Following the theoretical discussions put forward by Meyer in 1975 [25] to account for the physical factors which lead to the formation and character of the ferroelectric SmC* phase, an additional speculation was put forward by Michelson *et al.* in 1977 [50]. This postulated that, based on local symmetry and dipole-dipole interactions, a phase with an alternately-tilted local smectic C-like structure could exist (although no such phase had been observed at the time). Such a phase was in fact identified experimentally, just over a decade later, by Fukuda *et al*[App.B]. A newly synthesized FLC, (*R*)-MHPOBC (*figure 31*), intended to verify the relationship between rotational viscosity, spontaneous polarisation and optical purity [51], showed unusual switching behaviour in response to an applied electric field [52]. Instead of showing a characteristic single peak in response to an applied triangular-voltage wave [25, 53], corresponding to a transition between the two ferroelectric states, the material showed two peaks. This suggested that an intermediate third stable form was present on switching between the two ferroelectric states.
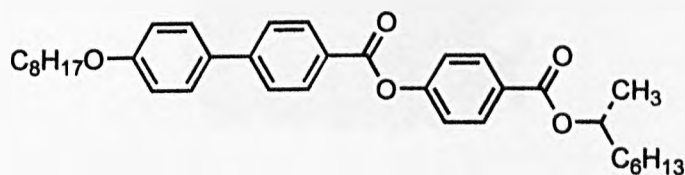
Figure 31:- Structure of (*R*)-MHPOBC
Cr 65.5 (SmI$_A$* 60) SmC$_A$* 119.9 SmC$_\gamma$* 120.5 SmC* 122.2 SmC$_\alpha$* 122.9 SmA*
148.7 I

The early speculations as to the structure of this third stable form [54, 55] were later

modified to take into account the observation of a number of other phase transitions, by DSC, between the SmA* and (what was at the time believed to be) the SmC* phase [56]. These other transitions implied the existence of additional novel phases in both the pure (R) and (S) enantiomers of the material (see next sub-section). Within a year a picture of the phase was constructed which could account for the unusual observations. The third stable form observed was postulated to be a SmC*-like phase in which the molecules in adjacent layers are tilted by the same angle, relative to the smectic layer normal, but in opposite directions [57] (figure 32). The overall effect of the alternating SmC*-layers conferred antiferroelectric character on the phase, since the direction of polarisation of the individual layers (originating from the spontaneous polarisation of the molecules), lay in opposing directions (not unlike the domains of opposing magnetic moments in an antiferromagnet). The phase was consequently designated "SmC$_A$*", similar to but distinct from, the standard SmC* phase with which it was immiscible (hence not identical in structure to) [58].
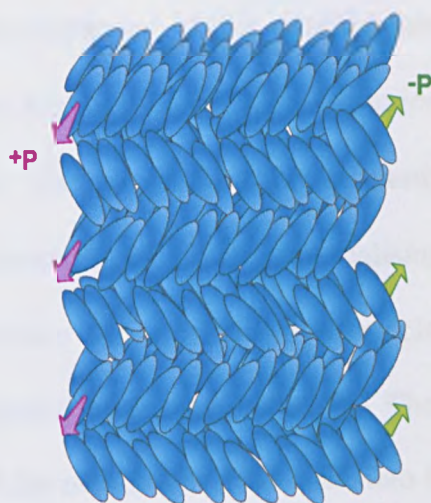
Figure 32:- Structure of the SmC$_A$* phase; smectic layers with alternating directions of tilt and polarisation (+P and -P).

The observation of two current responses, signifying two switching events on application of a triangular-wave AC field, could be explained as a field-induced phase

transition from one ferroelectric state to the other *via* this antiferroelectric state, and *vice versa* (*figure 33*).

| Ferroelectric (FO+) | Antiferroelectric (AFO) | Ferroelectric (FO-) |
| (SmC*) | (SmC$_A$*) | (SmC*) |
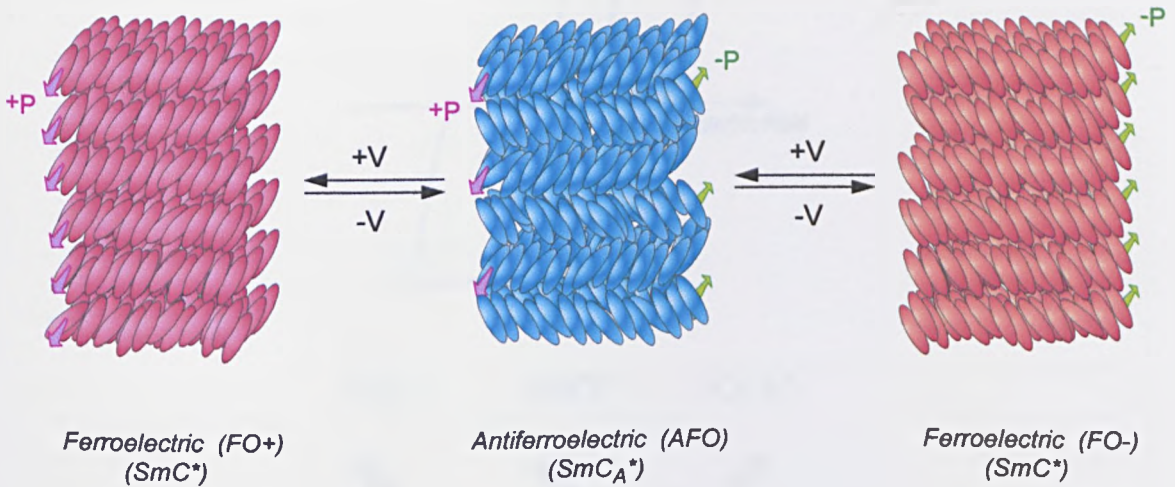
Figure 33:- Field-induced phase transition between the SmC* and SmC$_A$* phases (unwound states)

This "tristate" switching (originally referred to as "tristable switching"[App.C]) was characterised by two steep transmission *vs.* voltage curves, with a threshold voltage between the three states, accompanied by a characteristic "double hysteresis" (*figure 34*). This suggested that multiplexing of this modification of the ferroelectric effect could be possible to a very high degree (ie. high resolution, high information-content LCDs should be feasible). The potential use of the antiferroelectric SmC$_A$* phase presented an attractive alternative to FLCDs for realising video-frame rate display devices, as the fast response times of the antiferroelectric SmC$_A$* phase were comparable with those observed for the SS-FLCDs. The absence of bistability, as shown by the tendency of the material to relax back into the *neutral* antiferroelectric state on removal of the applied electric field, was also seen as a potential solution to the problem of "image sticking" in FLCDs. The similarity in the manner of switching with FLCDs ("in-plane" switching) had the potential to generate wide viewing angles and relatively good contrast ratios in practical devices.
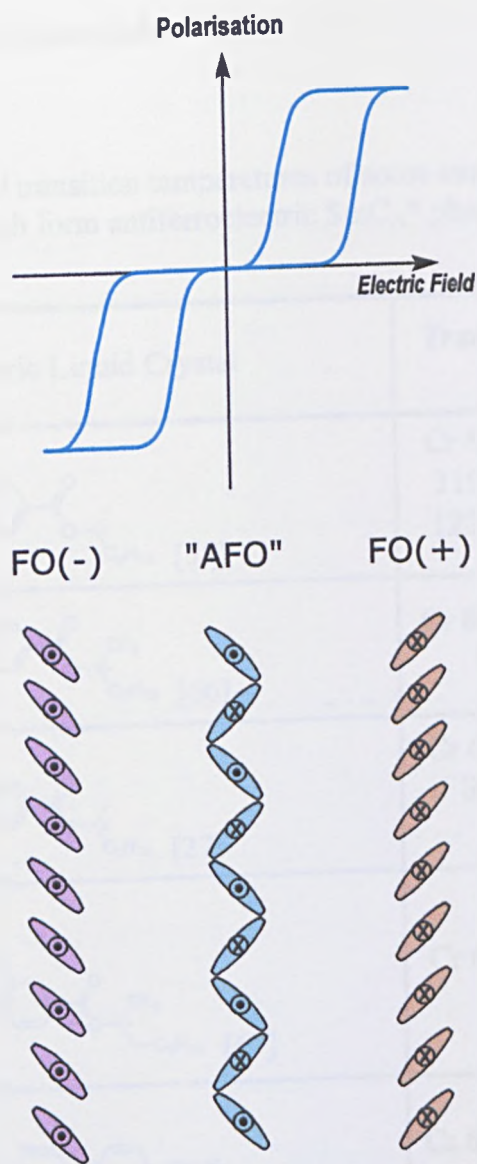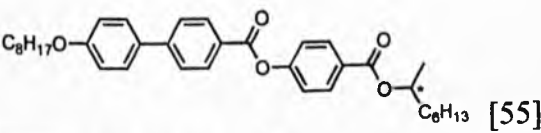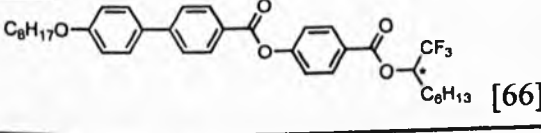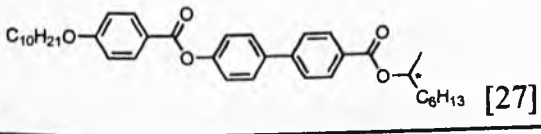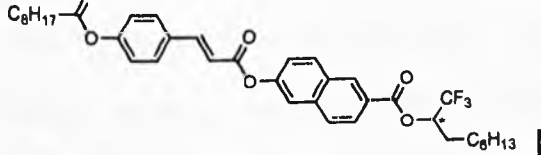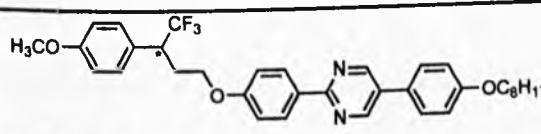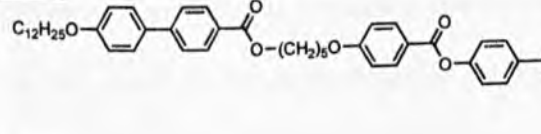
Figure 34:- "Tristate switching"; double polarisation-hysteresis of an antiferroelectric liquid crystal (AFLC) and corresponding directions of orientation of the molecules (dots represent spontaneous polarisation going "into" the page and crosses "coming out" of the page).

Since the SmC_A^* phase was discovered in the (R) and (S) enantiomers of MHPOBC, a number of structurally-related liquid crystals were prepared which also showed identical antiferroelectric phases [59-61]. Driven by the demonstration of several prototype display devices using the SmC_A^* phase [62-64], a large number of materials have been prepared which exhibit the antiferroelectric SmC_A^* phase [65]. Some examples of the structures of these materials, together with their transition

temperatures, are collated below (*table 4*).

Table 4:- Structures and transition temperatures of some examples of liquid crystals which form antiferroelectric SmC$_A$* phases.

Antiferroelectric Liquid Crystal	Transition Temperatures / °C
[55]	Cr 65.5 (SmI$_A$* 60) SmC$_A$* 119.9 SmC$_\gamma$* 120.5 SmC* 122.2 SmC$_\alpha$* 122.9 SmA* 148.7 I
[66]	Cr 84.3 SmC$_A$* 108.0 SmC* 109.0 SmA* 121.0 I
[27]	Cr 65.2 (J* 47.8) SmC$_A$* 69 SmC$_\gamma$*5.9 SmC* 105.4 SmA* 124.5 I
[67]	Cr 64 SmC$_A$* 67 SmA* 84 I
[68]	Cr 68 SmC$_A$* 90 SmA* 106 I
[69]	Cr 95 SmC$_A$* 106 SmC$_\gamma$* 106 SmC* 162 SmA* 180 I

At the microscopic level three key molecular factors responsible are speculated to be for contributing to the formation of the antiferroelectric SmC_A^* phase:

(i) pairing of the permanent transverse dipole moments between molecules in adjacent layers,

(ii) the bent "zig-zag" shape of the molecules,

(iii) steric interactions between the terminal chains of molecules in adjacent layers to form "dimers".

In the first case, the transverse dipoles, believed to be responsible for the formation of the SmC_A^* phase on cooling from the SmA^* phase [70, 71], are speculated to be larger in size than those observed in the SmC^* phase. The consequence of these large dipoles, characterised by the large values of spontaneous polarisation common to SmC_A^*-forming materials, leads to coupling of these dipoles between molecules in adjacent layers to form "molecular pairs". In this sense the in-plane spontaneous polarisation associated with each layer is "cancelled out" within the bulk material (since the dipoles act in equal but opposite directions) as a result of the alternating directions of the tilt between adjacent smectic layers (*figure 35*).
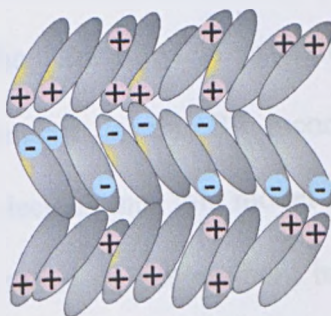
Figure 35:- Coupling of opposing transverse dipoles in the SmC_A^* phase between molecules in adjacent layers (resulting in the absence of a net spontaneous polarisation).

Electrostatic attraction and coupling of spontaneous polarisation cannot, however, account for the observation of the SmC$_A$* phase alone. The rapid thermal motion of the component molecules in liquid-crystalline phases (since liquid crystals are fluids after all) must to a degree diminish or at least act against the formation of molecular pairs by electrostatic means. Consequently the second and third of the above contributions, (ii) and (iii); molecular shape and steric interactions must also play a key role in stabilising the SmC$_A$* phase.

Examining the second of the two contributions, molecular shape, it is generally accepted that the bent "zig-zag" shape of the component molecules [72] is a more significant contribution to the formation of the *synclinic* SmC* and SmC phases than the coupling of lateral dipoles within the smectic layers. The fact that molecules with minimal transverse dipoles (eg. molecules without ether linking-groups) are never-the-less able to form SmC phases is tangible evidence for this [73]. Recent investigations [74] and computer simulations [75] have suggested that molecules which form anticlinic smectic (SmC$_A$*, SmC$_{alt}$) phases are in fact more *bent* at one end (the branched end) than the other (the unbranched end). The "bent-toothpick" model below (*figure 36(a)*) consists of a simplified smectic phase in which the molecules are bent at only one end [76]. In this arrangement the molecules can only pack effectively in pairs if they are tilted in opposite directions (in an anticlinic manner) between adjacent smectic layers. By incorporating alkyl chains at the "heads" and "tails" of the molecules into this model the "zig zag" character of the molecules is preserved while the more acutely-bent branched alkyl chains maintain the anticlinic packing of the phase (*figure 36(b)*) [28].
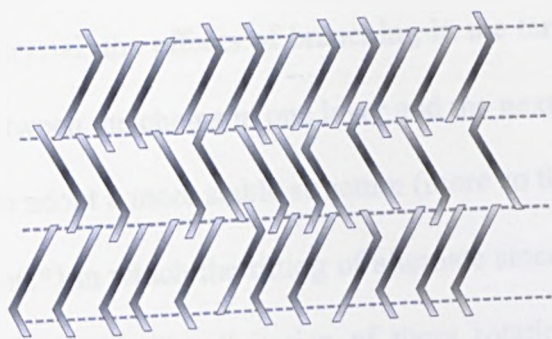
Figure 36(a):- "Bent-toothpick" model of the SmC$_A$* phase

Figure 36(b):- Bent "zig-zag" structure of the SmC$_A$* phase (the "cones" represent the rotational distributions of the terminal branched and unbranched chains)

It should of course be taken into account that there are as many "head-to-tail" interactions as there are "head-to-head" and "tail-to-tail" interactions. The pictures of the models presented show only "head-to-tail" interactions in order to make the nature of the interactions clearer.

The third contribution, steric interactions, are closely related to the contributions of molecular shape. These interactions take place between the branched (ie. chiral) terminal chain of one molecule, and the unbranched terminal chain of a molecule in an adjacent layer. As the rotation of the molecules about their long axes slows down,

on cooling the liquid crystal, the effects of branching in the terminal chains increase the steric hindrance between the chains in one layer and the next. The result is that the molecules are forced to adopt a more stable structure (more so than the usual *synclinic* arrangement of the SmC*) in which the tilting of alternate smectic layers, in opposite directions, is facilitated by the interdigitation of these rotationally-hindered chains (*figure 37*).
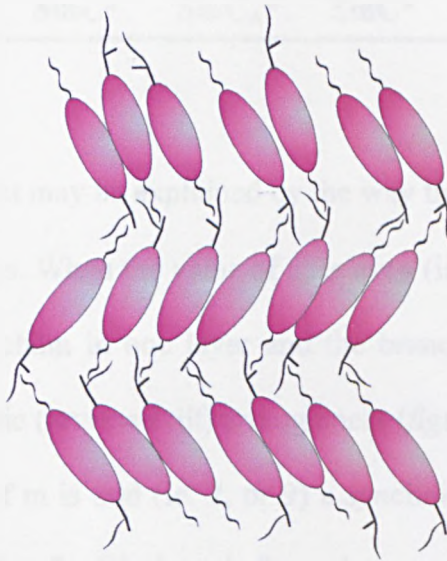
Figure 37:- Interdigitation of branched and unbranched terminal chains in the SmC$_A$* phase.

We would imagine that the significance of these steric interactions would be reflected in the physical properties of materials that form anticlinic SmC phases. This is in fact observed as strong odd-even effects due to the overlap of the alkyl chains between molecules in adjacent smectic layers [77]. In fact, in a homologous series of a "strong" antiferroelectric material such as 10B1MFm (m = 6 to 10) this is observed as the variation in the formation of either a SmC* (when m is an odd number) or a SmC$_A$* phase (when m is even) [78]. The presence one of the phases excludes the other (*table 5*).

Table 5:- Strong odd-even effect observed as the occurrence of either a SmC* or a SmC$_A$* phase in the homologous series of 10B1MFm (m = 6 – 10)
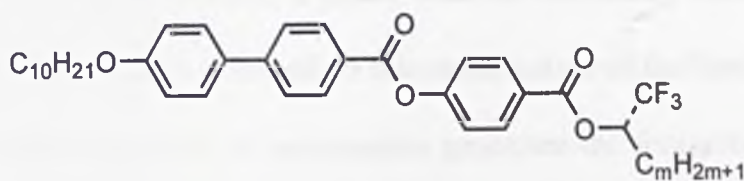
m				
6	7	8	9	10
SmC$_A$*	SmC*	SmC$_A$*	SmC*	SmC$_A$*

This strong odd-even effect may be explained by the way the alkyl chains "overlap" at the smectic layer interfaces. When the value of m is even (ie. 6, 8 or 10) the "overlap" between the unbranched chain in one layer and the branched chain in the adjacent layer promotes an *anti*clinic (reversed tilt) arrangement *(figure 38(a))*; a SmC$_A$* phase results. When the value of m is odd (ie. 7, or 9) a *syn*clinic arrangement is favoured *(figure 38(b))* consequently a SmC* phase is formed.

(a)
*anti*clinic ordering favoured (SmC$_A$*)

(b)
*syn*clinic ordering favoured (SmC*)
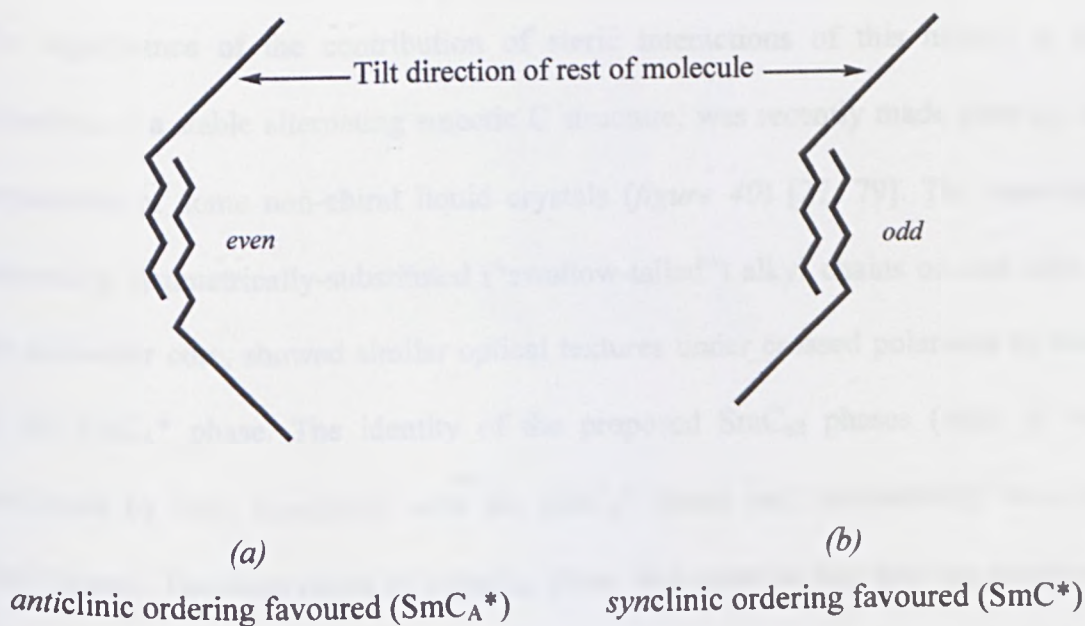
Figure 38:- Simplified picture of the odd-even effects due to steric interactions in the homologous series of 10B1MFm.

In the case of racemic mixtures, consisting of equal proportions of (S) and (R) enantiomers of the same material, a phase with an alternating SmC-like structure (designated "SmC$_{alt}$") is also observed. In this modification of the SmC$_A$* phase local spontaneous optical resolution of enantiomers promotes the formation of molecular pairs between like enantiomers (*figure 39*).
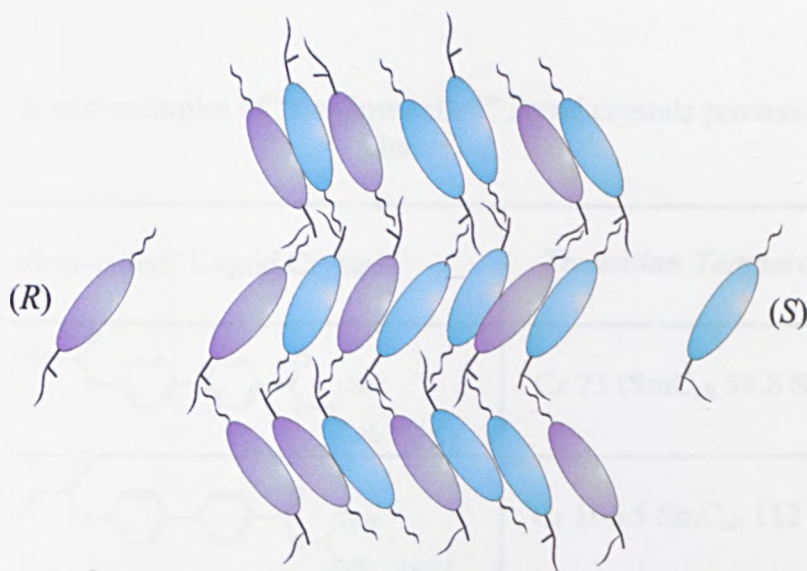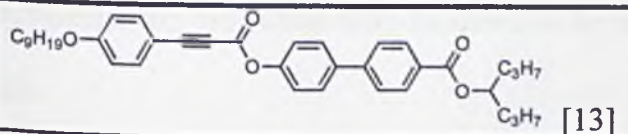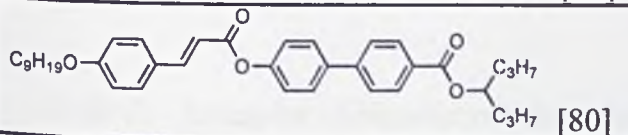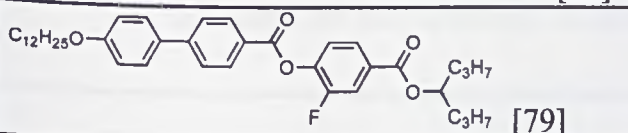
Figure 39:- Structure of the racemic modification of the SmC$_A$* phase (the "SmC$_{alt}$") phase.

The significance of the contribution of steric interactions of this nature, to the formation of a stable alternating smectic C structure, was recently made clear by the preparation of some non-chiral liquid crystals (*figure 40*) [27, 79]. The materials, possessing symmetrically-substituted ("swallow-tailed") alkyl chains on one side of the molecular core, showed similar optical textures under crossed polarisers to those of the SmC$_A$* phase. The identity of the proposed SmC$_{alt}$ phases (*table 6*) was confirmed by their miscibility with the SmC$_A$* phase and immiscibility with the SmC* phase. The observation of a SmC$_{alt}$ phase in a material that was not composed of equal quantities of enantiomers, as in a racemic mixture (ensured by the symmetrical alkyl chains), added weight to the speculation of the importance of steric

interactions. The transverse dipoles of the molecules could not be considered large enough to couple with each other, and local optical resolution could not arise, due to the absence of any chiral centres in the molecules. This implied that the formation of the phase was promoted to a considerable extent by the interdigitation of the rotationally-hindered alkyl chains.

Table 6:- Some examples of "swallow-tailed" liquid crystals possessing SmC$_{alt}$ phases.

"Swallow-tailed" Liquid Crystal	*Transition Temperatures / °C*
C$_9$H$_{19}$O⟨⟩≡⟨⟩⟨⟩ C$_3$H$_7$ C$_3$H$_7$ [13]	Cr 73 (SmC$_{alt}$ 54.8 SmA 70.3) I
C$_9$H$_{19}$O⟨⟩⟨⟩⟨⟩ C$_3$H$_7$ C$_3$H$_7$ [80]	Cr 106.5 SmC$_{alt}$ 112 SmA 126 I
C$_{12}$H$_{25}$O⟨⟩⟨⟩ F C$_3$H$_7$ C$_3$H$_7$ [79]	Cr 65.9 (SmC$_{alt}$ 56.8) SmA 72.9 I
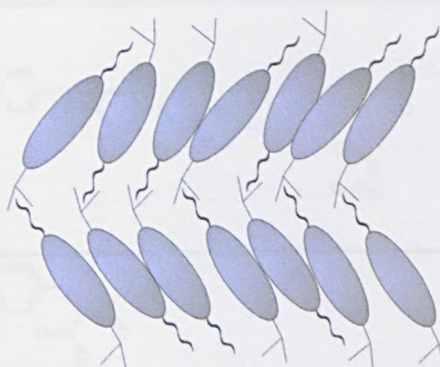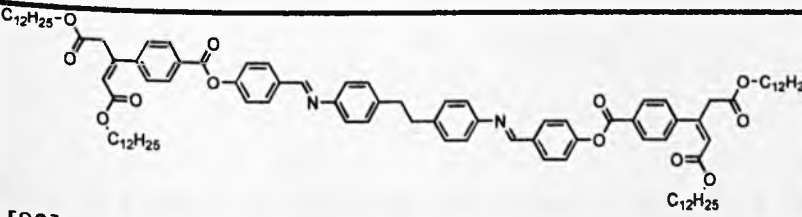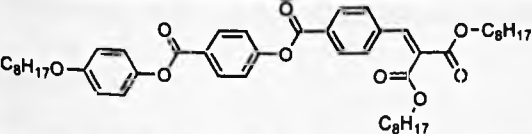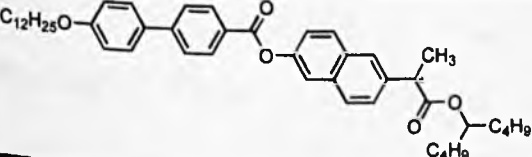
Figure 40:- SmC$_{alt}$ phase formed by the interdigitation of the "swallow-tailed" and straight-chained alkyl substituents.

In order to form a stable SmC$_A$* phase a balance between the contributions of steric interaction, molecular shape and coupling of large transverse dipoles is required. Clearly all three should be present for SmC$_A$* formation. This is evident from the fact that many ferroelectric SmC* materials, possessing very large transverse dipoles (high values of spontaneous polarisation) [81, 82], do not form SmC$_A$* phases when the steric interactions which favour alternate tilting of the smectic layers are not present simultaneously. Furthermore, if the steric interactions between the molecules are too pronounced or obstructive, (such as the "double swallow-tailed", chiral swallow-tailed and unsuitably-positioned swallow-tailed materials shown below (*table 7*), the molecules are too rotationally hindered to be able to form phases with an alternating tilt.

Table 7:- Examples of liquid crystals in which the structure of the molecules is unsuitable for the formation of alternating smectic C phases.

"Swallow-tailed" Liquid Crystal	Transition Temperatures / °C
[83]	Cr 95 SmC$_{(re)}$ 117 D$_{ob}$ 154 SmC 187 N 209 I
[84]	Cr 40 SmC 51 N 88 I
[85]	Cr 85.7 (SmC* 75) SmA* 115.4 TGB$_A$ 117.5 N* 128.7 BP 132.2 I

The discovery of several other novel phases in the region of, and between, the SmC* and SmC$_A$* phases brought to the fore the very nature of the factors which govern the formation of tilted and alternately-tilted disordered smectic phases. Particularly the contribution, to the formation of the SmC$_A$* phase, of the pairing of transverse dipole moments. These phases, generally classed as the *Smectic C* Subphases*, are speculated to be formed as a result of the competition between the intermolecular forces which stabilise the SmC* and SmC$_A$* phases. Consequently, the phases occur almost always in materials which possess both SmC* and SmC$_A$* phases. The sequence of formation of all *possible* intermediary phases (not all of the phases are always observed), on cooling the SmA* phase, is as follows (determined by mixing experiments) [86];-

SmI$_A$* – SmC$_A$* - SmC$_{FI(L)}$* – SmC$_\gamma$* - SmC$_{FI(H)}$* – "AF" – SmC* - SmC$_\alpha$*

$\longleftarrow$

Cooling
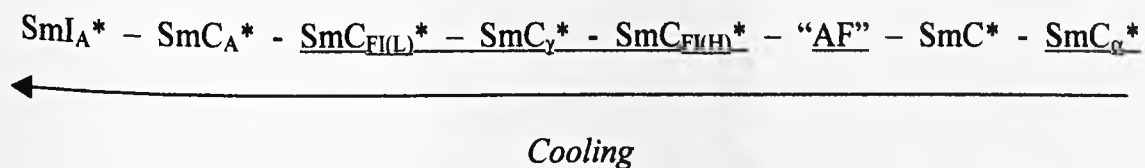
As it is beyond the scope of this thesis to provide a detailed account of these subphases only a brief description, of some key phases (underlined above), is given below:-

The SmC$_\alpha$* Phase

Little is known about this phase, although X-ray, conoscopic [87], electrooptic [88] and dielectric [89] investigations suggest it may be a continuously changing phase [90] (in which the structure changes with temperature); in the higher temperature-

region the phase appears to be antiferroelectric, on cooling the phase adopts a uniform ferroelectric-like structure (via a ferrielectric-like structure) just above the SmC* phase. The tilt angles of the molecules within the phase are believed to be much smaller that those observed in the other SmC* subphases [87].

The "AF" Phase

This phase can usually only be observed by dielectric means and is believed to be similar to the antiferroelectric SmC$_A$* phase, the difference being that the phase is formed by the alternating tilt direction of pairs of SmC* layers (*figure 41*). The "AF" phase is thought to facilitate the formation of the ferrielectric smectic C* phases on cooling from the SmC* phase [60, 91].
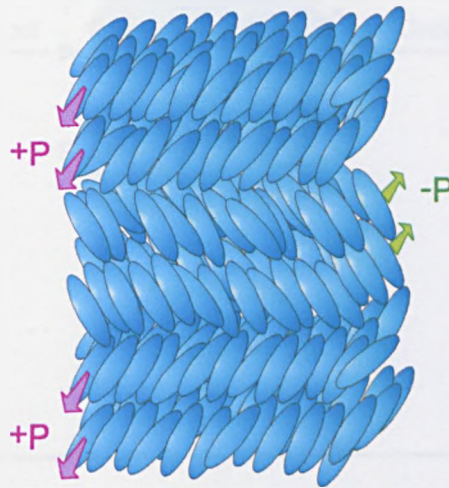
Figure 41:- Structure of the "AF" phase

The SmC$_{FI(L)}$*, SmC$_γ$* and SmC$_{FI(H)}$* Phases

These are the ferrielectric phases, observable between the SmC* and SmC$_A$* phases on cooling. Although usually only the SmC$_γ$* phase (often referred to as the "Devil's Staircase"[App.D]) is visible, if at all, some similar ferrielectric phases may exist between the SmC* and SmC$_A$* phases above and below the SmC$_γ$*. These are tentatively

referred to as the high-temperature and low-temperature ferrielectric SmC* phases (SmC$_{FI(H)}$* and SmC$_{FI(L)}$* respectively) and vary, hypothetically, in the fraction of *ferroelectric ordering* in an *antiferroelectric* structure [86, 92, 93].

In the "unwound" state the ferrielectric SmC$_\gamma$* phase(s), as a consequence of increased antiferroelectric character and decreased ferroelectric character, the spontaneous polarisation value of a macroscopically aligned domain of the phase would lie between that of the sample oriented in the SmC* and SmC$_A$* phases (*figure 42*).
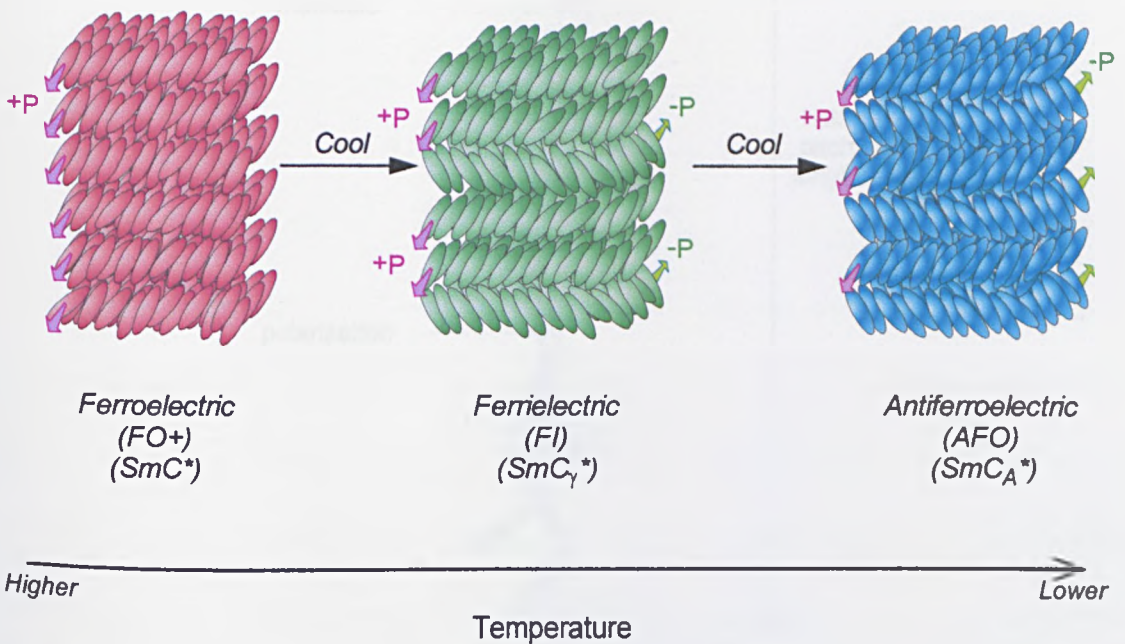
Figure 42:- Formation of ferrielectric and antiferroelectric phases on cooling from the ferroelectric phase

The Surface-Stabilised Antiferroelectric Liquid Crystal Display Device

As with the SmC* phase a macroscopic helix, a consequence of the optical activity of the constituent molecules, is induced in the domains that make up the bulk of the

SmC_A^* phase. This helix is also generated in the phase by the rotation of the long molecular axis of the molecules, in pairs, around a hypothetical cone (*figure 43*). As a consequence the director is parallel to the local helical axis, which varies randomly throughout a non-macroscopically aligned sample.
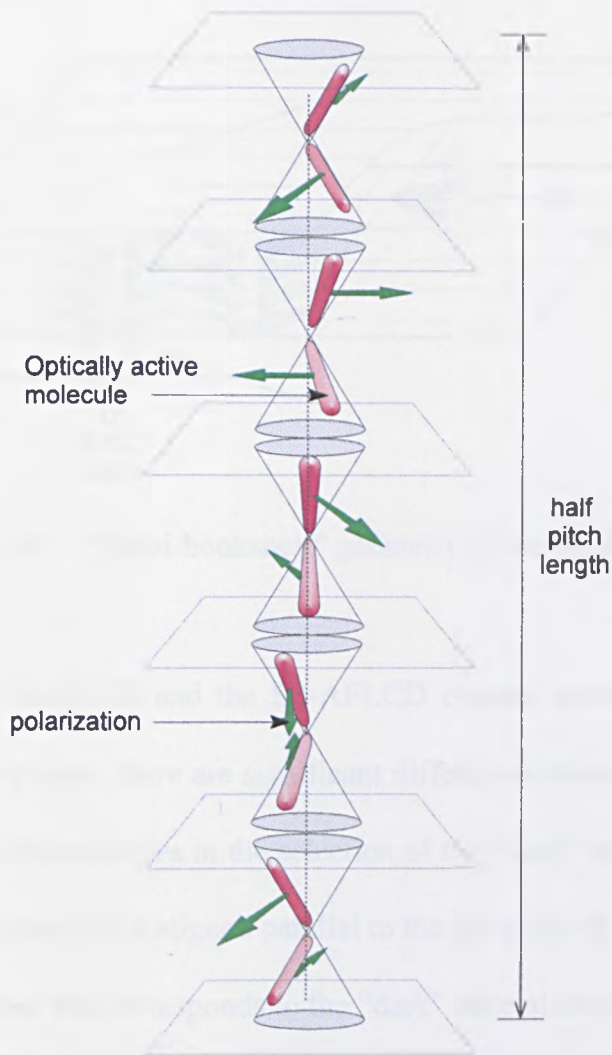
Figure 43:- Helical structure of the SmC_A^* phase (half-pitch)

In a similar manner to the SmC^* phase this helix can be permanently unwound by surface forces, in order to exploit the tristate switching by an electric field, by confining the material in a thin cell with suitable alignment layers. The potential use of the SmC_A^* phase in a display device, using this effect, was demonstrated in 1990

in a modification of the SS-FLCD [62]. As a result of the similarity in operation to the SS-FLCD, the device, utilising the SmC_A^* phase instead of the SmC^* phase, is more accurately referred to as the Surface Stabilised Antiferroelectric Liquid Crystal Display (SS-AFLCD) (*figure 44*).
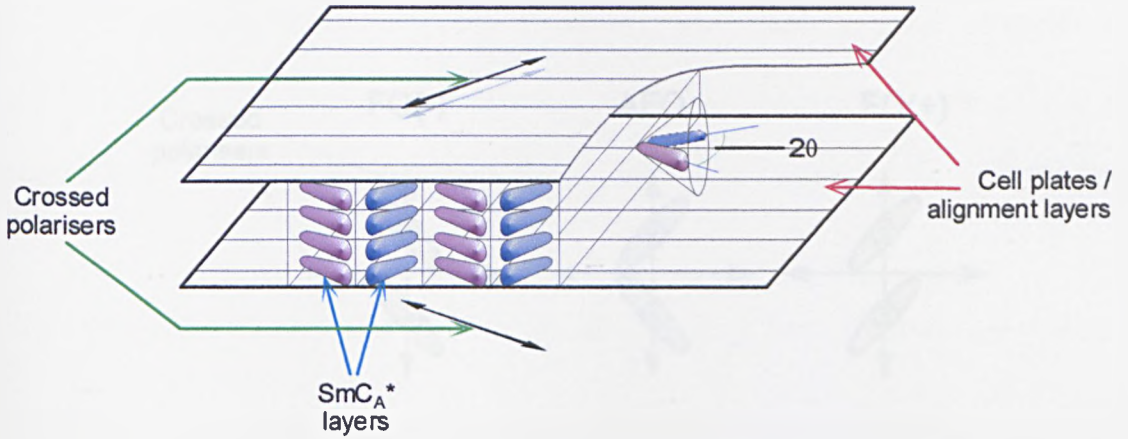
Figure 44:- "Quasi-bookshelf" geometry of the SS-AFLCD.

Although both the SS-FLCD and the SS-AFLCD operate under the principal of a switchable half-wave plate, there are significant differences between the two types of device. One major difference lies in the selection of the "dark" state. In the SS-FLCD one of the crossed polarisers is aligned parallel to the direction of orientation of one of the ferroelectric states; this corresponds to the "dark" state of the device, consequently the opposite ferroelectric state corresponds to the "light" state (switching angle $2\theta = 45°$ in the ideal case). In the SS-AFLCD the "dark" state is usually set to the neutral antiferroelectric state by this method; the two extreme ferroelectric states constitute two "light" states of equal transmittance (*figure 45*). The antiferroelectric state can be switched to one light state with a positive voltage and to the other light state with a negative voltage. This eliminates the problem of image-sticking ("ghost images") associated with SS-FLCDs due to the local build-up of ionic charge. Although the

antiferroelectric state can also be selected as an intermediate "grey" state with the two ferroelectric states corresponding to the "dark" and "light" states, switching between both "light" ferroelectric states via the middle "dark" state in the arrangement described is chosen for a further advantage: spatial dithering can be simplified to obtain suitable greyscale [94, 95].
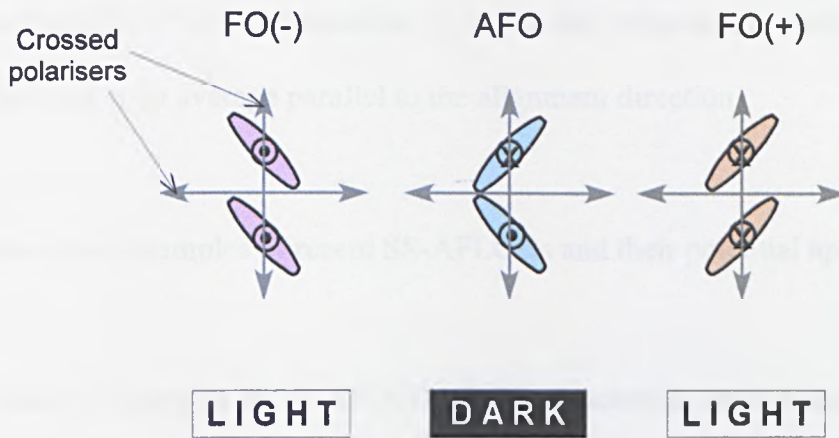
Figure 45:- Switching between the dark and light states in an SS-AFLCD.

A consequence of the selection of the antiferroelectric state, however, is that for maximum contrast between the light and dark states the tilt angles of the molecules should ideally be 45 ° (2θ = 90 °) in the smectic layers. Although materials with such large tilt angles are often very difficult to realise mixtures of materials, with tilt angles up to 35 °, have yielded contrast ratios (in devices) of over 100:1.

Since the switching behaviour of SS-AFLCDs is based on the same ferroelectric phenomenon as SS-FLCDs, they also possess fast response times, relatively good contrast ratios and wide viewing angles. In addition to the other advantage over SS-FLCDs described above, AFLCDs are regarded as being less susceptible, or to be more precise more easily recovered, from mechanical shock [39, 96]. This is believed

to be due to the fact that the average direction of orientation of the molecular long axis (the "optic axis") in the unwound SmC_A^* phase is parallel to the direction of alignment (the "rubbing direction") [78]. There is consequently a constant driving force for the molecules to return to the more stable alternating antiferroelectric state, even after deformation of the smectic layers by imposing physical stress on the device [38]. Whereas in the SS-FLCD in one of the supposedly bistable states the optic axis makes an angle of 22.5 ° with the direction of alignment, whereas the optic axis in the other bistable state is on average parallel to the alignment direction.

Table 8 shows some examples of recent SS-AFLCDs and their potential applications.

Table 8:- Examples of SS-AFLCDs and their potential applications.

Group	Year	Size / Resolution	Potential Application
NipponDenso Co. [62]	1990	• 6" diagonal, • 128 x 96 (monochrome)	- Prototype display -
Citizen Watch Co. [64]	1993	• 5.5" diagonal • 640 x 480 (monochrome)	Car navigation display
NipponDenso Co. [94]	1993	• 6" diagonal • 320 x 240 • Colour • Video frame-rate	Television
Toshiba [36]	1997	• 15" diagonal • 1024 x 768 • Colour	Desktop monitor

Aims

AIMS

Chiral Dopant Mixtures

The field-induced phase transition between the antiferroelectric SmC_A^* and uniform ferroelectric SmC^* states is generally optimised for use in SS-AFLCDs by the blending of individual materials to form multi-component mixtures. This technique provides the means to extend the operating temperature range (-40 °C to 100 °C is the present target [97]) and enhances the physical properties (tilt angles, switching speeds and contrast ratios) of the SmC_A^* phase. However, uniform alignment of the mixture is a critical factor in generating suitable "dark" and "light" states in the device. As AFLCD mixtures are generally composed of optically active materials with very tight pitches (helical twisting power, HTP), there inevitably exists a tendency for the materials to try to adopt a helical macrostructure in the device, despite anchoring at the surfaces. This is manifested in cells of liquid crystals as the imperfect alignment of the mixtures on cooling into the liquid crystal phases from the isotropic liquid. The presence of inhomogeneous domains degrades the optical performance of the display, by allowing light to "leak" through in the "dark" state with the effect of lowering the overall contrast ratio. Whereas the controlled formation of domains is favourable for the generation of greyscale [94], in both SS-FLCDs and SS-AFLCDs, the existence of unlike domains present in the display due to imperfect alignment in the first instance reduces the capacity to yield suitable greyscale.

Alignment can most conveniently be achieved, on cooling from the isotropic liquid, in mixtures which possess an N^* phase in addition to the desired smectic phase(s). Very

few materials which form SmC$_A$* phases actually possess a N* phase [98]. For this reason alignment in a device is takes place predominantly in the SmA* phase. In the case of mixtures for SS-FLCDs a solution to the problems of alignment are the use of chiral dopant mixtures. A small quantity of an optically-active *dopant (figure 46a)* added to a racemic or achiral *host* mixture of SmC – forming liquid crystals *(figure 46b)*, induces in the overall mixture a spontaneous polarisation with which the molecules can be reoriented [99] *(figure 47)*.

(a)   (b)

Cr 46.1 I   Cr 50 SmC 126 N 143 I
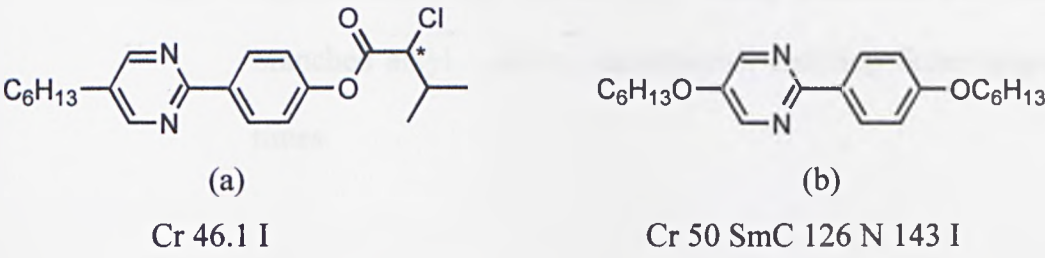
Figure 46:- Example of a chiral dopant (a) [100], and host material (b) [101], used in chiral-dopant ferroelectric mixtures.
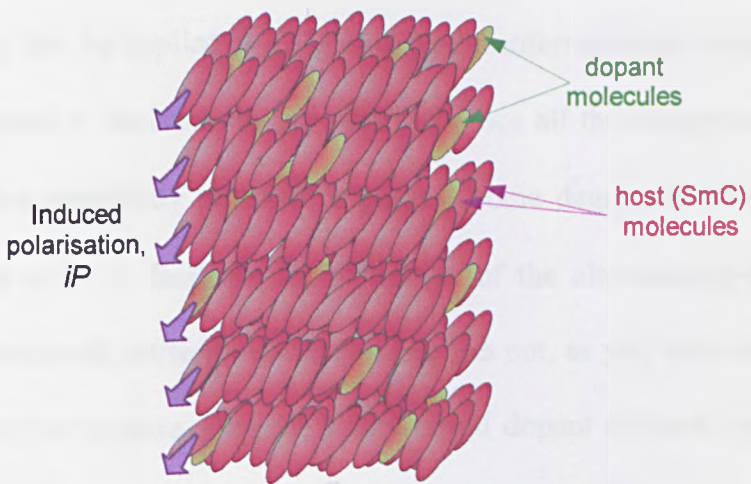
Figure 47:- simplified structure of an induced SmC* phase consisting of achiral molecules with a small quantity of a chiral dopant .

In SS-FLCDs practical mixtures based on this technique possess some clear advantages over those composed of purely chiral components:

(i)   The tendency to form the helix in the cell can be more readily suppressed, allowing for improved alignment in the device;

(ii)   The technique provides the means to tailor more effectively the physical and mesomorphic properties of the mixtures, and allows access to a greater variety of materials (since not all chiral groups are obtainable);

(iii)   The lowering of viscosity by using materials with fewer branched alkyl / alkoxy substituents, enabling faster response times.

Materials which form the SmC$_{alt}$ phase, the non-chiral or racemic analogue of the SmC$_A$* phase, are of interest for their potential applications as host materials for fast-switching antiferroelectric mixtures (*figure 48*). Although points (i) and (ii) above could in theory also be applied to a chiral-dopant *anti*ferroelectric system, (iii) cannot truly be compared to antiferroelectric systems, since all the compounds which form these phases are essentially required to possess some degree of "branching" of the alkyl chain, in order to facilitate the formation of the alternatingly-tilted phase. A practical chiral-dopant antiferroelectric mixture has not, as yet, been demonstrated. A previous attempt to prepare a model binary chiral dopant mixture, using a standard ferroelectric dopant with a series of swallow-tailed materials, could not effect any discernible switching in the subsequent SmC$_A$* phase despite application of large electric fields [79]. This was principally a consequence of the high stability of the (induced) SmC$_A$* phase due, to a large extent, to the speculated high degree of

interdigitation of the branched and unbranched alkyl chains between the molecules in adjacent smectic layers. It is postulated that in order to effect switching in the SmC$_{alt}$ phase, dopants with the potential to induce a larger spontaneous polarisation in the host material may be of more practical use, by increasing the size of the "handle" with which an applied electric field can switch the molecules.
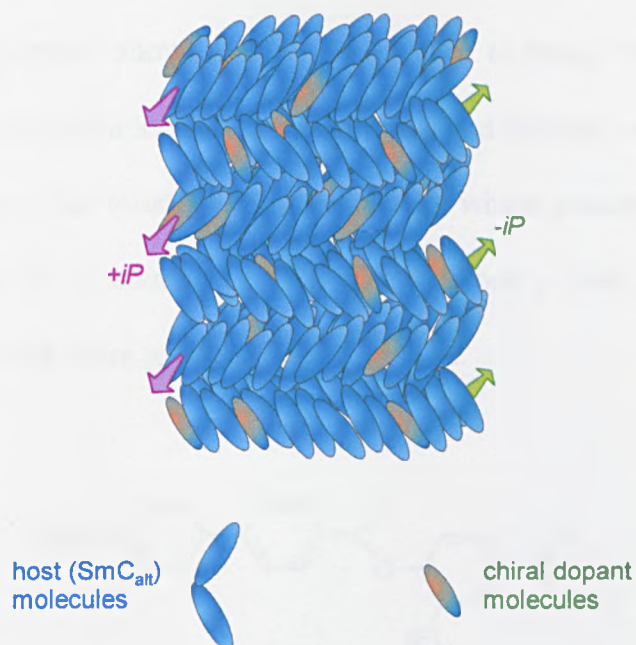
Figure 48:- Simplified structure of an induced SmC$_A$* phase consisting of achiral (or racemic) molecules with a small quantity of a chiral dopant (+iP, -iP are the induced polarisations).

The aims of this thesis are primarily two-fold:

(i)   To investigate the structural factors necessary for the formation of wide-temperature SmC_{alt} phases in a series of related liquid crystals (with the general structure shown below, *figure 49*); to study the effect of simple structural modifications on the occurrence and stability of the phase, and by this method, the selection of the materials which possess the most suitable properties (ie. occurrence of the phase across a wide temperature range encompassing room temperature).
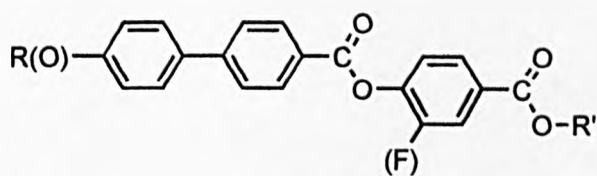
Figure 49:- General structure of the target host materials;
{R(O) = alkyl / alkoxy, R' = symmetrically- / unsymmetrically-substituted alkyl}

(ii)   To evaluate the use of the materials as hosts for practical fast-switching chiral-dopant antiferroelectric mixtures; to study the effect and suitability of different types of dopants for these applications by observing the changes in the physical properties of the model binary mixtures (transition temperatures, overall spontaneous polarisation, tilt angles, etc).

The feasibility of this technique for application in "real" devices will be discussed and suggestions made for further work in this field.

Results and Discussion

RESULTS and DISCUSSION

This chapter is divided into five sections; due to the similarity in the structure of both the chiral and non-chiral materials, the syntheses of both groups of materials are outlined in the first section, **section (i)**. The subsequent sections deal with;- the mesomorphic properties of the host materials, **section (ii)**; the mesomorphic properties, physical measurements and selection of the dopant materials, **section (iii)**; the evaluation of the ferroelectric dopant and antiferroelectric dopant mixtures, **sections (iva)** and **(ivb)**, respectively. The last section of this chapter, **section (v)**, is concerned with the study of unusual mesomorphic behaviour in some of the non-chiral materials, observed during the course of this work.

Section (i):

SYNTHESIS

Overview of Target Materials

The general structure of the target compounds is shown below (_figure 50_). The materials are structurally related to MHPOBC, the first reported antiferroelectric liquid crystal, and consequently the most widely studied "standard". The structure was therefore regarded to be an appropriate template for the purpose of this study. The key difference between the standard material and the target materials, however, is the presence of the additional lateral fluoro substituent in the target materials. The effect of the attachment of a single fluorine atom to the aromatic core in many examples of liquid-crystalline materials is to lower the melting points and transition temperatures of the phases [102]. The purpose of lowering the mesophase temperatures for this study was to attempt to generate lower-temperature SmC_{alt} phases, in the host materials, in order to demonstrate the potential application of chiral-dopant antiferroelectric mixtures to devices for operation at room temperature. The presence of the fluoro substituent is also postulated to be able to lower the viscosity (and consequently shorten the response time), in many systems, and also to reduce the tendency of the materials to form _ordered_ phases.
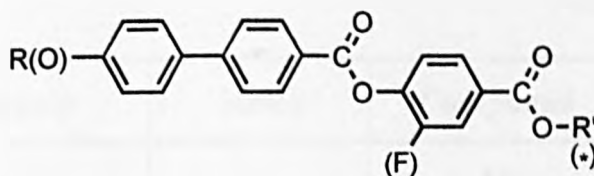
Figure 50:- General structure of the materials prepared;
{R(O) = alkyl / alkoxy, R' = symmetrically- / unsymmetrically-substituted alkyl}

In order to elucidate the structural factors, which favour the formation of stable SmC$_{alt}$ phases, the structure of the host materials was varied systematically for the different categories of racemic and non-chiral materials. The target hosts prepared can be divided into the series of materials listed below (*Tables 9a – 9e*). A brief description of the variation in the structures is now offered.

Unlike the majority of the compounds prepared, the structures in Series 1 possess *alkyl*, rather than *alkoxy*, chains attached to the biphenyl section of the core (*Table 9a*). The materials are the decyl analogues of some of the decyloxy *symmetrically* ("swallow-tailed") and *unsymmetrically*-substituted materials presented in *Tables 9b* and *9d* (below); the purpose of preparing these materials was to investigate the contribution of the ether linking-group to the stability of the corresponding SmC$_{alt}$ phases.

Table 9a:- Structure of the *alkyl* (R) *unsymmetrically* and *symmetrically-substituted* (R') host materials (Series 1);
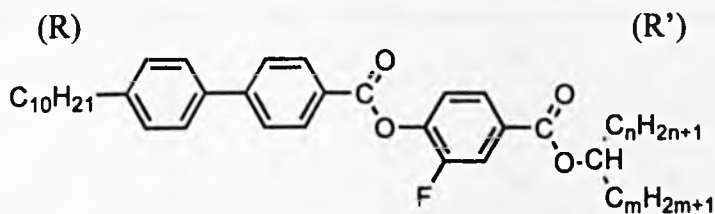
Category	Series	Compound	n	m
R (*alkyl*) constant, R' variable,	1	1a	1	6
		1b	2	6
		1c	4	4

Table 9b summarises the *symmetrically-substituted* materials prepared with varying sizes of unbranched alkyl chains (R, Series **2**) and swallow-tail moieties (R', Series **3** and **4**). A complete variation of these substituents may provide a clearer indication, as to the significance of the size of both groups of alkyl chains, on the formation of the SmC_{alt} phase.

Table 9b:- Structure and categories of the *symmetrically-substituted* host materials (Series **2**, **3** and **4**);

(R)   (R')
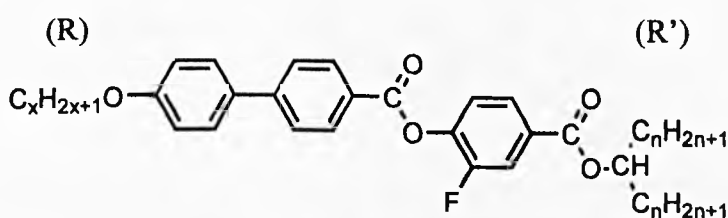
Category	Series	Compound	x	n
R variable, R' constant	2	2a	6	4
		2b	7	4
		2c	8	4
		2d	9	4
		2e	10	4
		2f	12	4
		2g	14	4
R constant, R' variable	3	3a	8	1
		3b	8	2
		3c	8	3
		3d	8	4
		3e	8	5
	4	4a	12	1
		4b	12	4
		4c	12	5

70

In addition to the variation of R and R', of the swallow-tailed materials, structures with alternative core components (than the usual biphenyl units) were also synthesised (*Table 9c*). Note that some of these structures do not possess a lateral fluoro substituent.

Table 9c:- Structure of the *symmetrically-substituted* (dibutyl swallow-tailed, R') host materials (Series **5**)
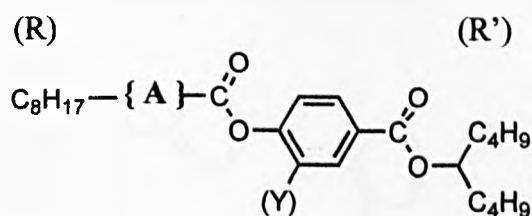
Category	Series	Y	Compound	{ A }
R & R' constant, -{A}- variable	5	F	5a	
		H	5b	
		H	5c	
		H	5d	

In order to compare, firstly, the effect of the lateral fluoro substituent on the transition temperatures of a model swallow-tailed host material; and secondly, the occurrence of unusual mesomorphic behaviour observed in one of the swallow-tailed host materials (compound **2c**), the corresponding non-fluorinated homologue was prepared (compound **9a**, *Table 9d*). The mesomorphic properties of this material are also compared against the analogues in *table 9c*. A second published non-fluorinated host

material, which appeared to show similar behaviour, was also prepared (compound **9b**) for comparison with **2c**. This material also provided the means to investigate the effect of increasing the size of one of the symmetrical alkyl chains, from **m** = 4 to **m** = 6.

Table 9d:- Structures of the model *symmetrically-substituted* fluorinated and non-fluorinated host materials; and an *unsymmetrically-substituted* non-fluorinated host material (compound **9b**).
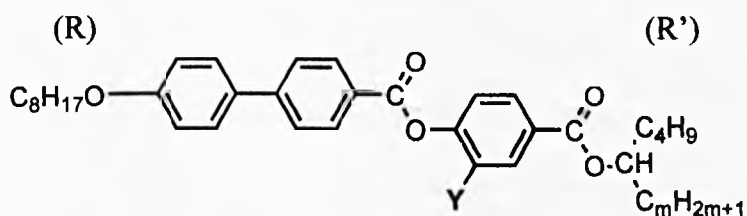
Category	Compound	m	Y
R constant,	*2c*	4	F
R' and Y variable	**9a**	4	H
	9b	6	H

Table 9e shows the variation in the structures of the *unsymmetrically-substituted* host materials. In Series **7** the length of the "off axis" branching alkyl chain, in R', is increased from **m** = 2 to **m** = 7, whilst the length of the unbranched alkyl chain, R, is maintained at **x** = 8.

Table 9e:- Structure and categories of the *unsymmetrically-substituted* host materials (Series **6**, **7** and **8**);
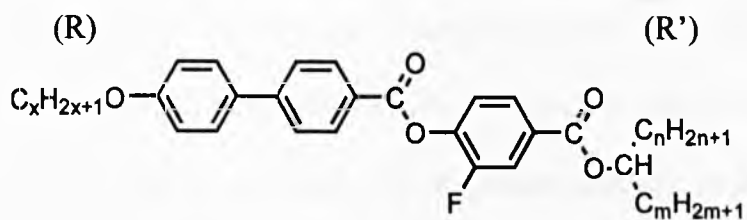
Category	Series	Compound	x	n	m
R variable, R' constant	6	6a	7	3	5
		6b	8	3	5
		6c	12	3	5
R constant R' variable	7	7a	8	1	2
		7b	8	1	3
		7c	8	1	4
		7d	8	1	5
		7e	8	1	6
		7f	8	1	7
		7g	8	2	5
		7h	8	2	6
R constant	8	8a	10	1	6
		8b	10	2	6
R' variable		8c	12	1	6
		8d	12	2	6

A number of optically-active materials, structurally related to the host materials, were also prepared. The materials were intended to compare the use of antiferroelectric materials and one ferroelectric material, with a similar structure to that of the host material, as a dopant in comparison to (S)-MHPOBC as a dopant. Two additional materials (compounds **10e** and **11d**), synthesized by Dr. R. A. Lewis, were also evaluated for their potential uses as dopants (*table 10*).

Table 10:- Structure and categories of the optically-active liquid crystalline materials intended for use as dopants
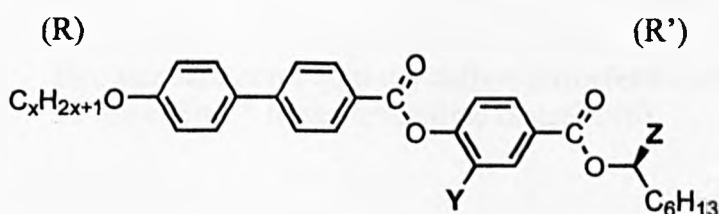
Category	Series	Compound	x	Y	Z
R variable, R' and Y constant	10	10a	8	F	CH_3
		10b	9	F	CH_3
		10c	10	F	CH_3
		10d	11	F	CH_3
		10e	12	F	CH_3
R and Y variable, R' variable	11	11a {(S)-MHPOBC}	8	H	CH_3
		11b	8	F	CH_2CH_3
		11c	10	H	CH_2F
		11d	12	H	CF_3

Two standard ferroelectric two-ring non liquid-crystalline dopants [103], and one three-ring smectic C*-forming material (synthesized by Dr. N. Gough) [30], were also evaluated for their potential applications as dopants for these systems (*figure 51*).

(a)   (b)
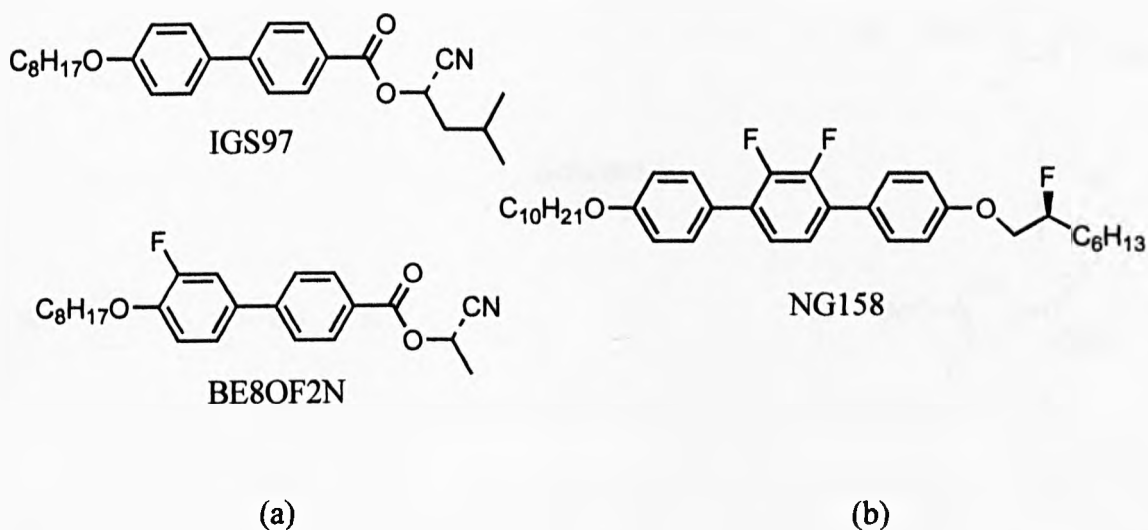
Figure 51:- Two standard non liquid-crystalline ferroelectric dopants (a);
a novel SmC* liquid crystalline material (b).

Synthetic Discussion

The target host and dopant materials, possessing a lateral fluoro substituent on the phenyl ring (ie. all the racemic and non-chiral compounds in *Tables 9a – 9d*, and most of the chiral compounds in *Table 10*), were mostly prepared according to the synthesis outlined in *Scheme 1* below.
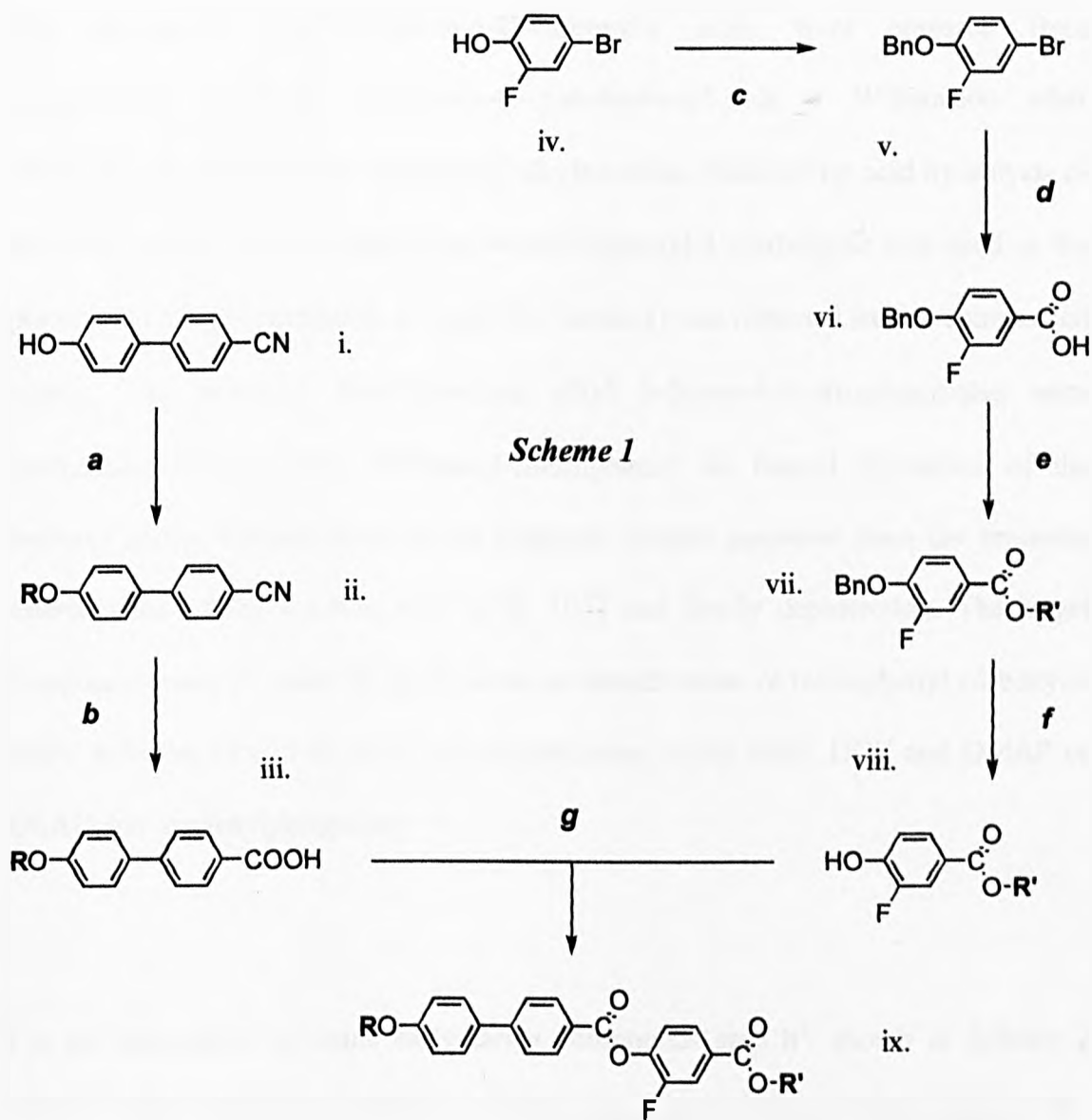
Scheme 1: – Synthesis of the fluorinated target compounds ("ix.")

a RBr, K_2CO_3, *butanone, reflux*

b c.H_2SO_4, H_2O, CH_3CO_2H, *reflux*

c BnBr, K_2CO_3, *butanone, reflux*

d i) Mg, *THF* ii) CO_2(s) iii) HCl

e R'OH, DEAD, PPh_3, *THF*

f Pd/C, H_2, *ethanol*

g DEAD, PPh_3, *THF* **or** DCC, DMAP, *DCM*

{Eg. where R = $C_{10}H_{21}$, and R' = -$CH(C_4H_9)_2$ (compound **2e**, *Table 9b*)}

The appropriate 4-alkoxybiphenyl-4'-carboxylic acids were prepared from commercially available 4-hydroxy-4'-cyanobiphenyl *via* a Williamson ether alkylation reaction with the appropriate alkylbromide, followed by acid hydrolysis of the nitrile group. The corresponding 4-decylbiphenyl-4'-carboxylic acid used in the preparation of the compounds in *Table 9a* (Series 1) was obtained from a commercial source. The necessary branched-chain alkyl 3-fluoro-4-hydroxybenzoates were synthesised starting from 4-bromo-2-fluorophenol *via* benzyl protection of the hydroxy group, carbonylation of the Grignard reagent prepared from the bromide, esterification of the resulting acid [104, 105] and finally deprotection. The target compounds were prepared in good yields by esterification of the biphenyl carboxylic acids, with the alkyl 3-fluoro-4-hydroxybenzoates, using either DCC and DMAP or DEAD and triphenylphosphine.

For the preparation of some early target compounds step **b'**, shown in *Scheme 2* below, replaced step **b** in *Scheme 1* in the preparation of the 4-alkoxybiphenyl-4'-carboxylic acids. The starting material (labelled "i'.") for this reaction, 4-bromo-4'-hydroxybiphenyl, was alkylated in the same manner as in *Scheme 1* (step **a**). The subsequent 4-*n*-alkoxybiphenyl-4'-bromides were lithiated at low temperature, carbonylated, and hydrolysed to the corresponding acids (compound "iii.").

HO—⟨benzene⟩—⟨benzene⟩—Br   i.

|
a
↓

RO—⟨benzene⟩—⟨benzene⟩—Br   ii'.   *Scheme 2*

|
b'
↓   iii.

RO—⟨benzene⟩—⟨benzene⟩—COOH
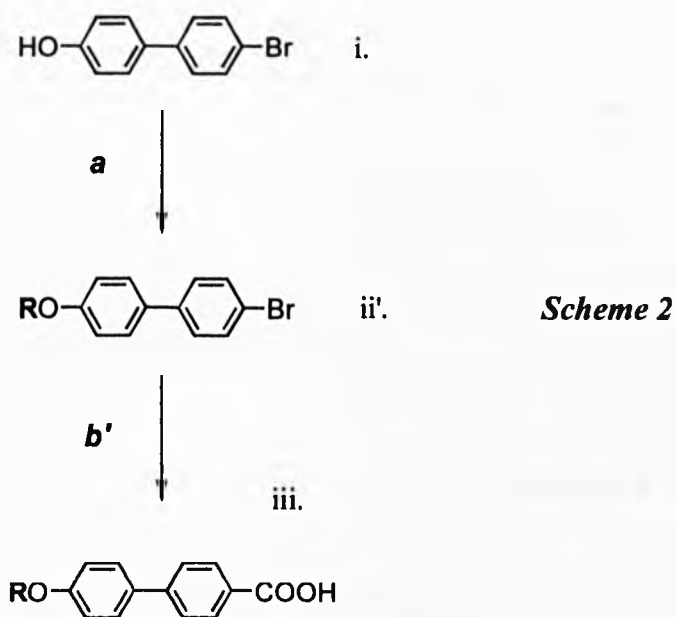
Scheme 2:- Alternative preparation of the 4-*n*-alkoxybiphenyl-4'-carboxylic acids

a RBr, K_2CO_3, *butanone, reflux*
b' i) *n*-BuLi, *THF*, *–78°C* ii') CO_2(s) iii) HCl

The non-fluorinated target compounds (**10a, 10b** and **12c**) were prepared from 4-hydroxybenzoic acid *via* methyl formate protection of the hydroxyl group (step **c'**), esterification with the branched alcohol as in *Scheme 1* (step **e**), and deprotection to the substituted non-fluorinated intermediate (*scheme 3*).

x.

$$\downarrow c'$$

xi.

$$\downarrow e$$ ***Scheme 3***

xii.

$$\downarrow f'$$

xiii.
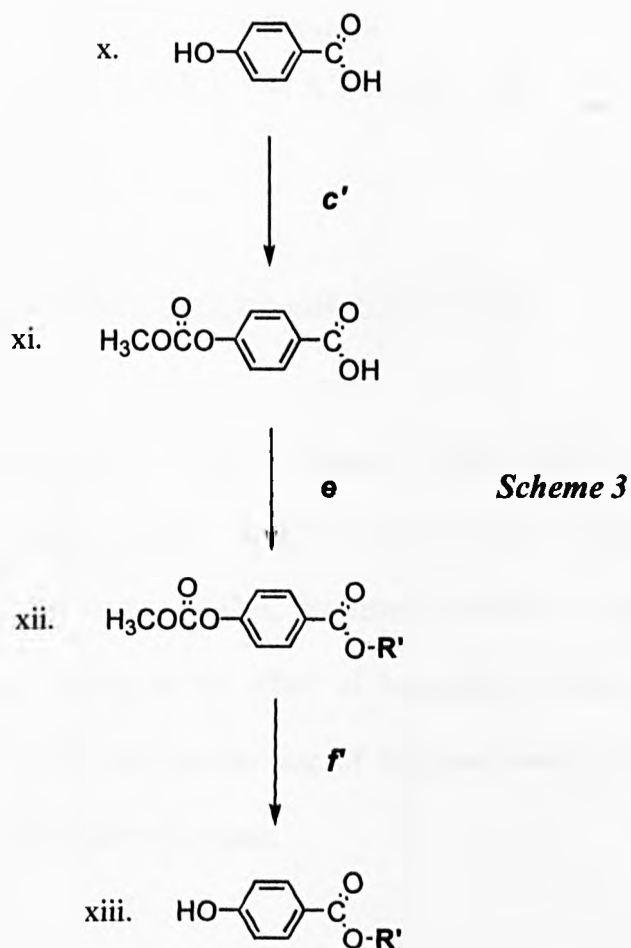
Scheme 3:- Preparation of the non-fluorinated phenol intermediates

c' i) CH_3OOCCl, NaOH, *distilled water*, 0 °C ii) HCl (aq)

e R'OH, DEAD, PPh_3, *THF*

f' NH_3(aq), *ethanol*

{Eg. where R' = $-CH(C_4H_9)_2$ (compound **10a**, *Table 7e*) or $-CH(CH_3)C_6H_{13}$}

Section (ii):
HOST MATERIALS

a. Symmetrically-Substituted ("Swallow-tailed") Materials

The transition temperatures and phase sequence of the first homologous series of symmetrically–substituted dibutyl "swallow-tailed" liquid crystals, determined by polarising optical microscopy and DSC are listed in *table 11*. These materials were prepared in order to investigate the effect of increasing the size of the unbranched alkoxy chains (R), while keeping the size of the swallow-tail (R') constant, on the thermal stability of the observed phases.

Table 11:- Transition temperatures (°C, on cooling) for the dibutyl swallow-tailed compounds
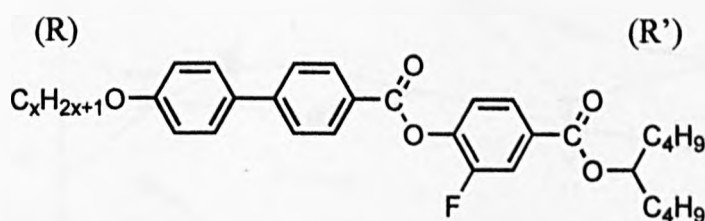
Compound	x	mp	"SmY"		SmC$_{alt}$		SmA		I	Recrys
2a	6	46	-	-	•	(43.0)	•	88.2	•	31
2b	7	53	•	(36.6)	•	55.0	•	91.1	•	26
2c	8	56	•	(28.0)	•	(54.0)	•	85.0	•	<25
2d	9	77	-	-	•	(46.6)	•	(70.3)	•	24
2e	10	73	-	-	•	(46.1)	•	(64.6)	•	<25
2f	12	49	-	-	•	(45.7)	•	58.1	•	40
2g	14	56	-	-	•	(41.0)	•	54.0	•	<25

( ) Represents a monotropic transition

All the compounds show monotropic SmC_{alt} phases and SmA phases, two of the compounds show an additional (as yet unidentified) phase, denoted "SmY" (see **section (iv)** of this chapter). No SmC phase was observed in any of the compounds. *Graph 1* below shows the relationship between the length of the unbranched alkoxy chain and the stability of the SmC_{alt} phase in this series of materials.

Graph 1:- Transition temperatures of the dibutyl swallow-tailed compounds
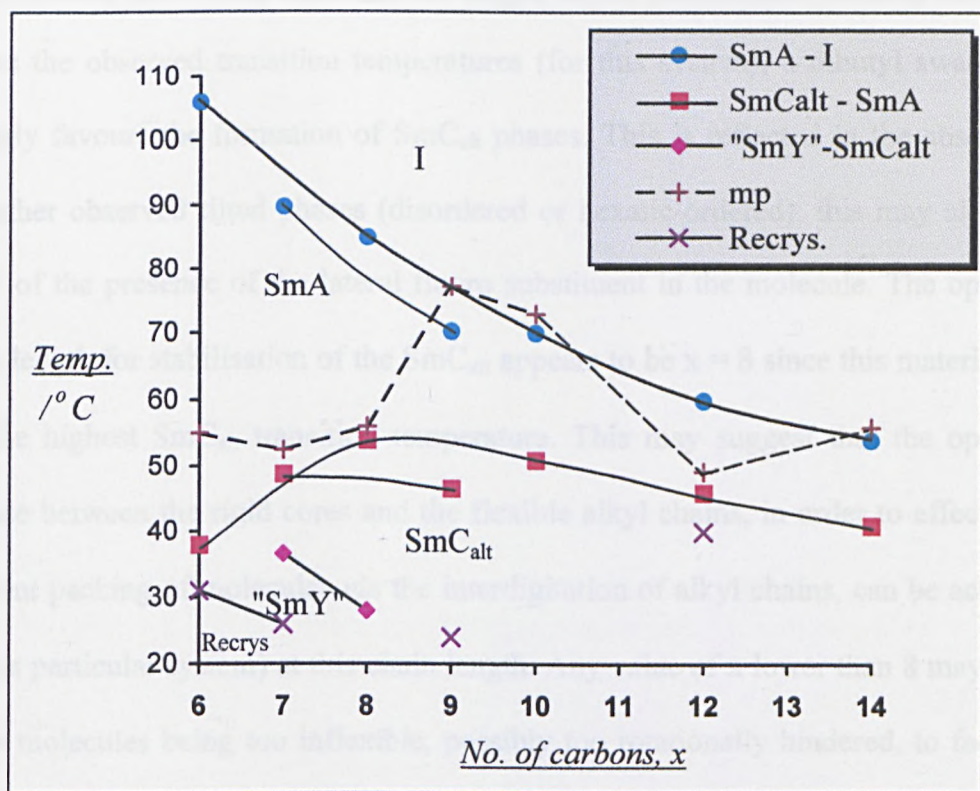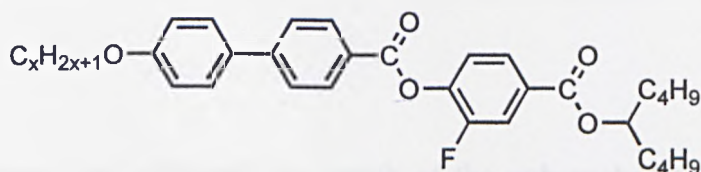
There is a general decline in SmA-I transition temperatures from compound **2a** (x = 6) to compound **2g** (x = 14); the SmC_{alt}-SmA temperatures increase to a maximum at x = 8 (compound **2c**) then decrease gradually to x = 14 (compound **2g**). As expected, there does not appear to be any observable trend for the melting points. A decrease in

the transition temperatures of the "SmY" phase from x = 7 (**2b**) to x = 8 (**2c**) is also observed. It is interesting to note that an "odd-even" effect is visible in the transition temperatures of the SmA-I transitions from x = 6 (**2a**) to x = 10 (**2e**). This odd-even effect is not truly observed between x = 10 and x = 14 since the intervening compounds, x = 11 and x = 13, were not prepared for this study. The transition temperatures of the SmC_{alt}-SmA phase between the x = 6 to x = 10 compounds do not appear to show this odd-even effect.

The materials show that, although the length of the unbranched terminal chain (R) affects the observed transition temperatures (for this system), a dibutyl swallowtail strongly favours the formation of SmC_{alt} phases. This is reflected in the absence of any other observed tilted phases (disordered or hexatic-ordered); this may also be a result of the presence of the lateral fluoro substituent in the molecule. The optimum chain length for stabilisation of the SmC_{alt} appears to be x = 8 since this material (**2c**) has the highest SmC_{alt} transition temperature. This may suggest that the optimum balance between the rigid cores and the flexible alkyl chains, in order to effect more efficient packing of molecules *via* the interdigitation of alkyl chains, can be achieved in (this particular system) at this chain length. Any value of x lower than 8 may result in the molecules being too inflexible, possibly too rotationally hindered, to facilitate stable "pair formation" in the alternating-tilt layers (*figure 52a*). Any value of **x** greater than 8 may result in the molecules being too flexible to permit strong pair formation (*figure 52c*).

(a)   (b)   (c)

Figure 52:- Postulated pair formation in the dibutyl swallow-tailed materials;-

(a) x = 6 (**2a**), the molecules are too rotationally restricted, the SmC_{alt} is less stable;
(b) x = 8 (**2c**), optimum chain length, strong pair formation occurs,
ie. the SmC_{alt} is the most stable;
(c) x = 14 (**2g**), the molecules are too flexible, the pair formation is weak,
consequently the SmC_{alt} is also less stable.

The material considered to be the most interesting as a potential host, principally due to presence of the unidentified "SmY" phase, which remained unrecrystallized for several hours at room temperature, is compound **2c**.

The decyl homologue of compound **2e** was also prepared (compound **1c**) but showed much lower transition temperatures in comparison to the decyloxy material (*table 12*).

Table 12:- Transition temperatures (°C) and phase sequence of the decyl and decyloxy compounds:
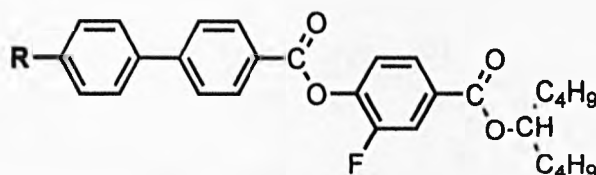
Compound	R	mp	SmC$_{alt}$		SmA		I	Recrys.
2e	C$_{10}$H$_{21}$O-	46	•	46.1	•	88.2	•	<25
1c	C$_{10}$H$_{21}$-	<0	•	(0)	•	28.0	•	<0

The SmC$_{alt}$ phase for compound **1c** could only be observed by cooling the heating stage of the microscope with liquid nitrogen; the actual temperature of the transition was determined by DSC. The very large reduction in the stability of all the transition temperatures in the decyl material, in comparison with the decyloxy material, suggests that the ether linkage in the unbranched terminal chain (R) plays a crucial role in stabilising the phases in a swallow-tailed liquid crystal of this type. This is a general trend on the whole, which has in fact been observed in other non-related liquid crystal systems, and may be attributed to the *mesomeric relay* of π electrons across the molecules (*figure 53a*). The "flow" of electrons, in opposite directions in adjacent molecules, appears to stabilise the formation of smectic phases through quadrupolar coupling. This is believed to be due to increased electrostatic attraction between adjacent molecules, as a result of the flow of electrons in opposite directions, favouring the packing of the molecules in this manner. By comparison the decyl-

substituted systems appear to show a reduced degree of this *mesomeric relay* due to the absence of the terminal ether linkage (*figure 53b*). This may then account for the lower transition temperatures of the decyl compound (**1c**) in comparison with the decyloxy homologue (**2e**).
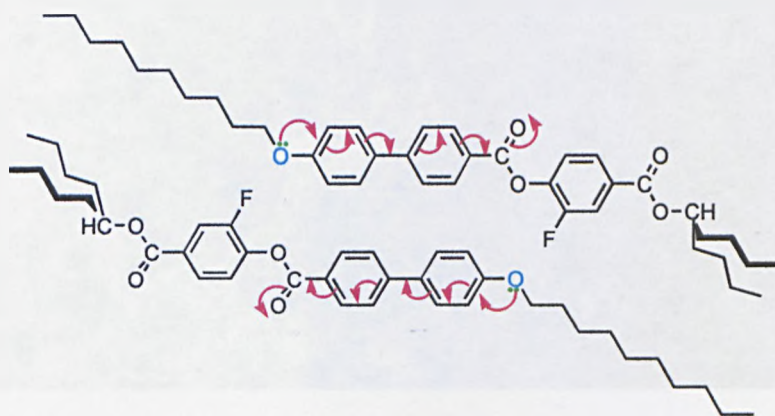
Figure 53a:- Postulated *mesomeric relay* in adjacent molecules of compound **2e** (initiated by the ether oxygen).
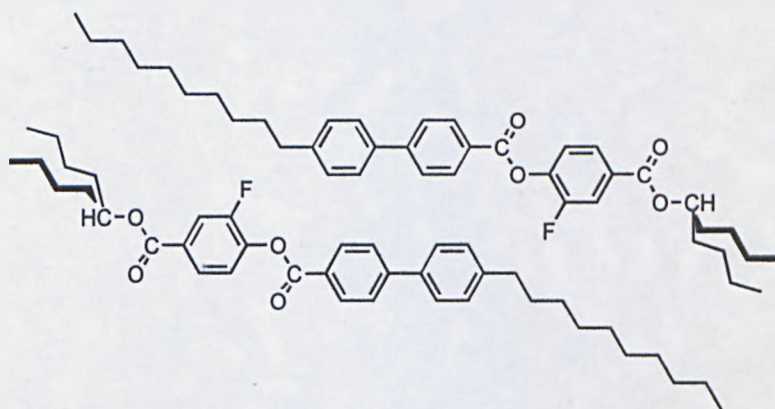
Figure 53b:- Greatly reduced mesomeric relay in compound **1c** due to the absence of the ether linkage in the unbranched terminal chain.

The photographs below show the characteristic optical textures, observed through crossed polarisers, of the SmA and SmC$_{alt}$ phases of compound **2e** (*figures 54(a)* and *(b)* respectively).
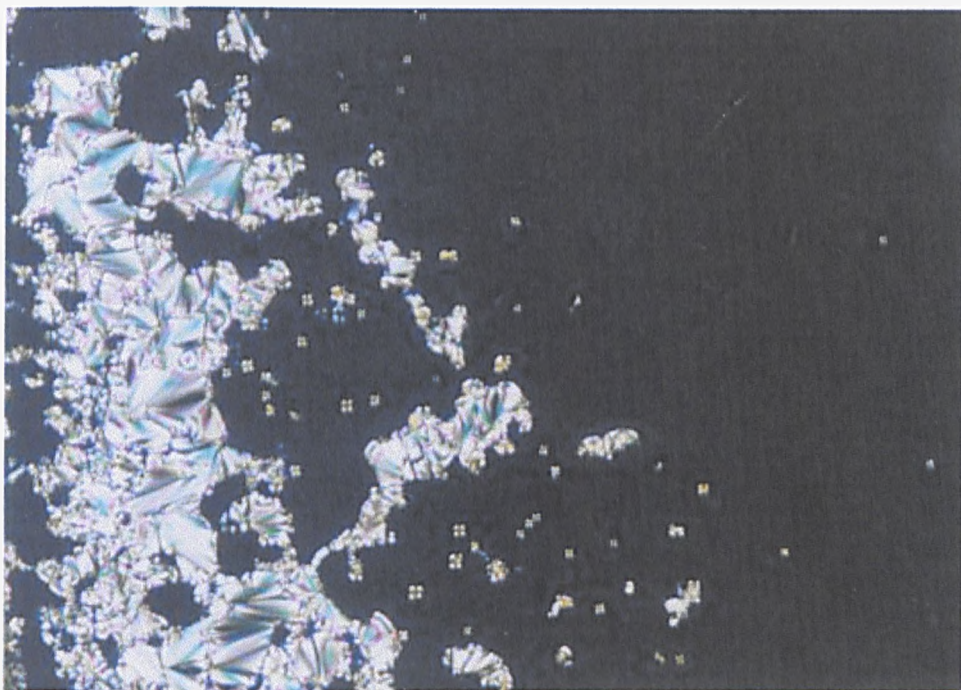
(a)
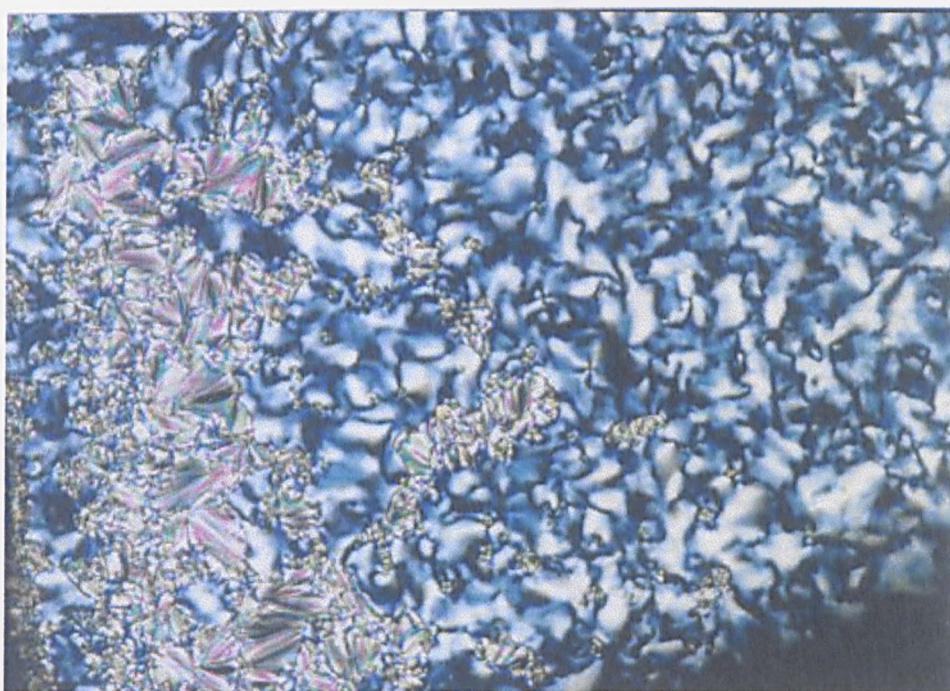
(b)

Figure 54:- Optical textures of the SmA (a), and SmC$_{alt}$ (b) phases of compound **2e** (59.7 °C and 43.4 °C respectively).

For the next series of swallow-tailed materials **R** was kept constant (at **x** = 8 and 12) while **R'** was varied, from n = 1 to 5 (*tables 13a* and *13b*). These materials were prepared in order to study the relationship between the size of the swallowtail moiety on the occurrence and stability of the SmC_{alt} phases. For the dodecyloxy compounds (*table 13b*) three of the materials were prepared which complete the series of materials prepared initially by Booth *et al* [79] (shown in parantheses { }).

Table 13a:- Transition temperatures (°C) and phase sequence of the octyloxy swallow-tailed compounds (n = 1 to n = 5)
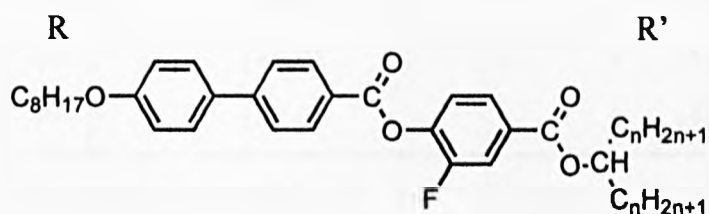
Compound n		mp	"SmY"		SmC_{alt}		SmC		SmA		I	Recrys
3a	1	83	-	-	-	-	•	(81.3)	•	157.2	•	75
3b	2	77	-	-	•	(74.2)	-	-	•	119.6	•	43
3c	3	86	-	-	•	(67.4)	-	-	•	96.7	•	39
2c	4	56	•	(28.0)	•	(54.0)	-	-	•	85.0	•	<25
3d	5	42	-	-	•	(38.8)	-	-	•	71.5	•	<25

Table 13b:- Transition temperatures (°C) and phase sequence of the dodecyloxy swallow-tailed compounds (**n** = 1 to **n** = 5)

R $\qquad\qquad$ R'

$C_{12}H_{25}O$—〔 〕—〔 〕—C(=O)—O—〔 〕—C(=O)—C_nH_{2n+1} O—CH C_nH_{2n+1} (with F)
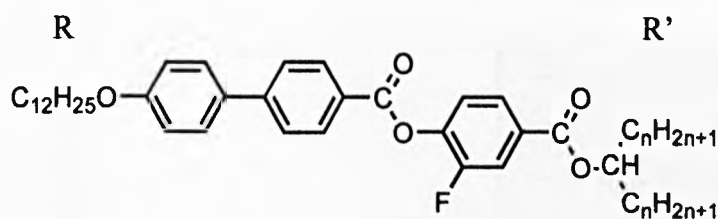
Compound	n	mp	SmC$_{alt}$		SmC		SmA		I	Recrys
4a	1	69	-	-	•	89.7	•	146.2	•	45
{}	2	46	•	82.2	-	-	•	108.6	•	32
{}	3	66	•	(56.8)	-	-	•	72.9	•	40
{4b}	4	49	•	(45.7)	-	-	•	58.1	•	40
4c	5	49	•	(27.0)	-	-	•	(43.8)	•	-

{ } previously reported materials $\qquad$ { } previously reported, also prepared for this study

All the compounds exhibit a SmA phase. Only Compounds **3a** and **4a** (n = 1) exhibit an additional SmC phase whereas compounds where n = 2 to n = 5 exhibit a SmC$_{alt}$ phase in its place. Compound **2c** in *table 13a* is the only material that appeared to exhibit the unidentified "SmY" phase. *Graphs 2a* and *2b* below show the relationship between the length of the branched swallow-tail chains and the stability of the SmC$_{alt}$ phase in these two series of materials.

Graph 2a:— Transition temperature trends of the octyloxy substituted swallow-tailed compounds (**series 3**)
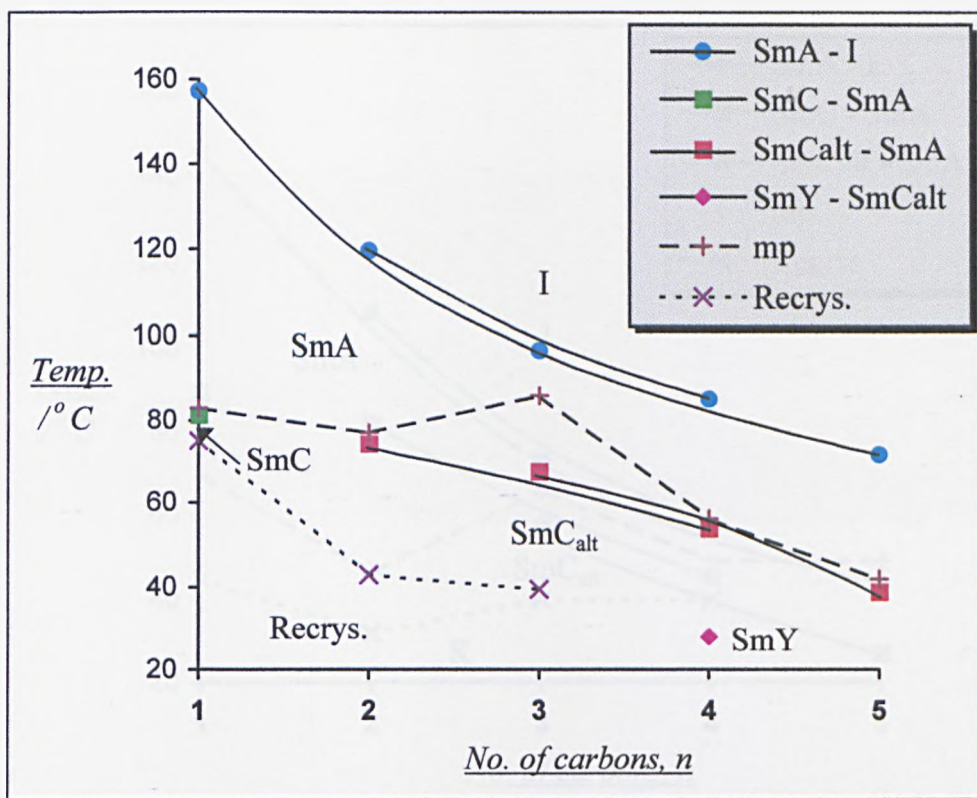
Graph 2b:— Transition temperature trends of the dodecyloxy substituted swallow-tailed compounds (**series 4**)
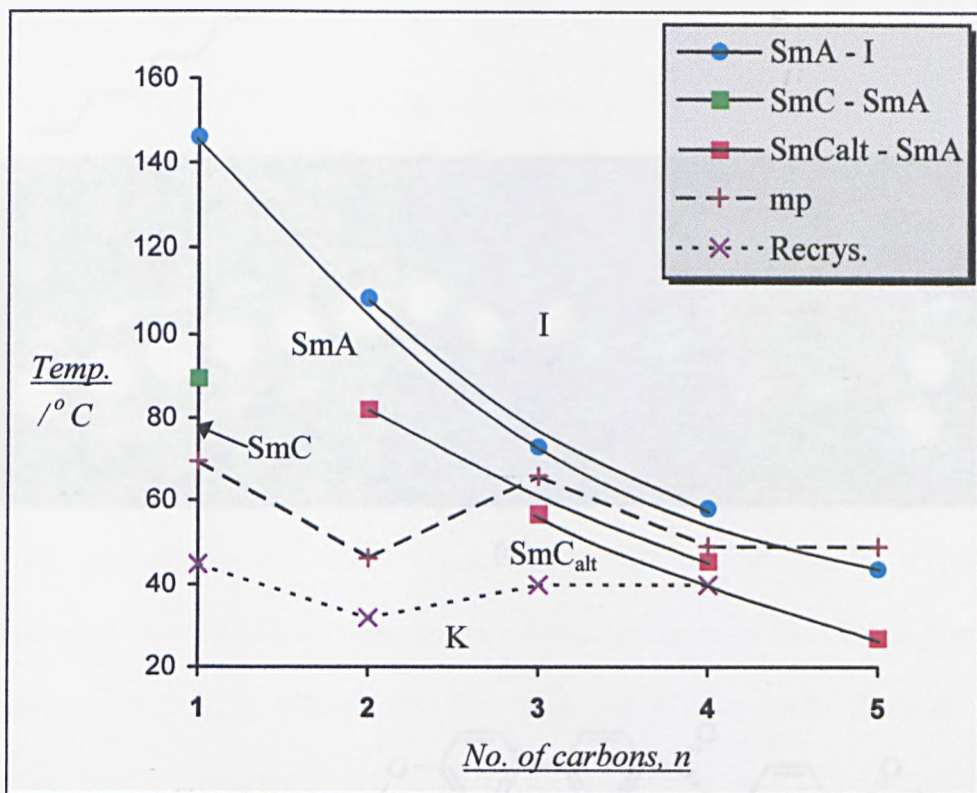
In both series of materials there is a general decrease in the SmA - I transition temperature from $n = 1$ to $n = 5$. A general decrease is also observed for the SmC_{alt} - SmA temperatures from $n = 2$ to $n = 5$. These compounds also form SmC_{alt} phases directly from the SmA phase without an intermediate SmC phase; this suggests that the minimum size of the swallow-tail moiety required to effect sufficient steric interaction, between molecules in adjacent smectic layers, is $n = 2$. The size of this swallow-tail appears to promote the formation of a SmC_{alt} phase in preference to a smectic C phase regardless of the length of R. *Figure 55* shows the energy-minimised structure of the dodecyloxy compounds in which $n = 2$ (compounds **4a** and **4b**).
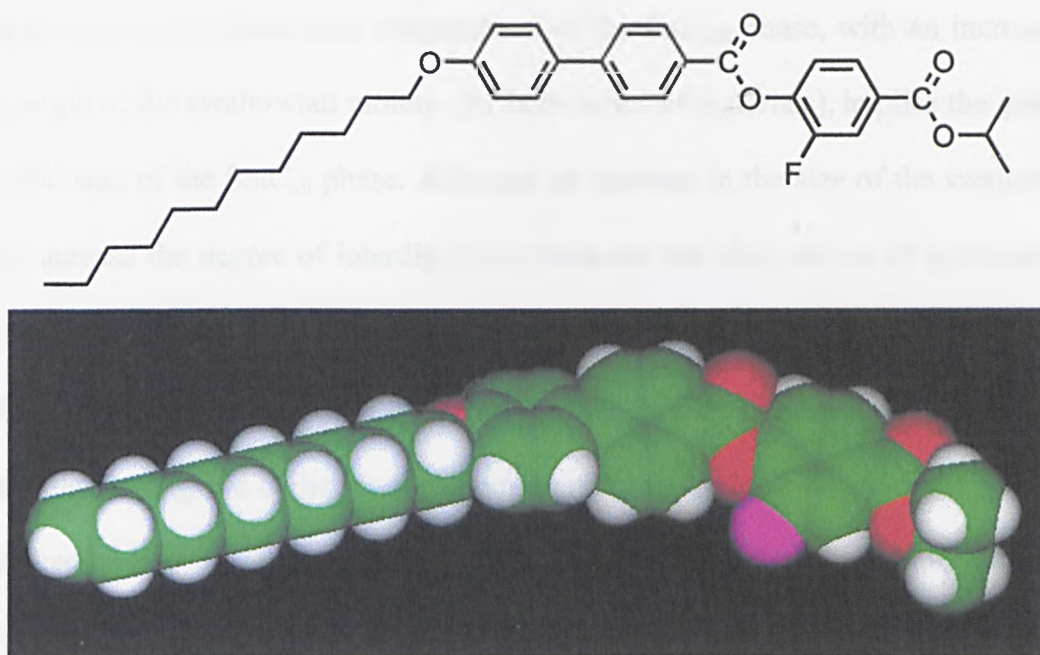
(a)
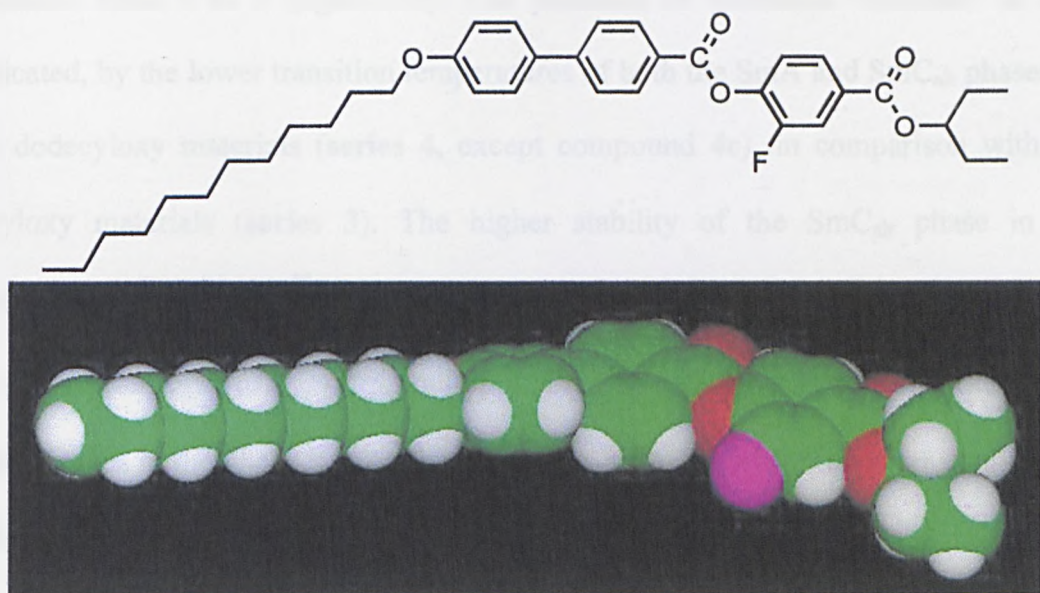
(b)

Figure 55:- Space-filling energy-minimised molecular models (Nemesis Interactive Modelling; COSMIC force-field) of compounds **4a** and **4b** ((a) and (b) respectively); the diethyl (**n** = 2) swallowtail appears to be large enough to allow steric interactions to facilitate the packing of the molecules in an anticlinic manner.

The decrease in the transition temperatures of the SmC_{alt} phase, with an increase in the length of the swallowtail moiety (for both series of materials), implies the gradual destabilising of the SmC_{alt} phase. Although an increase in the size of the swallowtail may increase the degree of interdigitation, between the alkyl chains of molecules in adjacent layers, a second factor must be taken into account when considering the stability of these alternatingly-tilted phases. As with the first series of swallow-tailed materials investigated earlier (series **2**) an increase in the length of the symmetrically branched alkyl chain (R'), above the "optimum value" (n = 2), generally increases the "flexible" parts of the molecules. There is as a consequence a greater degree of "fluidity" and increased freedom of movement between the smectic layers; this is accompanied by a decrease in the transition temperatures of the SmC_{alt} phases as n increases from 2 to 5 (*figure 56*). The presence of increased "disorder" is also indicated, by the lower transition temperatures of both the SmA and SmC_{alt} phases, in the dodecyloxy materials (**series 4,** except compound **4c**), in comparison with the octyloxy materials (**series 3**). The higher stability of the SmC_{alt} phase in the dodecyloxy n = 2 swallow-tailed compound, (**4c**, 82.2°) in comparison with the octyloxy homologue (**3b**, 74.2°), could possibly be due to the most stable arrangement of molecules in the phase being achieved in the materials with the longer unbranched chain. This appears to be specific to the size of the swallowtail since from the first series of swallow-tailed materials (**series 2**, n = 4) the *optimum* length of the unbranched chain is octyloxy (x = 8).

The observation that a swallow-tail moiety with a relatively short alkyl chain (n = 2) is sufficient to generate a SmC_{alt} phase in preference to a SmC phase, however, may be regarded as further evidence to support the postulation that steric interactions are a

major contribution towards the formation of stable SmC$_{alt}$ phases. It is also interesting to note that in **series 4** the n = 2 swallowtail is the only material to show an enantiotropic SmC$_{alt}$ phase. The other materials showed only monotropic SmC$_{alt}$ phases; this may be a further indication as to the increased strength of the steric interactions which favour the formation of alternating-tilt smectic phases in this series of materials.

Reduced freedom of movement (ie."fluidity"); SmC$_{alt}$ more stable & occurs at a higher temperature

Greater freedom of movement; SmC$_{alt}$ less stable & occurs at a lower temperature

Compound **3b**
(n = 2)
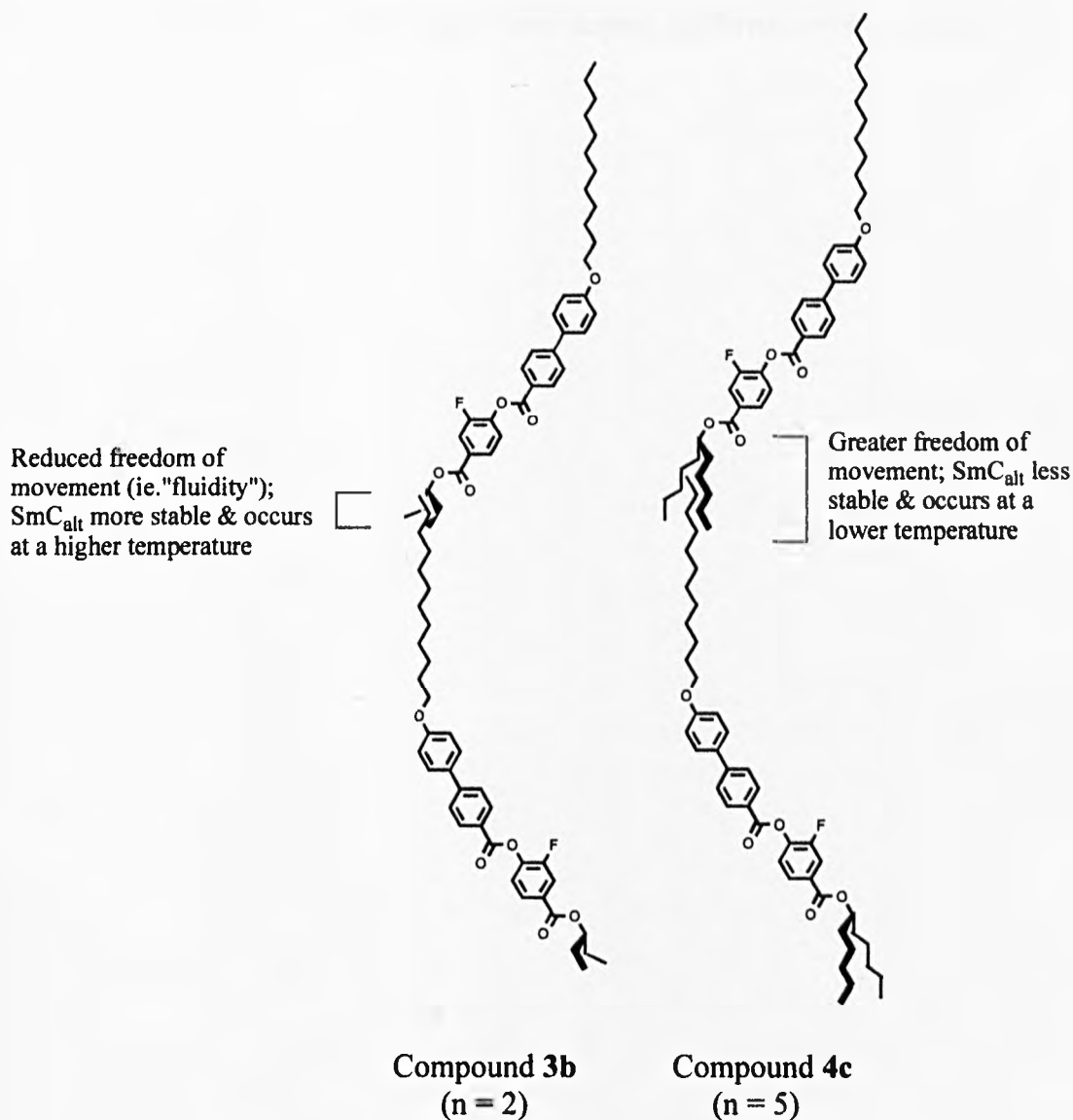
Compound **4c**
(n = 5)

Figure 56:- Comparison of the "fluidity" the dodecyloxy n = 2 and n = 5 swallow-tailed materials

The non-chiral anticlinic structure of the SmC_{alt} phase in one of the swallow-tailed materials, compound **4c**, was confirmed by a miscibility test with the standard chiral antiferroelectric material, (*S*)-MHPOBC. The material showed complete miscibility with the SmC_A^* phase (*graph 3*). In fact, by mixing the material with another with a high SmC_A^* phase stability, the transition temperature of the induced SmC_A^* phase in the resulting binary mixture is raised. This may allow the material to act as a host despite possessing a low SmC_{alt} transition itself. For this reason, this material was also selected as a host for the model binary chiral dopant antiferroelectric mixtures.

Graph 3:- Miscibility phase diagram of compound **4c** with (*S*)-MHPOBC

(*S*)-MHPOBC

Compound **4c**
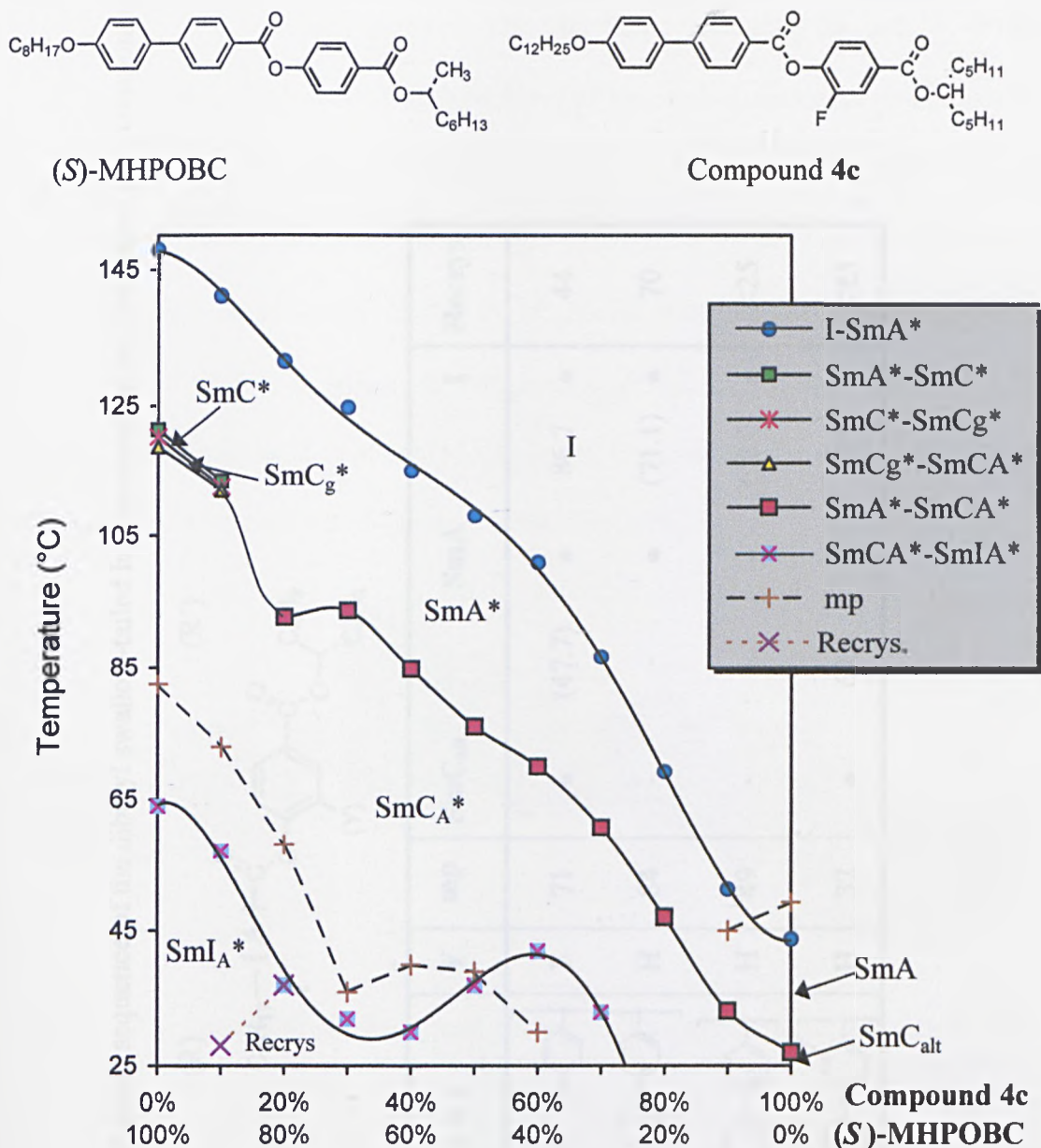
In order to study the effect, on the SmC$_{alt}$ phase, of changing part of the core component of dibutyl (**n** = 4) swallow-tailed materials, a series of materials with alternative core components were prepared (*table 14*).

Table 14:- Transition temperatures (°C) and phase sequence of the dibutyl swallow-tailed host materials with alternative core components.
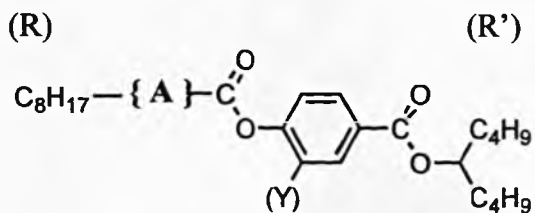
Compound	{A}	Y	mp	SmC$_{alt}$		SmA		I	Recrys
5a		F	71	●	(47.7)	●	86.7	●	44
5b		H	84	-	-	●	(71.1)	●	70
5c		H	49	-	-	●	(40.0)	●	<25
5d		H	32	●	68.4	●	87.9	●	<25

All the materials exhibited SmA phases; only compounds **5a** and **5d** showed an additional monotropic SmC$_{alt}$ phase. The fact that compounds **5b** and **5c** showed only SmA phases suggests that the structures of the core components, in comparison with the biphenyl component in compound **2c** for example, is unsuitable for the formation of tilted (SmC) or alternatingly-tilted (SmC$_{alt}$) phases. In the case of compound **5c**, the presence of the bulky lateral bromo-substituent may have a disrupting, or hindering effect, on the packing of the molecules (*figure 57*); this could inhibit the formation of any tilted phases. Consequently the only phase which is observed to be stabilised in any way is the SmA phase.
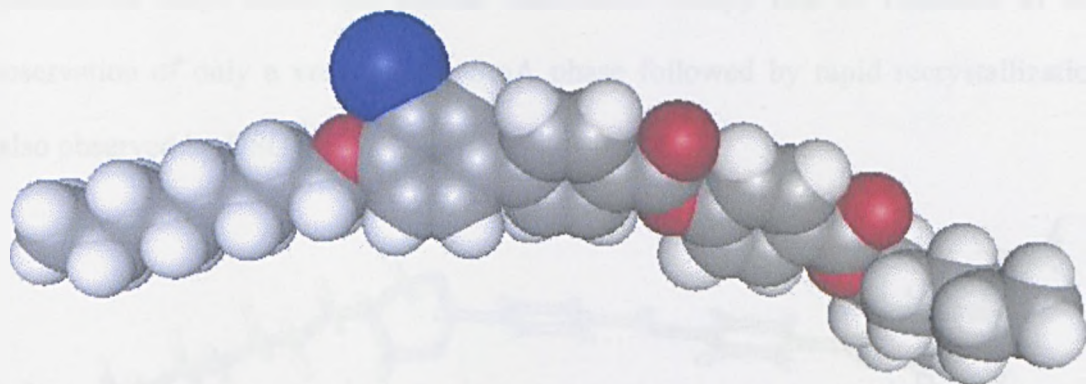
Figure 57:- Energy-minimised space-filling molecular model (rendered with MSI Weblab Viewer) of compound **5b** showing the bulky lateral bromo substituent.

Compound **5c** possesses a lateral fluoro substituent in the biphenyl component of the molecular core. The substituent is much smaller in size in comparison with the bromo substituent in compound **5b**, the hindering effect on the packing of the molecules is lower, and the SmC$_{alt}$ phase is observed. In fact the transition temperature of the phase appears to be raised, by over 14 °C in comparison with compound **2c**, by the presence of the fluoro substituent in the biphenyl component of the core rather than the phenylcarboxylate component. This increase in stability of

the SmC$_{alt}$ phase may reflect the enhanced packing of the molecules in the anticlinic structure of the phase.

In compound **5b** a 2,5-dioxanyl unit replaces one of the phenyl rings in the biphenyl component of the core. *Figure 58* below shows the energy-minimised structure of a molecule of the material; the heterocyclic dioxanyl unit, due to its dissimilarity to the planar phenyl ring(s), appears to hinder the packing of the molecules in either a tilted or alternatingly-tilted manner. Together with the absence of an ether bond in the unbranched alkyl chain (to initiate mesomeric relay) this is reflected in the observation of only a very narrow SmA phase followed by rapid recrystallization (also observed by DSC).

2,5-dioxanyl
heterocycle
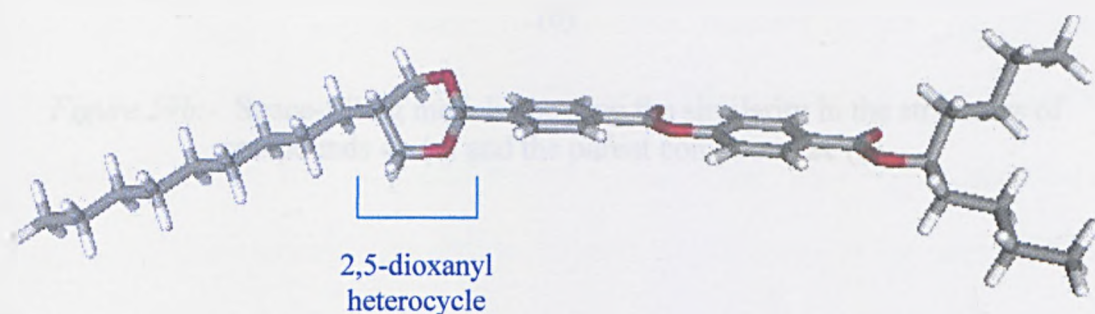
Figure 58:- Energy-minimised "stick" model of a molecule of compound **4b**, showing the hindering non-planar 2,5-dioxanyl heterocyclic ring.

The inclusion of an extra ester group, between the two phenyl rings in the biphenyl component of the core, appeared to maintain the occurrence of a SmC$_{alt}$ phase. The structure (*figure 59a*) of this material is similar to that of the parent molecule (compound **2c**, *figure 59b*) containing the biphenyl component. This most likely accounts for the preservation of the SmC$_{alt}$ phase.
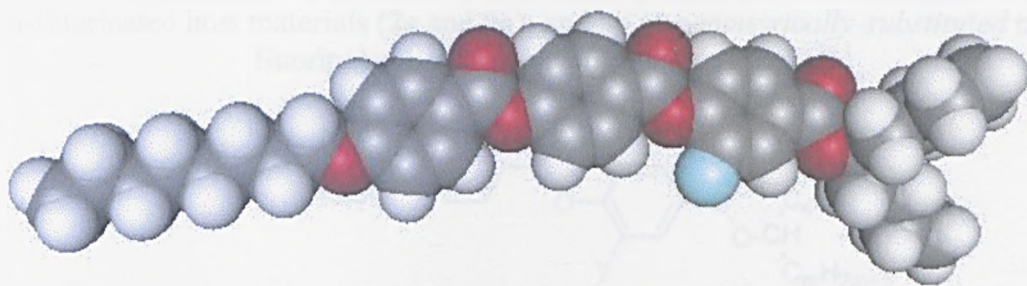
(a)
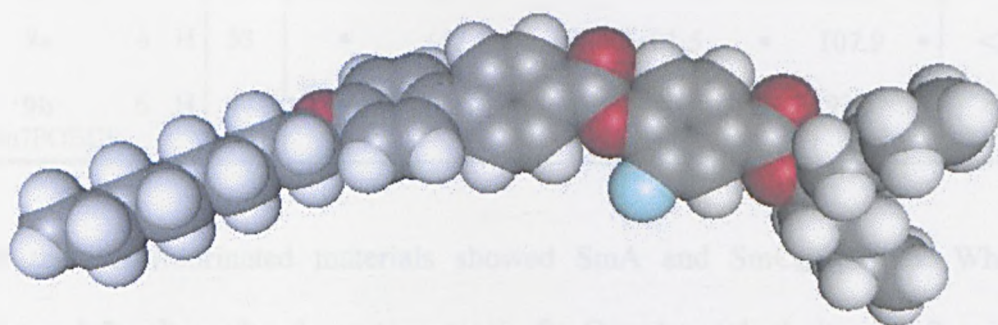
(b)

Figure 59b:- Space-filling models showing the similarity in the structures of compounds **4a** (a) and the parent compound **2c** (b).

The final swallow-tailed material prepared for this part of the sub-section is the non-fluorinated version of compound **2c** ie. **9a**. The effect of increasing the length of one of the branching chains, making up the swallow-tail moiety, was also investigated by preparation of a published material ("1Bu7POBC") [70] (*table 15*).

Table 15:- Structures and transition temperatures (°C) of the model fluorinated and non-fluorinated host materials (**2c** and **9a**); and an *unsymmetrically-substituted* non-fluorinated host material (compound **9b**).
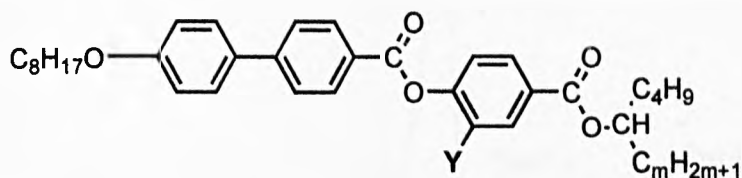
Compound	m	Y	mp	"SmY"		SmC$_{alt}$		SmA		I	Recrys
2c	4	F	56	•	(28.0)	•	(54.0)	•	85.0	•	<25
9a	4	H	53	•	(47.5)	•	91.5	•	107.9	•	<25
9b {1Bu7POBC}	6	H	44	•	(35.4)	•	75.4	•	93.1	•	<25

Both the non-fluorinated materials showed SmA and SmC$_{alt}$ phases. Whereas compound **2c** showed only a monotropic SmC$_{alt}$ phase, both its non-fluorinated homologue, **9a**, the unsymmetrically-substituted homologue (**9b**, 1Bu7POBC) showed enantiotropic SmC$_{alt}$ phases (confirmed by DSC, *figure 60*). Both **9a** and **9b** also showed a phase with an optical texture similar to the "SmY" phase observed in compound **2c** (see **section (iv)** of this chapter). The absence of the lateral fluoro-substituent in compound **9a** has the effect of increasing the transition temperatures of all the phases, including the unidentified phase, in comparison with the model dibutyl swallow-tailed material (**2c**). This is also consistent with observations that related smectic materials, possessing lateral fluoro-substituents, generally show lower transition temperatures than the non-fluorinated homologues [102].
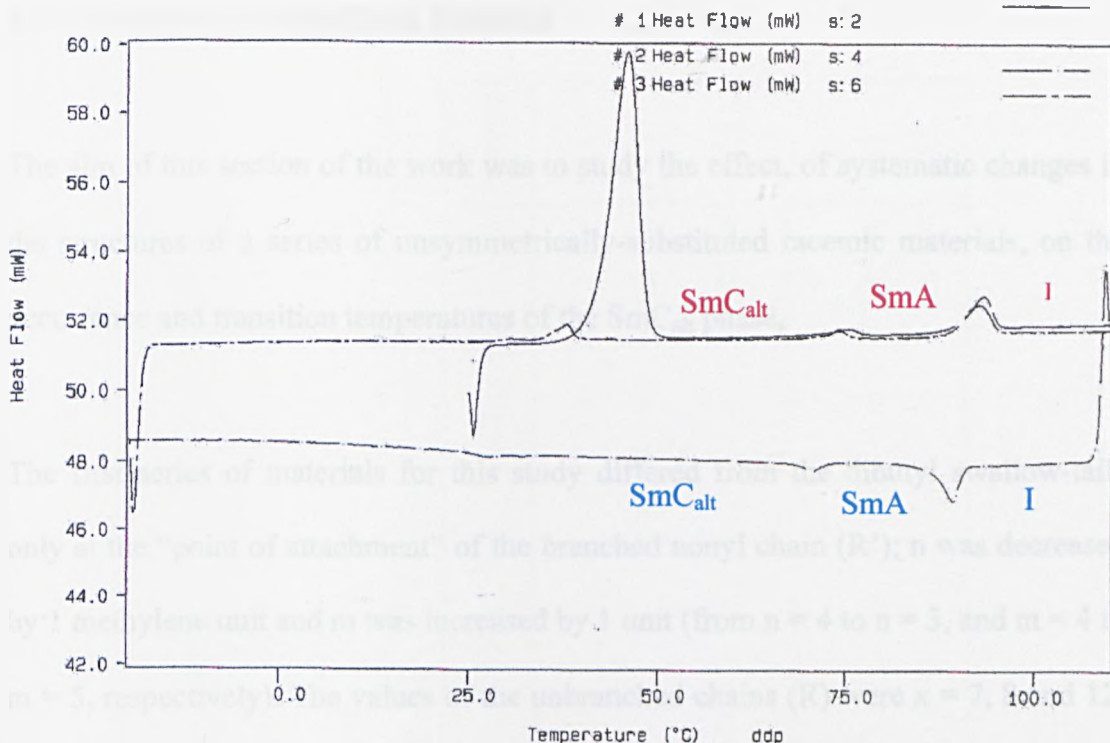
Figure 60:- DSC trace of compound **9b** showing the enantiotropic SmC$_{alt}$ phase.

An increase in the length of one of the branched swallow-tail chains, in the non-fluorinated materials (**9a** and **9b**) by two methylene units (from **m** = 4 to **m** = 6), has the effect of lowering the transition temperatures of the observed phases. This is believed to be due to an increase in the "fluidity" of the system in comparison to the dibutyl material. This is generally consistent with the results, discussed earlier in this thesis, for the other swallow-tailed materials in which both the lengths of R and R' were varied.

b. Unsymmetrically-Substituted Materials

The aim of this section of the work was to study the effect, of systematic changes in the structures of a series of unsymmetrically-substituted racemic materials, on the occurrence and transition temperatures of the SmC_{alt} phase,

The first series of materials for this study differed from the dibutyl swallow-tails only at the "point of attachment" of the branched nonyl chain (R'); n was decreased by 1 methylene unit and m was increased by 1 unit (from n = 4 to n = 3, and m = 4 to m = 5, respectively). The values of the unbranched chains (R) were x = 7, 8 and 12; the x = 7 and 8 materials were of interest since the dibutyl swallow-tailed homologues showed the "SmY" phase. The transition temperatures of the unsymmetrically-substituted materials, in comparison with the original symmetrical swallow-tailed materials, are listed in *table 16* below.

Table 16:- Transition temperatures (°C) and phase sequence of the n = 3, m = 5 compounds:
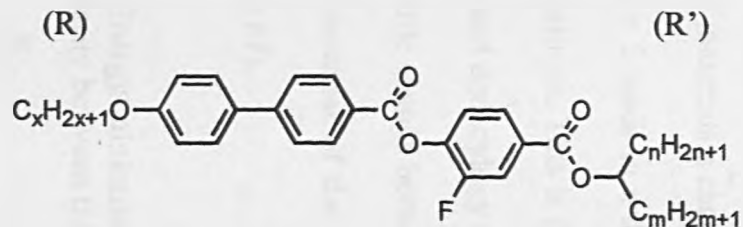
Compound	x	n	m	mp	SmX	"SmY"	SmC$_{alt}$	SmC	SmA	I	Recrys.
2a	7	4	4	83	- -	• (36.6)	• (55.0)	- -	• 91.1	•	26
6a	7	3	5	40	• (32.0)	- -	- -	• 44.6	• 88.2	•	27
2c	8	4	4	56	- -	- (28.0)	• (54.0)	- -	• 85.0	•	<25
6b	8	3	5	46	- -	- (28.0)	• 54.6	- -	• 82.4	•	27
2f	12	4	4	49	- -	- -	• (45.7)	- -	• 58.1	•	40
6c	12	3	5	39	- -	- -	• (45.0)	- -	• 61.0	•	<25

All the materials showed SmA and *monotropic* SmC$_{alt}$ phases except compound **6a**, which showed an *enantiotropic* SmC phase in place of the SmC$_{alt}$, and compound **6b** which showed an *enantiotropic* SmC$_{alt}$ phase. The "SmY" phase was observed in both the octyloxy compounds **2c** and **6b**, but only in the **n** = 4, **m** = 4 heptyloxy homologue, **2a**. The **n** = 3, **m** = 5 homologue did show an additional phase below the SmC$_{alt}$, however, the microscopic texture was not identical to the SmY phases observed in the other materials, hence the phase is assigned "SmX". Neither of the dodecyloxy materials **2f** or **6c** showed any other additional phases. For the heptyloxy and decyloxy materials a change in the branched substituents (R') from **n** and **m** = 4 to **n** = 3, **m** = 5 leads to a decrease, by a few degrees, in the temperatures of the SmA − I transitions. This is the reverse case for the dodecyloxy materials. For both the octyloxy and dodecyloxy materials the transition temperature of the SmC$_{alt}$ phase shows very little change between the two different values of R'. The similarity in the swallow-tail moieties of the **n** and **m** = 4 and **n** = 3, **m** = 5 materials are shown below (*figure 61*).

Figure 61:- Energy-minimised models of compounds **2c** (a), and **6b** (b) showing the similarity between the sizes of R' (for the octyloxy (R) compounds).

(a)

(b)
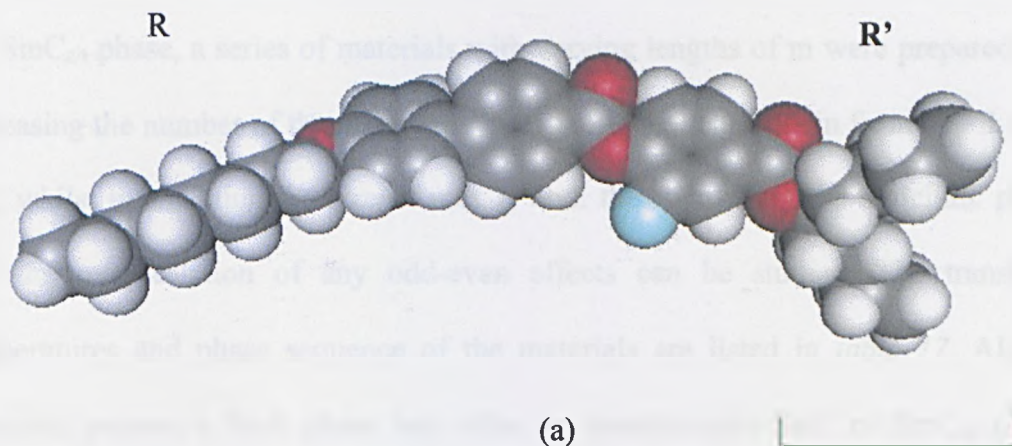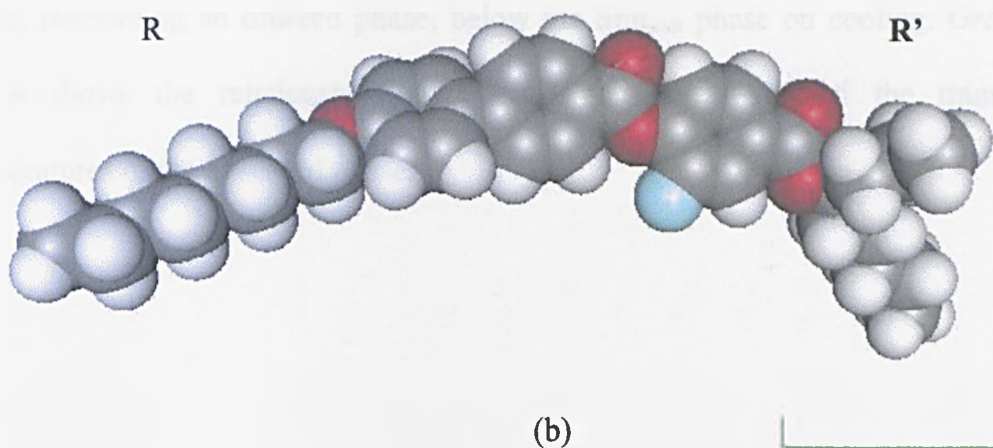
The observation of a SmC phase in place of the SmC$_{alt}$ in the heptyloxy n = 3, m = 5 material (**6a**) may be tentatively attributed to the manifestation of part of an odd-even effect. The packing of the molecules with certain numbers of carbons in the unbranched chain may favour the arrangement of the molecules in a SmC phase rather than a SmC$_{alt}$ phase. Obviously many more unbranched (R) homologues would have to be prepared in order to clarify this.

In order to carry out a detailed investigation of the significance of the unsymmetrically substituted terminal chain, **R'**, on the occurrence and stability of the SmC$_{alt}$ phase, a series of materials with varying lengths of m were prepared. By increasing the number of the methylene units in the branched chain from m = 1 to m = 7, whilst maintaining the size of n at 1, both the stability of the anticlinic phase and the manifestation of any odd-even effects can be studied. The transition temperatures and phase sequence of the materials are listed in *table 17*. All the materials possess a SmA phase and either an enantiotropic SmC or SmC$_{alt}$ phase (with the exception of compound **7e**, which shows a monotropic SmC phase). The compounds that possess a SmC$_{alt}$ phase appear to show an additional unknown

phase, resembling an ordered phase, below the SmC$_{alt}$ phase on cooling. *Graph 4* below shows the relationship between the length of m and the transition temperatures of the observed phases.

Table 17:- Transition temperatures (°C) and phase sequence of the n = 1, m = 1 – 7 compounds.

(R)   (R')

$C_8H_{17}O$ —⬡—⬡—C(=O)—O—⬡(F)—C(=O)—O—CH(CH_3)(C_mH_{2m+1})
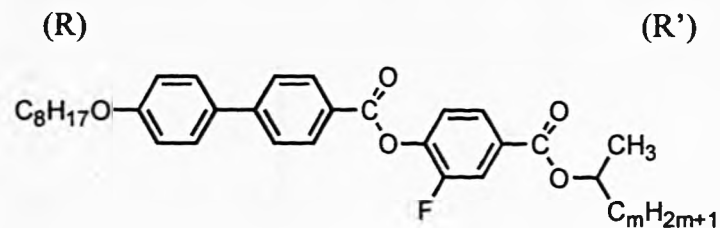
Compound	m	mp	SmX₃		SmX₂		SmC$_{alt}$		SmC		SmA		I	Recrys
3a	1	83	-	-	-	-	-	-	•	(81.3)	•	157.2	•	75
7a	2	71	-	-	-	-	-	-	•	(68.3)	•	144.0	•	47
7b	3	60	-	-	•	(58.3)	•	78.8	-	-	•	132.6	•	47
7c	4	51	-	-	•	(36.0)	•	64.5	-	-	•	127.9	•	28
7d	5	51	•	(34.8)	-	-	-	-	•	63.1	•	123.2	•	34
7e	6	48	-	-	•	(38.0)	•	49.0	-	-	•	117.0	•	27
7f	7	74	-	-	-	-	-	-	•	(28.0)	•	115.0	•	26

(R)   (R')

$C_8H_{17}O$ — ... — CH_3
C_mH_{2m+1}
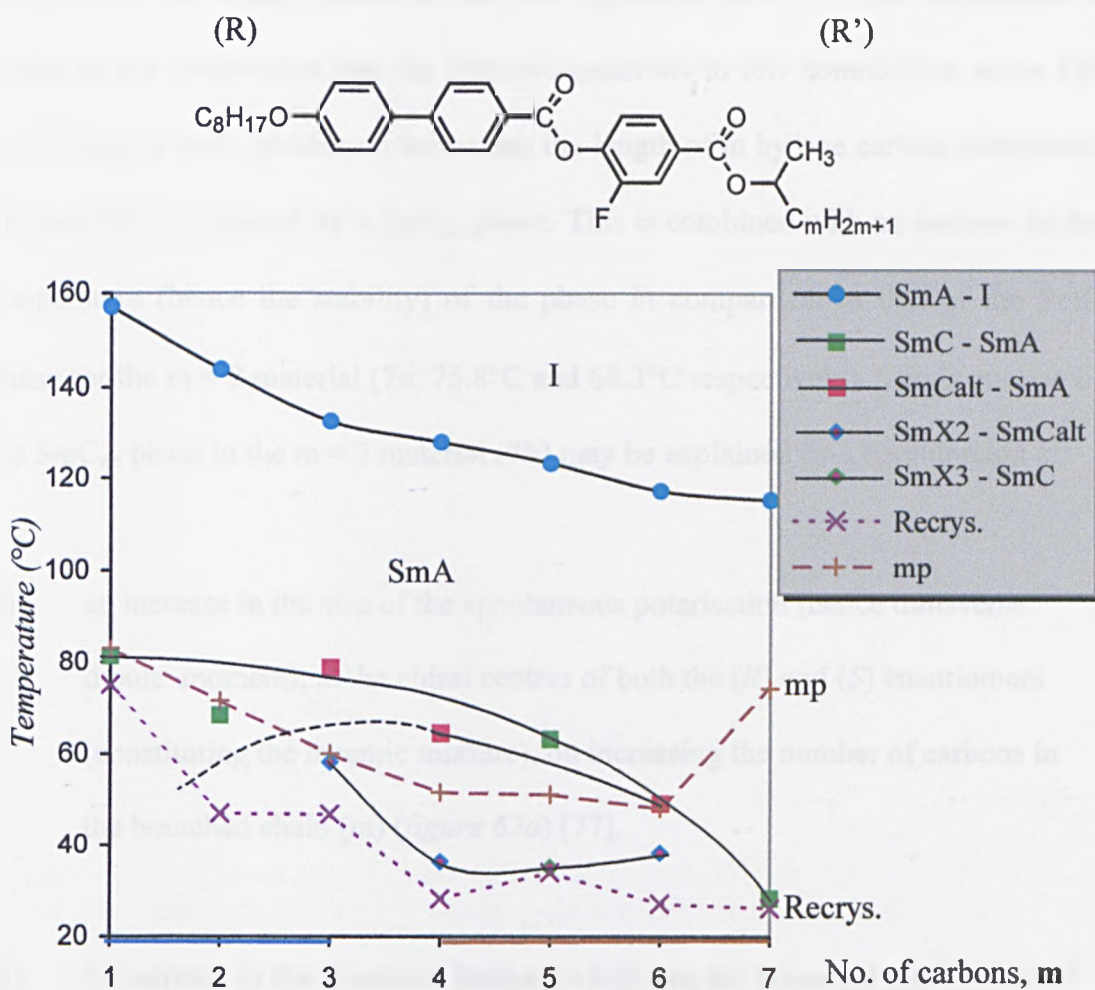
The transition temperatures of the SmA phases decrease as the length of m increases from m = 1 to m = 7. The occurrence of the tilted smectic phases below the SmA phases in the overall series can be better understood by dividing the homologous series into two parts;

(i)   compounds m = 1 to m = 3 (**3a, 7a** and **7b**), and

(ii)   compounds m = 4 to m = 7 (**7c** to **7f**)

In the first part of the series the smallest value of m which appears to promote the formation of the SmC_{alt} phase over the SmC appears to be m = 3. This assumption is based on the observation that the first two materials in this homologous series (**3a** and **7b**) show SmC phases; on increasing the length of m by one carbon (compound **7c**) the SmC is replaced by a SmC_{alt} phase. This is combined with an increase in the temperature (hence the stability) of the phase in comparison to that of the SmC phase for the m = 2 material (**7a**, 78.8°C and 68.3°C respectively). The formation of the SmC_{alt} phase in the m = 3 material (**7b**) may be explained by a combination of:

(i)   an increase in the size of the spontaneous polarisation (hence transverse dipole moment), at the chiral centres of both the (R) and (S) enantiomers (constituting the racemic mixture), on increasing the number of carbons in the branched chain (m) (*figure 62a*) [77].

(ii)   an increase in the rotational hindrance between the branched alkyl chains of the molecules in one smectic layer and the unbranched chains in the adjacent layer, relative to the m = 1 and 2 materials, sterically favouring alternatingly-tilt phases (*figure 62b*).

increasing transverse dipole (hence spontaneous polarisation)
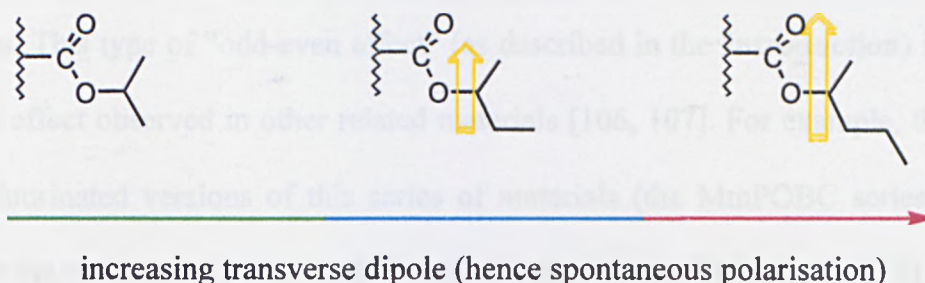
Figure 62a:- Increase in the size transverse dipoles at the chiral centres (of both the (R) and (S) enantiomers) as the value of m increases from m = 1 to m = 3.
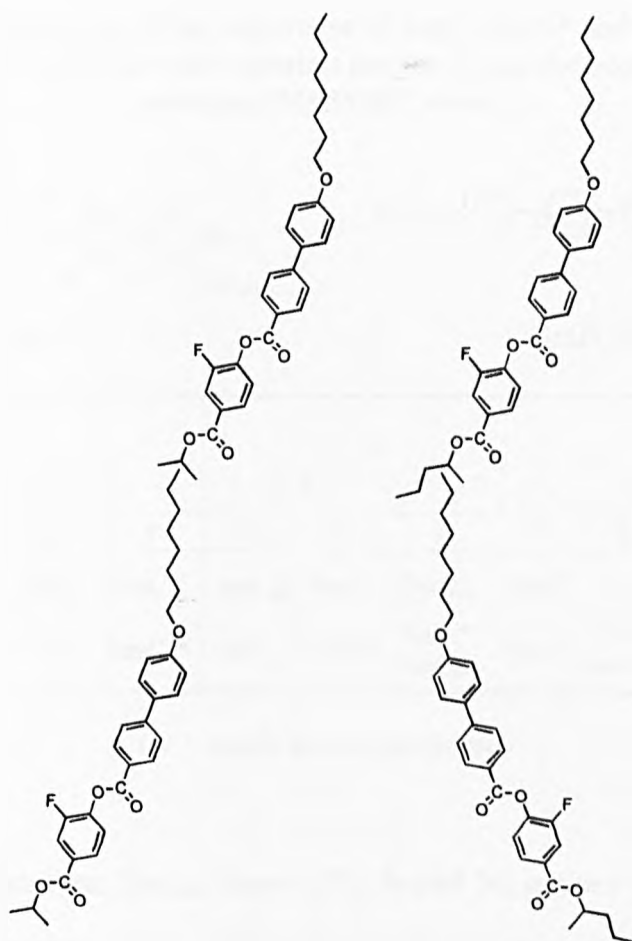
Figure 62b:- Increased steric interactions which favour the formation of the SmC$_{alt}$ phase in the m = 3 material (relative to the m = 1 material).

In the second part of the homologous series steric contributions, to formation of either the SmC (*syn*clinic) or the SmC$_{alt}$ (*anti*clinic) phase, may play an increased role in comparison to the coupling of transverse dipoles. This is believed to be the case since above the value of m = 2 the transverse dipole appears to be large enough to allow anticlinic phases to form, but not all the materials in the series form these phases. This type of "odd-even effect" (as described in the **Introduction**) is similar to the effect observed in other related materials [106, 107]. For example, the chiral, non-fluorinated versions of this series of materials (the MmPOBC series) closely match the occurrence of phases in the above series (**series 7**) (*table 18*) [78].

Table 18:- Comparison of the occurrence of SmC / SmC* and SmC$_{alt}$ / SmC$_A$* phases in the fluorinated racemic materials (**series 7**) and the non-fluorinated chiral materials (MmPOBC series).

Series 7   MmPOBC series
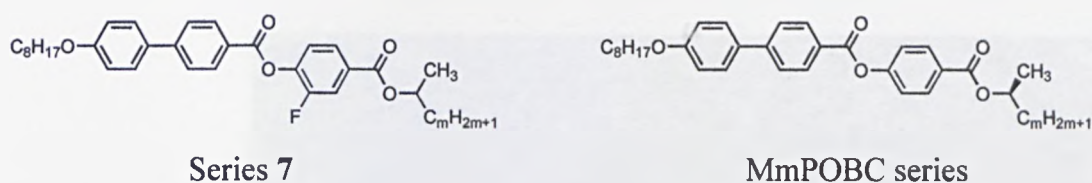
Series	m									
	1st p a r t			2nd p a r t						
	1	2	3	4	5	6	7	8	9	10
7	SmC	SmC	SmC$_{alt}$	SmC$_{alt}$	SmC	SmC$_{alt}$	SmC	/	/	/
MmPOBC	/	SmC*	SmC$_A$*	SmC$_A$*	SmC*	SmC* SmC$_A$*	SmC*	SmC* SmC$_A$*	SmC*	SmC$_A$*

('/' materials not prepared)

The materials which form SmC$_{alt}$ phases (**7b, 7c** and **7e**) possess underlying smectic phases, denoted "SmX$_2$", the textures of which bear some resemblance the "SmY" phases observed in some of the materials discussed previously (*figure 63a*). Only one SmC-forming compound, **7d** (**m = 5**), formed an ordered phase (SmX$_3$), the texture for which appeared to be dissimilar to the SmX$_2$ (*figure 63b*). As some of the non-fluorinated chiral homologues form ordered (SmI* and SmI$_A$*) phases below the SmC* and SmC$_A$* phases we may expect the underlying SmX$_2$ and SmX$_3$ phases to be similar in structure (ie. ordered).

Figure 63:- Comparison of the optical textures of the SmX_2 phase in compound 7e (25 °C) (a), and the SmX_3 phase in compound 7d (25 °C) (b); before (i), and after (ii) shearing.
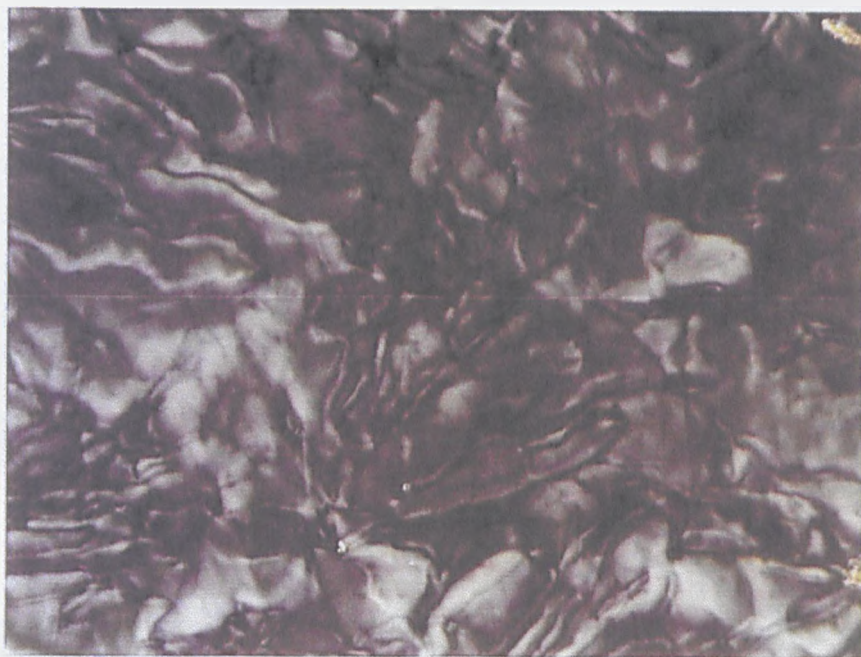
(i)
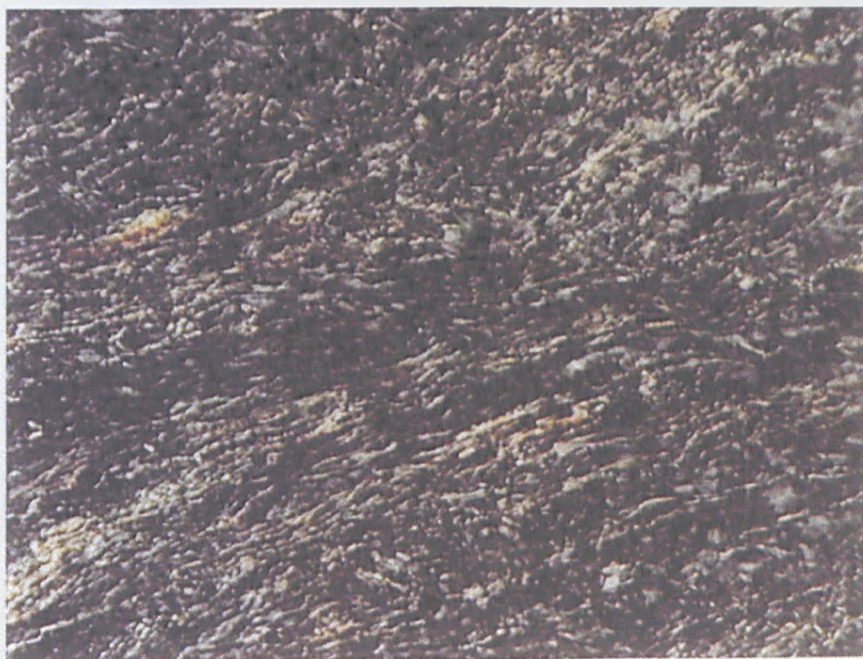
(ii)

(a)
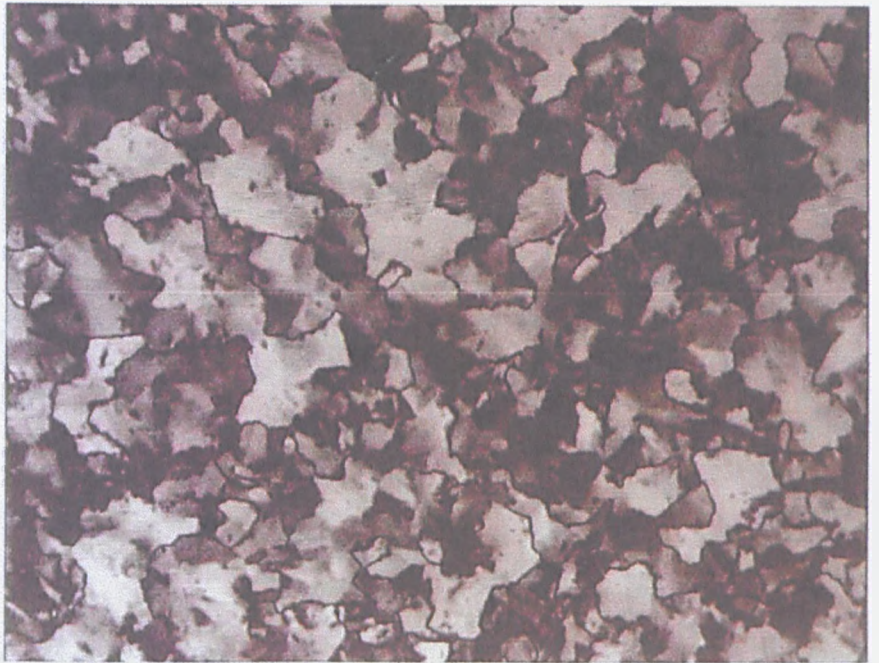
(i)

(ii)

(b)

The significance of the alkoxy chain in *unsymmetrically-substituted* materials was investigated by the preparation of two groups of materials differing only in the presence or the absence of the ether oxygen in the unbranched chain of the

113

molecules. *Table 19* below shows the transition temperatures, for the decyl- and decyloxy-substituted (R) homologues, of the materials possessing methylheptyl (n = 1, m = 6) and ethylheptyl (n = 2, m = 6) branched chains (R').

Table 19:- Transition temperatures (°C) and phase sequence of the decyl- and decyloxy-substituted compounds;

(R)   (R')
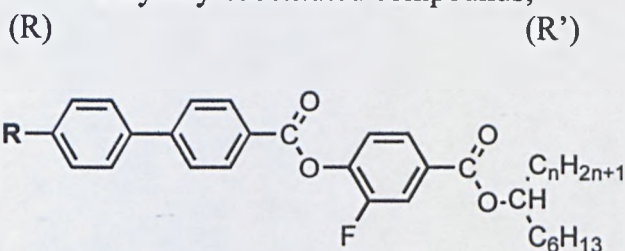
Compound	R	n	mp	SmC$_{alt}$		SmC		SmA		I	Recrys
1a	C$_{10}$H$_{21}$-	1	51	-	-	-	-	●	76.0	●	39
1b	C$_{10}$H$_{21}$-	2	<25	●	(9.0)	-	-	●	43.0	●	<0
8a	C$_{10}$H$_{21}$O-	1	38	●	79.5	●	83.0	●	111.0	●	<25
8b	C$_{10}$H$_{21}$O-	2	34	●	57.0	-	-	●	79.0	●	<25

Both the decyloxy-substituted materials show enantiotropic SmA and SmC$_{alt}$ phases; compound **8a** (n = 1) show an additional SmC phase. Of the two decyl homologues only compound **1b** (n = 2) shows a monotropic SmC$_{alt}$ phase which appears below room temperature. This supports the observation that alkoxy, rather than alkyl, terminal chains are more effective for the formation of stable SmC$_{alt}$ phases. The significance of the observation of a SmC$_{alt}$ phase on cooling from the SmA phase, without an intermediate SmC phase, in compound **8b** (in comparison to compound **8a**) can be better understood by placing both materials in a table of related homologues (*table 20*).

All the compounds exhibit a SmA phase; all the homologues possess either a SmC and/or a SmC$_{alt}$ phase. The transition temperatures of the n = 1, m = 6 compounds are generally higher than those of the n = 2, m = 6 compounds with the exception of the octyloxy compounds (**7e** and **7h**). This is consistent with the *general* trend that increasing the length of terminal alkyl chains lowers the transition temperatures of the observed phases [102]. Only the octyloxy materials, except **7f** (n = 1, m = 7), form an unidentified "SmX$_2$" phase.

In the n = 1, m = 6 homologues (**8a** and **8c**) of the decyloxy and dodecyloxy compounds the SmC$_{alt}$ phase forms from a SmC phase, whereas in the n = 2, m = 6 homologues (**8b** and **8d**), the SmC$_{alt}$ phase forms directly from the SmA phase. This is consistent with observations made for related chiral systems [80, 108], ie. an increase in one of the alkyl chains at the point of branching, from methyl to ethyl, increases the tendency of the compounds to form SmC$_{alt}$ phases rather than SmC phases. This may be attributed to the increased interdigitation of the terminal branched and unbranched chains in the n = 2, m = 6 compounds, and subsequent restricted rotational freedom at the point of branching of the molecules, compared with the situation for the n = 1, m = 6 compounds (*figure 64*).

Table 20:- Transition temperatures (°C) and phase sequences of the unsymmetrically-substituted compounds.

(R) $C_xH_{2x+1}O$—[biphenyl]—C(=O)—O—[phenyl(F)]—C(=O)—O—CH(C_nH_{2n+1})(C_mH_{2m+1}) (R')
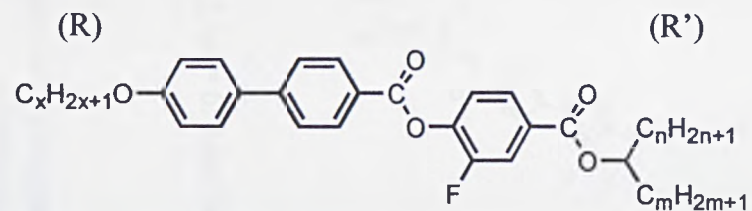
Compound	x	n	m	mp	SmX$_2$		SmC$_{alt}$		SmC		SmA		I	Recrys
7e	8	1	6	48	•	38.0	•	49.0	-	-	•	117.0	•	27
7h	8	2	6	37	•	20.0	•	56.5	-	-	•	94.0	•	-3
7g	8	2	5	34	•	22.0	•	53.5	-	-	•	93.5	•	-4
6b	8	3	5	46	•	28.6	•	54.6	-	-	•	82.4	•	28
7f	8	1	7	74	-	-	-	-	•	(28)	•	115.0	•	26
8a	10	1	6	38	-	-	•	79.5	•	83.0	•	111.0	•	-10
8b	10	2	6	34	-	-	•	57.0	-	-	•	79.0	•	-35
8c	12	1	6	52	-	-	•	75.0	•	88.6	•	105.0	•	16
8d	12	2	6	42	-	-	•	60.0	-	-	•	75.4	•	-2
6c	12	3	5	39	-	-	•	45.0	-	-	•	61.0	•	2
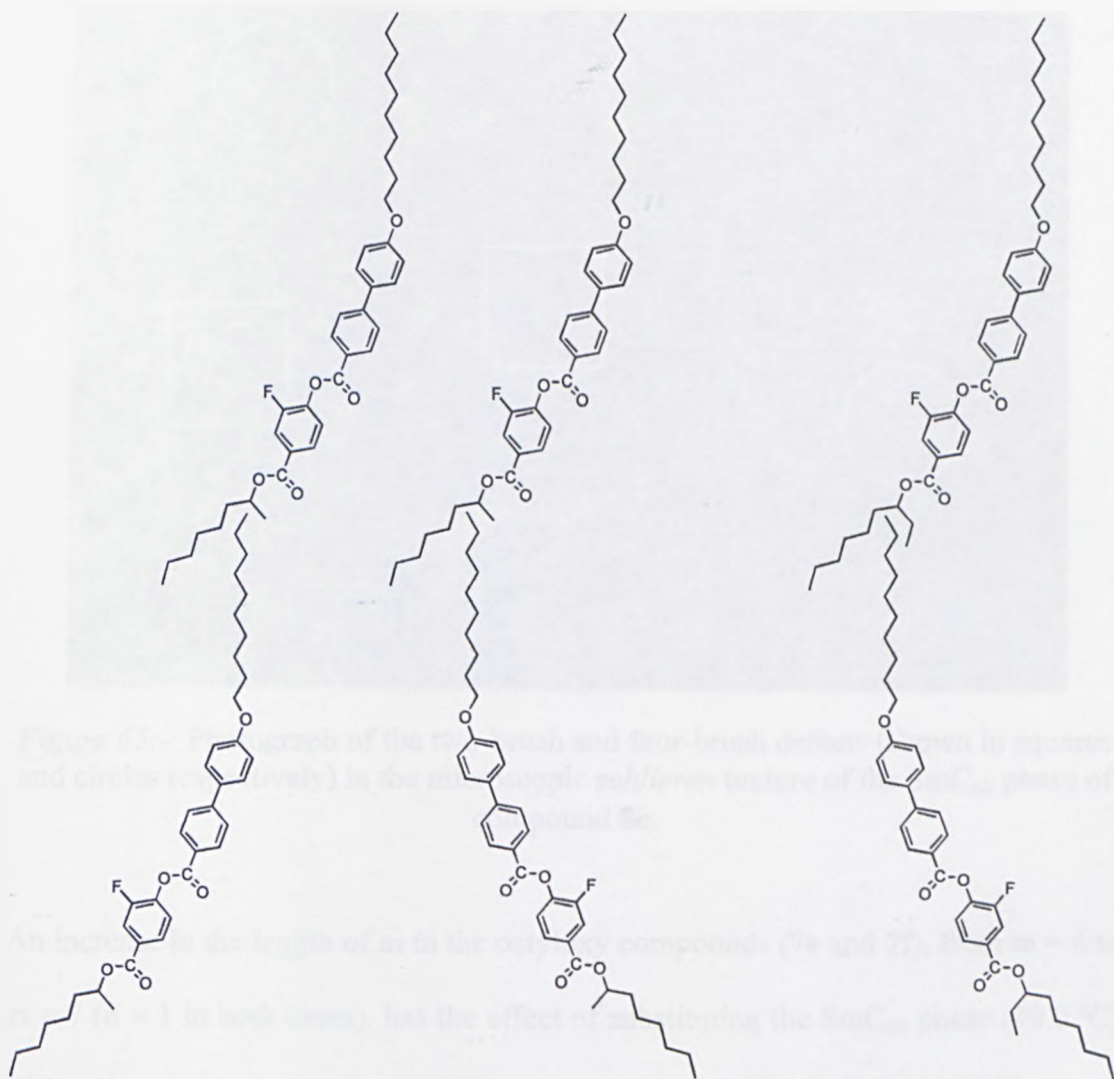
n = 1, m = 6: both SmC and SmC$_{alt}$ possible   n = 2, m = 6: restricted rotation, greater interdigitation; SmC$_{alt}$ sterically favoured

Figure 64:- Comparison of the interdigitation between the unsymmetrically-substituted methyl and ethyl-heptyl branched chains (R')
in the decyloxy (R) compounds **8a** and **8b**.

The photograph below (*figure 65*) shows the *schlieren* texture of the SmC$_{alt}$ phase of compound **8c** through crossed polarisers. The characteristic two-brush and four-brush defects common to anticlinic SmC phases are clearly visible (marked).
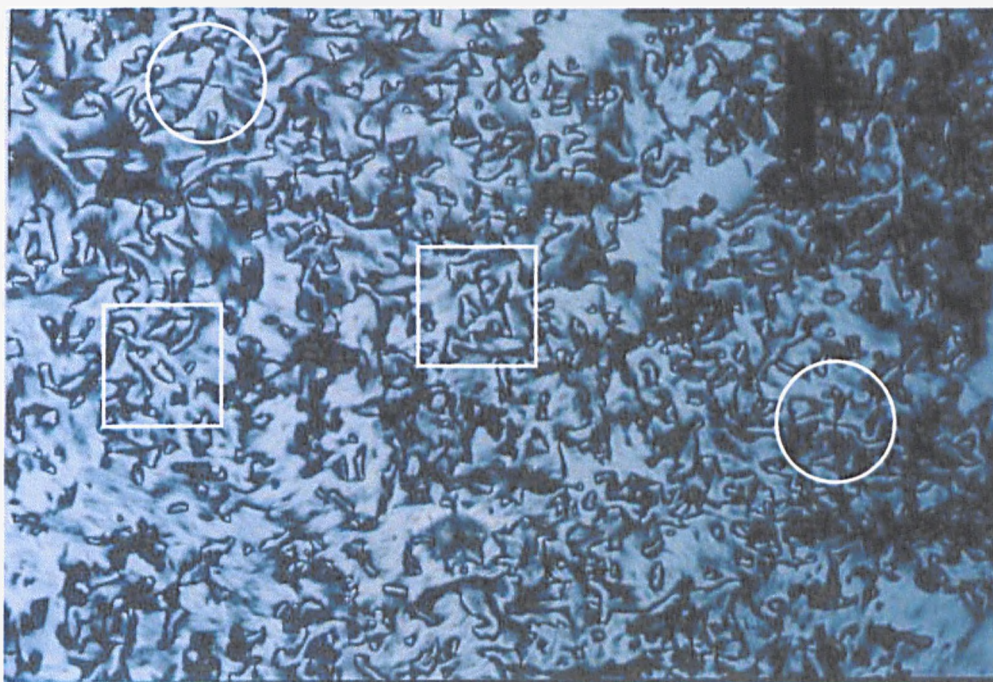
Figure 65:- Photograph of the two-brush and four-brush defects (shown in squares and circles respectively) in the microscopic *schlieren* texture of the SmC_{alt} phase of compound **8c**.

An increase in the length of m in the octyloxy compounds (**7e** and **7f**), from m = 6 to m = 7 (n = 1 in both cases), has the effect of substituting the SmC_{alt} phase (49.0 °C) with a SmC phase at a lower temperature (28.0 °C). A reduction in the length of m in the octyloxy compounds (compounds **7h** and **7g**) from m = 6 to m = 5 (n = 2 in both cases) has the effect of lowering all of the transition temperatures by only a few degrees. Increasing the length of n from 2 to 3 carbons for this material (compound **6b**, m = 5) lowers the SmA transition temperature, but does not affect the SmC_{alt} transition temperature greatly.

Graphs 5a and *5b* below show the transition temperatures and phases of the octyloxy, decyloxy and dodecyloxy compounds with n = 1, m = 6 (compounds **7e**, **8a** and **8c**); and n = 2, m = 6 (compounds **7h**, **8b** and **8d**). Compound **7e** is the only

material of this type (n = 1, m = 6) which forms a SmC_{alt} phase without an intermediate SmC phase.

Graph 5a:- Transition temperatures and phase sequences of the n = 1, m = 6 compounds.
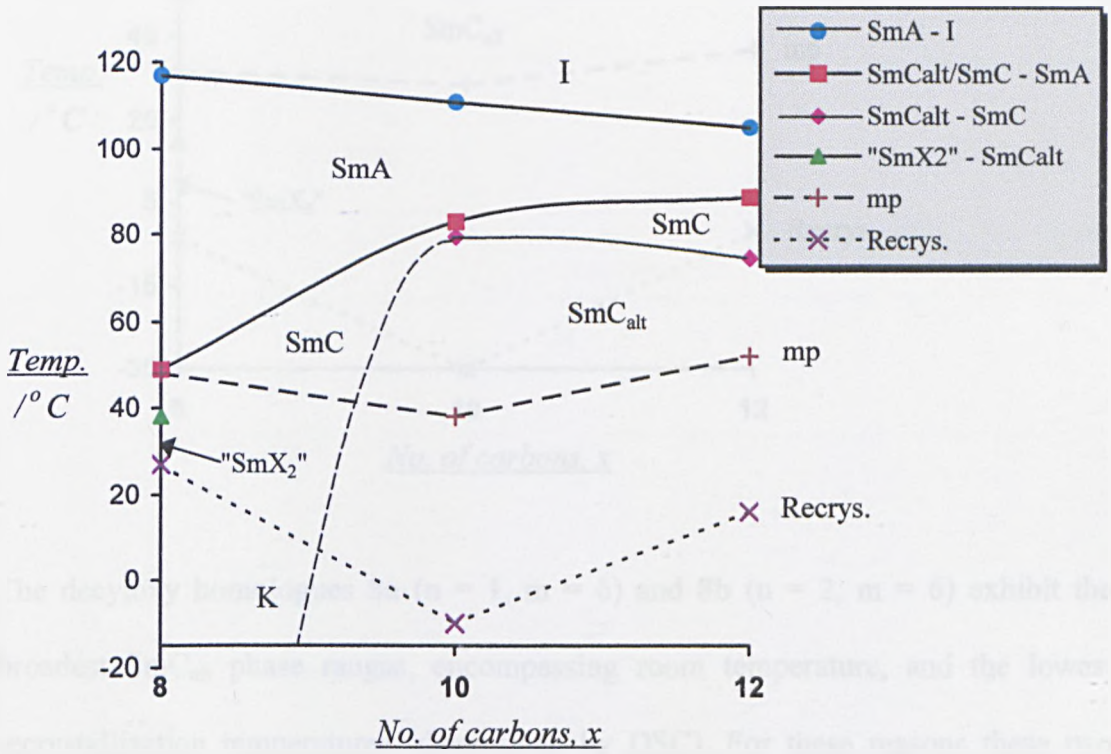
Graph 5b:- Transition temperatures and phases of the n = 2, m = 6 compounds.
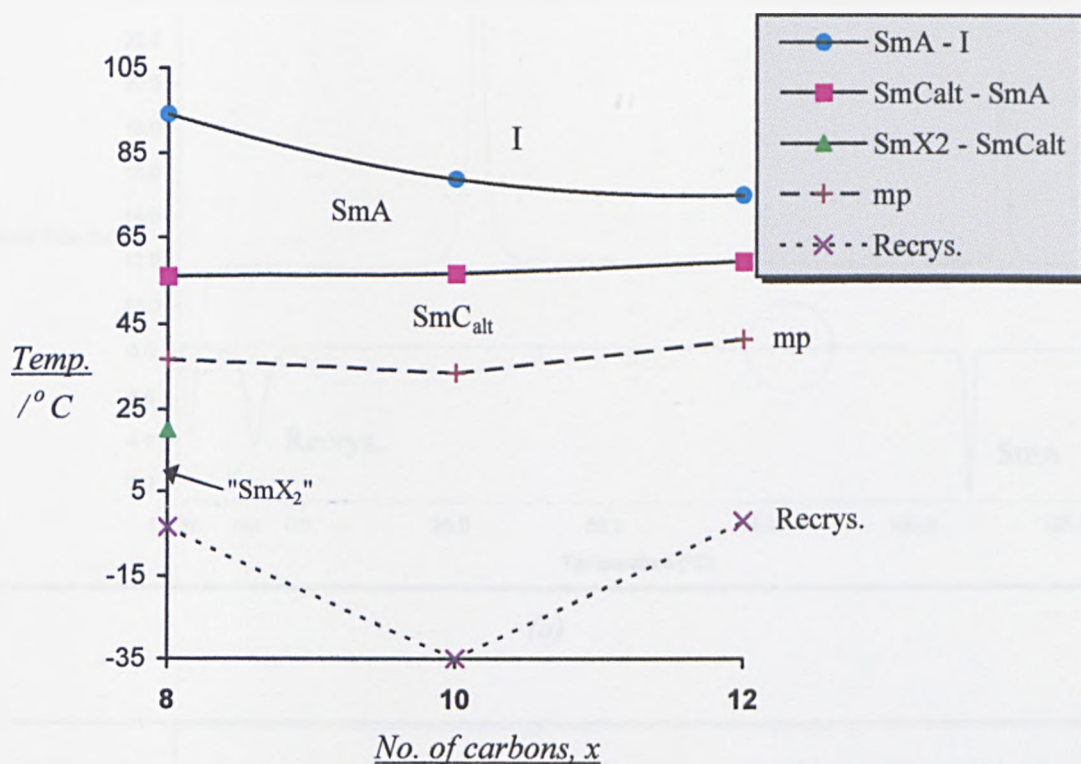
The decyloxy homologues **8a** (n = 1, m = 6) and **8b** (n = 2, m = 6) exhibit the broadest SmC$_{alt}$ phase ranges, encompassing room temperature, and the lowest recrystallization temperatures (determined by DSC). For these reasons these two materials would be the most suitable materials from this series (and indeed all the unsymmetrically-substituted materials discussed in this sub-section) as hosts for model binary chiral-dopant antiferroelectric mixtures.

The expanded region of the DSC plot of compound **8a** (*figure 66*) shows that the SmC and SmC$_{alt}$ phases arise *via* an apparent weak first order and first order phase transitions, respectively, on cooling from the SmA phase. The expanded region of the DSC plot for compound **8b** shows that as in chiral antiferroelectric systems the SmC$_{alt}$ phase arises directly from the SmA phase via a first order transition (*figure 67*).
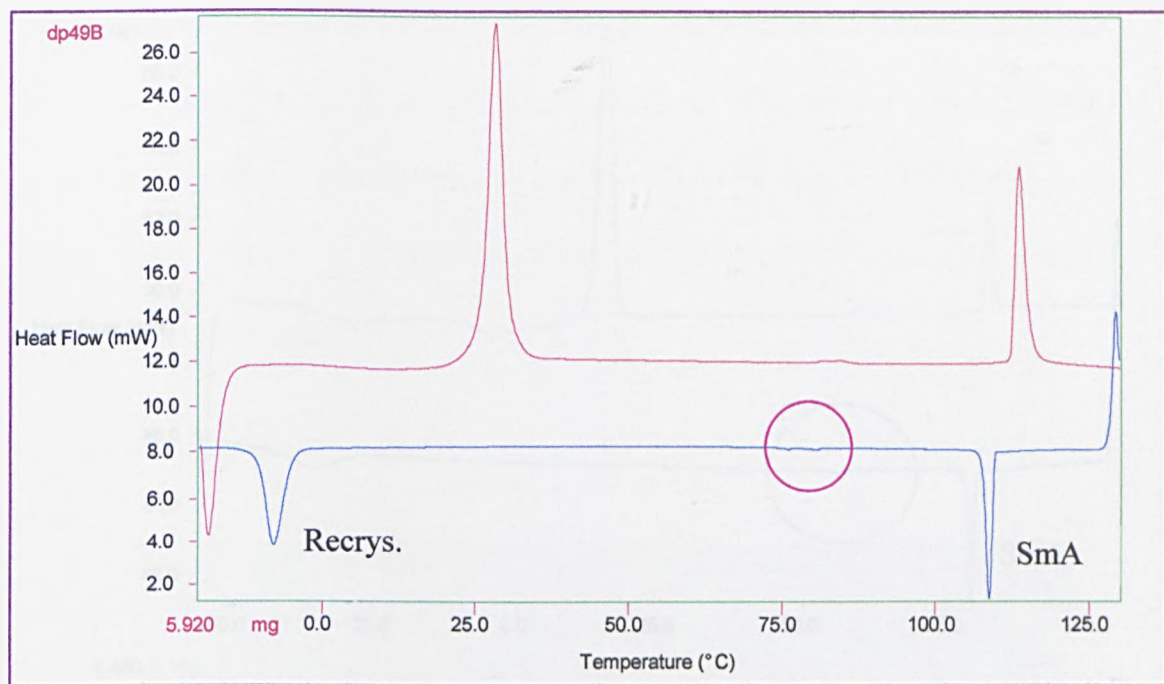
(a)
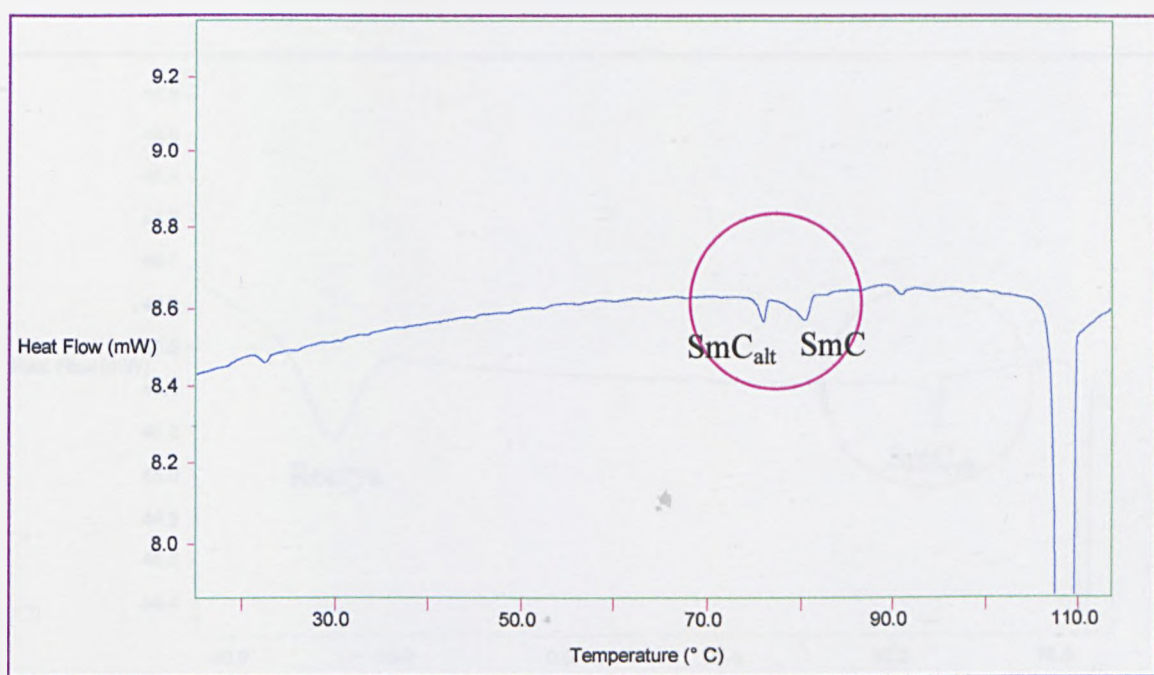
(b)

Figure 66:- DSC plot of compound **8a** *(a)*, and expanded region showing the SmC and SmC$_{alt}$ phase transitions (circled) *(b)*.
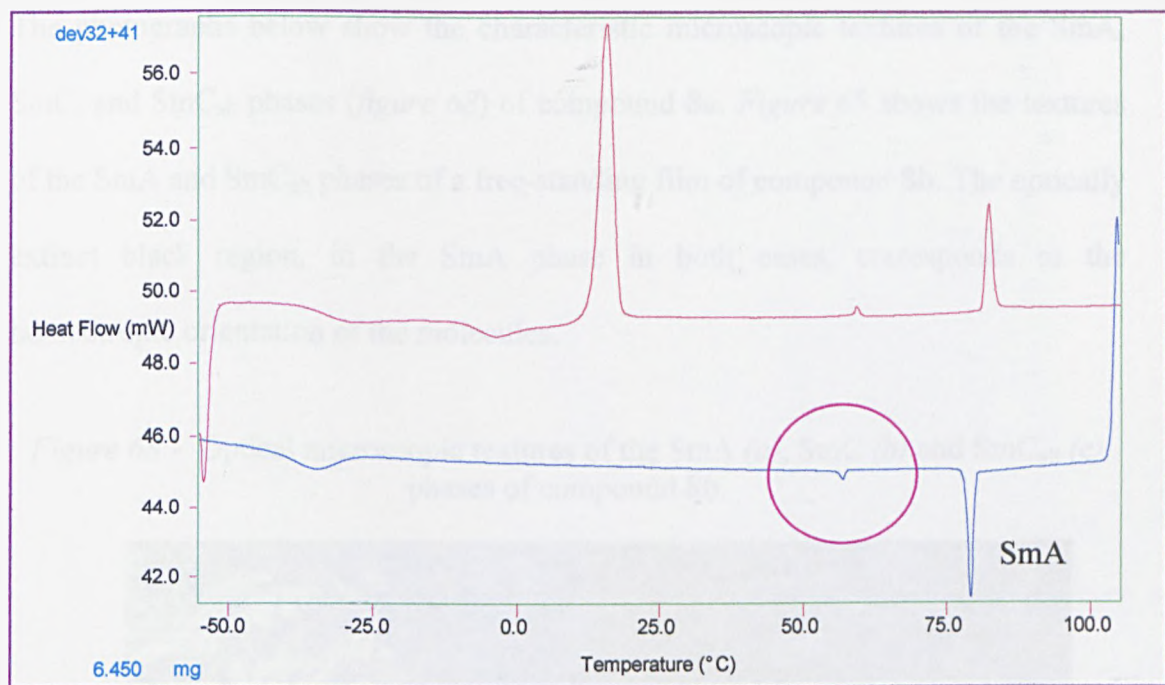
(a)
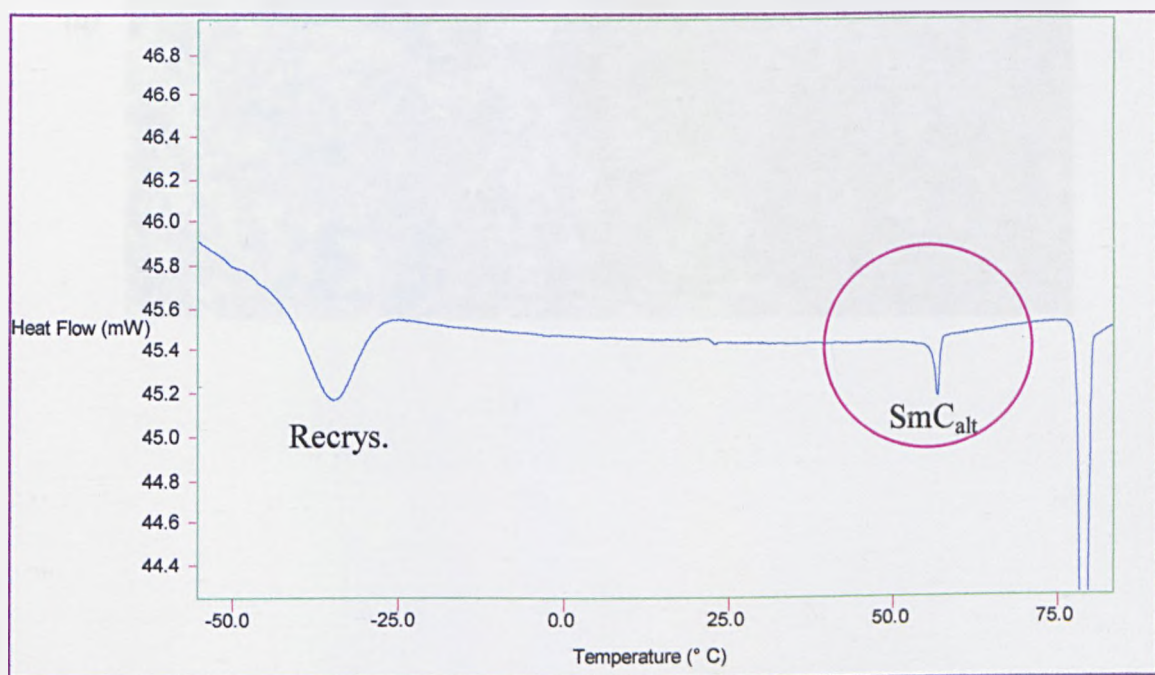
(b)

Figure 67:- DSC plot of compound **8b** *(a)*, and expanded region showing the SmC$_{alt}$ phase transition (circled) *(b)*.

The photographs below show the characteristic microscopic textures of the SmA, SmC, and SmC$_{alt}$ phases (*figure 68*) of compound **8a**. *Figure 69* shows the textures of the SmA and SmC$_{alt}$ phases of a free-standing film of compound **8b**. The optically extinct black region, in the SmA phase in both cases, corresponds to the homeotropic orientation of the molecules.

Figure 68:- Optical microscopic textures of the SmA *(a)*, SmC *(b)* and SmC$_{alt}$ *(c)* phases of compound **8b**.

(a)
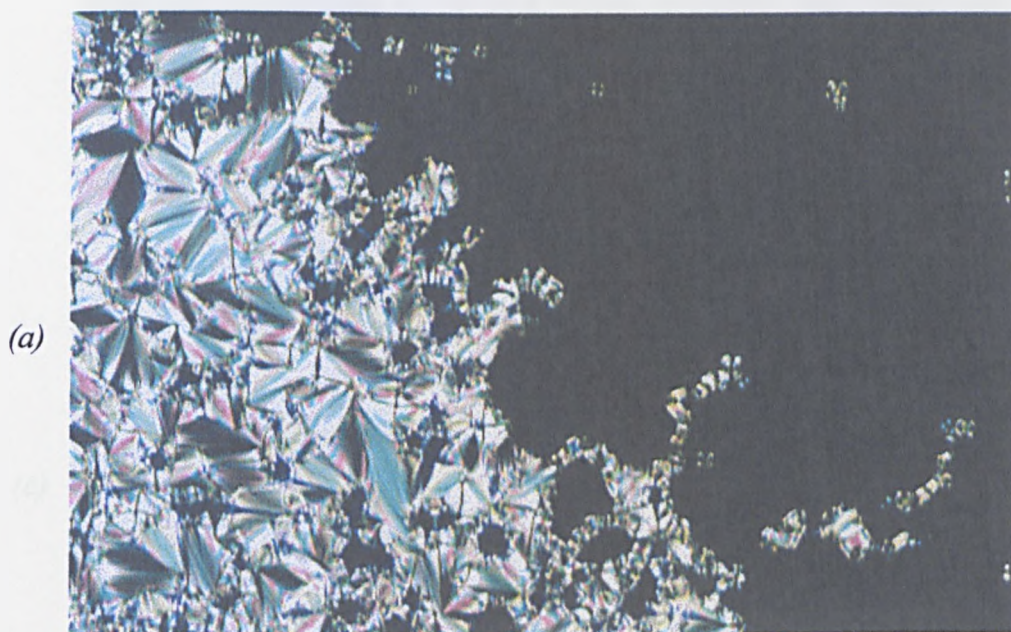
(b)
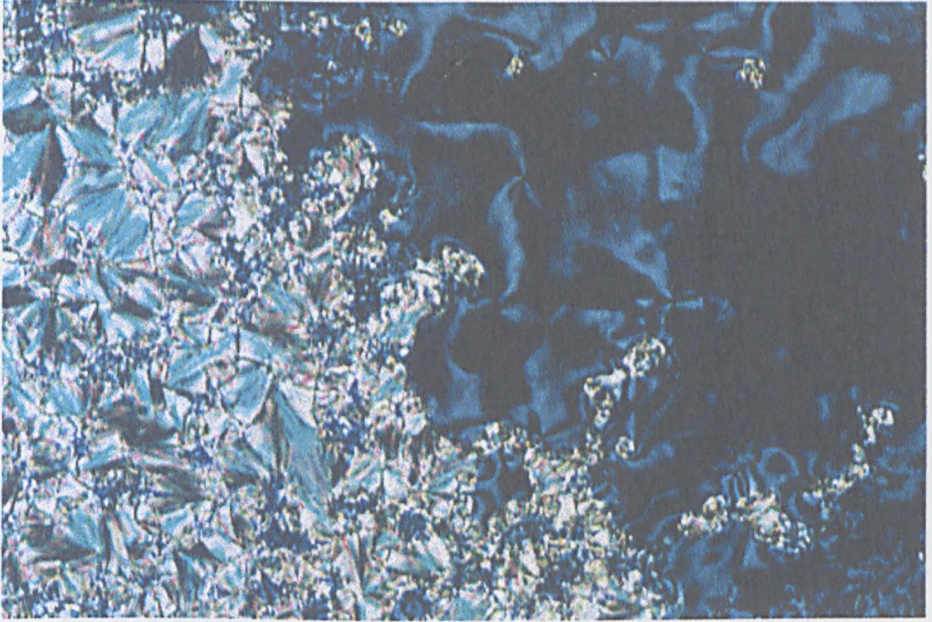
(c)
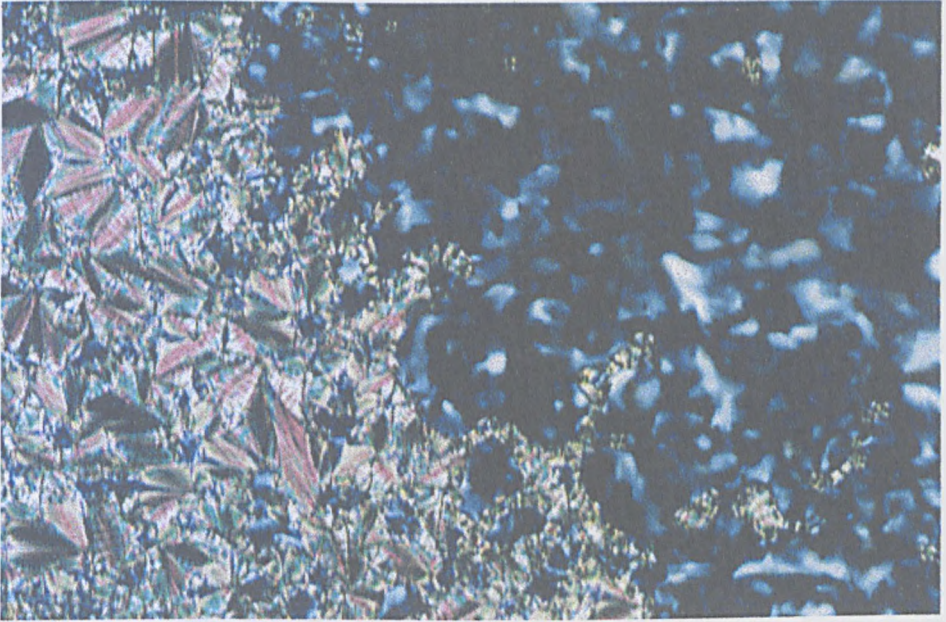
Figure 69:- Microscopic optical textures of the SmA *(a)* and SmC$_{alt}$ *(b)* phases of a free-standing film of compound **8b**.

(a)
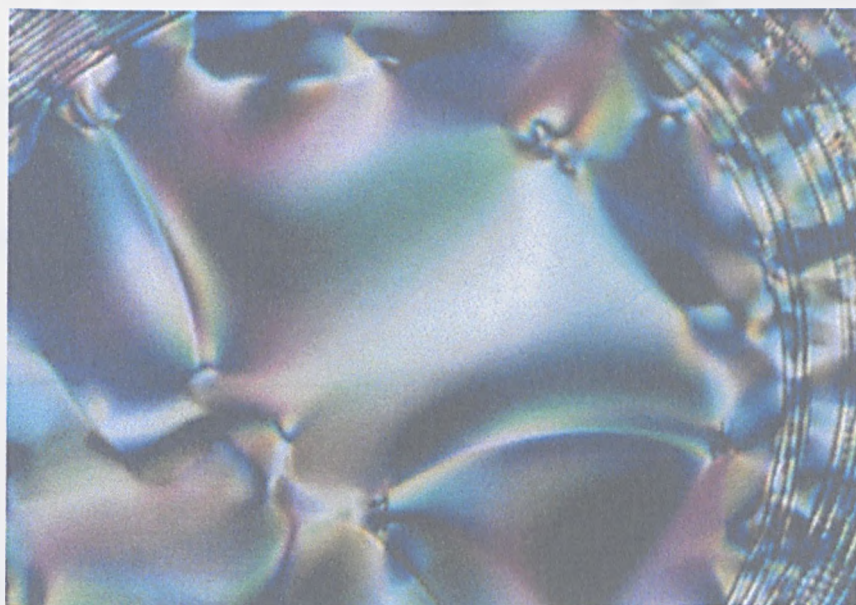
(b)

The identification of the SmC$_{alt}$ phases, in these two host materials, was confirmed by miscibility phase diagrams with the standard material, (*S*)-MHPOBC. Complete

miscibility was observed between the SmC_A^* phase of the standard material and the SmC_{alt} phase of both test materials across the entire phase diagrams (*figures 70(a) and (b)*).
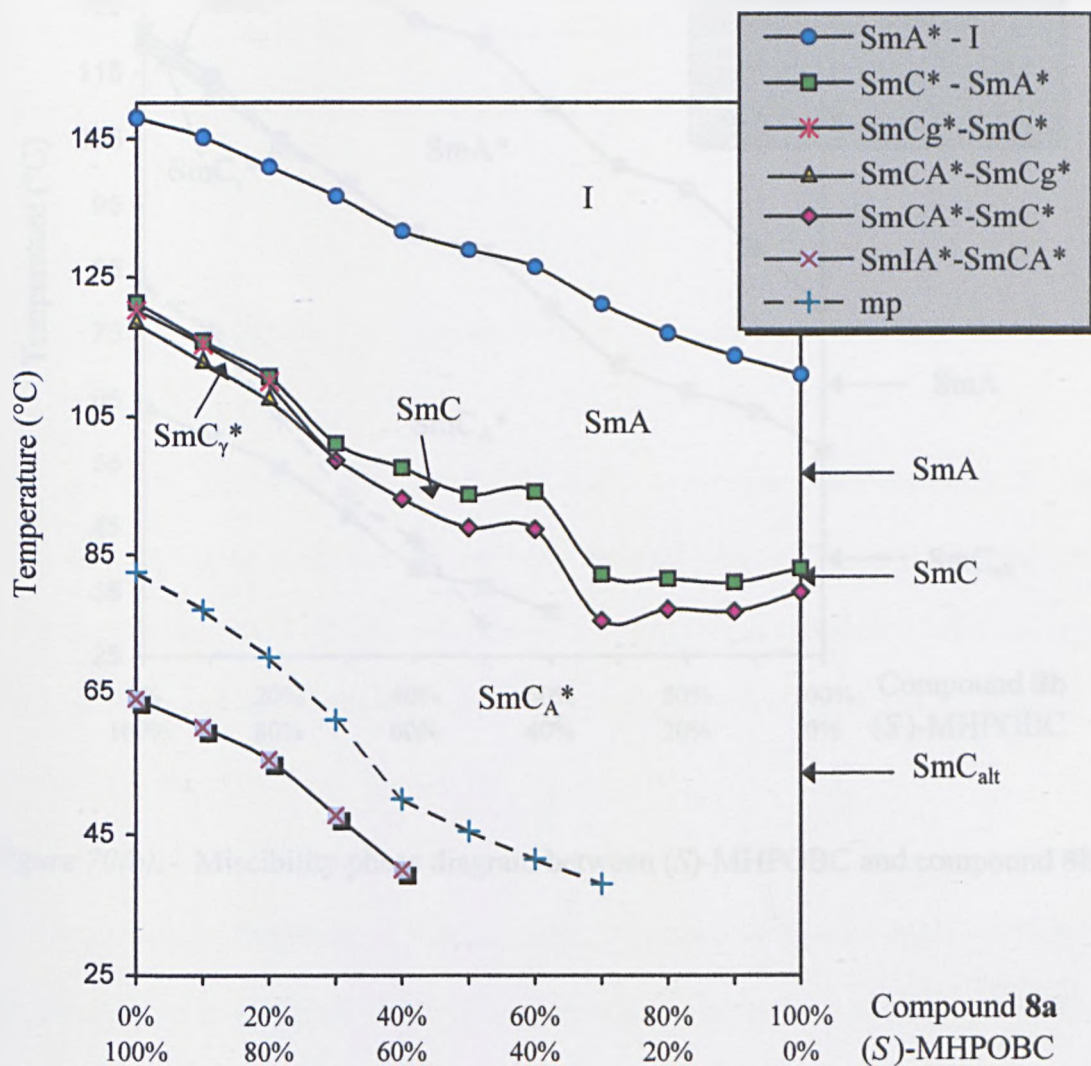
Figure 70(a):- Miscibility phase diagram between (S)-MHPOBC and compound **8a**.
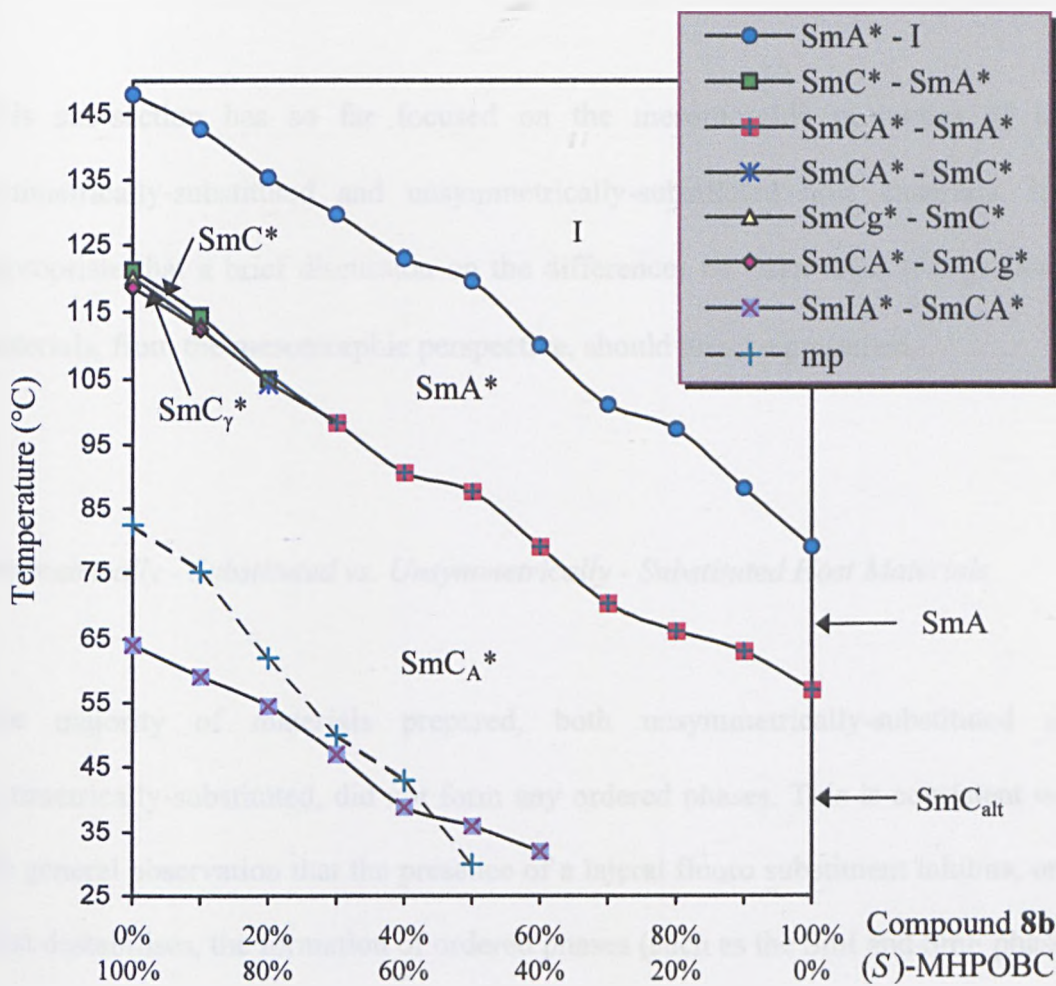
Figure 70(b):- Miscibility phase diagram between (S)-MHPOBC and compound **8b**.

This sub-section has so far focused on the mesomorphic properties of both symmetrically-substituted and unsymmetrically-substituted host materials. It is appropriate that a brief discussion on the differences between these two groups of materials, from the mesomorphic perspective, should now be presented.

Symmetrically - Substituted vs. Unsymmetrically - Substituted Host Materials

The majority of materials prepared, both unsymmetrically-substituted and symmetrically-substituted, did not form any ordered phases. This is consistent with the general observation that the presence of a lateral fluoro substituent inhibits, or at least destabilises, the formation of ordered phases (such as the SmI and SmF phases) in smectic systems.

With regard to the formation of SmC_{alt} phases, two observations are apparent; firstly, the symmetrically-substituted materials generally appear to form monotropic SmC_{alt} phases (determined by optical microscopy and DSC), whereas the unsymmetrically-substituted materials generally exhibit enantiotropic SmC_{alt} phases (*table 21*). Secondly, the SmC_{alt} phase stabilities of the unsymmetrically-substituted materials are generally higher than those of the symmetrically substituted materials. An explanation for these observations may lie in the differences in the steric and transverse dipole contributions, to the formation of alternatingly-tilted phases, between the swallow-tailed and non swallow-tailed materials.

Table 21:- Comparison of the occurrence of monotropic and enantiotropic SmC$_{alt}$ phases between the symmetrically-substituted and unsymmetrically-substituted materials.

Compound	Symmetrically-Substituted	Unsymmetrically–Substituted	Monotropic SmC$_{alt}$	Enantiotropic SmC$_{alt}$
1c	●		◆	
2a	●		◆	
2b	●		◆	
2c	●		◆	
2d	●		◆	
2e	●		◆	
2f	●		◆	
2g	●		◆	
3a	●		◆	
3b	●		◆	
3c	●		◆	
3d	●		◆	
4a	●		◆	
4b	●		◆	
4c	●		◆	
5a	●		◆	
5d	●			▲
9a	●			▲
6a		■	◆	
6b		■		▲
6c		■	◆	
7b		■		▲
7c		■		▲
7e		■		▲
7g		■		▲
7h		■		▲
8a		■		▲
8b		■		▲
8c		■		▲
8d		■		▲
9b		■		▲

Swallow-tailed materials are believed to form SmC$_{alt}$ phases principally by the interdigitation of the branched and unbranched alkyl chains between molecules in neighbouring smectic layers [79, 109]. The contribution, to the formation of this

phase, may then be regarded as being mostly steric in nature. The transverse dipole in the molecule is minimal in comparison with unsymmetrically-substituted materials (*figure 71*), which possess a chiral centre, hence a measurable spontaneous polarisation (in the optically pure forms) [25]. In the racemic form the contributions to the formation of SmC_{alt} phases are also speculated on as being close to a balance between these two contributions, in conjunction with the pair formation of like enantiomers [78]. It may of course also be the case that since symmetric substitution results in higher melting points the likelihood of a monotropic phase would be greater in comparison with the unsymmetrically-substituted materials. An increase in the length of the short alkyl unit, at the chiral centre from $n = 1$ to $n = 2$ (*figure 72*) increases steric interactions and favours an alternatingly-tilted smectic phase. This is observed as the exclusion of the SmC phase in many examples of antiferroelectric materials, both chiral and racemic [110], on cooling from the SmA* / SmA phase. The observation that the stability of the SmC_{alt} phase sometimes decreases (as in the decyl and dodecyl racemic materials 8a – 8d) may relate to the scale of interaction of branched chains in one smectic layer with the unbranched alkyl chains in the adjacent layer. With longer unbranched chains we could expect the interactions, between the molecules, to be more disordered. The rotational entrapment of the ethyl group may favour a direct SmA to SmC_{alt} transition, although a decrease in the transition temperature may result, due to the "fluidity" of the molecules.

Unsymmetrically-substituted   Unsymmetrically-substituted

(Minimal / negligible transverse dipole)   *(transverse dipole arises)*
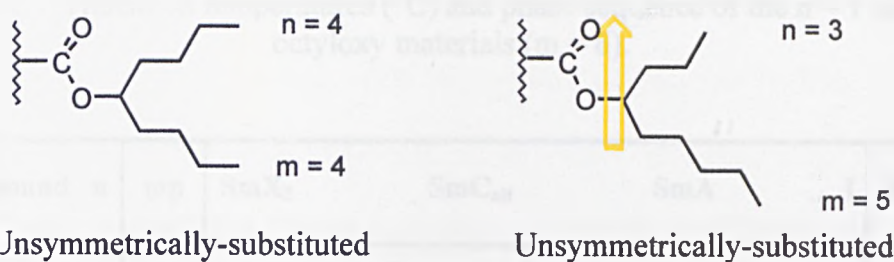
Figure 71: – Comparison between the transverse dipoles present at the branching carbon atom in symmetrically and unsymmetrically-substituted materials (only branching sections of molecules shown).

8a   **8b**

Steric interactions small   Steric interactions
                                    (rotational hindrance) greater
                                    $\therefore$ SmC$_{alt}$ phase stabilised
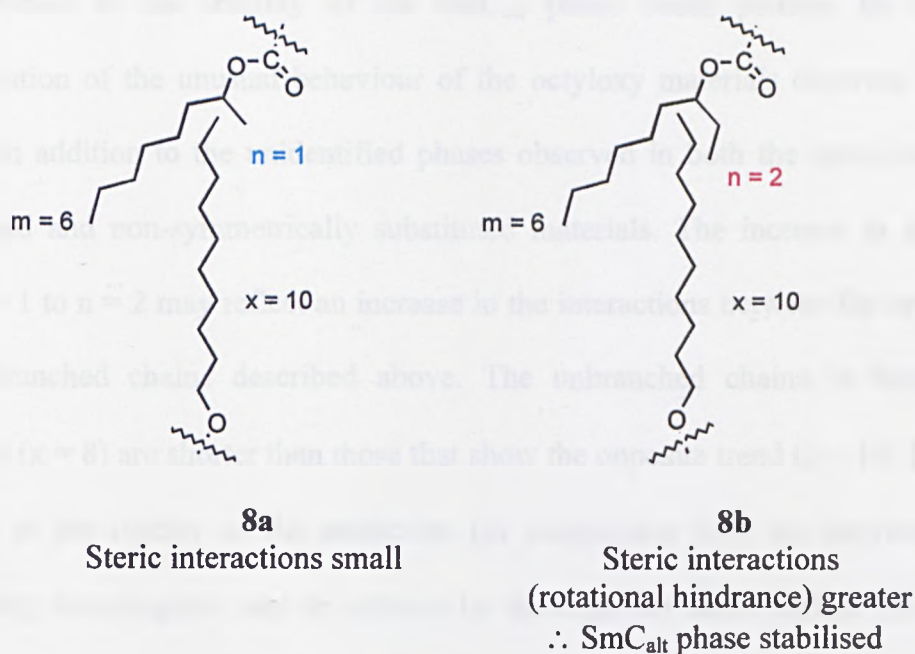
Figure 72:- Effect on steric interactions on increasing the length of the shorter branched unit at the chiral centre, from methyl (n = 1) to ethyl (n = 2) for the decyloxy compounds **8a** and **8b** (only branched & unbranched chains shown).

An obvious exception to this is the behaviour in the racemic octyloxy materials **7e** and **7h**; in this case the reverse of the *general* trend described above appears to be the case. The n = 2 material has lower transition temperatures than the n = 1 material (m = 6 in both cases, *table 22*) for all transitions except the SmC$_{alt}$ phase.

Table 22:- Transition temperatures (°C) and phase sequence of the n = 1 and n = 2 octyloxy materials (m = 6).

Compound	n	mp	SmX$_2$		SmC$_{alt}$		SmA		I	Recrys
7e	1	48	•	38.0	•	49.0	•	117.0	•	27
7h	2	37	•	28.0	•	56.2	•	94.2	•	<25

The increase in the stability of the SmC$_{alt}$ phase could perhaps be another manifestation of the unusual behaviour of the octyloxy materials observed so far. This is in addition to the unidentified phases observed in both the symmetrically-substituted and non-symmetrically substituted materials. The increase in stability from n = 1 to n = 2 may reflect an increase in the interactions between the branched and unbranched chains described above. The unbranched chains in these two materials (x = 8) are shorter than those that show the opposite trend (x = 10, 12). An increase in the rigidity of the molecules (in comparison with the decyloxy and dodecyloxy homologues) may be inferred by the relatively short chains. The effect of increased hindered rotation of the n = 2 material (7h), in comparison with the n = 1 material (7e), together with the reduced "fluidity" of the molecules, may account for the increase in the stability of the SmC$_{alt}$ phase. The effect on the spontaneous polarisation, in the purely chiral versions of these two octyloxy materials, will be investigated in the following section of this chapter.

In terms of suitable host materials for the model chiral-dopant antiferroelectric mixtures, the unsymmetrically-substituted materials appear to display the more

desirable properties than the symmetrically-substituted materials. These include: enantiotropic SmC_{alt} phases with wide temperature ranges, low melting points and high SmC_{alt} phase stabilities. For this reason more attention was paid to the evaluation of the selected unsymmetrically-substituted host materials, than the symmetrically-substituted materials, in **section (iv)** of this chapter. The structures of the most suitable materials intended for further studies in **section (iv)**, selected from both categories, are shown in *table 23* below.

Table 23:- Structures and transition temperatures (°C) of the selected SmC_{alt}-forming host materials for evaluation in the model binary chiral-dopant antiferroelectric mixtures.
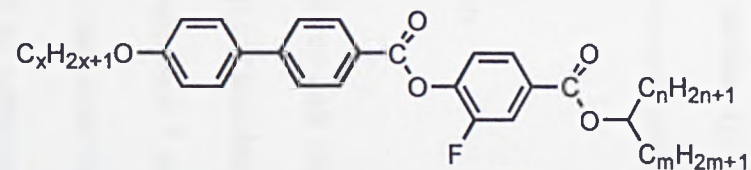
Compound	x	n	m	mp	"SmY"		SmC_{alt}		SmC		SmA		I	Recrys.
2c	8	4	4	56	•	(28.0)	•	(54.0)	-	-	•	85.0	•	<25
4c	12	5	5	49	-	-	•	(27.0)	-	-	•	(43.8)	•	<25
8a	10	1	6	38	-	-	•	79.5	•	83.0	•	111.0	•	<25
8b	10	2	6	34	-	-	•	57.0	-	-	•	79.0	•	<25

Section (iii):

DOPANT MATERIALS

Overview

The aim of this section was to identify the most suitable materials for use as dopants for mixing with the selected achiral host materials. The first series of potential dopants, antiferroelectric liquid-crystalline materials, were prepared according to the syntheses described in **Section (i)**. The second series of materials, the ferroelectric dopants [103], were previously synthesised by Dr. N. Gough.

Antiferroelectric Dopants

The transition temperatures and phase sequences of the first series of materials, related to (S)-12F1M7 [111] are shown below (*table 24*). All the compounds exhibit a SmA* phase. Only compound **1** (n = 8) shows a direct SmA* - SmC$_A$* transition whereas in compounds **2** and **3** the SmC$_A$* phase arises via a SmC* phase. A SmC$_\alpha$* phase was observed only in compound **10d** (*figures 73a – e*). The SmC$_A$* phases in compounds **10b – 10d** arise *via* the formation of a SmC$_\gamma$* phase.

Graph 6 shows the phases and transition temperatures of the chiral materials (compounds 10a – 10e) which were determined by optical microscopy and verified by DSC. An odd-even effect is clearly visible between the compounds from x = 9 to x = 12. The material with the lowest melting point, lowest recrystallization temperature, and widest SmC$_A$* phase was found to be 10c ("(S)-10F1M7").

135

Table 24:- Transition temperatures (°C) and phases of the homologous series of chiral antiferroelectric liquid crystals (related to (*S*)-12F1M7).
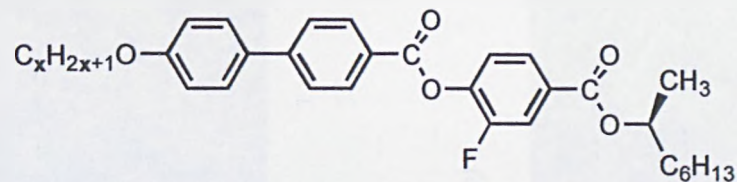
Compound	x	mp	SmC$_A$*		SmC$_\gamma$*		SmC*		SmC$_\alpha$*		SmA*		I	Recrys.
10a	8	55	●	(47.5)	-	-	-	-	-	-	●	118.4	●	39
10b	9	56	●	67.2	●	70.8	●	73.4	-	-	●	112.4	●	30
10c	10	45	●	78.8	●	80.3	●	82.3	-	-	●	109.2	●	24
10d	11	56	●	67.6	●	69.2	●	76.1	●	84.0	●	107.5	●	28
10e {(*S*)-12F1M7}	12	54	●	77.0	●	81.7	●	89.3	-	-	●	107.0	●	37

Figures 73a – e:- Changes in the focal-conic texture of compound **10d** on cooling from the isotropic liquid.
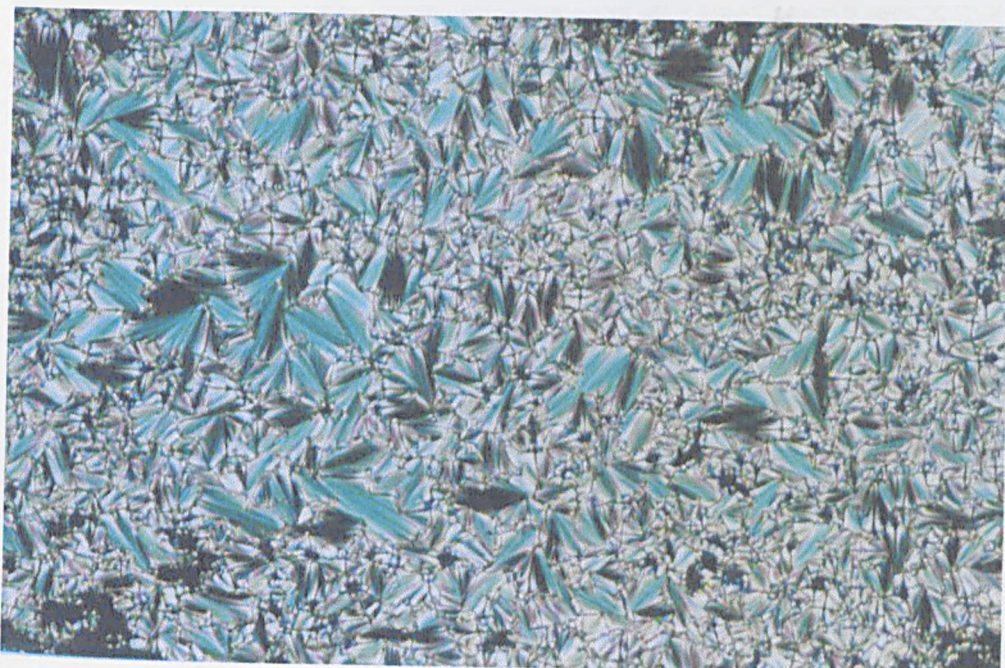
(a) SmA*
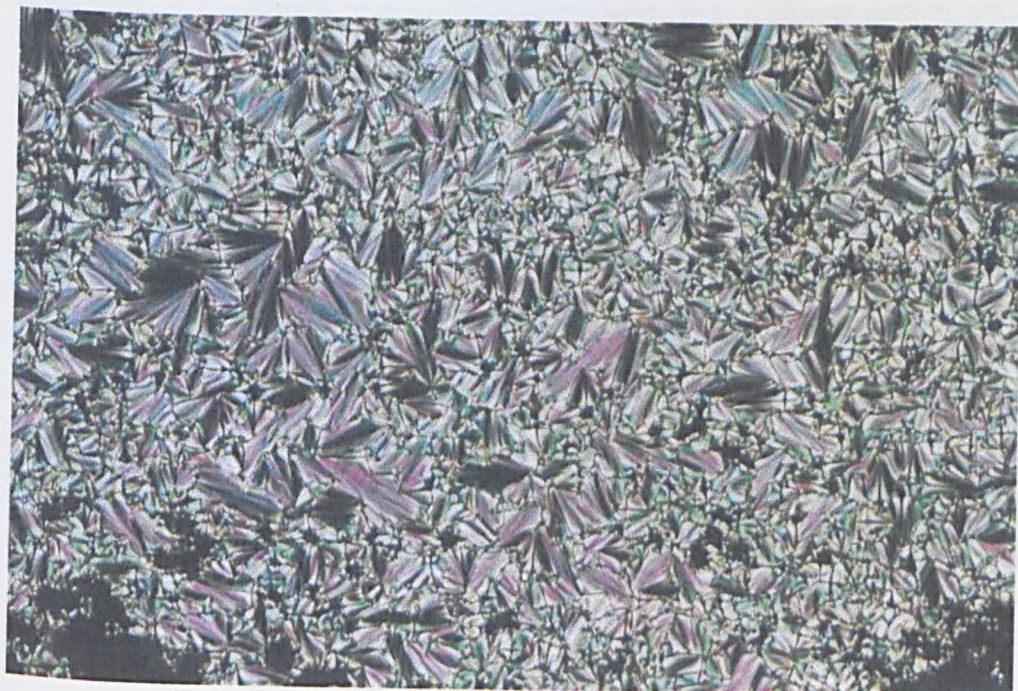
(b) SmC$_\alpha$*
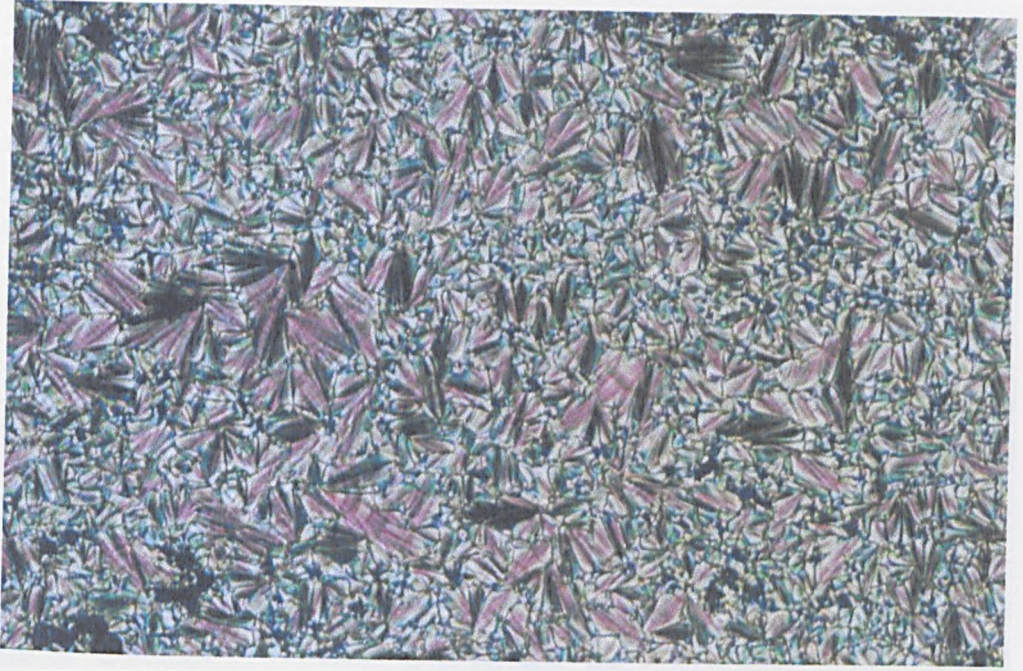
(c) SmC*
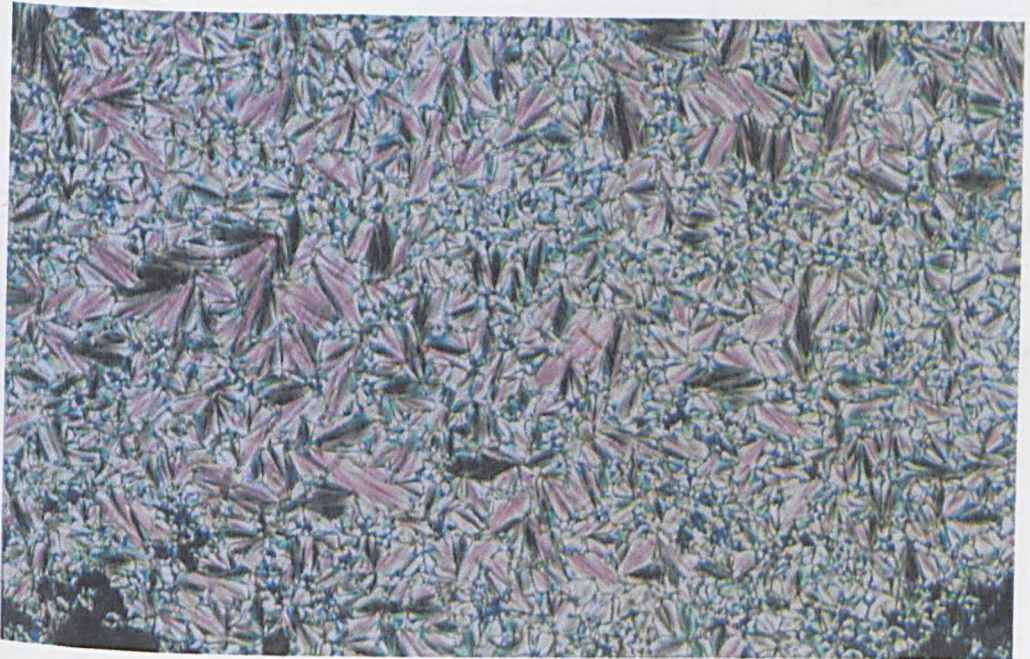
(d) SmC$_\gamma$*

(e) SmC$_A$*
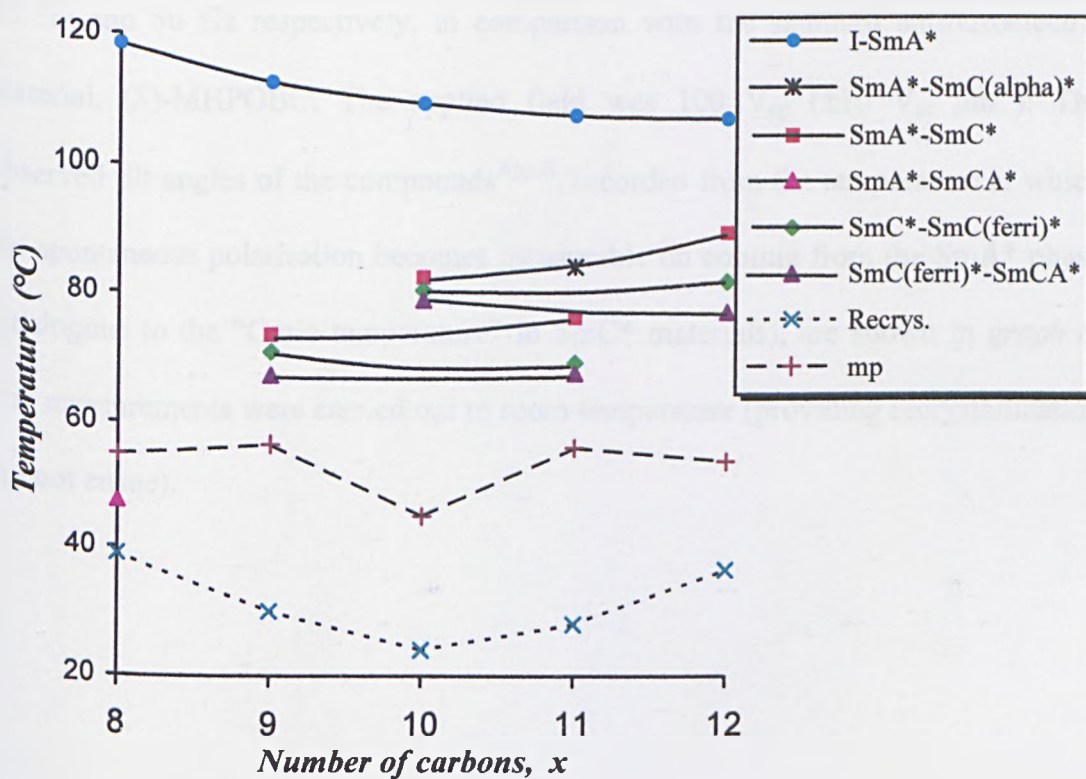
Graph 6:- Transition temperatures and phases of the chiral materials
11a – 11e (x = 8 to x = 12).

Although compound **10c** possesses the most advantageous mesomorphic properties in the series, for a potential mixture consisting only of chiral (antiferroelectric) components, the most useful material for a chiral dopant would in fact be the material with the largest spontaneous polarisation. A large spontaneous polarisation is an important property for a dopant since only a small quantity of a dopant should be utilized in chiral-dopant mixtures, in order to preserve the phase width of the host material(s) [99]. To determine the most suitable material (from the series), for use as a dopant in the doped antiferroelectric mixtures, the spontaneous polarisation of all the materials was measured as a function of *reduced temperature*[App.E].

Graphs 7(a) and *7(b)* show the spontaneous polarisation values obtained for the materials (**10a** – **10e**) in test cells with 5 μm plate separation[App.F], at a frequency of 20 Hz and 50 Hz respectively, in comparison with the standard antiferroelectric material, (*S*)-MHPOBC. The applied field was 100 V_{pp} (±10 V_{ac} μm^{-1}). The observed tilt angles of the compounds[App.G], recorded from the temperature at which the spontaneous polarisation becomes measurable on cooling from the SmA* phase (analogous to the "Curie temperature" in SmC* materials), are shown in *graph 8*. The measurements were carried out to room temperature (providing recrystallization did not ensue).

Graph 7:- Measured spontaneous polarisation values of compounds **10a** – **10e** in comparison to (*S*)-MHPOBC (**10a**), at 20 Hz *(a)*, and 50 Hz *(b)*.

141
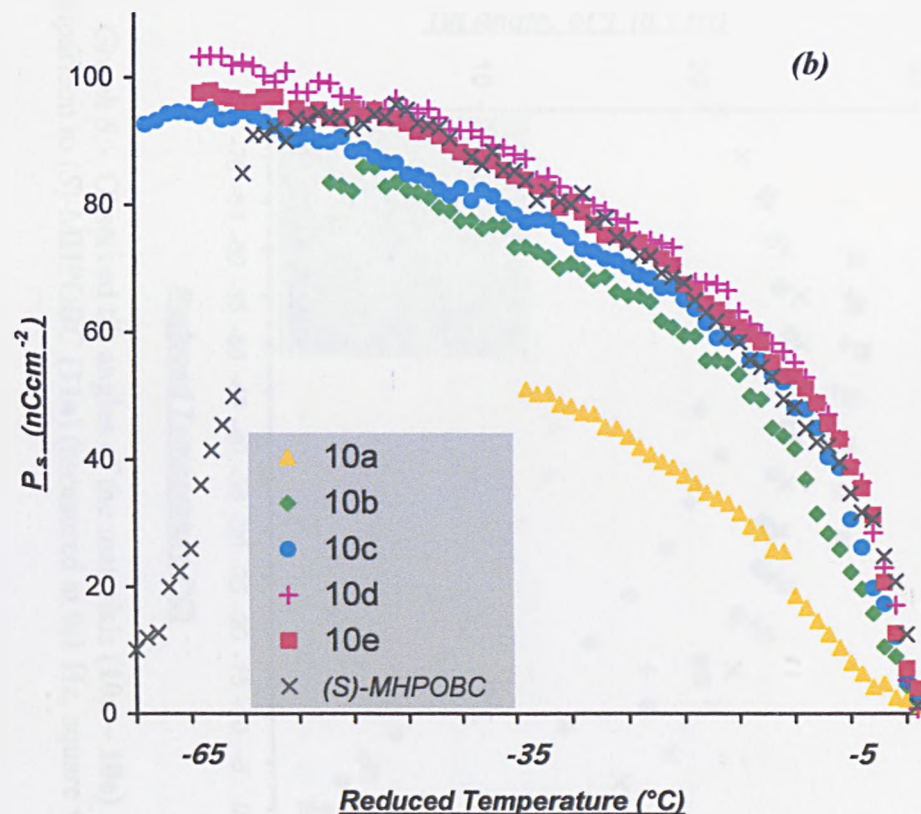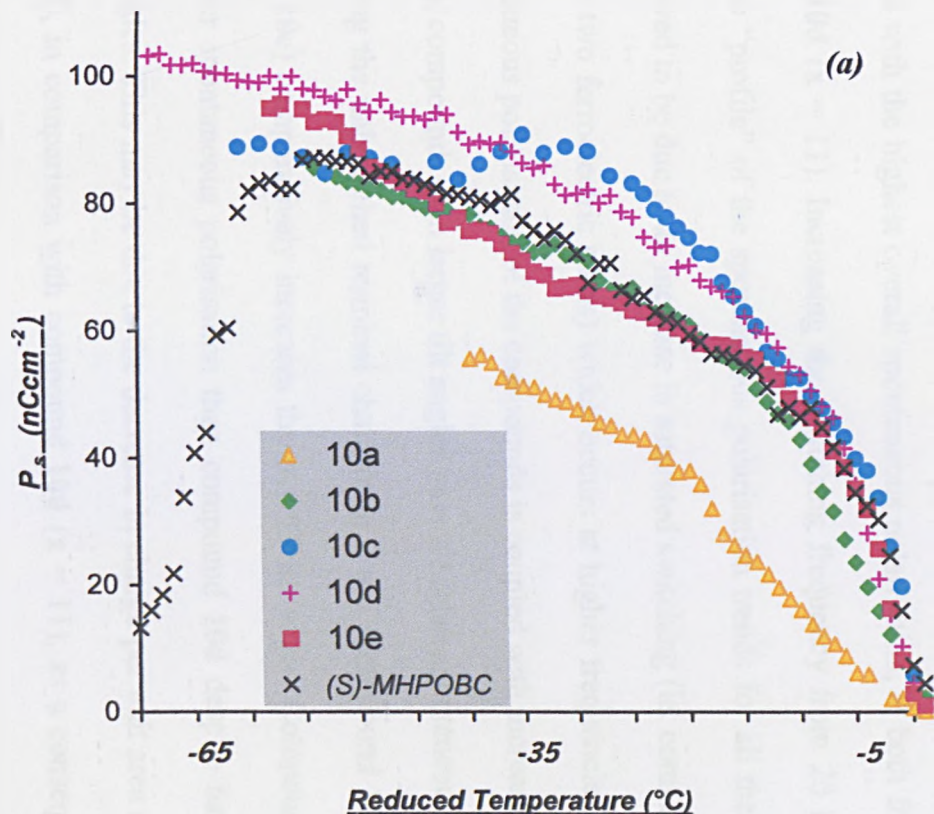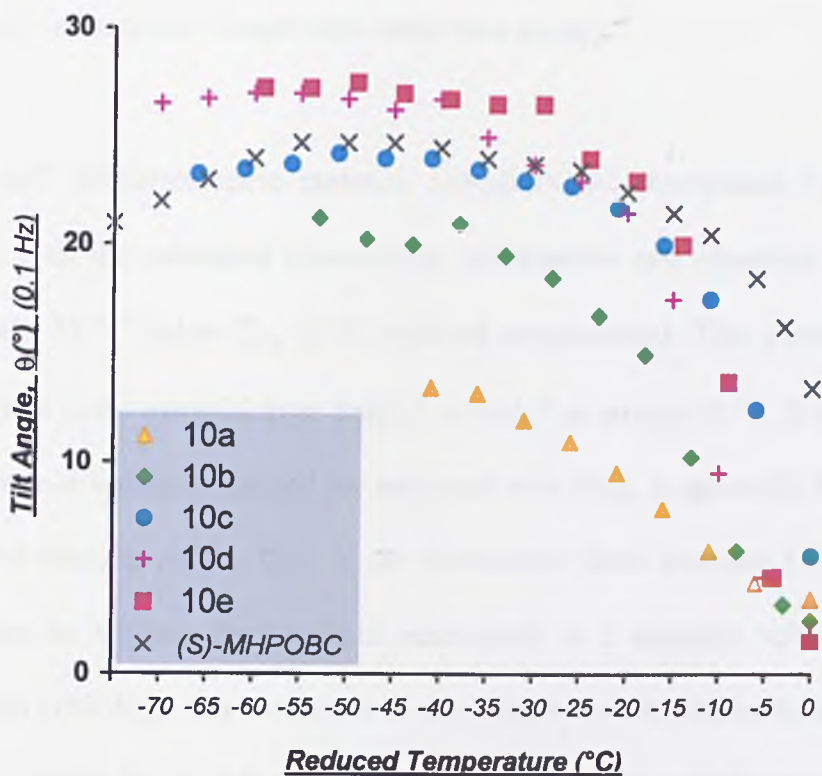
Graph 8:- Observed tilt angles of the materials (**10a – 10e**)
in comparison to (*S*)-MHPOBC (**11a**) (measured at 0.1 Hz, square wave).

The material with the highest overall spontaneous polarisation, at both frequencies, is compound **10d** ($x = 11$). Increasing the switching frequency from 20 Hz to 50 Hz improves the "profile" of the spontaneous polarisation trends for all the compounds. This is believed to be due to an increase in saturated switching (ie. complete switching between the two ferroelectric states) which occurs at higher frequencies. An increase in the spontaneous polarisation of the compounds is coupled with increases in tilt angle (on cooling); compounds with larger tilt angles have a higher spontaneous polarisation, and increasing the unbranched terminal chain from $x = 8$ (compound **10a**) to $x = 12$ (compound **10e**) comparatively increases the overall tilt angle. Compound **10e** has a slightly lower spontaneous polarisation than compound **10d** despite having slightly larger tilt angles. This may be due to the decrease in charge per unit area of compound **10e** ($x = 12$), in comparison with compound **10d** ($x = 11$), as a consequence of the

small increase in molecular length (one methylene group).

The "standard" antiferroelectric material, (S)-MHPOBC (compound **11a**) shows a decrease in both the measured spontaneous polarisation and observed tilt angle at approximately 55 °C below T_{Cx} (0 °C reduced temperature). This corresponds to a phase transition in the material from SmC_A^* to SmI_A^* at around 60 °C. It is understood that the threshold voltage, required for saturated switching, is generally higher in the ordered tilted smectic phases than in the disordered tilted smectics [112]. For this reason, under an applied electric field maintained at a constant value during the measurements (100 V_{pp}), this behaviour is not unexpected. At higher fields we would expect the trends in the both the tilt angles and spontaneous polarisation to continue until recrystallization.

Compound **10a** has a similar structure to (S)-MHPOBC (the only difference being an additional fluorine atom) but comparatively possesses a smaller spontaneous polarisation. This may be due to the opposing effect of the transverse dipole due to the lateral fluoro substituent in compound **10a**. The energy-minimised molecular model shown in *figure 74* shows the fluoro points *away* from the direction of the chiral methyl group, hence diminishing the observed value of the spontaneous polarisation.
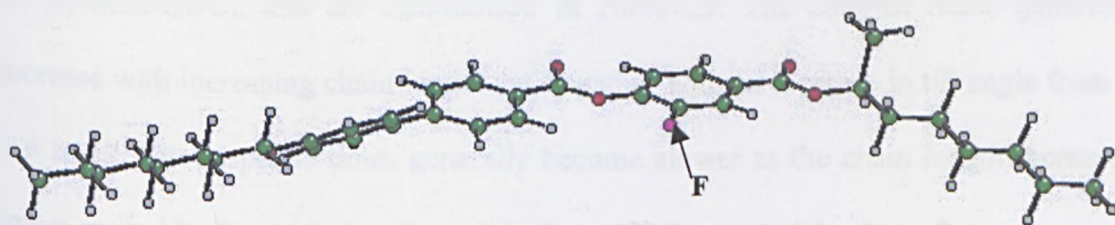
Figure 74:- Energy-minimised ('ball and stick') molecular model of compound **10a**.

Although a SmC$_\alpha$* phase could not be observed in compound **10c**, either by microscopy or DSC, the current response trend in *figure 75* clearly shows the presence of a SmC$_\alpha$* phase above the SmC* phase of the material. The double-peak response (labelled) corresponds to a "double-flow" of charge which is characteristic for antiferroelectric switching (SmC* - SmC$_A$* - SmC*) in aligned cells. The SmC$_\alpha$* phase is believed to be antiferroelectric in nature at higher temperatures and ferroelectric at lower temperatures (on cooling to the SmC* phase).
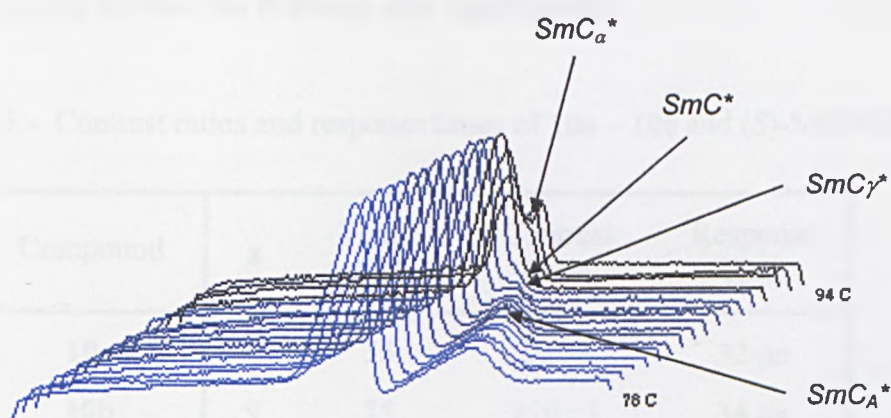
Figure 75:- Current response trend of compound **10c** on cooling from 94 °C to 78 °C (applied triangular-wave voltage of 100 V, at a frequency of 20 Hz).

The contrast ratios and response times for switching between the ferroelectric states of the materials were measured[App.G] 15 °C above the recrystallization temperature (confirmed by repeated cooling runs), or the transition to the SmI$_A$* phase (in the case of (S)-MHPOBC), and are summarised in *Table 25*. The contrast ratios generally increase with increasing chain length (x), together with an increase in tilt angle from x = 8 to 12. The response times generally become slower as the chain length increases (most probably due to increasing viscosity). All the materials show faster response times than those measured for the SmC$_A$* phase of (S)-MHPOBC under the above conditions. This may be indicative of the lower viscosity of the materials, despite

longer unbranched alkyl chains (x), due to the presence of the lateral fluoro substituent.

The most suitable material as a potential antiferroelectric dopant, in this category, is compound **10d** because it possesses the highest spontaneous polarisation in comparison to the other materials in the series. It is interesting to observe that, despite the general trend, an increase in the number of carbons in the unbranched chain (x) does not appear to increase the response time significantly.

Table 25:- Contrast ratios and response times of **10a – 10e** and (*S*)-MHPOBC

Compound	x	Temp. (°C)	Contrast Ratio	Response Time
10a	8	55	20 : 1	32 μs
10b	9	55	>20 : 1	34 μs
10c	10	45	30 : 1	36 μs
10d	11	50	30 : 1	37 μs
10e	12	60	>30 : 1	38 μs
(*S*)-MHPOBC	8	75	10 : 1	73 μs

A homologue (**11b**) of compound **10a** was also prepared which possessed an ethyl substituent at the chiral centre in place of a methyl substituent. The effect on the transition temperatures is shown in *table 26*.

Table 26:- Transition temperatures and phase sequence for compounds **10a** and **11b**
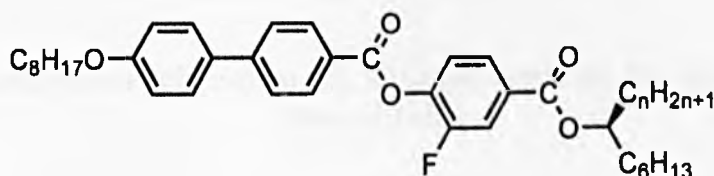
Compound	n	mp	SmC$_A$*		SmA*		I	Recrys.
10a	1	55	•	(47.5)	•	118.4	•	39
11b	2	52	•	52.2	•	93.6	•	<25

Increasing the length of the substituent, C_nH_{2n+1}, from methyl (**n** =1) to ethyl (**n** = 2) has the effect of lowering all the transition temperatures except those of the SmC$_A$* phase. This is actually stabilised by several degrees, which is a similar observation to those made in similar systems [113] and also for the racemic homologues of these materials (from the previous section). The spontaneous polarisation and tilt angles of compound **11b** were also measured and are compared with those obtained for **10a** in *Graph 9*.
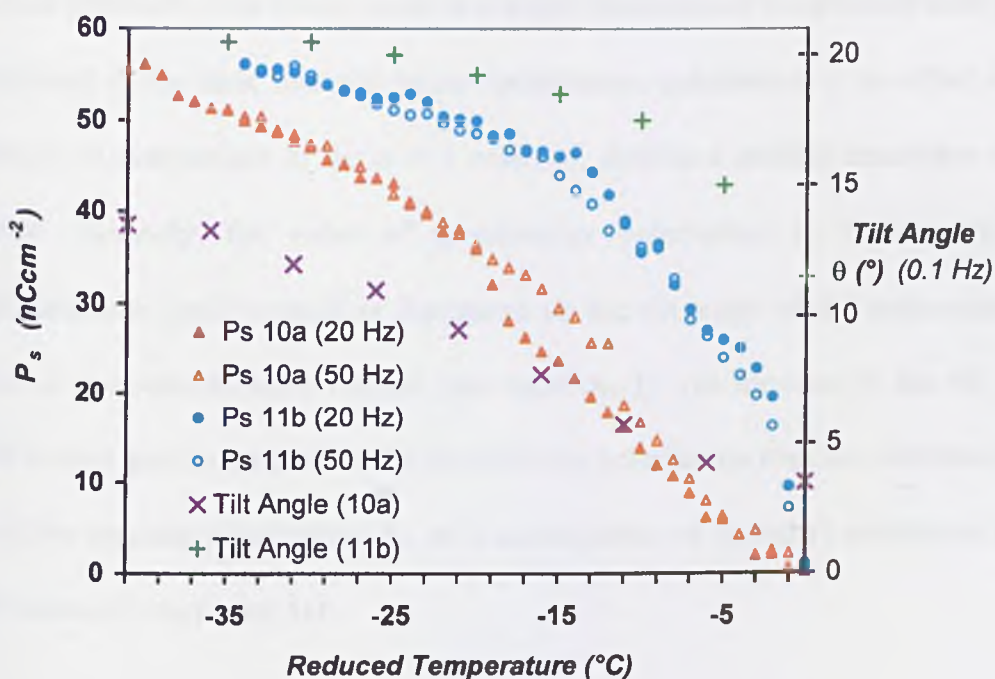
Graph 9:- Spontaneous polarisation and tilt angle trends for the chiral compounds **10a** and **11b**.

It is interesting to observe that the n = 2 material (**11b**) also possesses a higher spontaneous polarisation than for **10a** (n = 1). At first glance this is perhaps the opposite of what we would expect based on the discussion in the previous section. We might speculate that a decrease in the transverse dipole would be inferred by increasing the length of n from 1 to 2. However, other factors must be taken into account when considering the contribution of the transverse dipole to the overall spontaneous polarisation of the molecules. Firstly, the stability of the anticlinic of the n = 2 racemic homologue (**7h**) was greater than the n = 1 racemic homologue (**7e**) from the previous section. This was speculated as being due to the combined effects of increased interdigitation, decreased "flexibility", and restricted rotation (specifically for the octyloxy materials). The fact that rotation of the molecules may be hindered suggests that the transverse dipole moment is directed in a preferred direction. That is, the dipole moment may spend a greater amount of time on average "pointing" in a particular direction. This would result in a higher spontaneous polarisation than would be expected in the bulk material (since spontaneous polarisation is in effect a bulk property), in comparison to the n = 1 material, despite a smaller transverse dipole moment. Secondly, the value of spontaneous polarisation in ferroelectric and antiferroelectric liquid crystals is dependant on the tilt angle of the molecules with respect to the smectic layer normal (see equation **1**). An increase in the tilt angle would show a greater increase in the spontaneous polarisation than the decrease in the size of the absolute polarisation, P_o, as a consequence of the ethyl substituent at the chiral centre of compound **11b**.

$$(1) \qquad \text{spontaneous polarisation } (P_s) = P_o \sin \theta$$

An analogue of (S)-MHPODBC (the decyloxy version of (S)-MHPOBC) was also prepared and characterised. The material, (S)-FMHPODBC, differs in the substitution of the methyl group at the chiral centre with a fluoromethyl (-CH$_2$F) group. The transition temperatures of the material (11c) and maximum spontaneous polarisation values, in comparison with those of (S)-MHPODBC and the trifluoromethyl homologue ((S)-TFMHPODBC), are shown in *table 27*. It was hoped that the highly electronegative fluoro substituent, on the methyl group at the chiral centre, would raise the antiferroelectric phase stability by increasing the size of the overall transverse dipole (and consequently spontaneous polarisation), in comparison to (S)-MHPODBC. However, although the table shows this is the case for the homologue with three fluoro substituents at the chiral centre ((S)-TFMHPODBC), this is clearly not the case for (S)-FMHPODBC. A SmC$_A$* phase is observed in both (S)-MHPODBC and (S)-TFMHPODBC; the only tilted phase observed in (S)-FMHPODBC was a SmC*. The tilt angles and spontaneous polarisation measured for (S)-FMHPODBC are shown in *graph 10*. The material showed a very low spontaneous polarisation (maximum 8.8 nCcm^{-2}) whereas (S)-TFMHPODBC showed a very high spontaneous polarisation (maximum ~150.0 nCcm^{-2}). The values of maximum spontaneous polarisation and tilt angle for (S)-MHPODBC were not available for a valid comparison to be made between the materials. However, the homologue with the highest SmC$_A$* transition temperature is the trifluoromethyl homologue, (S)-TFMHPODBC.
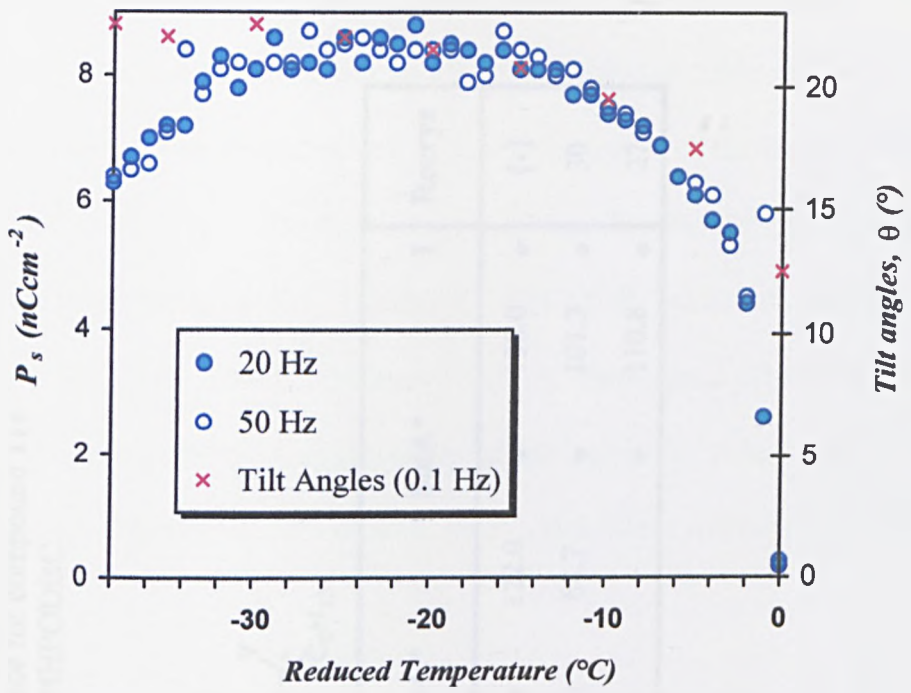
Graph 10:- Spontaneous polarisation and tilt angles measured for **11c**
((*S*)-FMHPODBC).

Table 27:- Transition temperatures (°C) and phase sequence for compound **11c** in comparison with (*S*)-MHPODBC and (*S*)-TFMHPODBC.
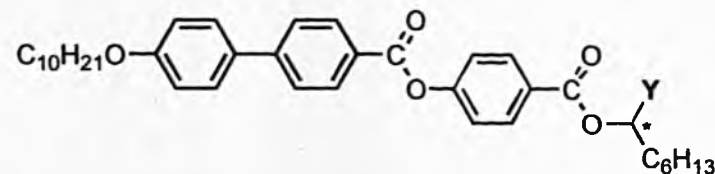
Compound	Y	Max P_s (nCcm^{-2})	Max θ (°)	mp	SmC$_A$*		SmC*		SmA*		I	Recrys
(*S*)-MHPODBC	CH$_3$	{-}	{-}	67	●	115.0	●	122.0	●	138.0	●	{-}
11c {(*S*)-FMHPODBC}	CH$_2$F	8.8	22.5	60	-	-	●	68.7	●	101.3	●	30
(*S*)-TFMHPODBC	CF$_3$	>150	36.5	53	●	104.9	-	-	●	110.8	●	27

{-} = Value not available

Replacing a hydrogen substituent on the methyl group at the chiral centre of (S)-MHPODBC by a fluoro substituent results in the disappearance of the SmC$_A$* phase altogether. This may be explained by examining the nature of the dipole moments at the chiral centre itself. *Figure 76* shows the postulated direction of the transverse dipole moment in the chiral environment of the (S)-MHPODBC molecule. The methyl group attached to the chiral carbon possesses identical (hydrogen) substituents with equal values of electronegativity. Rotation of the single carbon – carbon bond, between the methyl group and the chiral carbon atom, results in a dipole moment directed along this bond.
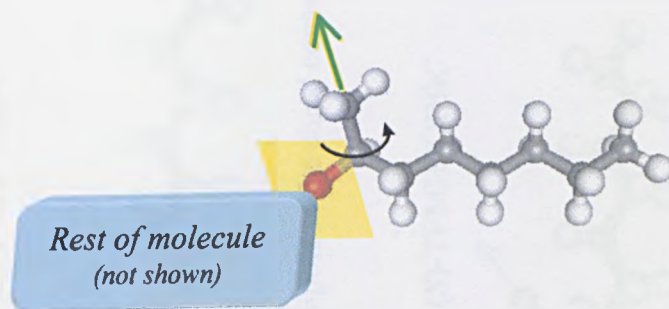
Figure 76:- Idealised structure of the chiral environment in (S)-MHPODBC showing
the direction of the dipole at the chiral centre (green arrow).
The methyl substituent rotates about the sp^3 carbon - carbon bond.
(Only the branched chain of the molecule is shown).

Figure 77 shows the effect of replacing the hydrogen substituent(s) on the methyl group with a single fluoro ((S)-FMHPODBC, *(a)*) and three fluoros ((S)-TFMHPOBC, *(b)*).

Figure 77:- Effect of mono-fluoromethyl- and trifluoromethyl- substituents (blue) on the dipole at the chiral centre of the above molecules
(green arrows = dipole (at the chiral centre);
blue dashed arrows = direction of "secondary" dipoles due to the fluoro substituents)

(a) (*S*)-FMHPODBC
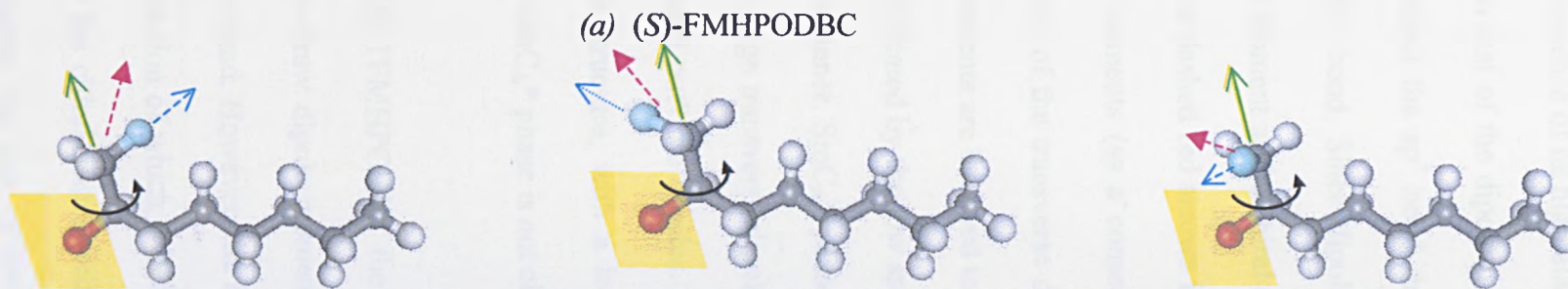
Presence of a single fluoro reduces the size of the overall dipole at the chiral centre (red arrow); the spontaneous polarisation is low.
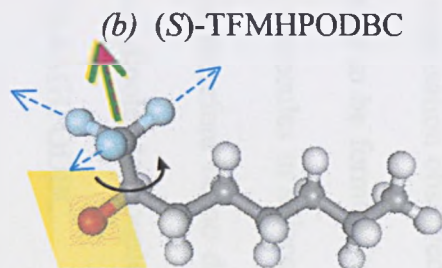
(b) (*S*)-TFMHPODBC

The direction of the dipole on account of the presence of three fluoros results in a strong increase in the overall dipole at the chiral centre.

In the first example ((S)-FMHPODBC) the fluoro substituent draws a dipole moment itself, as a consequence of its high electronegativity (dashed blue arrow(s) in *figure 77*), perpendicular to that of the dipole due to the chiral centre. As the monofluoromethyl group rotates about the sp^3 bond the direction of the "fluoro-dipole moment" also rotates about this bond. Since dipole moments are in essence vector quantities the resultant dipole moment at the chiral centre lies in a direction different to that of either dipole (shown as dashed red arrows in the figure). As there is no "common" direction for the dipole moments (as a consequence of the rotating carbon-carbon bond) the overall magnitude of the transverse dipole moment at the chiral centre is diminished. These dipole moments are believed to be too small to couple with those of the adjacent smectic layer (indicated by the low spontaneous polarisation observed for this material) in an anticlinic manner. SmC$_A$* phases are believed to be formed (to some extent) by the coupling of large transverse dipoles between molecules in adjacent smectic layers, in order to "cancel out" the dipoles. There would therefore be no driving force for a material of this structure, with a low transverse dipole, to couple in this manner. Consequently a SmC$_A$* phase is not observed in (S)-FMHPODBC.

In the case of (S)-TFMHPODBC the three fluoro substituents on the methyl group at the chiral centre draw dipole moments, of equal magnitude, perpendicular to the sp^3 carbon – carbon bond. However, the rotation of this bond results in an averaged dipole moment, the direction of which is believed to coincide with the direction of the dipole moment due to the chiral centre (red and green arrows in *figure 77(b)*). The overall effect is to increase the size of the transverse dipole moment at the chiral centre (indicated by the large spontaneous polarisation value), which effectively couples with the transverse dipoles of molecules in adjacent smectic layers to form the anticlinic

structure. This is believed to account for the high thermal stability of the SmC$_A$* phase of this material in comparison with (S)-MHPODBC.

(S)-FMHPODBC possesses a similar structure to those of (S)-MHPODBC and (S)-TFMHPODBC, but does not exhibit a SmC$_A$* phase. This supports the postulation that structure and steric interactions, between molecules of this type, cannot themselves account for the observation of stable enantiotropic SmC$_A$* phases. A contribution from the coupling of transverse dipole moments must be present to stabilise the anticlinic phase (see **section (ii)**). These observations are consistent with those made for systems closely related to the above [59].

A third antiferroelectric liquid crystalline material with a high value for its spontaneous polarisation, (S)-TFMHPODDBC (synthesised by Dr. R. A. Lewis), was selected for its use as an antiferroelectric dopant. The structure and transition temperatures of the material are shown in *table 28* below.

Table 28:- Structure and transition temperatures (°C) of (S)-TFMHPODDBC
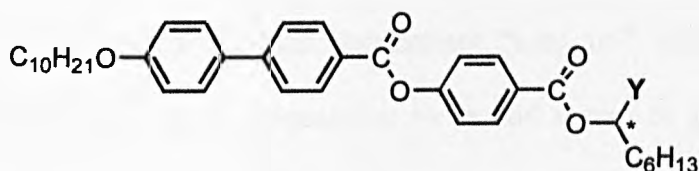
Compound	mp	Recrys.		SmC$_A$*		SmC*		SmA*		I
(S)-TFMHPODDBC	61	•	30.0	•	96.2	•	96.9	•	101.1	•

The presence of the highly polar trifluoromethyl substituent at the chiral centre confers a high spontaneous polarisation on the material (*Graph 11*). However, in addition to the

high thermal stability of the antiferroelectric phase (as with the decyloxy homologue above), a consequence of the large transverse dipole is the high stability for switching to the ferroelectric states [66]. This is also believed to be a consequence of strong pair formation between molecules in adjacent layers. We would also expect that strong pair formation leads to large tilt angles (>22.5 °) [114]. *Graph 11* shows that the spontaneous polarisation increases from the Curie Point, "0 °C", (at both frequencies), then decreases rapidly to zero on further cooling. The tilt angle decreases from approximately 18 ° (at 0 °C) to 9.5 ° (at "zero spontaneous polarisation"; bearing in mind the low frequency for measuring tilt angles). The apparently contradictory behaviour of both the spontaneous polarisation and tilt angle can be explained by the fact that the measurements were carried out with a constant applied AC electric field of $100 V_{pp}$ ($\pm 10 V\mu m^{-1}$). The magnitude of the field may not have been sufficient, firstly, to overcome the high stability of the antiferroelectric phase, and secondly, to induce complete switching to the ferroelectric state. This is supported by the observation that the measured spontaneous polarisation is higher at 20 Hz than at 50 Hz, which is the opposite of the observations made for the (S)-12F1M7-related series discussed earlier. For (S)-TFMHPODDBC, since saturated switching is not achieved in the first instance with the applied field, the partial switching cannot "keep up" with the field as the frequency is increased. At higher frequencies we would expect to further reduce the degree of ferroelectric switching contributing to the spontaneous polarisation; consequently the magnitude of the observed spontaneous polarisation is lower.
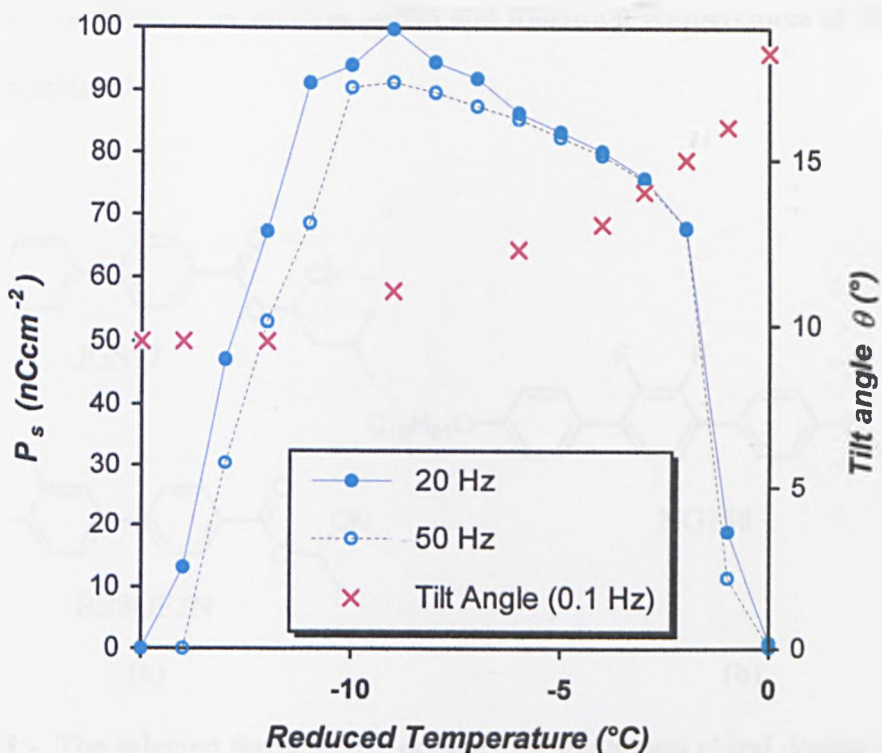
Graph 11:- Spontaneous polarisation and tilt angles measured for (*S*)-TFMHPODDBC

Ferroelectric Dopants

The ferroelectric dopants below (*figure 78*) are regarded as being suitable for use in the model chiral-dopant mixtures. Two of the materials, IGS97 and BE8OF2N are standard non liquid-crystalline dopants and are commonly used in ferroelectric mixtures [115]. IGS97 generally induces a much larger spontaneous polarisation, in SmC host materials, than the same quantity of BE8OF2N. Consequently, usually only a small quantity of IGS97 (ca. 5 %) is required in order to induce effective switching in chiral-dopant ferroelectric mixtures. The third material, NG158, is a SmC*-forming liquid crystal. This material was selected for its close similarity to the structure of the host materials (three phenyl rings, similar alkoxy and alkyl chain lengths). A SmC* material was also selected in order to study the effect of combining SmC* materials with the

anticlinic SmC$_{alt}$ phase. The melting points and transition temperatures of the materials are listed in *table 29*.
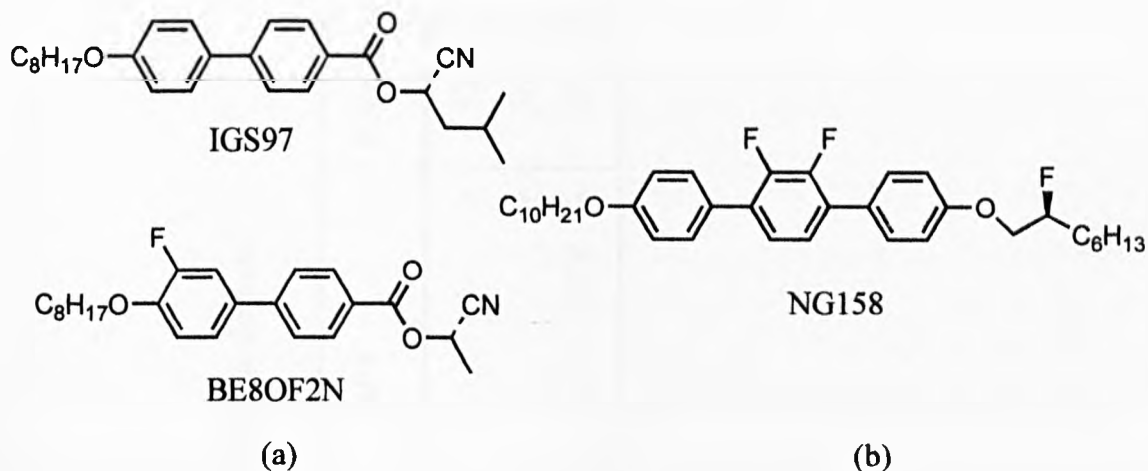
Figure 78:- The selected ferroelectric dopants for the binary chiral dopant mixtures; two standard non liquid-crystalline ferroelectric dopants (a), and a novel SmC* liquid-crystalline material (b).

At first glance it may seem a little unusual to use non liquid-crystalline materials as dopants in a liquid-crystalline host. A small amount of a non-mesogenic material can in fact be incorporated (or "doped"), into a liquid-crystalline host material, without greatly depressing the phase stability or mesomorphic properties of the host. This is also believed to be the case for a SmC* material in a SmC$_{alt}$ host. Since these materials, and indeed these techniques, have not been successfully demonstrated in materials with a SmC$_{alt}$ phase, miscibility tests were first carried out in order to determine the compatibility of the materials with the SmC$_{alt}$ phase. These tests, between the dopants and the selected host materials, are also practical for ascertaining the maximum quantity of dopant which can be added to the host before completely destabilising the induced SmC$_A$* phase. These will be presented in the following section of this chapter.

Table 29:- Transition temperatures (°C) of the selected ferroelectric dopants.

Compound	mp	SmC*		SmA*		N*		BP I		I	Recrys.
(*S*)-IGS97	67	-	-	-	-	-	-	-	-	•	32
(*S*)-BE8OF2N	56	-	-	-	-	-	-	-	-	•	36
(*S*)-NG158	89	•	114.1	•	154.9	•	157.3	•	157.8	•	80

Summary of this Section

A systematic series of antiferroelectric materials was prepared and their physical properties were investigated. The materials selected for use as antiferroelectric dopants for the model chiral dopant mixtures are (*S*)-MHPOBC and compound **10d** ((*S*)-11F1M7), and (*S*)-TFMHPODDBC. A number of ferroelectric dopants were also selected; IGS97, BE8OF2N (non liquid-crystalline materials) and NG158 (liquid-crystalline, SmC*-forming material) for evaluation.

Section (iv):

BINARY MIXTURE STUDIES

Overview

This section describes the investigations carried out on the model chiral-dopant mixtures. The use of both antiferroelectric liquid crystalline dopants and ferroelectric liquid-crystalline / non liquid-crystalline dopants, has been evaluated and are discussed in turn. A brief discussion of the suitability of the two different techniques, for the formulation of practical antiferroelectric mixtures, is to be found towards the end of this section.

The mixtures were prepared by carefully weighing the required quantities of the appropriate components onto a clean glass slide placed on a balance (Sartorius, accuracy to ±0.01 mg). A ±0.25 % to ±0.75 % margin of error (0.01 mg to 0.03 mg in 4.00 mg) was considered an acceptable level of accuracy for the purpose of these studies. The mixtures were blended in the isotropic phase on a heating bank (Leica Reichert). The spontaneous polarisation, tilt angles, response times and contrast ratios of the mixtures were measured in the same manner as for the antiferroelectric materials described in the previous section[Apps.E - G]. The materials were also aligned in the cells in the same way.

(a) Antiferroelectric Dopant Mixtures

In order to make as valid a comparison as possible between the binary mixtures, for the first study, the quantity of antiferroelectric dopants used in the mixtures was maintained at 15 % (by weight). The mixtures consist of the host materials selected from **section (ii)** (unsymmetrically and symmetrically-substituted) and the chiral antiferroelectric dopants from **section (iii)**. The composition and transition temperatures of the first three mixtures, and those of the undoped material (compound **8a**), are listed in *table 30*. The phase sequence of the undoped host material is preserved in the binary mixtures (the phases are of course chiral modifications due to the presence of the chiral dopants). The high thermal stability of the SmC_A^* phase in the (S)-MHPOBC and (S)-TFMHPODDBC dopants was conferred on **Mix1** and **Mix3**, which exhibit a higher SmC_A^* transition temperature than the SmC_{alt} transition temperature than those of the host compound, **8a**. All the mixtures showed supercooling in the induced SmC_A^* phase to below room temperature.

Table 30:- Composition and transition temperatures (°C) of the first series of antiferroelectric chiral-dopant mixtures
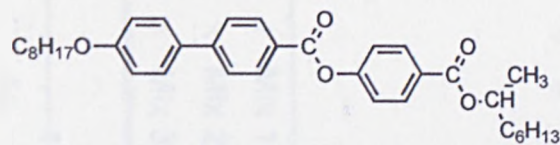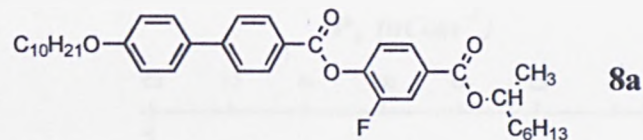
host material:

$C_{10}H_{21}O$—⬡—⬡—C(=O)—O—⬡—C(=O)—O·CH(CH₃)—C₆H₁₃ (F) **8a**

dopants:

$C_8H_{17}O$—⬡—⬡—C(=O)—O—⬡—C(=O)—O·CH(CH₃)—C₆H₁₃

(*S*)-MHPOBC

$C_{11}H_{23}O$—⬡—⬡—C(=O)—O—⬡—C(=O)—O·CH(CH₃)—C₆H₁₃ (F)

11d {(*S*)-11F1M7}

$C_{12}H_{25}O$—⬡—⬡—C(=O)—O—⬡—C(=O)—O·CH(CF₃)—C₆H₁₃
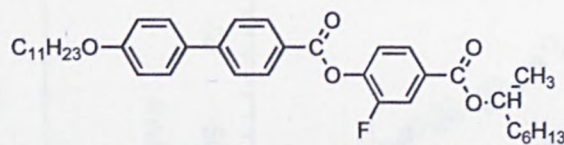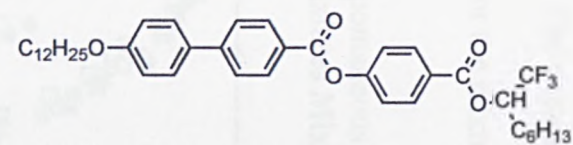
(*S*)-TFMHPODDBC

Host / Mixture	Composition (% dopant b.w.)	mp	SmC_alt / SmC_A*		SmC / SmC*		SmA / SmA*		I	Recrys.
8a	(Host Material)	38	●	79.5	●	83.0	●	105.0	●	<25
Mix1	15% (*S*)-MHPOBC	40	●	82.6	●	87.1	●	116.1	●	<25
Mix2	15% **11d** {(*S*)-11F1M7}	37	●	77.8	●	83.2	●	110.2	●	<25
Mix3	15% (*S*)-TFMHPODDBC	38	●	85.5	●	89.4	●	114.1	●	25

The mixtures appeared to show good alignment in the test cells despite the absence of a chiral nematic phase. The values and trends of both the spontaneous polarisation and tilt angles measured for the mixtures are shown in *graphs 12a* and *12b* below.

Graphs 12(a), 12(b):- Spontaneous polarisation (P_s) values (a), and tilt angles (b), measured for mixtures **Mix1 – Mix 3** (100 V_{pp}, 20 Hz and 50 Hz)
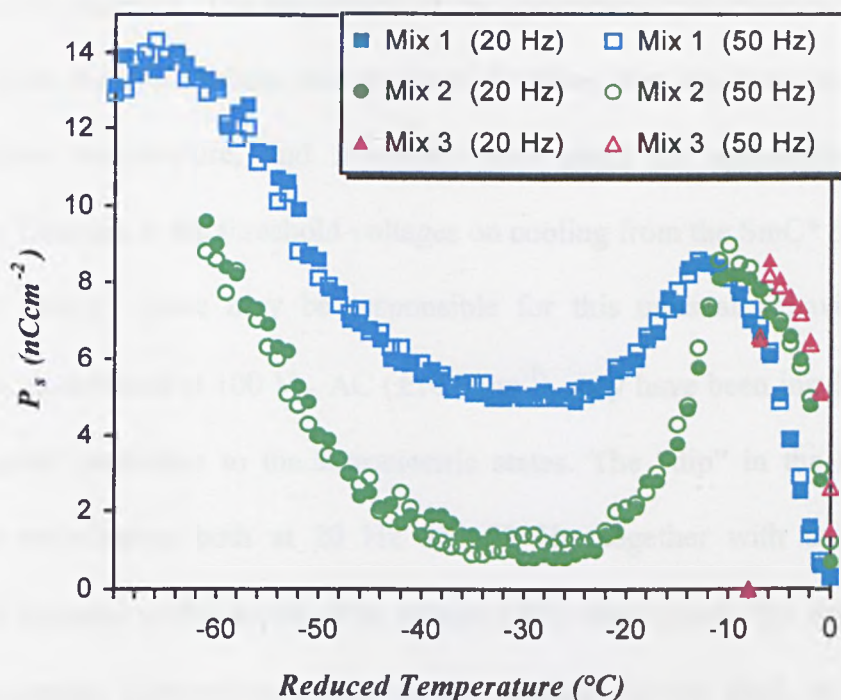
(a)

(b)
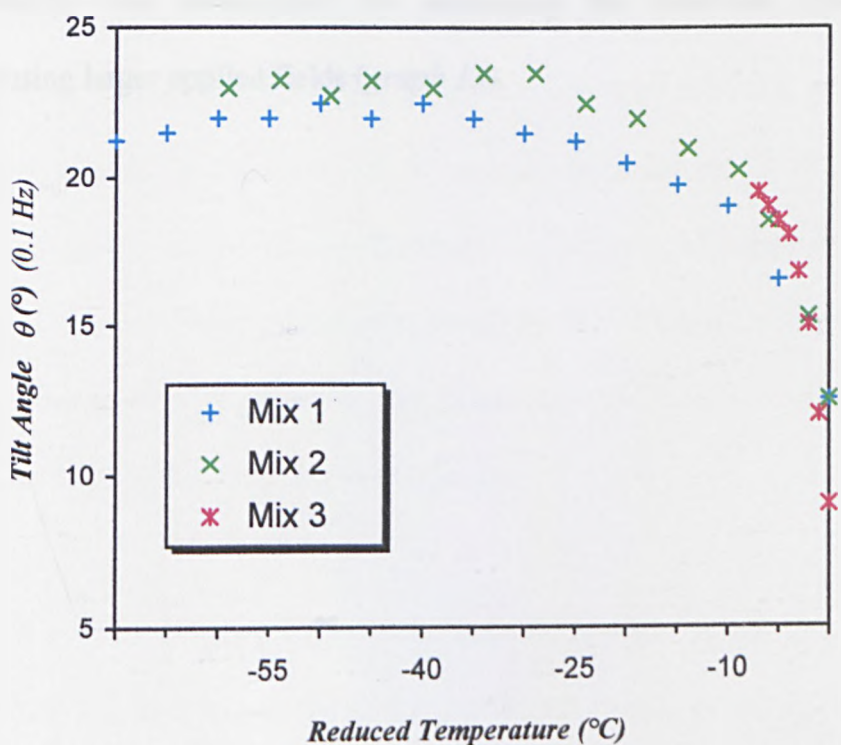
The spontaneous polarisation values obtained at 20 Hz and 50 Hz for the mixtures were found to be almost equal; the maximum value of spontaneous polarisation was found to be approximately 14 $nCcm^{-2}$ (at room temperature). The tilt angle trends for both **Mix1** and **Mix2** are typical for chiral antiferroelectric materials. The trends in the spontaneous polarisation are, however, not typical for the majority of antiferroelectric materials. The magnitude of the spontaneous polarisation increases on cooling from the SmC* phase into the SmC_A* phase, then decreases to around - 36 °C reduced temperature, and increases once again on approaching room temperature. Changes in the threshold voltages on cooling from the SmC* phase into the induced SmC_A* phase may be responsible for this unusual behaviour. The applied field, maintained at 100 V_{pp} AC (±10 $V\mu m^{-1}$), may have been insufficient to induce complete switching to the ferroelectric states. The "dip" in the measured spontaneous polarisation both at 20 Hz and 50 Hz, together with only partial switching of domains visible in the cells, supports this observation. The dependence of the spontaneous polarisation trends on the applied electric field, in the first mixture (**Mix1**), was investigated by measuring the observed spontaneous polarisation using larger applied fields (*graph 13*).

Graph 13:- Effect of increasing applied field on spontaneous polarisation of **Mix1** (measured at 50 Hz).
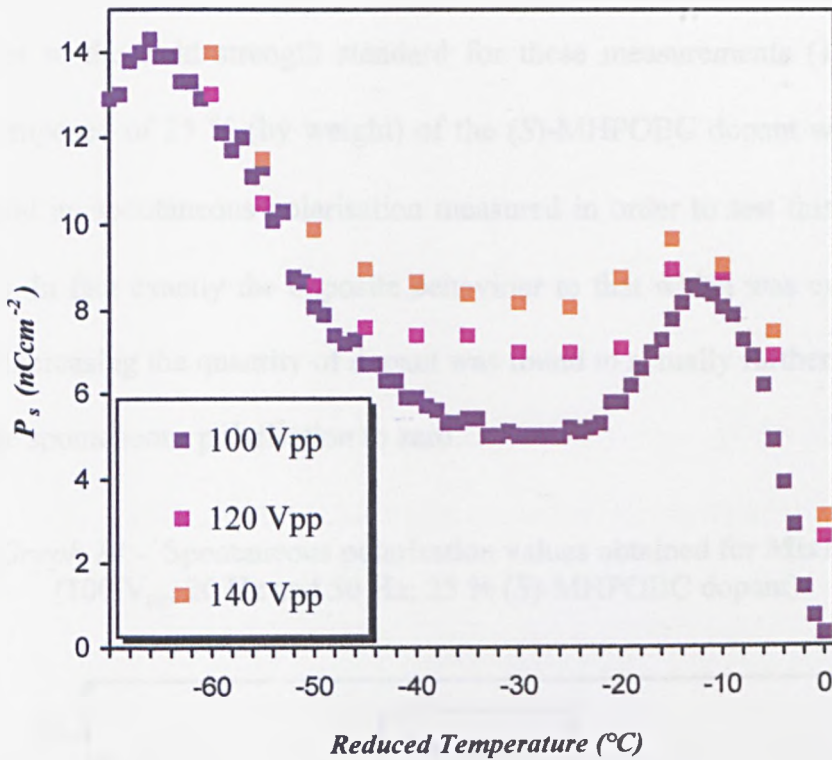
Increasing the applied field from 100 V_{pp} to 140 V_{pp} increases the value of the observed spontaneous polarisation, particularly in the region of the "dip" in *graph 13*. This supports the postulation that the threshold voltages in the mixture increases in this "dip", then decreases with decreasing temperature until saturated switching is achieved, close to room temperature (-66 °C reduced temperature). With increasing applied field the appearance of the spontaneous polarisation trend begins to resemble the characteristic spontaneous polarisation trend for the antiferroelectric materials from the previous section. A greater degree of saturated switching is believed to be achieved in the "dip" with increasing field strength.

An alternative method to using larger electric fields in order to achieve saturated switching in **Mix1** is to increase the quantity of chiral dopant in the mixture. This

would induce a larger spontaneous polarisation into the host matrix that could couple more readily to the electric field. This could then allow saturated switching to take place closer to the field strength standard for these measurements (100 V_{pp}). A mixture composed of 25 % (by weight) of the (S)-MHPOBC dopant was prepared (**Mix1b**) and its spontaneous polarisation measured in order to test this hypothesis (*graph 14*). In fact exactly the opposite behaviour to that which was expected was observed. Increasing the quantity of dopant was found to actually further depress the "dip" in the spontaneous polarisation to zero.

Graph 14:- Spontaneous polarisation values obtained for **Mix1b** (100 V_{pp}, 20 Hz and 50 Hz; 25 % (S)-MHPOBC dopant)
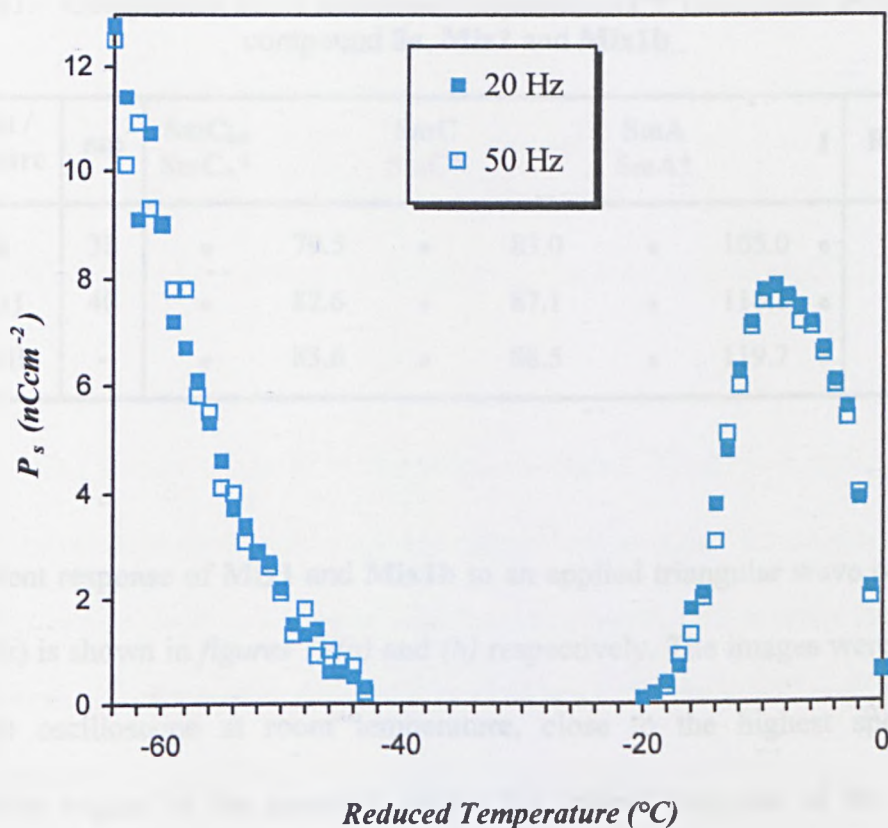
The maximum value for the spontaneous polarisation was found to be 12.5 $nCcm^{-2}$ at room temperature, which was a little lower than that of **Mix1**. Increasing the concentration of dopant molecules in the mixture may, in effect, raise the threshold

for switching to over that of **Mix1**. The increased stability of the antiferroelectric phase in this mixture is also indicated by an increase in the transition temperature of the anticlinic phase in comparison with that of the host material and **Mix1** (*table 31*). As an applied field of 100 V_{pp} is sufficient to permit complete switching of the pure dopant itself (see previous section), it is not unreasonable to assume that there exists a relationship, perhaps even a "balance", between the amount of dopant present and threshold voltage. It may be the case that for this system a much larger quantity of dopant would be required, which may defeat the objective of the chiral dopant concept, but may lead to improved switching properties in the mixtures.

Table 31:- Comparison of the transition temperatures (°C) and phase sequence for compound **8a**, **Mix1** and **Mix1b**

Host / Mixture	mp	SmC$_{alt}$ SmC$_A$*		SmC SmC*		SmA SmA*		I	Recrys.
8a	38	●	79.5	●	83.0	●	105.0	●	<25
Mix1	40	●	82.6	●	87.1	●	116.1	●	<25
Mix1b	-	●	83.6	●	88.5	●	119.7	●	<25

The current response of **Mix1** and **Mix1b** to an applied triangular wave of 100 V_{pp} (at 20 Hz) is shown in *figures 79(a)* and *(b)* respectively. The images were captured from the oscilloscope at room temperature, close to the highest spontaneous polarisation region of the mixtures, where the optical response of the mixtures appeared to be the strongest. In both cases an applied frequency of 20 Hz appears to be sufficient to effect direct switching between the ferroelectric states (assuming at room temperature the ferroelectric states could be achieved at the applied field strength).
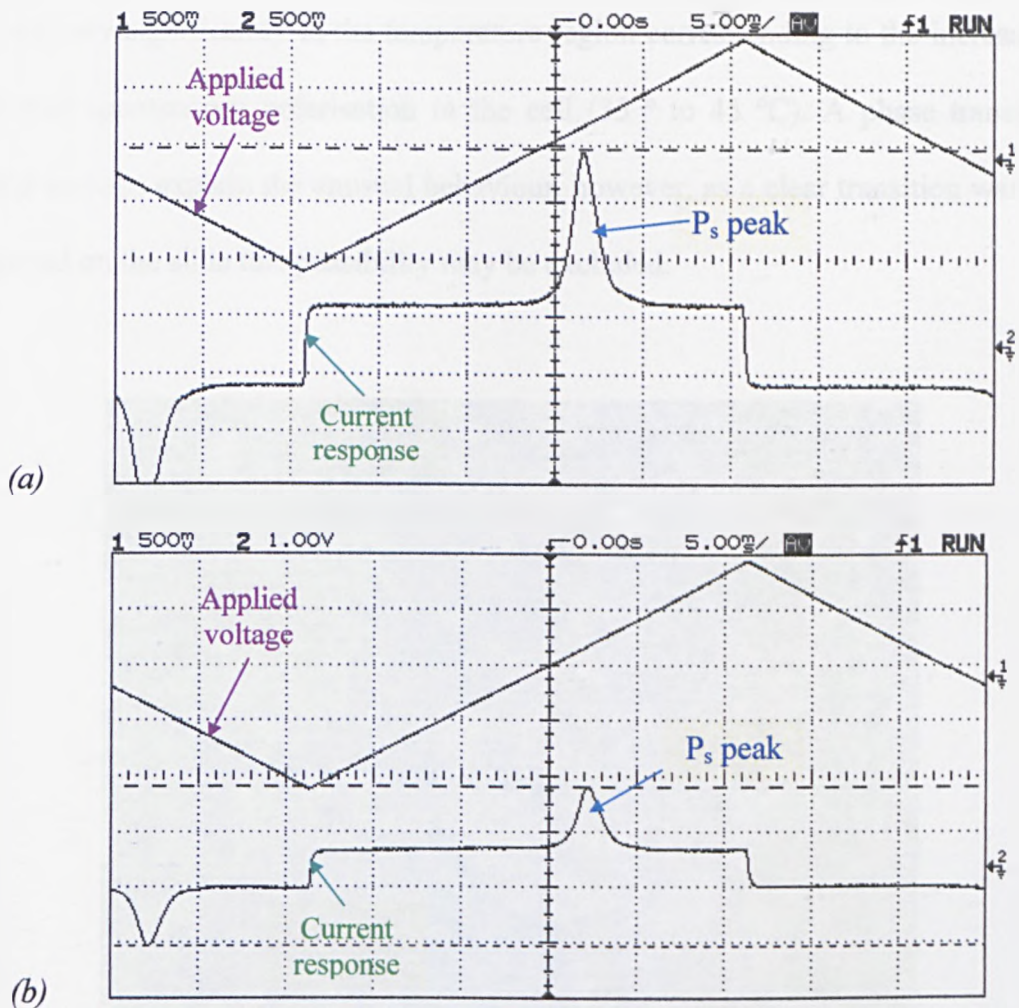
Figure 79(a), *(b)*:- Current response of **Mix1** *(a)*, and **Mix1b** *(b)* at 20 Hz, 100 V_{pp}.

An interesting feature of the first two mixtures (**Mix1, Mix2**) is that the switching observed in the cells could not be clearly categorised, as either ferroelectric (bistate) or antiferroelectric (tristate), even at low frequencies (0.1 Hz) at room temperature. This was mainly due to the difficulty in observing the "middle" antiferroelectric state (characterised by a "striped" purple or blue texture) on switching between the two ferroelectric (one yellow-coloured "bright" and one brown-coloured "dark") state. This was despite the observation, on a glass slide, of both schlieren and broken focal conic microscopic textures characteristic for a smectic C phase with an antiferroelectric structure [116] (*figure 80*). The appearance of this texture did not

change very significantly in the temperature region corresponding to the increase in observed spontaneous polarisation in the cell (35 ° to 45 °C). A phase transition would perhaps explain the unusual behaviour, however, as a clear transition was not observed on the slide this possibility may be excluded.
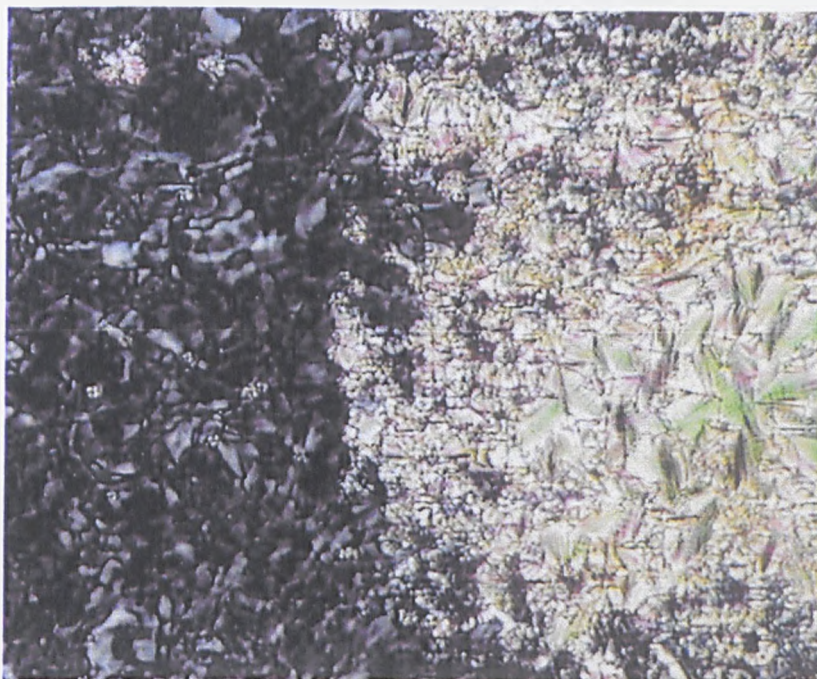
Figure 80:- Microscopic texture of the induced SmC_A^* phase of **Mix1** (25 °C).

The third mixture, **Mix 3**, showed clear ferroelectric switching in the SmC^* phase on cooling from the Curie point ("0 °C"). This was followed by a sharp decline in the switching (the measured spontaneous polarisation) at the transition to the induced SmC_A^* phase. As discussed in the previous section of this chapter antiferroelectric materials, possessing trifluoromethyl groups at the chiral centre, are known to possess high thresholds for switching as a consequence of the high stability of the antiferroelectric phases. This stability is believed to be transferred to the mixture as the threshold field, required for switching to the ferroelectric state, appears to be much higher than the equipment used could safely generate. The effect

of increasing the size of the applied field on the spontaneous polarisation and tilt angles of the mixture is shown in *graph 15(a)* and *(b)*; the effect on the current response, at 20 Hz and 50 Hz, is shown in *figure 81 (a)* and *(b)*.

Graph 15(a), (b):- Effect of increasing the applied field on the spontaneous polarisation *(a)* and tilt angle *(b)*, of **Mix3**
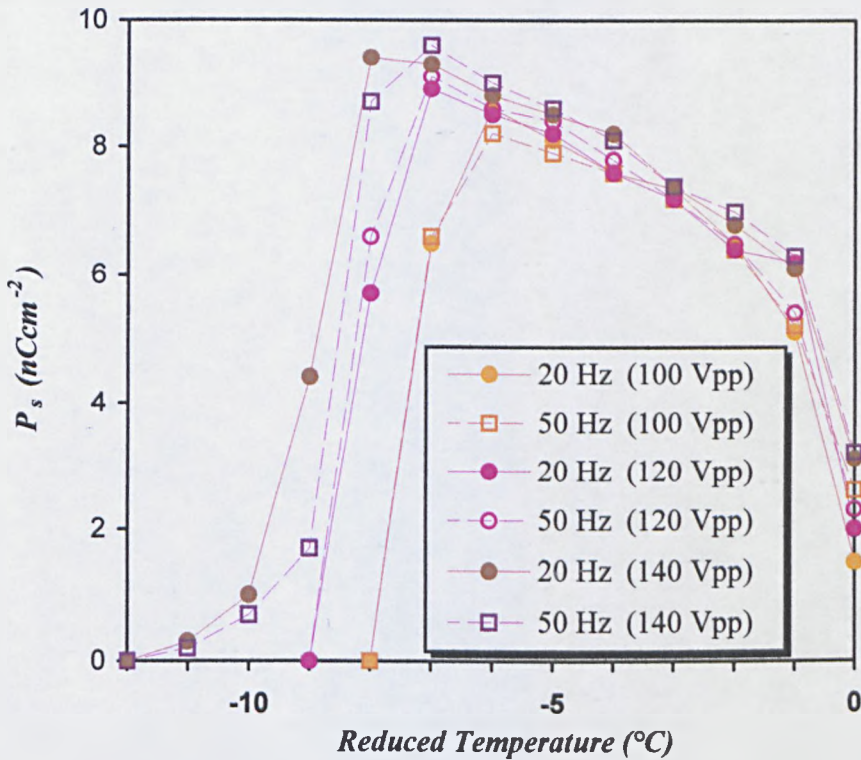
(a)
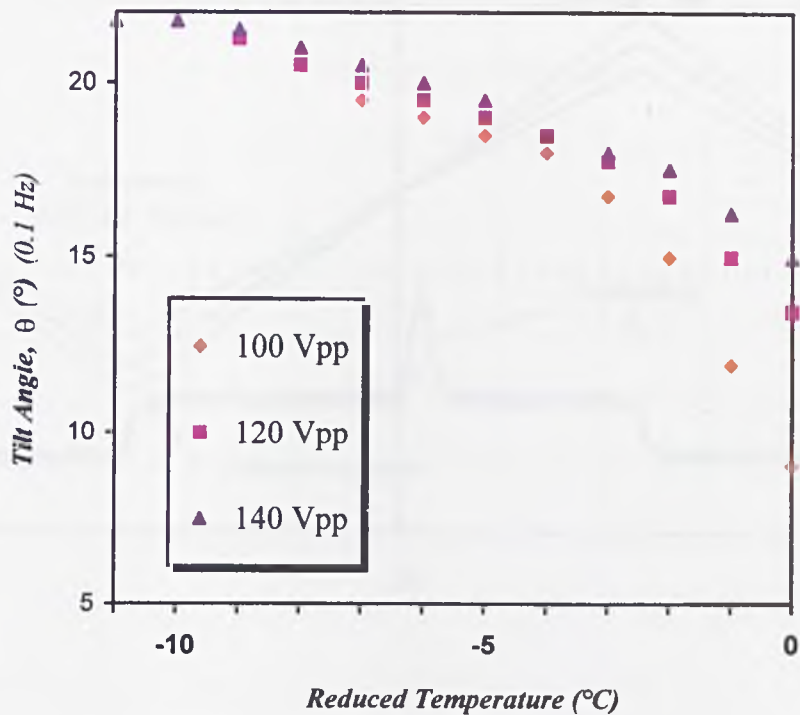
(b)

Figure 81 (a), (b):- Effect of increasing the applied field on the current response of **Mix3** at 20 Hz *(a)*, and 50 Hz *(b)*.
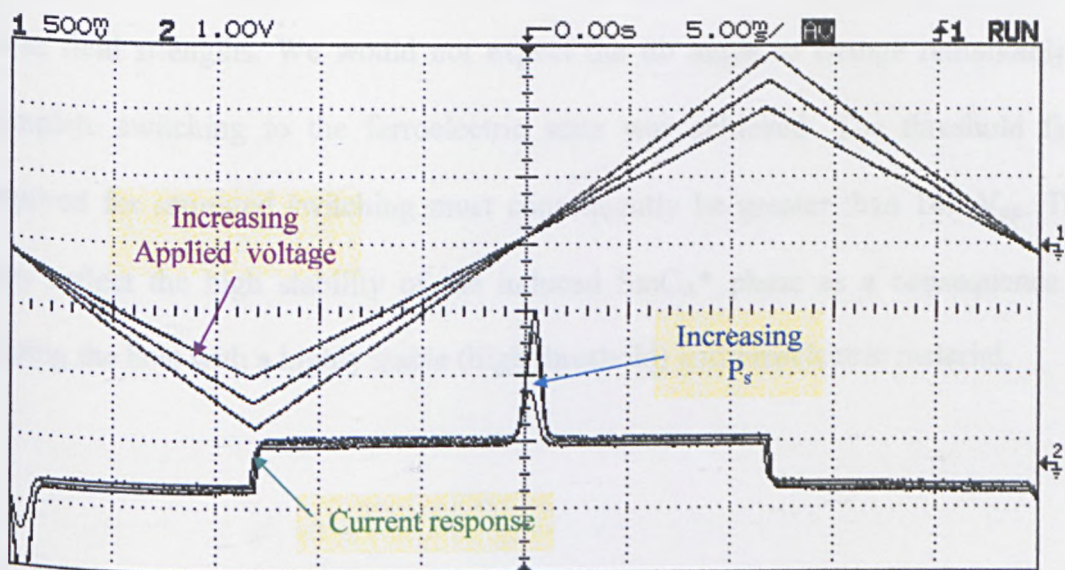
(a)
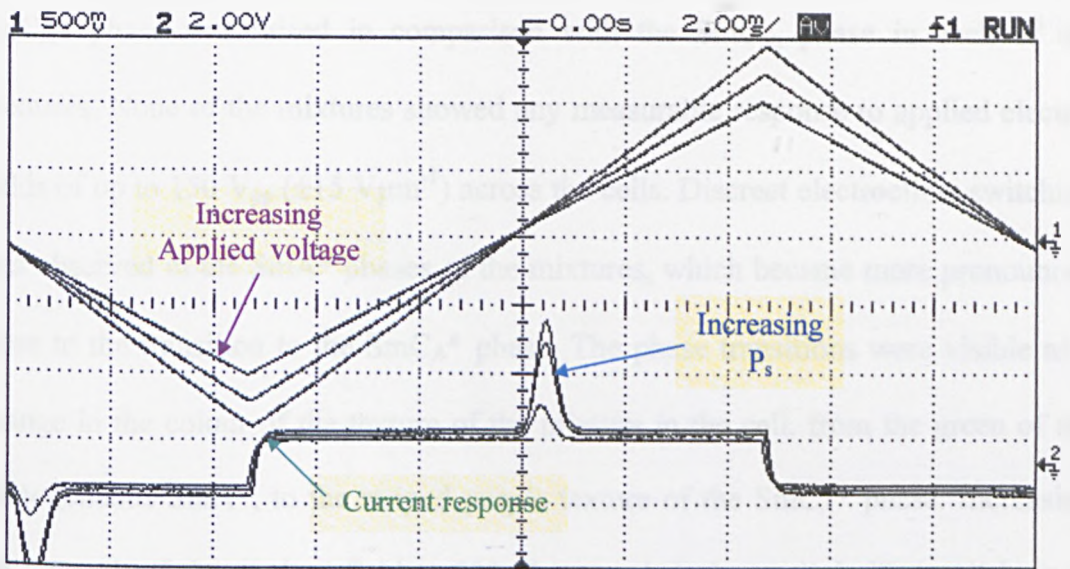
(b)

Increasing the applied field both augments the temperature range at which switching is observed and increases the size of the current response and value of the calculated spontaneous polarisation. The fact that the tilt angles also increase, with increasing field, is clear evidence that switching to the ferroelectric state cannot be achieved at these field strengths. We would not expect the tilt angle to change remarkably if complete switching to the ferroelectric state was achieved. The threshold field required for saturated switching must consequently be greater than 140 V_{pp}. This may reflect the high stability of the induced SmC_A^* phase as a consequence of doping the host with a highly stable (high threshold) antiferroelectric material.

The second series of mixtures, **Mix4** to **Mix6**, consist of the same antiferroelectric dopants as the first series of mixtures above, but with a different host material, compound **8b** *(table 32)*. All the mixtures showed the same chiral phase sequence as that observed for the undoped racemic host material. The stability of the induced

SmC_A^* phase was raised in comparison with the SmC_{alt} phase in each of the mixtures. None of the mixtures showed any measurable response to applied electric fields of up to 150 V_{pp} (±15 $V\mu m^{-1}$) across the cells. Discreet electroclinic switching was observed in the SmA^* phases of the mixtures, which became more pronounced close to the transition to the SmC_A^* phase. The phase transitions were visible as a change in the colour of the texture of the mixture in the cell, from the green of the homogeneous SmA^*, to the striped purple texture of the SmC_A^* phase. Increasing the strength of the applied field to 180 V_{pp} revealed electroclinic-like switching in this phase. The switching was too shallow to allow any practical tilt angle measurements to be carried out and decayed as the temperature of the cell was lowered.

In **section (ii)** of this chapter we discussed the greater relative stability of the SmC_{alt} phase in the n = 2 materials compared to that of the n = 1 materials (*figure 82*). Although the n = 2 materials often exhibit lower transition temperatures than the n = 1 materials, the transition to the SmC_{alt} phase in the x = 10 and x = 12 materials arises directly from the SmA phase on cooling from the isotropic phase (without an intermediate SmC phase). The anticlinic SmC_{alt} phase is believed to be much more favoured than the synclinic SmC phase in these materials as a consequence of increased steric interactions (ie. interdigitation), between the branched and unbranched chains of molecules in adjacent layers, in comparison with the n = 1 materials [80, 108]. As the cores of the two types of host molecules are identical it is possible to speculate that these steric interactions must be responsible for "locking" the molecules in an anticlinic structure.

Table 32:- Composition and transition temperatures (°C) of the second series of antiferroelectric chiral-dopant mixtures

host material:

8b

dopants:

(S)-MHPOBC

11d {(S)-11F1M7}
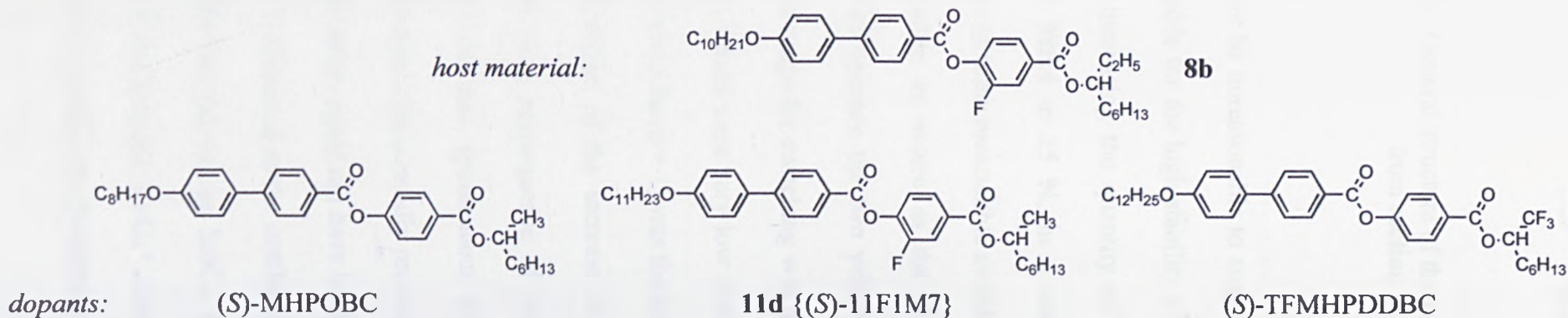
(S)-TFMHPDDBC

Host / Mixture	Composition (% dopant b.w.)	mp	SmC_alt / SmC_A*		SmA / SmA*		I	Recrys.
8b	(Host material)	34	●	57.0	●	79.0	●	<25
Mix4	15% (S)-MHPOBC	-	●	64.5	●	93.4	●	<25
Mix5	15% **11d {(S)-11F1M7}**	42	●	59.1	●	84.9	●	<25
Mix6	15% (S)-TFMHPODDBC	-	●	62.4	●	85.1	●	<25
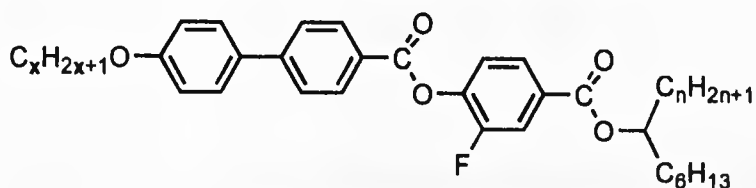
Figure 82:- General structure of the unsymmetrically-substituted racemic materials from **section (ii)** (x = 10, 12; n = 1, 2).

It would not be unreasonable to suggest then that the same steric interactions must be responsible for the high stability of the induced antiferroelectric phases in **Mix4** to **Mix6**. Increasing the quantity of the (*S*)-MHPOBC dopant, from 15 % (by weight) in **Mix4** to 25 %, in a subsequent mixture, **Mix4b**, did result in the observation of some measurable switching (*graph 16*). The switching appeared to be antiferroelectric in nature as the third "middle" blue-coloured state could be distinguished between the two yellow-coloured ferroelectric states. However, the temperature range for switching was quite small (only 7.0 °C) and the spontaneous polarisation values were very low (maximum 3.7 nCcm^{-2}), compared with **Mix1**, in which compound **8a** (n = 1) was the host. The fact that switching could be measured at all may reflect of the increase in the magnitude of the induced spontaneous polarisation as a consequence of the presence of a larger quantity of dopant. Conversely, the low spontaneous polarisation and the fact that the measured response decayed rather rapidly presumably indicates that complete switching to the ferroelectric states could not have been achieved at the applied voltages of 100 V_{pp}. This may be attributed to the combined effects of the preservation of a high degree of interdigitation (as in the SmC_{alt} phase of the undoped host), with the high threshold of the induced $SmC_A{}^*$ phase (higher than in **Mix1**). As with **Mix1** an increase in the quantity of (*S*)-MHPOBC dopant raised the transition temperature of

the induced SmC$_A$* phase in comparison with **Mix4** (*table 33*).

Graph 16:- Measured spontaneous polarisation of **Mix4b**
(at 20 Hz and 50 Hz, 100 V$_{pp}$; 25 % (*S*)-MHPOBC dopant)
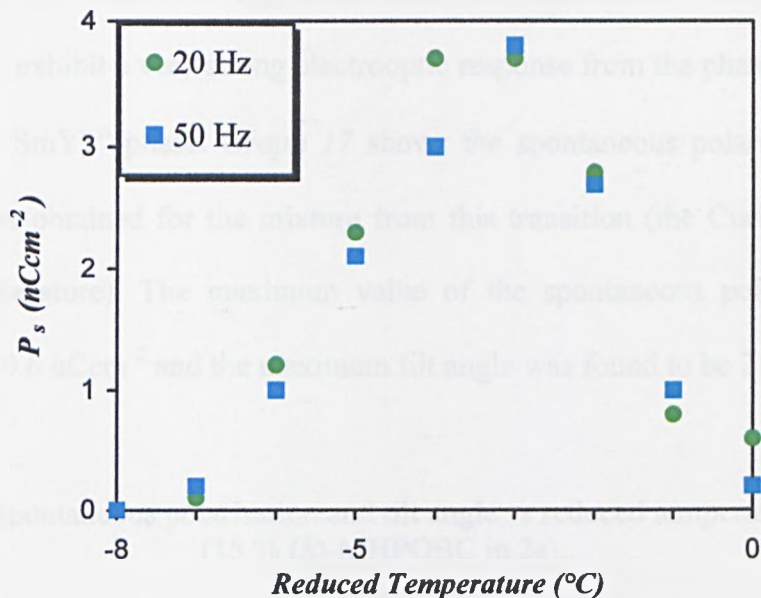
Table 33:- Comparison of the transition temperatures and phase sequence for
Mix4 and **Mix4b**

Mixture	mp	SmC$_A$*			SmA*		I	Recrys.
Mix4	-	•	64.5	•	93.4	•		<25
Mix4b	-	•	65.6	•	112.7	•		<25

In the next series of binary antiferroelectric dopant mixtures the selected symmetrically-substituted ("swallow-tailed") host materials, compounds **2c** and **4c**, were doped with 15 % (*S*)-MHPOBC (**Mix7** and **Mix8** *table 34)*. The chiral version of the anomalous "SmY" phase of the undoped host material in **Mix7** (compound **2c**) was observed in this mixture ("SmY*"). In an aligned cell of the mixture the

phase transition from the induced SmA* to the SmC$_A$* could be observed as changes in the colour of the texture (as in the cells of **Mix4** to **Mix6**). As with the earlier mixtures very weak electroclinic-like switching could be observed in the SmC$_A$* phase only at high fields (180 V$_{pp}$) and at fairly low frequencies (5 Hz). The mixture did, however, exhibit a very strong electrooptic response from the phase transition to the induced "SmY*" phase. *Graph 17* shows the spontaneous polarisation values and tilt angles obtained for the mixture from this transition (the Curie Point, 0 °C reduced temperature). The maximum value of the spontaneous polarisation was found to be 10.6 nCcm^{-2} and the maximum tilt angle was found to be 21.5 °.

Graph 17:- Spontaneous polarisation and tilt angle *vs* reduced temperature for **Mix7** (15 % (*S*)-MHPOBC in **2c**).
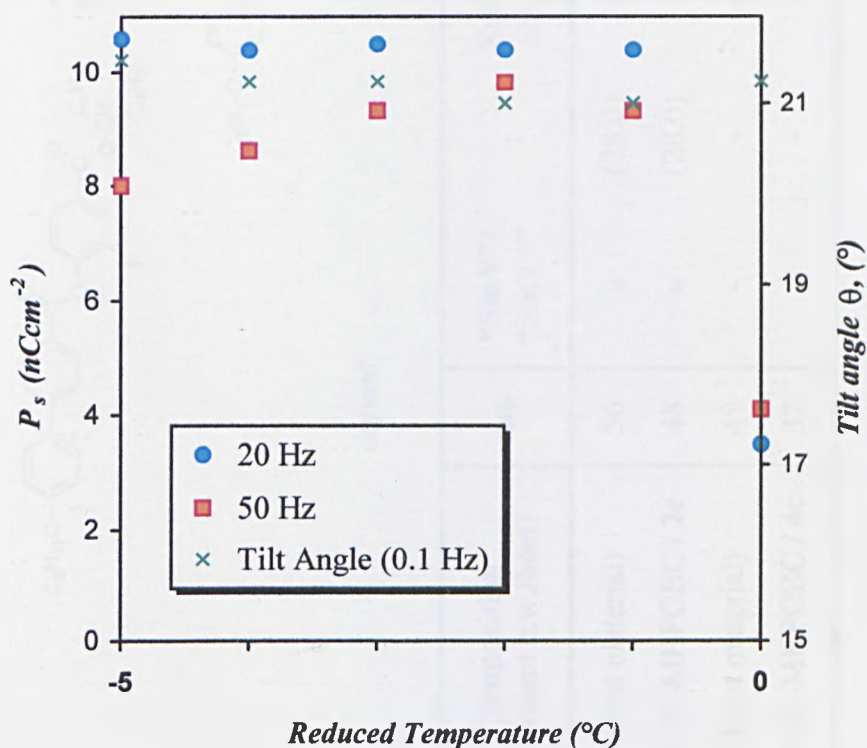
Table 34:- Composition and transition temperatures (°C) of the third series of antiferroelectric chiral-dopant mixtures

host materials:

2c

4c
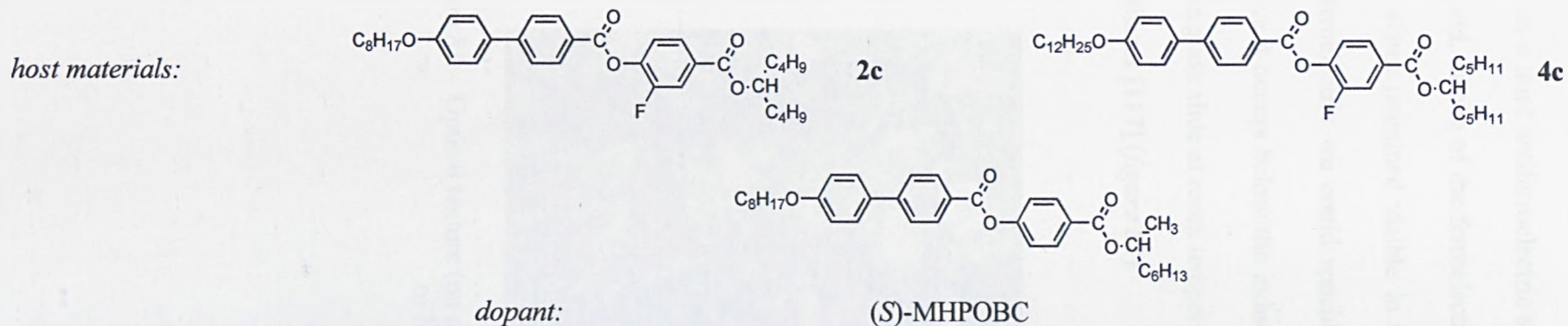
dopant:

(S)-MHPOBC

Host / Mixture	Composition (% dopant b.w./host)	mp	"SmY"/ "SmY*"		SmC$_{alt}$ / SmC$_A$*		SmC / SmC*		SmA / SmA*		I	Recrys.
2c	(Host material)	56	●	(28.0)	●	57.0	-	-	●	85.0	●	<25
Mix7	15% (S)-MHPOBC / 2c	48	●	(28.0)	●	64.5	-	-	●	93.4	●	<25
4c	(Host material)	49	-	-	●	(27.0)	-	-	●	(43.8)	●	<25
Mix8	15% (S)-MHPOBC / 4c	32	-	-	●	42.7	●	45.8	●	66.8	●	<25

The nature of the switching in the "SmY*" phase appeared to be ferroelectric in character as a third antiferroelectric state could not be observed. On removal of the applied field, in one of the ferroelectric states, regions of greenish-yellow partially-switched states remained visible in the cell. If this (as yet unidentified) phase is indeed ferroelectric we could speculate that it is a more-ordered SmI* or SmF* phase since it occurs below the induced SmC_A* phase. However the texture of the phase on a glass slide at room temperature did not appear to resemble those of either of these phases [117] (*figure 83*).
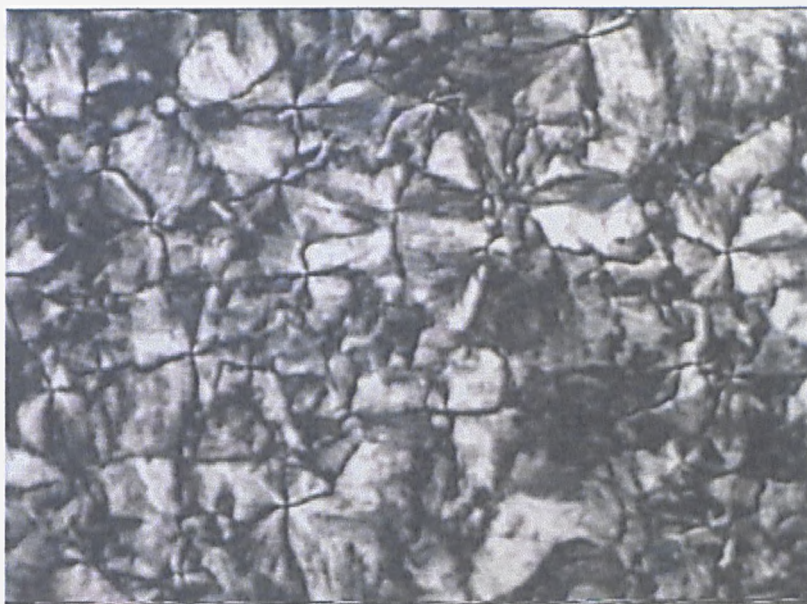
Figure 83:- Optical texture (on a glass slide) of the induced "SmY*" phase of **Mix7** (25 °C).

The possibility that the "SmY" phase could be a more ordered phase (ie. long range positionally ordered), such as the H* or G* (see *figure 7* in the **Introduction**), can be discounted since the material on the slide above could be sheared with almost as little force as that required to shear the SmC_A^* (*figure 84*). This is of course purely demonstrative since for a change to a more ordered phase, close to room temperature, we may (tentatively) expect to observe an increase in the viscosity that would make the material more difficult to shear. In addition, saturated switching appeared to take place at applied fields as low as 40 V_{pp}. This is also an unusual observation since the threshold for switching to the ferroelectric states in the induced SmC_A^* phase is evidently much higher than that of the "SmY*" phase. Transitions to hexatic-ordered phases are usually accompanied by a noticeable increase in the threshold voltages for switching [112].
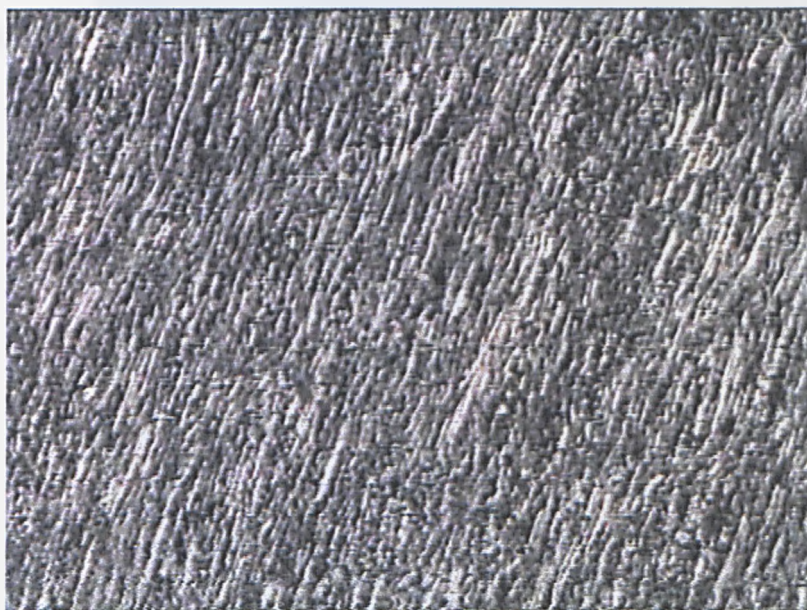
Figure 84:- Optical texture of the induced "SmY*" phase
of **Mix7** after shearing (25 °C).

The possibility that the "SmY*" phase could be a monotropic SmI_A* phase, as is found in chiral MHPOBC (below the SmC_A* phase), can also be discounted for the above reasons. The observed switching appeared to be bistate rather than tristate (SmI_A* is after all antiferroelectric) and the texture bore little or no resemblance to that of the SmI_A* phase in (S)-MHPOBC (*figure 85*).

(a) 74.0 °C

(b) 54.0 °C
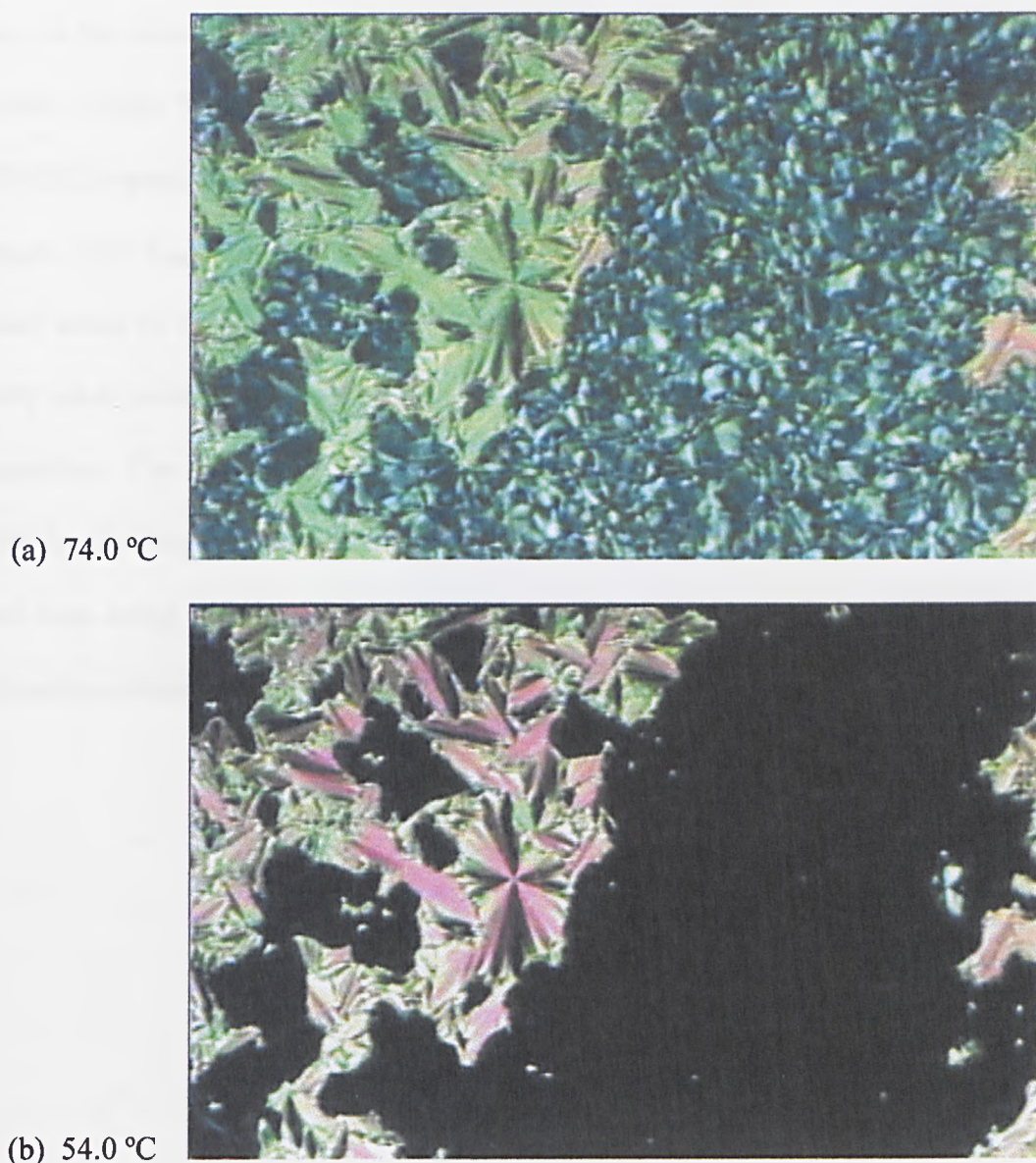
Figure 85:- Microscopic textures of the SmC_A* (a), and SmI_A* (b) phases of (S)-MHPOBC

The induced SmC_A^* phases, both in **Mix7** and **Mix8**, were found to be enantiotropic in contrast with the monotropic SmC_{alt} phases of the undoped host materials. This alone allows us to speculate that the very induction of a spontaneous polarisation into the bulk of the symmetrically-substituted material assists in stabilising the anticlinic phase. This is also observed as an increase in the transition temperature of the induced SmC_A^* phase in comparison with the SmC_{alt} phase of the undoped hosts. In the case of **Mix7** the melting point is also raised whereas in **Mix8** it is lowered. Unlike **Mix7**, the induced SmC_A^* phase, with the same quantity of (S)-MHPOBC dopant (15 % by weight), did show some switching at the "regular" field strength (100 V_{pp}). The observed spontaneous polarisation (*Graph 18*) showed a similar trend to that of **Mix1b**. The spontaneous polarisation decreases to zero shortly after switching is initially observed and increases sharply close to room temperature. The spontaneous polarisation was found to be higher at 20 Hz than at 50 Hz (suggesting that a smaller degree of saturated switching between ferroelectric states was being achieved at 50 Hz); the maximum value of the spontaneous polarisation obtained was 12.5 $nCcm^{-2}$.

Graph 18:- Spontaneous polarisation vs reduced temperature for **Mix8** (15 % (S)-MHPOBC in **4c**).
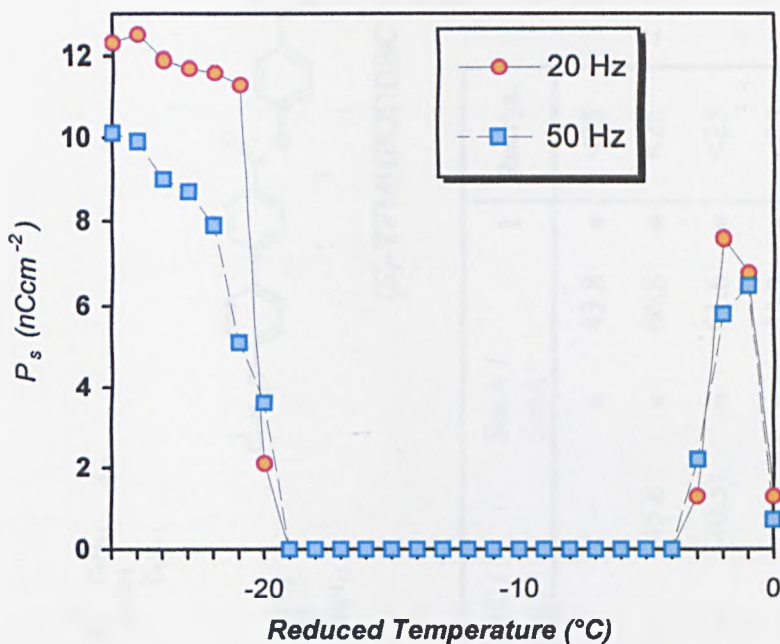
Table 35 shows the phase sequence and transition temperatures of the final series of antiferroelectric-doped mixtures in comparison with those of **Mix8**. The host, **4c**, was doped with 15 % (by weight) of (S)-11F1M7 and (S)-TFMHPODDBC (**Mix9** and **Mix10** respectively).

The SmC_A* phase in both **Mix9** and **Mix10** was also raised in temperature in comparison to the SmC_{alt} phase of the undoped hosts. In the mixtures possessing (S)-MHPOBC and (S)-11F1M7 dopants a SmC* phase was observed in the phase sequence despite the absence of a SmC phase in the undoped host. A SmC* phase was not observed in the mixture doped with (S)-TFMHPODDBC (**Mix10**).

The measured spontaneous polarisation values of the mixtures are shown in *Graph 19*.

Table 35:- Composition and transition temperatures (°C) of the third series of antiferroelectric chiral-dopant mixtures

host material:

4c
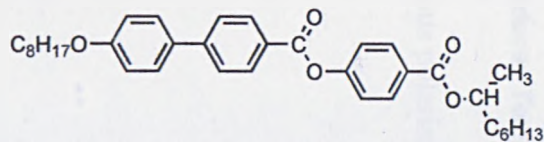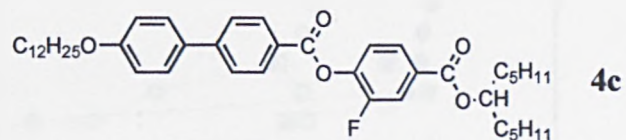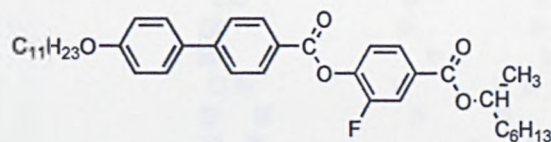
dopants:

(S)-MHPOBC

11d {(S)-11F1M7}

(S)-TFMHPODDBC

184
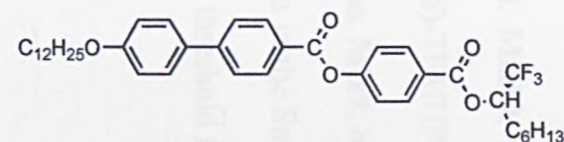
Mixture	Composition (% dopant b.w./host)	mp	SmC_alt / SmC_A*		SmC / SmC*		SmA / SmA*		I	Recrys.
4c	(Host material)	49	●	(27.0)	-	-	●	43.8	●	<25
Mix8	15 % (S)-MHPOBC	42	●	42.7	-	45.8	●	66.8	●	<25
Mix9	15 % 11d {(S)-11F1M7}	32	●	39.8	●	(40.5)	●	61.6	●	<25
Mix10	15 % (S)-TFMHPODDBC	32	●	40.2	-	-	●	55.2	●	<25

The trend in the spontaneous polarisation of **Mix9** and **Mix10** showed the opposite behaviour to that expected. **Mix10**, which possessed the dopant with the higher threshold for switching ((S)-TFMHPODDBC), actually showed almost saturated switching at all temperatures. **Mix9**, however, showed a slight "dip" in the value of the spontaneous polarisation in the SmC$_A$* phase region despite being doped with a chiral material with a lower threshold for switching.
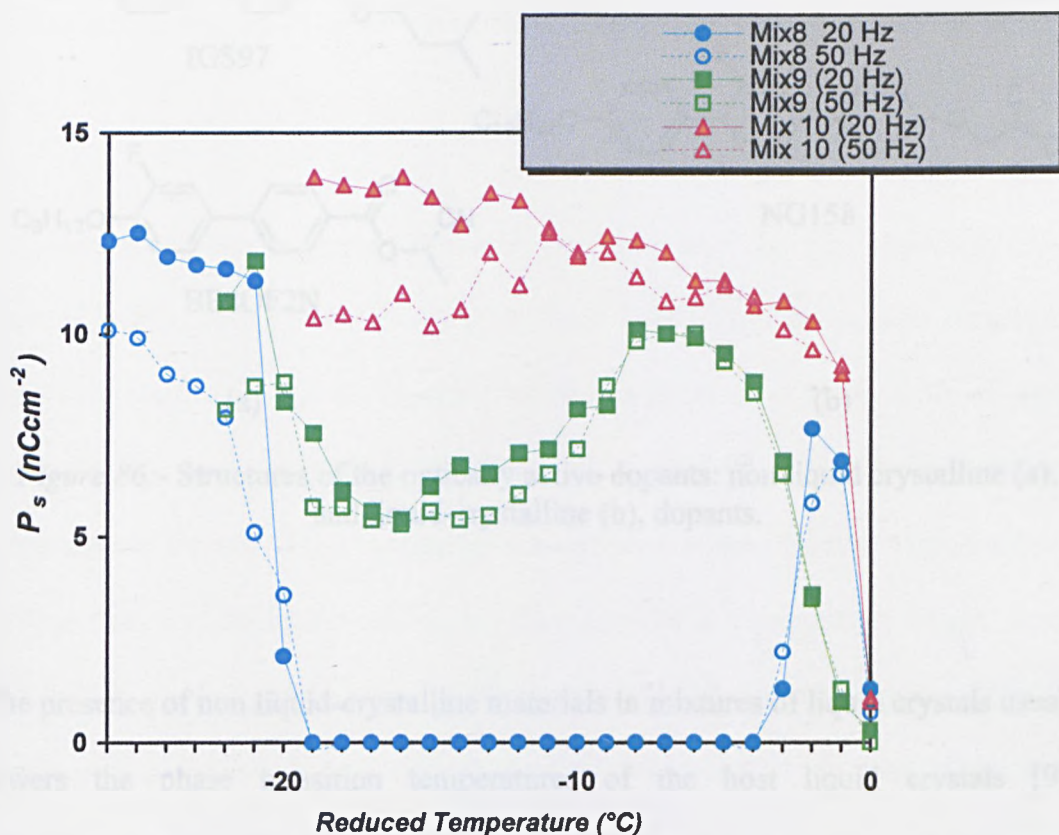
Graph 19:- Spontaneous polarisation values obtained for **Mix8 – Mix10**

(b) Ferroelectric Dopant Mixtures

Three optically active dopants were chosen for this study; one was a compound with an enantiotropic SmC* phase and the other two were standard dopants (*figure 86*) that did not exhibit liquid crystal phases.

(a)   (b)
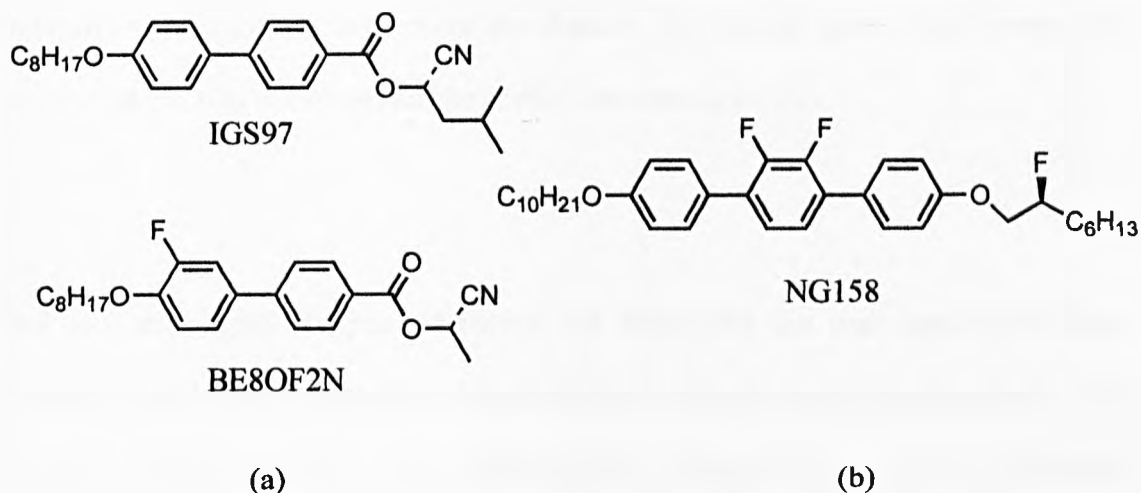
Figure 86:- Structures of the optically active dopants: non liquid crystalline (a), and liquid-crystalline (b), dopants.

The presence of non liquid-crystalline materials in mixtures of liquid crystals usually lowers the phase transition temperatures of the host liquid crystals [99]. Consequently there is a limit to the quantity of dopant a host mixture can incorporate either before the phase transition temperatures become too low for a given application or before the dopant separates out from the mixture. There are also miscibility considerations eg. a synclinic SmC (or SmC*) phase cannot be miscible across the whole phase diagram with an anticlinic SmC_{alt} (or SmC_A*) phase. In order to determine the quantities of dopants that can be usefully dissolved in the selected host materials, without lowering the SmC_A* phase below an acceptable limit, a

series of mixture studies were carried out using the dopants and the unsymmetrically-substituted hosts. Miscibility graphs are shown for the dopants in hosts **8a** and **8b** (*graphs 20a(i) – (iii)* and *20b(i) –(iii)* respectively). The quantities of dopants chosen for further study, based on the results of these miscibility studies, are listed in *table 36* (shown as dashed lines on the graphs) together with the transition temperatures of the binary mixtures. It was only necessary to prepare mixtures containing up to 50 % of the dopants (by weight) since, in all cases, the SmC_A^* phase was not observed above this concentration ratio.

All four miscibility diagrams between the hosts and the non liquid-crystalline dopants (IGS97 and BE8OF2N, *graphs 20a(i) – 20b(ii)*) show similar trends. The transition temperatures of all the observed phases decrease as the quantity of dopant increases. The decrease in the temperatures of the tilted (SmC^* or SmC_A^*) phases is more marked than the SmA^* phase ie. the decrease in the observed temperatures is *steeper* than for the SmA^* transition. This may be a consequence of the greater destabilisation (decrease in transition temperature) of phases which possess a higher degree of molecular ordering, such as the SmC^* and SmC_A^*, in comparison to the relatively disordered SmA^*.

The miscibility diagrams with NG158 as the liquid crystalline ferroelectric (SmC^*-forming) dopant (*graphs 20a(iii)* and *b(iii)*)) show an altogether different behaviour to those of the non liquid-crystalline dopants above. In this case an increase in the transition temperature of the SmA^* phase is observed with increasing dopant

concentration. This is to be expected since the pure dopant itself possesses a SmA* phase with a high thermal stability.

Graph 20:- Miscibility diagrams for binary mixtures (i) – (iii) of varying composition containing the dopants and the hosts **8a** and **8b**.

a(ii)

Legend:
- ● SmA* - I
- ■ SmC* - SmA*
- ▲ SmCA* - SmC*
- ◆ SmCA* - SmA*

I

SmA*

SmC$_A$*

Temperature (°C)

| 0% | 12.5% | 25% | 37.5% | 50% | (S)-BE8OF2N |
| 100% | 87.5% | 75% | 62.5% | 50% | **8a** |

b(ii)

Legend:
- ● I - SmA*
- ◆ SmA* - SmCA*

I

SmA*

SmC$_A$*

Temperature (°C)

| 0% | 12.5% | 25% | 37.5% | 50% | (S)-BE8OF2N |
| 100% | 87.5% | 75% | 62.5% | 50% | **8b** |

190

a(iii)

Legend:
- ● I - SmA*
- ■ SmA* - SmC*
- ▲ SmC* - SmCA*
- ✕ Recrys.

Axis labels: Temperature (°C); (S)-NG158; 8a

b(iii)

Legend:
- ● I - SmA*
- ◆ SmA* - SmCA*
- ▢ SmCA* - SmX*
- ✕ Recrys.
- ✚ mp

Axis labels: Temperature (°C); (S)-NG158; 8b
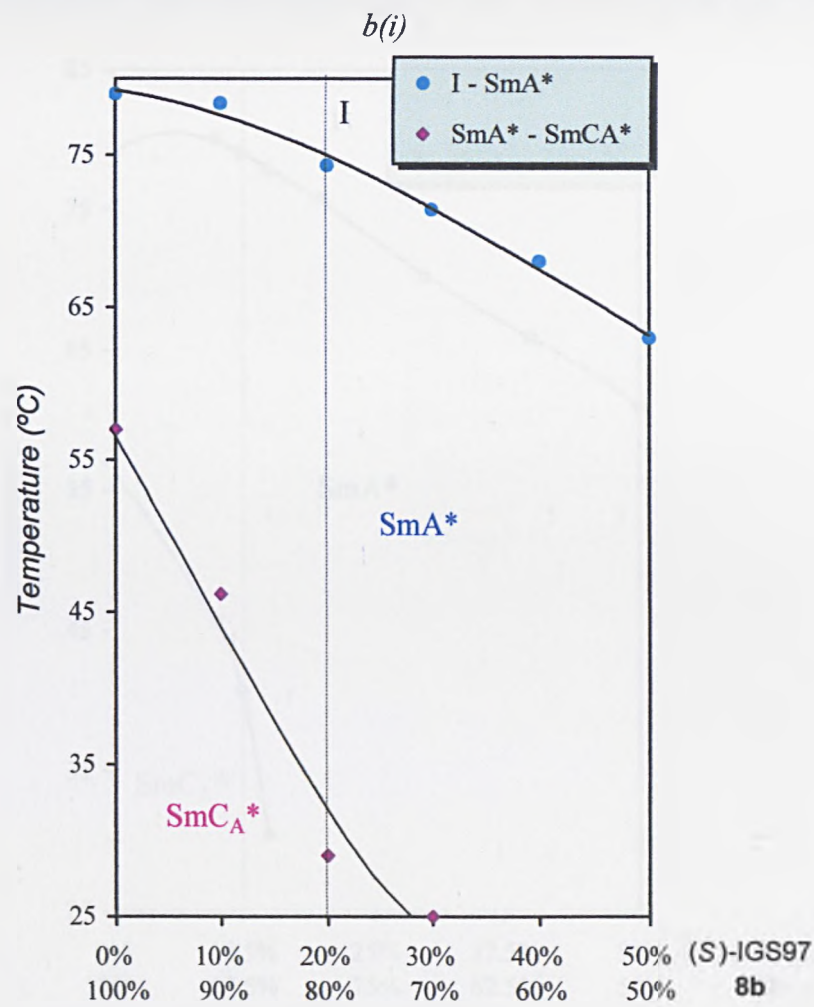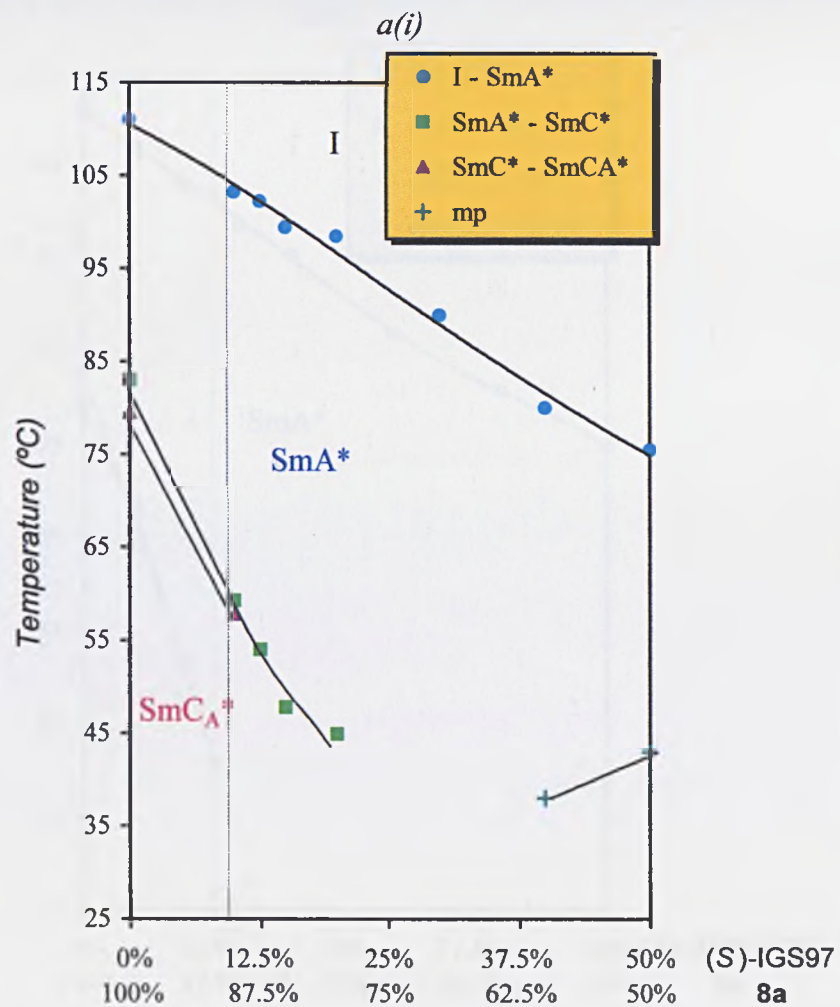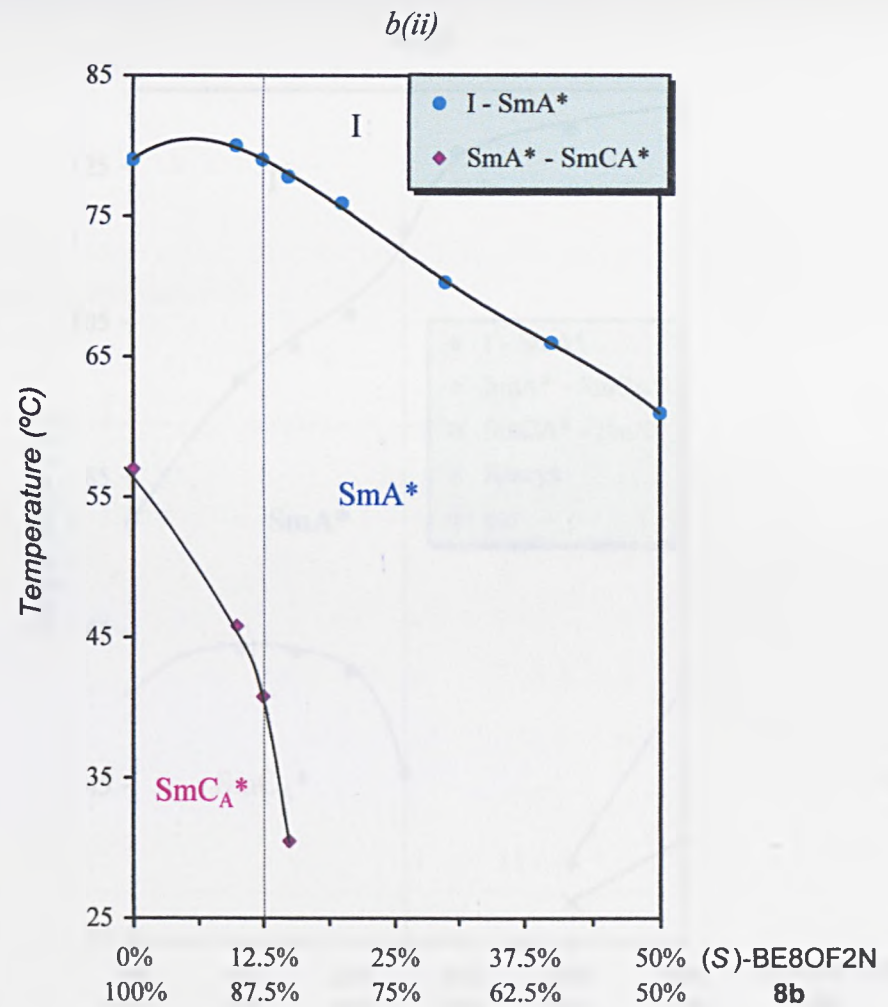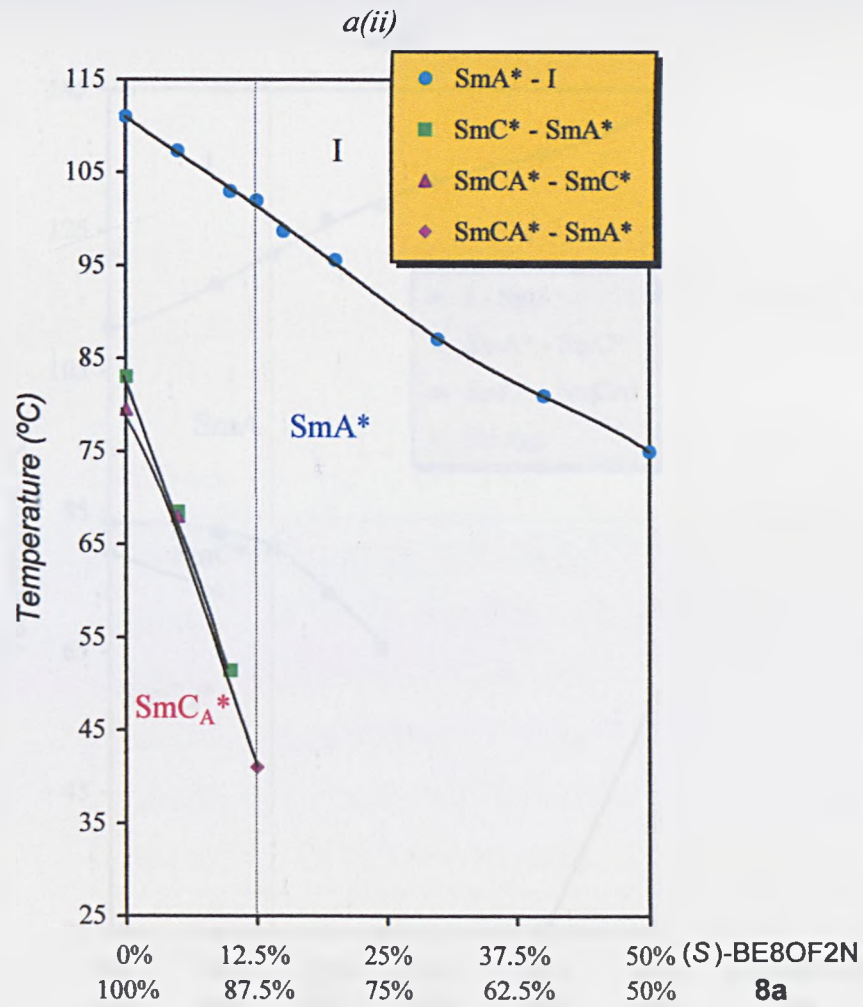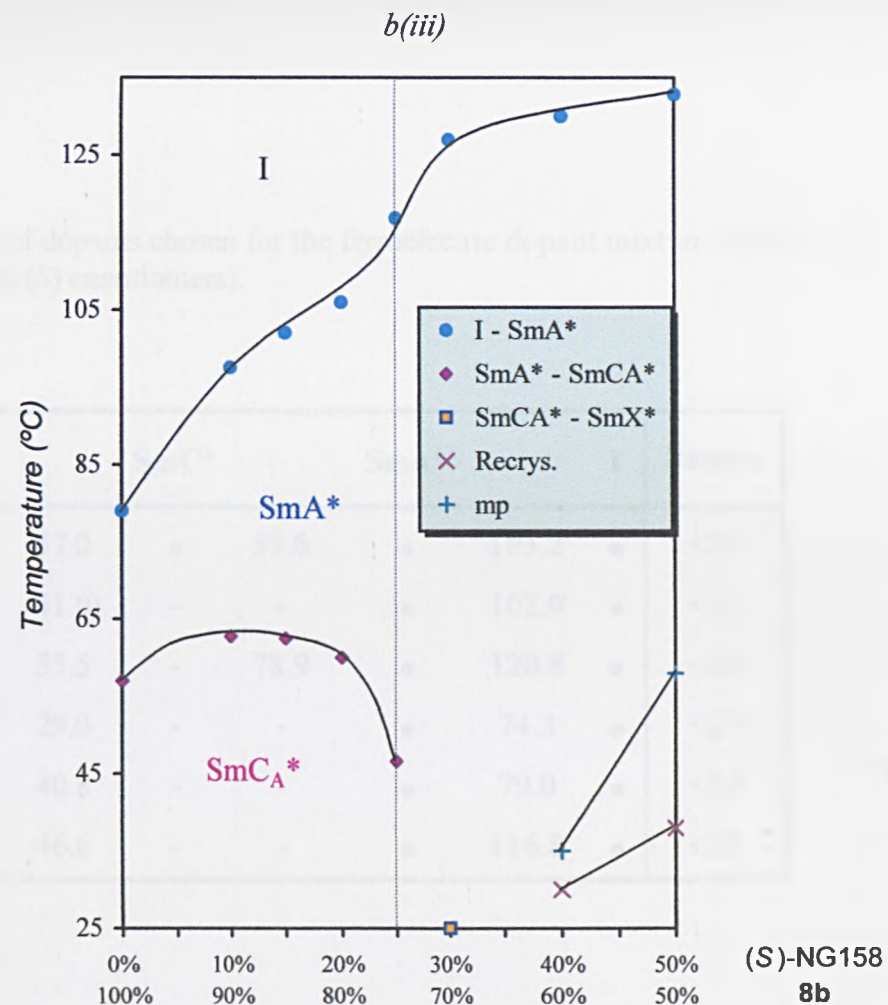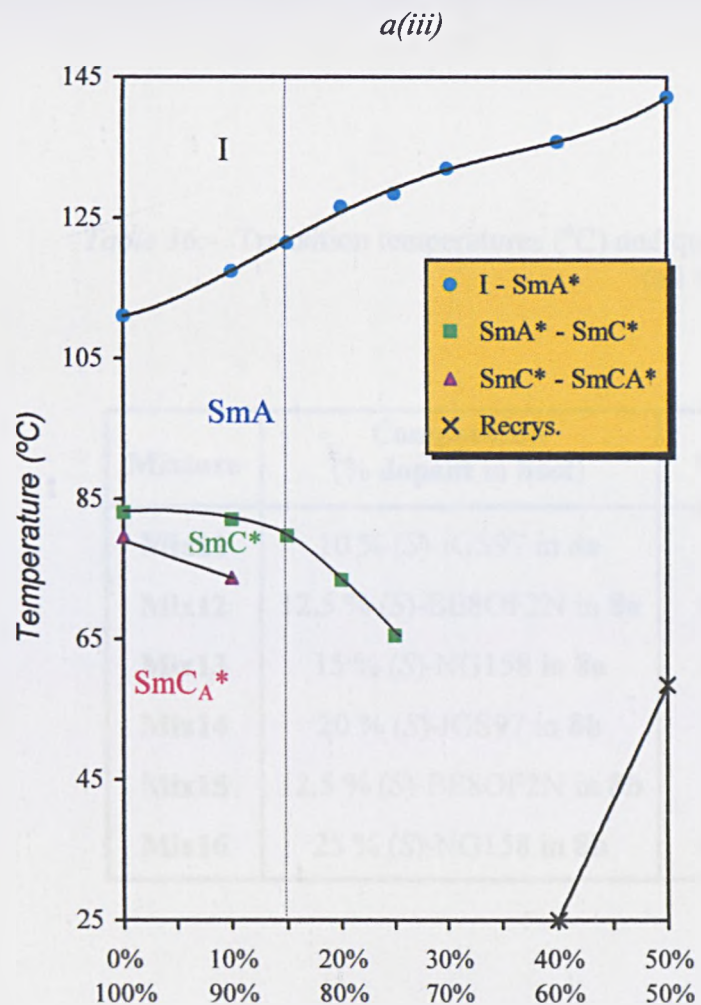
Table 36:- Transition temperatures (°C) and quantities (wt %) of dopants chosen for the ferroelectric dopant mixture studies (all the dopants were (*S*) enantiomers).

Mixture	Composition (% dopant in host)	mp	SmC$_A$*		SmC*		SmA*		I	Recrys.
Mix11	10 % (*S*)-IGS97 in **8a**	-	•	57.0	•	59.0	•	103.2	•	<25
Mix12	12.5 % (*S*)-BE8OF2N in **8a**	42	•	(41.0)	-	-	•	102.0	•	<25
Mix13	15 % (*S*)-NG158 in **8a**	52	•	55.5	-	78.9	•	120.8	•	<25
Mix14	20 % (*S*)-IGS97 in **8b**	-	•	29.0	-	-	•	74.3	•	<25
Mix15	12.5 % (*S*)-BE8OF2N in **8b**	-	•	40.8	-	-	•	79.0	•	<25
Mix16	25 % (*S*)-NG158 in **8b**	40	•	46.6	-	-	•	116.8	•	<25

The miscibility diagrams also allow us to compare the effect of the dopants on the stability of the SmC$_A$* phase in both series of mixtures with **8a** and **8b** as hosts. *Table 37* shows the change in the transition temperatures for the SmC$_{alt}$ phase of the host on addition of 10 % of dopant to form the observed SmC$_A$* phase.

Dopant (10 % b.w.)	ΔT(SmC$_A$* phase in comparison with SmC$_{alt}$ phase of -) Host 8a *(°C)*	ΔT(SmC$_A$* phase in comparison with SmC$_{alt}$ phase of -) Host 8b *(°C)*
(S)-IGS97	- 21.7	- 10.8
(S)-BE8OF2N	- 28.1	- 11.2
(S)-NG158	- 5.7	+ 5.8

Table 37:- Difference in transition temperatures of the induced SmC$_A$* phase in 10 %-doped mixtures of **8a** and **8b** (in comparison with the SmC$_{alt}$ phase of the individual hosts).

Of the two non liquid-crystalline dopants BE8OF2N causes a greater reduction in the transition temperatures of the observed SmC$_A$* phases, in both hosts, than IGS97. In the case of NG158 a smaller decrease in the thermal stability of the SmC$_A$* phase is observed in **8a** than that caused by the other dopants. This is no doubt due to a combination of the liquid-crystalline nature of the dopant and the similarity in structure between the dopant and the host. In fact the similarity in structure (three phenyl rings hence comparable molecular size) may enhance molecular packing in the phase which may be responsible for the increase in the thermal stability of the SmC$_A$* phase observed for the mixture of this dopant and **8b**. This is despite the absence of an antiferroelectric phase in NG158.

The spontaneous polarisation values and tilt angles measured for **Mix11** (10 % IGS97 in **8a**) are shown in *graph 21*. The highest values of the spontaneous polarisation and tilt angle observed were 35.7 nCcm^{-2} and 19 °, respectively, at room temperature. The spontaneous polarisation and tilt angles increase with order parameter as expected. The similarity between the values of spontaneous polarisation obtained at 20 Hz and 50 Hz suggest that saturated switching between ferroelectric states is achieved at 20 Hz. In fact it was not possible to distinguish the usual blue-coloured antiferroelectric phase between the two ferroelectric states (set at "dark" and "light" positions) in this mixture even at low frequencies (0.1 Hz and lower). This suggests that direct switching between the ferroelectric states occurs at relatively low frequencies. Unlike the analogous antiferroelectric-doped mixture (**Mix1**; 15 % MHPOBC in **8a**) the spontaneous polarisation trend for **Mix11** does not appear to indicate any changes in threshold voltage as indicated by a "dip" in the observed spontaneous polarisation on cooling to room temperature. This may also be due to the fact that the "standard" applied field (100 V_{pp}) is well above the threshold required for switching to the ferroelectric state. After reducing the applied field to 30 V_{pp} the antiferroelectric state still indistinguishable at frequencies as low as 0.1 Hz.

A further peculiarity of this mixture was that on disconnecting the power to the cell some regions of the cell appeared to remain fixed in the ferroelectric state (visible as bright green stripes across the cell) whereas some regions (domains) appeared to relax into the typical blue-coloured texture of the antiferroelectric phase (*figure 87*).
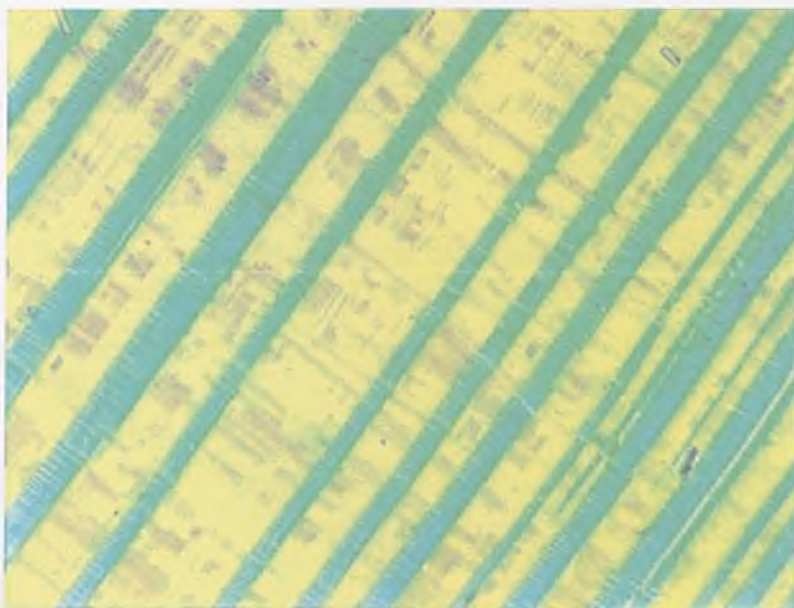
Figure 87:- Coexistence of ferroelectric (yellow and dark yellow regions) and antiferroelectric (blue stripes) domains in a cell of **Mix11**.

Although the relaxation time of antiferroelectric materials, from the ferroelectric to antiferroelectric state, is known to be quite long in the absence of a suitable applied field these ferroelectric stripes were still visible at zero voltage an hour later. In most cases the time taken for relaxation to the antiferroelectric phase is milliseconds [118]. Short-circuiting the cell by connecting a cable between the electrode sockets of the cell holder, to ensure that the persistence of the ferroelectric domains was not a consequence of a residual cell capacitance, had no observable effect on diminishing the number of yellow ferroelectric stripe domains visible through the crossed polarisers. These observations are similar to those made by Moritake *et al.* [119] and Hatano *et al.* [120] in cells of individual antiferroelectric materials. It was speculated that the occurrence of stripe domains such as these was due to a form of *coexistence*, between domains of molecules arranged in SmC* and SmC$_A$* geometries, in *thin* cells as a consequence of the greater influence of the alignment layers on the smectic layer structure. This is thought to be brought about by the preservation of the synclinic SmC* ordering in thin cells (due to surface pinning

effects, or "surface stabilisation") which results in a decreased tendency for the molecules to relax back to the anticlinic SmC_A^* ordering.

Graph 21:- Spontaneous polarisation and tilt angles as a function of temperature measured for **Mix11** (10 % (*S*)-IGS97 in **8a**)
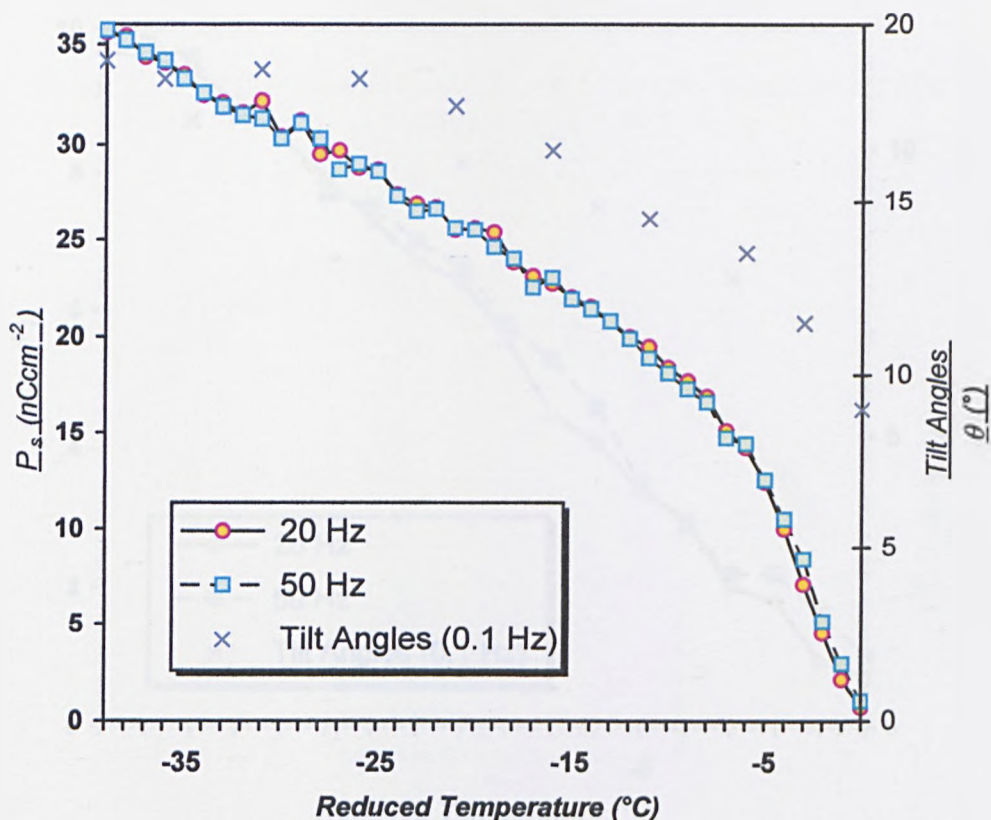
Graph 22 shows the spontaneous polarisation and tilt angles measured for **Mix12** (12.5 % (*S*)-BE8OF2N in **8a**). The values are smaller than those obtained for **Mix11** despite the presence of a slightly larger quantity of dopant. This is not an unusual observation as (*S*)-BE8OF2N is known to induce a smaller spontaneous polarisation in chiral-dopant ferroelectric SmC* mixtures than a similar quantity of IGS97 [115]. It would also be reasonable to expect a similar observation in chiral-dopant antiferroelectric mixtures. Furthermore the tilt angle of **Mix12** is lower than that observed for **Mix11** so this must clearly contribute to the lower overall spontaneous

polarisation, since the size of the spontaneous polarisation of course also depends on the tilt angle, θ.

Graph 22:- Spontaneous polarisation and tilt angles measured for **Mix12** (12.5 % (*S*)-BE8OF2N in **8a**)
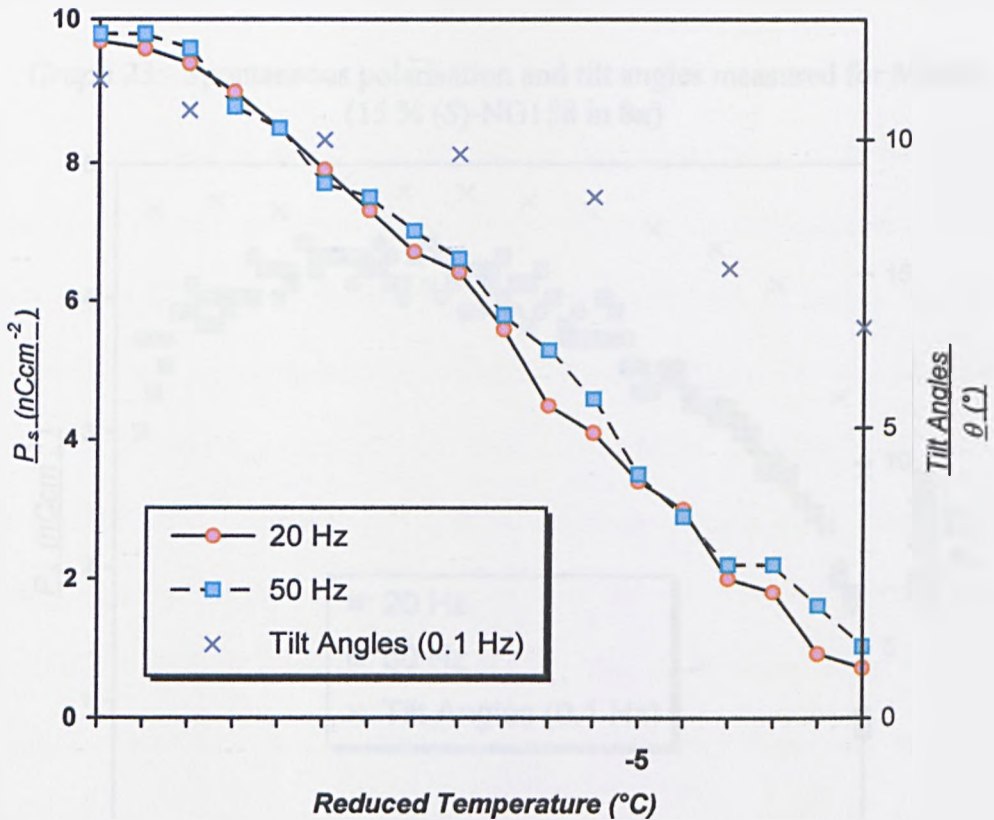
The spontaneous polarisation trend observed in **Mix13** (15 % (*S*)-NG158 in **8a**, *Graph 23*) shows a different behaviour to the trends observed in **Mix11** and **Mix12**. In this mixture the spontaneous polarisation increases to a temperature about 44 °C below the clearing point, but then decreases on further cooling to room temperature. In the case of **Mix1** (15 % (*S*)-MHPOBC in **8a**) the "dip" in spontaneous polarisation was postulated to be an artefact due to an increase in the threshold voltage required for switching to the ferroelectric state to a value above the applied field. We may also postulate that in **Mix13** the decrease in the spontaneous polarisation is due to an increase in threshold above the applied field on approaching

room temperature. This may be due to a very high viscosity at low reduced temperatures. We would consequently expect that a larger applied field would eliminate this apparent decrease in the value of the spontaneous polarisation at lower temperatures.

Graph 23:- Spontaneous polarisation and tilt angles measured for **Mix13** (15 % (*S*)-NG158 in **8a**)
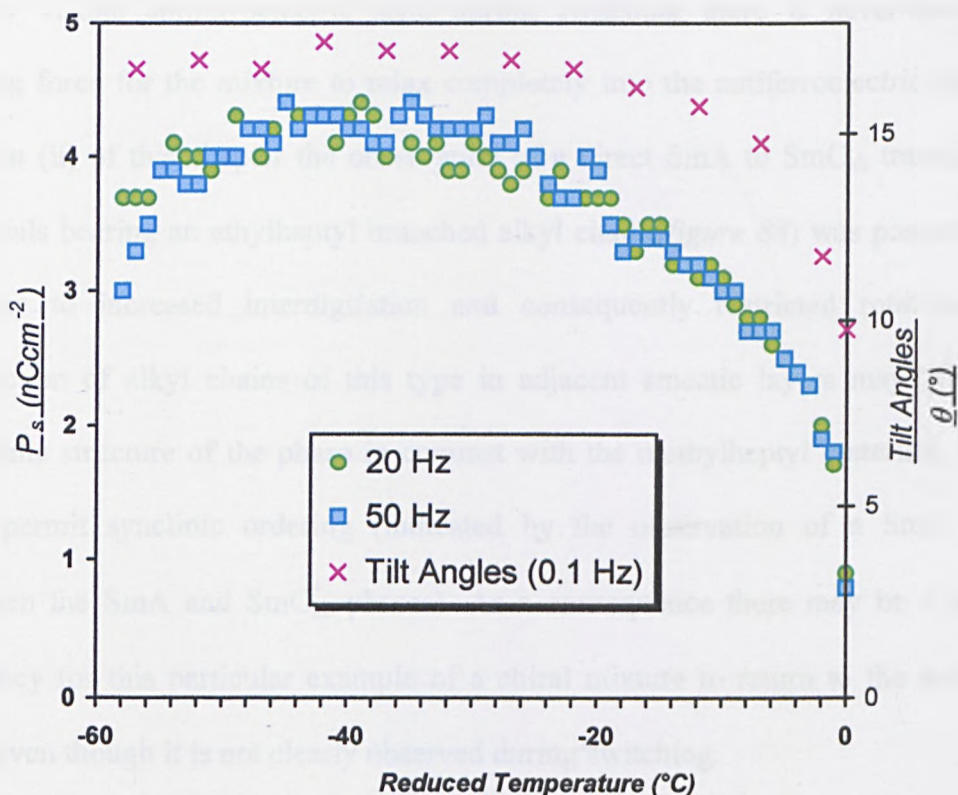
A larger quantity of dopant could be dissolved into the second of the selected host materials, **8b**. This gave rise to a higher spontaneous polarisation value for **Mix14** which contained twice the quantity of (*S*)-IGS97 dopant (20 % by weight, *Graph 24*) than **Mix11** (in which **8a** was the host). The range at which switching was observed was smaller than **Mix11** due to the lower transition temperature of the SmC$_A$* phase in **Mix14**. The spontaneous polarisation does not appear to reach saturation at room temperature (-14 °C reduced temperature), but perhaps by cooling the sample to

below room temperature a "levelling" of the spontaneous polarisation values would be observed indicating saturation. As with **Mix11** a clear antiferroelectric state could not be observed in this mixture. After disconnecting the power leads and short-circuiting the cell, however, the blue colour of the antiferroelectric phase could be observed throughout the entire cell after several seconds. The absence of the bright green ferroelectric stripes in this mixture indicates that despite the absence of a clearly visible antiferroelectric state during switching there is never-the-less a driving force for the mixture to relax completely into the antiferroelectric state. In **section (ii)** of this chapter the observation of a direct SmA to SmC$_{alt}$ transition in materials bearing an ethylheptyl branched alkyl chain (*figure 88*) was postulated to be due to increased interdigitation and consequently restricted rotation. The interaction of alkyl chains of this type in adjacent smectic layers may "fix" the anticlinic structure of the phase in contrast with the methylheptyl materials, which may permit synclinic ordering (indicated by the observation of a SmC phase between the SmA and SmC$_{alt}$ phases). As a consequence there may be a greater tendency for this particular example of a chiral mixture to return to the anticlinic state even though it is not clearly observed during switching.

	$\underline{n}$	Phases observed
	1	SmA, SmC, SmC$_{alt}$
	2	SmA, SmC$_{alt}$

$C_xH_{2x+1}O$ —

x = 10 or 12

C_nH_{2n+1}

C_6H_{13}

F
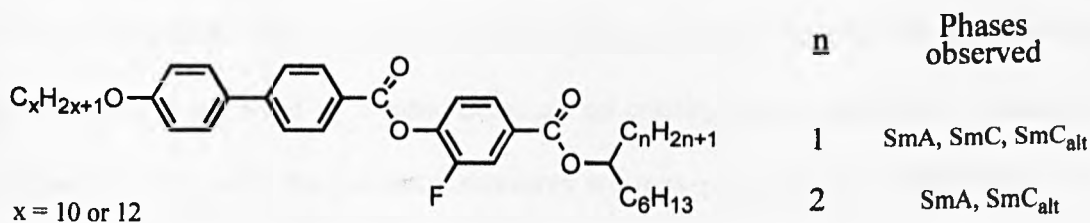
Figure 88:- General structure of the host materials in which an ethylheptyl alkyl substituent (**n** = 2) favours anticlinic ordering more than a methylheptyl substituent (**n** = 1).

Graph 24:- Spontaneous polarisation and tilt angles measured for **Mix14** (20 % (*S*)-IGS97 in **8b**)
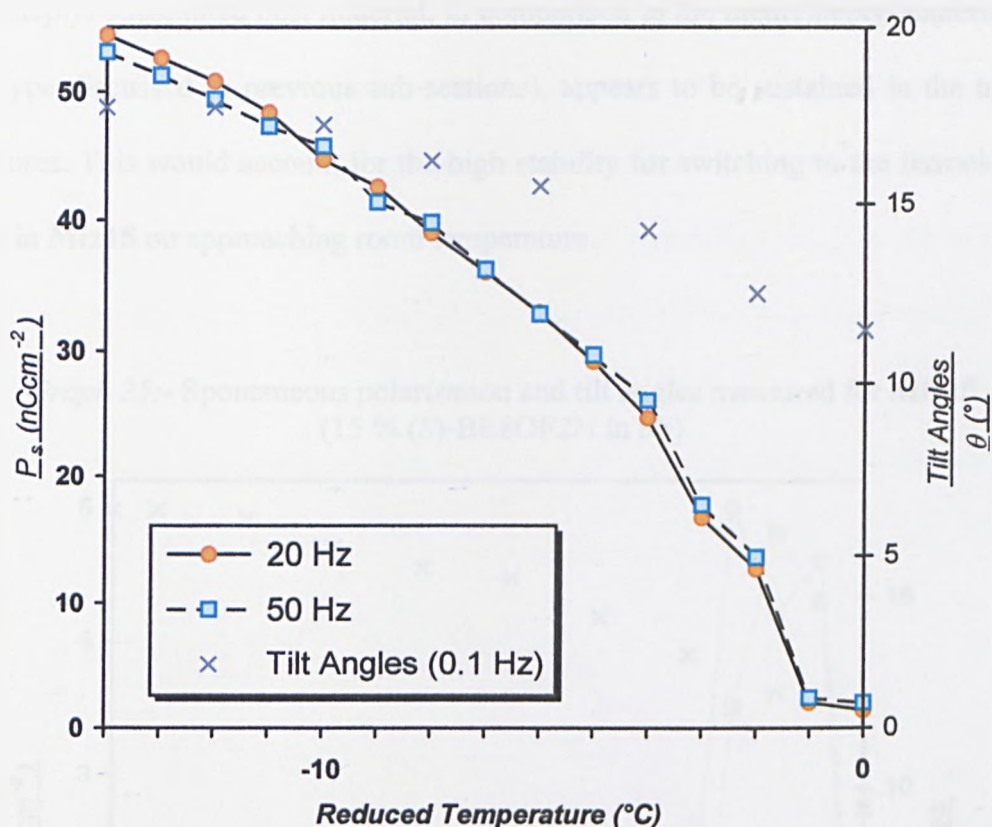
The spontaneous polarisation trend observed for the next mixture, **Mix15** (12.5 % (*S*)-BE8OF2N in **8b**, *Graph 25*), was completely different to **Mix12** (12.5 % (*S*)-BE8OF2N in **8a**) despite an identical quantity of dopant. As with some of the earlier binary mixtures containing a highly stable antiferroelectric dopant (such as **Mix3**, 15 % (*S*)-TFMHPODDBC in **8a**) an initial increase in the value of the spontaneous polarisation is followed by a rapid decrease on cooling below the SmC$_A$* transition temperature. As with the previous mixtures we may presume that this behaviour is due to a rapid increase in the threshold voltage above the applied field strength. The fact that two closely related systems, with the same quantity and type of dopant, behave so differently is consistent with the general observation that *simple* modifications in the structure of the host material *can* have a marked effect on the

physical properties of the binary mixture. Greater steric interaction in the ethylheptyl-substituted host material, in comparison to the methylheptyl material (of the type discussed in previous sub-sections), appears to be sustained in the binary mixtures. This would account for the high stability for switching to the ferroelectric state in **Mix15** on approaching room temperature.

Graph 25:- Spontaneous polarisation and tilt angles measured for **Mix15** (15 % (*S*)-BE8OF2N in **8b**)
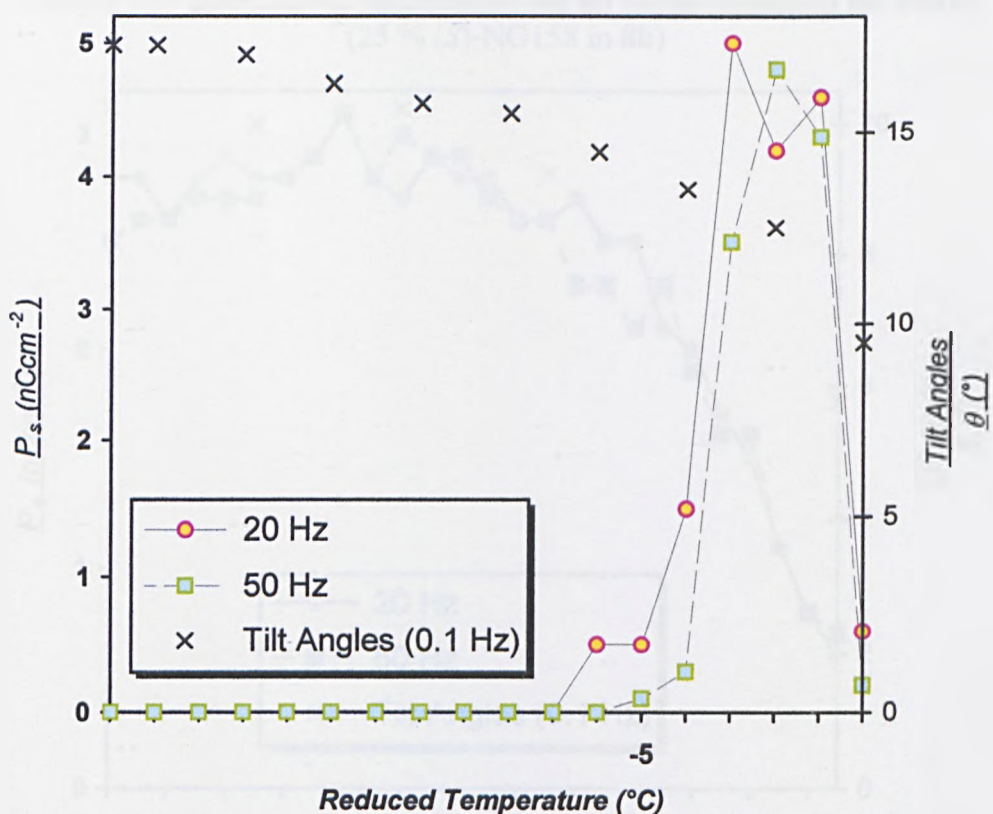
The final binary mixture in this series, **Mix16** (25 % (*S*)-NG158 in **8b**), showed the lowest spontaneous polarisation values of all the ferroelectric-doped series of mixtures (*Graph 26*). This was despite the largest quantity of dopant. A possible explanation is that, once again, the magnitude of the applied field did not allow complete switching between ferroelectric states to take place in the mixture either at 20 Hz or 50 Hz. This is partially supported by the slight decrease in the observed

spontaneous polarisation on approaching room temperature. Furthermore the liquid-crystalline dopant, NG158, itself possesses a moderate spontaneous polarisation of around 50 nCcm^{-2}. In combination with the above factors we would, therefore, not expect to observe a very large spontaneous polarisation in the binary mixture. As with the previous examples, however, saturated switching could be observed at much lower frequencies (0.1 Hz) which permitted the tilt angles to be measured[App.G].

Graph 26:- Spontaneous polarisation and tilt angles measured for **Mix16** (25 % (S)-NG158 in **8b**)
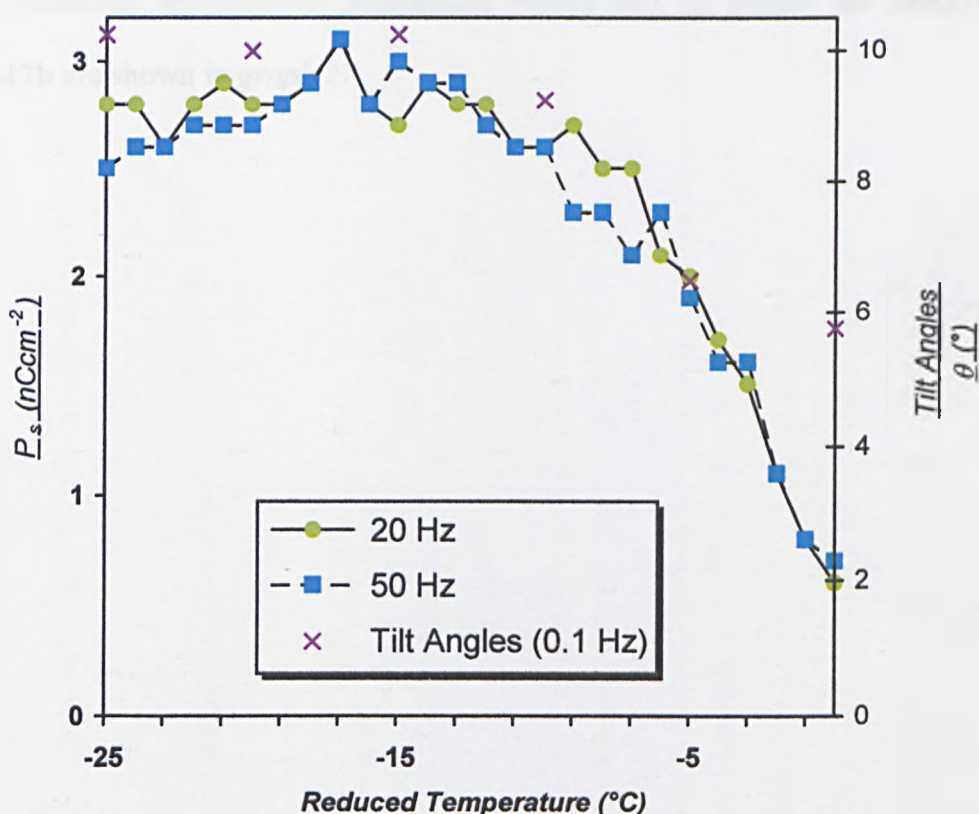
In the final series of binary mixtures a ferroelectric dopant was added to a swallow-tailed host material (**2c**). Measurements were carried out on mixtures with a lower concentration of dopant, ie. 2.5 % and 5 % (S)-IGS97 dopant and 2.5 % (S)-BE8OF2N in order to maintain the occurrence of the "SmY*" phase. The transition temperatures of these two mixtures (**Mix17a** and **Mix17b**), together with the mixture

containing 2.5% BE8OF2N dopant (**Mix18**), are listed in *table 38*.

Adding 5 % (by weight) of (*S*)-IGS97 to the host has the effect of lowering both the SmA* and SmC$_A$* transition temperatures more than that observed on adding 2.5 %. A curious observation is that the "SmY*" phase appears to be actually raised in temperature by a few degrees in **Mix17a** (2.5 % (*S*)-IGS97 in **2c**) in comparison with the SmY phase of the undoped host.

The measured spontaneous polarisation values and tilt angles for **Mix17a** and **Mix17b** are shown in *graph 27*.

Table 38:- Composition and transition temperatures (°C) of **Mix17a**, **Mix17b**, and **Mix18**.

host material:

2c

dopants:

(*S*)-IGS97

(*S*)-BE8OF2N
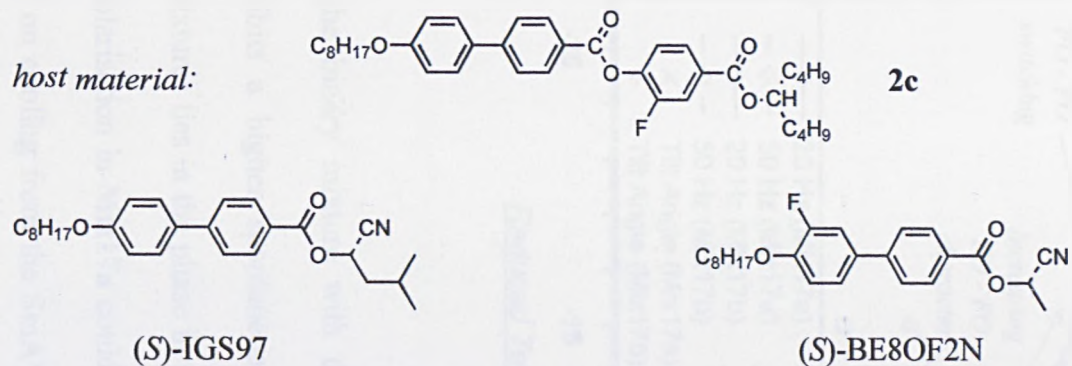
Host / Mixture	Composition (% dopant b.w.)	mp	"SmY" / "SmY"*		SmC_alt / SmC_A *		SmA / SmA*		I	Recrys.
2c	(Host Material)	56	●	(28.0)	●	(57.0)	●	85.0	●	<25
Mix17a	5 % (*S*)-IGS97 in **2c**	41	●	(27.6)	●	(45.6)	●	82.7	●	<25
Mix17b	2.5 % (*S*)-IGS97 in **2c**	44	●	(30.2)	●	(48.4)	●	83.6	●	<25
Mix18	2.5 % (*S*)-BE8OF2N in **2c**	45	●	(32.6)	●	(48.4)	●	83.4	●	<25

Graph 27:- Spontaneous polarisation and tilt angles measured for **Mix17a** and **Mix17b** (2.5 % and 5 % (*S*)-IGS97 in **2c** respectively)
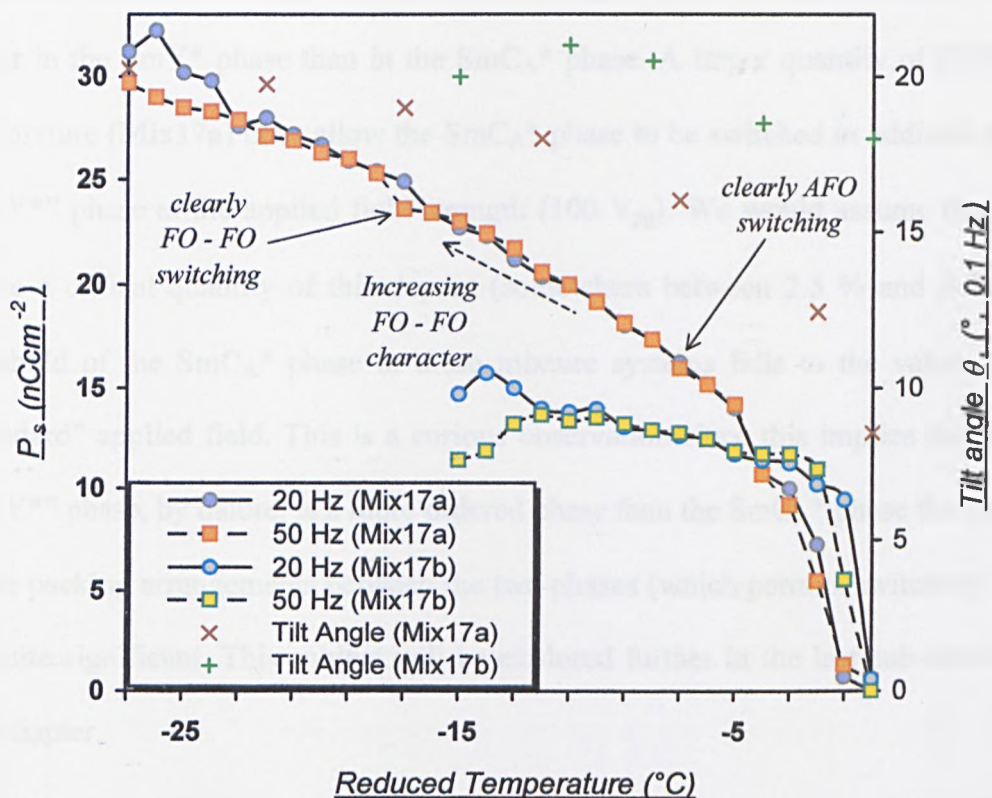
As expected the binary mixture with the larger quantity of (*S*)-IGS97 dopant (**Mix17a**) exhibits a higher spontaneous polarisation. The principal difference between the mixtures lies in the phase in which switching is observed. Whereas the spontaneous polarisation in **Mix17a** could be detected below the transition into the SmC$_A$* phase, on cooling from the SmA* phase, a spontaneous polarisation could only be observed in **Mix17b** below the transition into the SmY* phase. This was also observed in **Mix7** (15 % (*S*)-MHPOBC in **2c**). It appears that a small quantity of a high spontaneous polarisation-inducing dopant (2.5 % (*S*)-IGS97) is sufficient to allow the "SmY*" phase to be switched without switching the overlying SmC$_A$* phase above. Obviously a spontaneous polarisation is only visible when switching between ferroelectric states occurs and consequently it is not observed in the SmC$_A$*

phase. As with **Mix7** the absence of switching in the SmC_A^* phase is most probably due to the threshold voltage required for switching between ferroelectric states being lower in the SmY^* phase than in the SmC_A^* phase. A larger quantity of IGS97 in the mixture (**Mix17a**) does allow the SmC_A^* phase to be switched in addition to the "SmY^*" phase at the applied field strength (100 V_{pp}). We would assume then that above a critical quantity of this dopant (somewhere between 2.5 % and 5 %) the threshold of the SmC_A^* phase in these mixture systems falls to the value of the "standard" applied field. This is a curious observation since this implies that if the "SmY^*" phase, by nature, is a more ordered phase than the SmC_A^* phase the change in the packing arrangements between the two phases (which permits switching) may be quite significant. This subject will be explored further in the last sub-section of this chapter.

Another similarity of **Mix17a** to **Mix7** was the nature of the observed switching in the "SmY^*" phase. The absence of a clearly observable antiferroelectric phase even at fairly low frequencies suggests that the switching, and consequently the phase itself, may be ferroelectric in character. In **Mix17b** the switching in the SmC_A^* phase was clearly tristate (hence antiferroelectric) at 7 °C below the transition to the SmC_A^* phase (labelled on *graph 27*). On cooling to 2 °C above the transition temperature of the underlying "SmY^*" phase (-17 °C reduced temperature) the switching became increasingly ferroelectric in character. This is the opposite of what is commonly observed in the SmC_A^* phase of purely chiral materials. By cooling further into the phase the antiferroelectric state usually becomes more stable as the ability of the materials to be switched from the antiferroelectric to the ferroelectric states becomes increasingly more difficult (due to increased viscosity).

No clearly discernible change in texture could be observed on cooling into the "SmY*" phase from the SmC$_A$* phase in **Mix17b**. This suggests that as a consequence of the larger quantity of dopant present in this mixture there is some form of "overlap" between the SmC$_A$* and "SmY*" phases in the cell. The two types of switching may momentarily *coexist* around the transition to the "SmY*" phase. Similar forms of coexistence between phases with different structures have been observed and reported earlier [119-121].

The divergence observed in the values of spontaneous polarisation close to room temperature, at 20 Hz and 50 Hz in both **Mix17a** and **Mix17b**, may be due to a reduction in saturated ferroelectric switching at 50 Hz in comparison with the switching at 20 Hz. This difference may be due to the increased viscosity of the mixture close to room temperature, which makes it more difficult for the molecules to respond to the field. As a consequence only partial (unsaturated) switching may be achieved at higher frequencies, which would of course lead to a decrease in the observed spontaneous polarisation. A marked difference in the value of the spontaneous polarisation between the two frequencies was also observed in **Mix18** (2.5% (*S*)-BE8OF2N in **2c**) (*graph 28*).
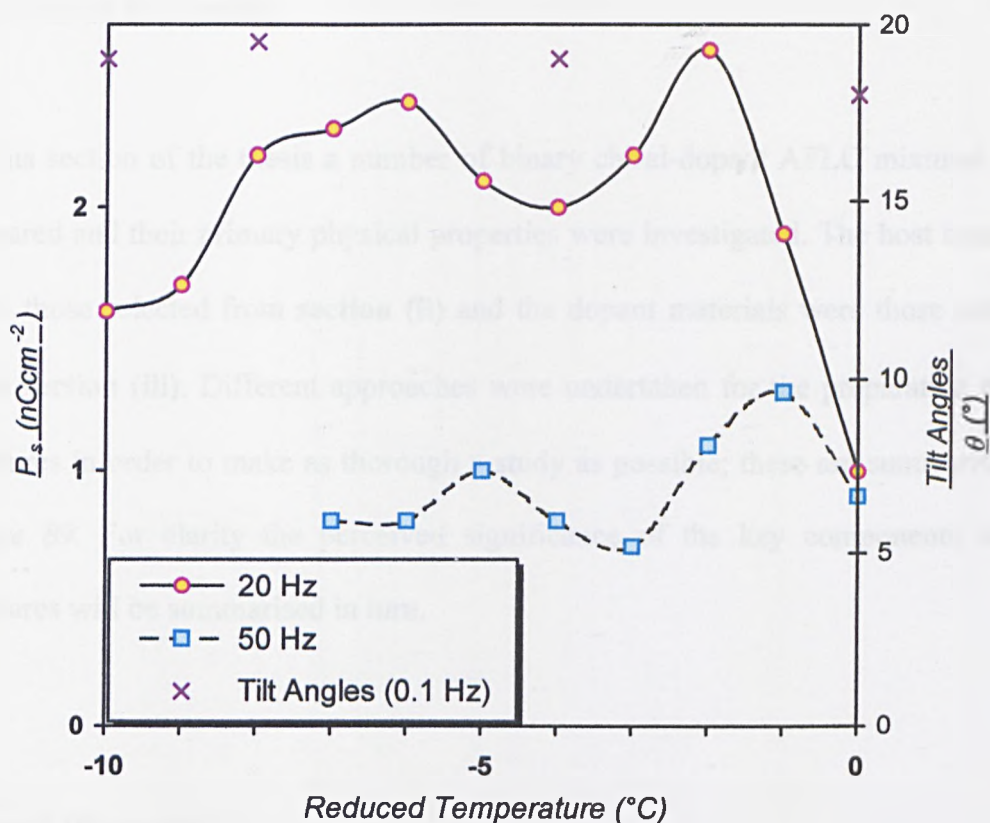
Graph 28:- Spontaneous polarisation and tilt angles measured for **Mix17a** and **Mix17b** (5% and 2.5% (*S*)-IGS97 in **2c** respectively)

Although the BE8OF2N dopant used in this mixture is known to induce, in mixtures, a lower spontaneous polarisation in comparison with the same quantity of IGS97 [115], the values of the observed spontaneous polarisation in this mixture were found to be even lower than expected. This, together with the very pronounced difference between the values obtained at 20 Hz and 50 Hz, indicates that saturated switching does not occur at the "standard" applied field strength. As with **Mix17a** above only the "SmY*" phase was found to switch between ferroelectric states. No clear trend is discernible at either frequency. This is most probably due to the relatively high level of error associated with measuring very small spontaneous polarisation values.

<u>Summary of this Section</u>

In this section of the thesis a number of binary chiral-dopant AFLC mixtures were prepared and their primary physical properties were investigated. The host materials were those selected from **section (ii)** and the dopant materials were those selected from **section (iii)**. Different approaches were undertaken for the preparation of the mixtures in order to make as thorough a study as possible; these are summarised in *figure 89*. For clarity the perceived significance of the key components in the mixtures will be summarised in turn.

General Observations

The investigations showed that the behaviour of the mixtures in test cells depends very strongly both on the type of dopant used and the nature of the host material itself. Although this is the case for virtually any kind of liquid crystal mixture based on the chiral-dopant concept, regardless of the actual phase of interest, it appears that this is of particular significance in the AFLC mixtures studied. The mode of switching of the induced SmC_A^* phase of certain mixtures, which were found to switch electrooptically at or close to room temperature, could be clearly classified as tristate (antiferroelectric) in character (eg. **Mix17b**). In certain other "switchable" mixtures (eg. **Mix1** and **Mix11**) the mode of switching could not be clearly identified as being tristate in nature. This was due firstly, to the absence of a clearly observable "third" (antiferroelectric) state and secondly, to the persistence of ferroelectric stripe-domains in the cells after removal of the applied field.
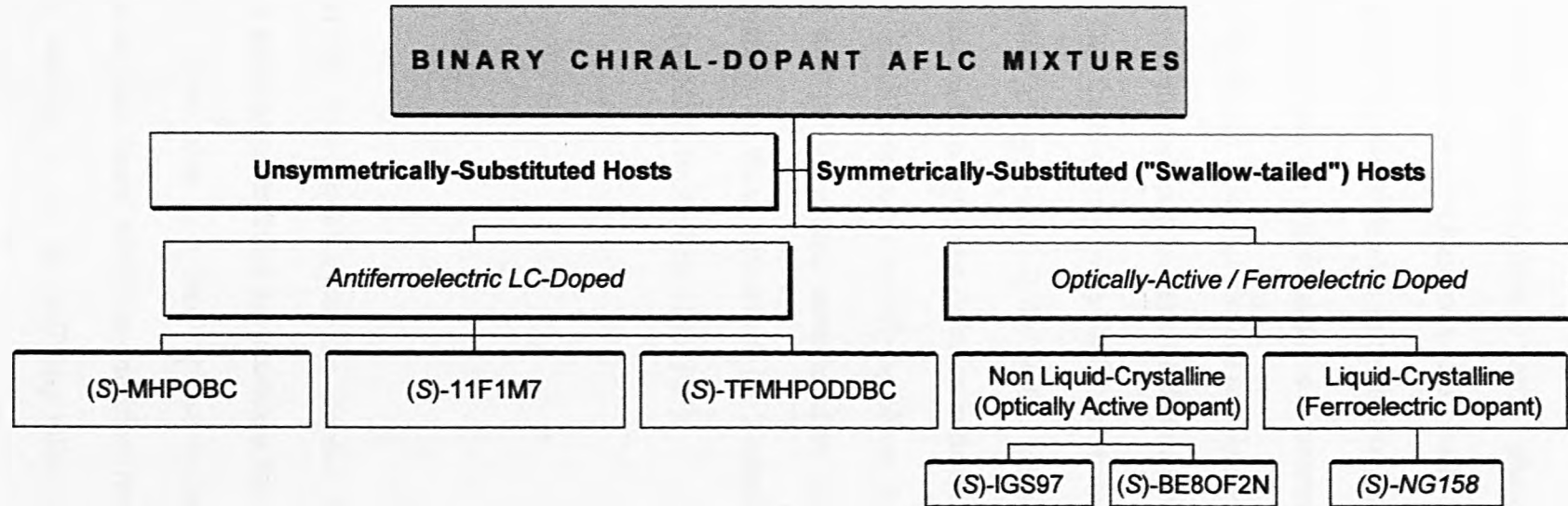
Figure 89:- Summary of the different types of binary chiral-dopant AFLC mixtures prepared in this section.

This is particularly interesting when taking into account the fact that the mixtures were classified as being antiferroelectric, in the first instance, by the observation of characteristic textural defects common to SmC_A^* phases [116]. The transition to the SmC_A^* phase from the SmC^* phase was also clearly visible on a glass microscope slide. It is apparent that the difference in the behaviour of the mixture in the cell, as compared to its behaviour on a glass slide, is a consequence of the alignment layers on the surfaces of the cell. The significance of alignment layers on the behaviour of chiral smectic systems confined in cells of different thickness is very well known [64, 122-125]. The observation of only SmC^* behaviour (direct FO – FO switching) in a mixture, which is supposedly in the SmC_A^* phase, suggests that the anticlinic order is suppressed and the synclinic ordering initiated in the SmC^* phase above the SmC_A^* phase is maintained in the underlying phase. A form of coexistence between the SmC^* and SmC_A^* phases was speculated to be present in certain mixtures. Further investigations on these mixtures at the Technical University of Berlin have recently confirmed this to be the case [126, 127].

Dopant Materials

It appears that the non liquid-crystalline dopant IGS97 in the methyl-heptyl substituted host material (compound **8a**) promotes the switching of the mixture in a manner which is more akin to a SmC^* phase rather than a SmC_A^* phase. The possible causes for this, based solely on empirical observations, were discussed in this section. In contrast to the destabilising effect of the non liquid-crystalline dopants on the SmC_A^* phase, on both the transition temperatures and the switching

characteristics, the antiferroelectric dopants generally have a stabilising effect on the SmC$_A$* phase. As we would expect, the relative stability of these dopants is conferred into the mixture; dopants with a high thermal stability and high threshold field for the SmC$_A$* phase confer a higher thermal stability and likewise a high threshold voltage into the mixture.

Host Materials

Only mixtures composed of methylheptyl-substituted host materials showed distinct electrooptic switching between ferroelectric states. In contrast the mixtures in which the host materials possess a greater driving force to maintain anticlinic ordering, such as the swallow-tailed materials or the ethylheptyl substituted materials (for the reasons outlined in **section (i)**), exhibit little or no electrooptic switching. This is most likely due to the high stability for switching the antiferroelectric state to the ferroelectric state, as a consequence of the greater degree of interdigitation of these hosts, in comparison to the methylheptyl-substituted hosts.

Field Strength

It is also clear from the results that the applied field was not sufficiently large enough to completely switch all of the mixtures to the ferroelectric states from the antiferroelectric state. Partial switching of the mixture across the cell more-than-likely accounts for the unusual trends of the measured spontaneous polarisation

values. A larger applied field would have certainly ensured that saturated switching was effected across the entire cell. However, it is unlikely that some of the unusual observations, such as the changes in thresholds of certain mixtures (**Mix1**) or the evidently large difference in threshold between the SmC_A^* phase and the "SmY^*" phase (**Mix17b**) would have been noticed in this case. In order to make a valid comparison, not only between all the mixtures but also all the chiral antiferroelectric materials from **section (iii)**, the strength of the applied field was maintained at 100 V_{pp} (10 $V_{ac}\mu m^{-1}$).

Response Times and Contrast Ratios

The response times of the mixtures were considered to be of significance since a relatively fast response time (or switching time, on the order of hundreds of microseconds and faster) is required to achieve video frame rate at high resolution. *Table 39* shows the response times of two of the binary mixtures with compound **8a** as the host. The values listed were measured for switching between FO – FO states rather than the AFO – FO states for qualitative reasons[App.G]. The response times appear to be fast enough to allow us to speculate that multi-component mixtures based on these binary mixtures may be able to support video frame rate at medium to medium-high resolutions (VGA and SVGA respectively).

Mixture	Composition (% dopant in host)	Response time (μs)
Mix11	10 % (S)-IGS97 in 8a	50 - 60
Mix12	12.5 % (S)-BE8OF2N in 8a	100 -110

Table 39:- Response times for switching between ferroelectric states in two of the binary chiral-dopant mixtures (25 °C, 100 V_{pp} square wave).

The contrast ratio of any type of liquid-crystalline mixture intended for use in a display device is an important parameter in the evaluation of the mixture. The measurement of the contrast ratio was not, however, regarded to be very useful for the binary AFLC mixtures studied since the cells available (5 μm Linkam) were too thick to achieve a phase shift of $\lambda/2$ of plane-polarised light. This is of course the reason why the "dark" and "light" states appeared coloured (usually dark brown and yellow/green, respectively) during the switching of the mixtures in the cells. Thinner cells (on the order of 1.5 – 2 μm) are usually used in order to achieve a black "dark" state and a white "light" state in AFLC mixtures.

The contrast ratios of several mixtures were however measured for the purpose of gaining experience of the technique but were not presented.

UNUSUAL MESOMORPHIC BEHAVIOUR

Overview

In this final section of the **Results and Discussion** chapter we study the unusual mesomorphic behaviour in some of the non-chiral materials observed during the course of this work.

The "SmY" Phase

A number of unidentified smectic phases were observed below the SmC or SmC$_{alt}$ phases of several undoped host materials. The non-fluorinated chiral versions of many of the materials, principally the MHPOBC series, are known to possess more ordered phases such as the SmI$_A$* or SmI* [58, 128]. Consequently it should not be unusual for similar non-chiral phases to be observed in the non-chiral fluorinated versions of the materials (albeit at lower temperatures). Some of the host materials, however, were found to exhibit a phase that could not be clearly classified as a hexatic-ordered phase. This phase, the "SmY" (as it is referred to in this thesis), was initially observed in compound **2c** and subsequently some of its homologues. *Table 40* summarises the transition temperatures of the materials that possess this phase in addition to those that were found to possess a phase with a similar optical texture to that of the "SmY" (denoted as "SmX$_2$"). *Figure 90* shows the optical textures of the "SmY" phase in thin and thick samples of compound **2c**.

Table 40:- Transition temperatures (°C) and phase sequence of the host materials showing "SmY" and "SmX$_2$" phases.
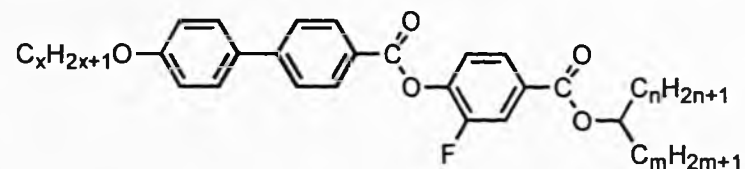
Host	x	n	m	mp	SmX$_2$		"SmY"		SmC$_{alt}$		SmA		I	Recrys.
2a	7	4	4	54	-	-	●	(36.6)	●	55.0	●	91.1	●	26
2c	8	4	4	56	-	-	●	(28.0)	●	(54.0)	●	85.0	●	<25
7e	8	1	6	48	●	(38.0)	●	-	●	49.0	●	117.0	●	27
7h	8	2	6	37	●	(20.0)	●	-	●	56.2	●	94.2	●	<25
7g	8	2	5	34	●	(22.0)	-	-	●	53.5	●	93.5	●	<25
6b	8	3	5	46	-	-	●	(28.0)	●	54.6	●	82.4	●	27

Figure 90:- Optical textures of the SmC$_{alt}$ and "SmY" phase in *thin* and *thick* samples of compound **2c** (a) and (b) respectively.

(a) thin sample
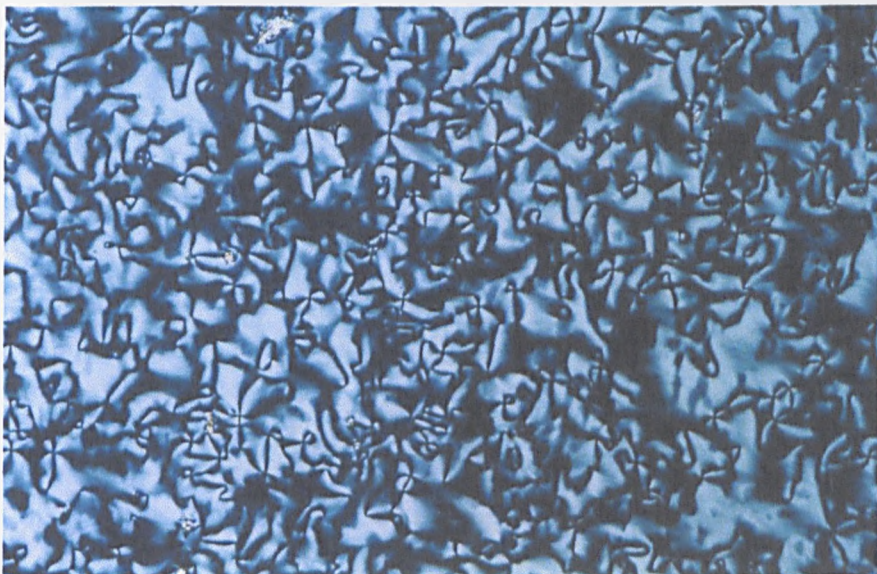
SmC$_{alt}$ (43.1 °C)
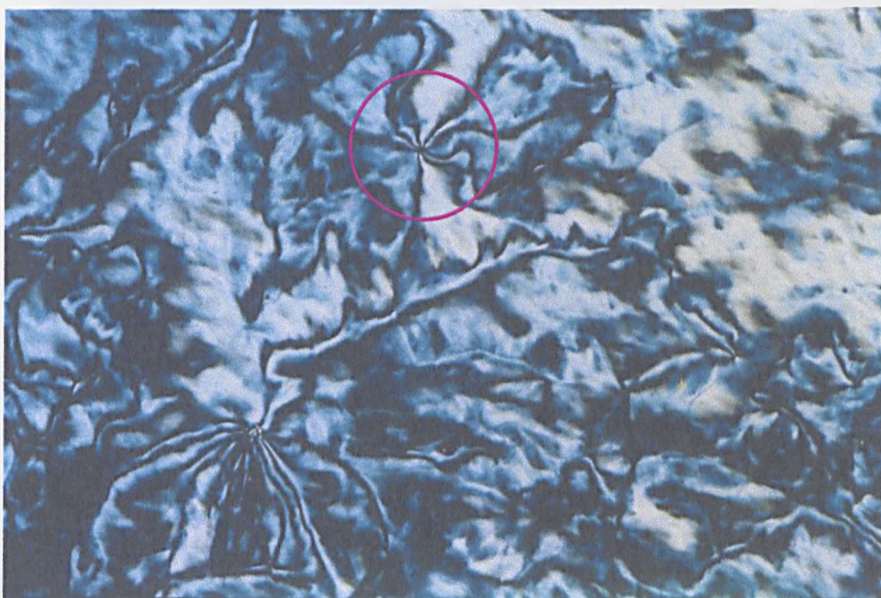
"SmY" (28.8 °C); note the apparent eight-brush defect (circled). Such a defect has not been reported in any other smectic materials.

(b) thick sample

SmC$_{alt}$
(48.2 °C)
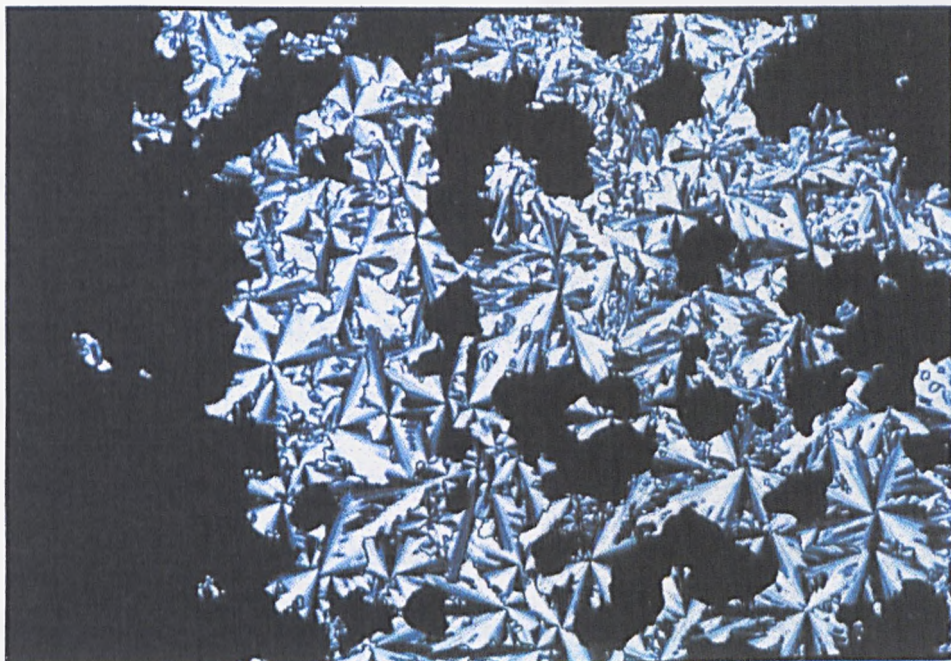
"SmY"
(25 °C)
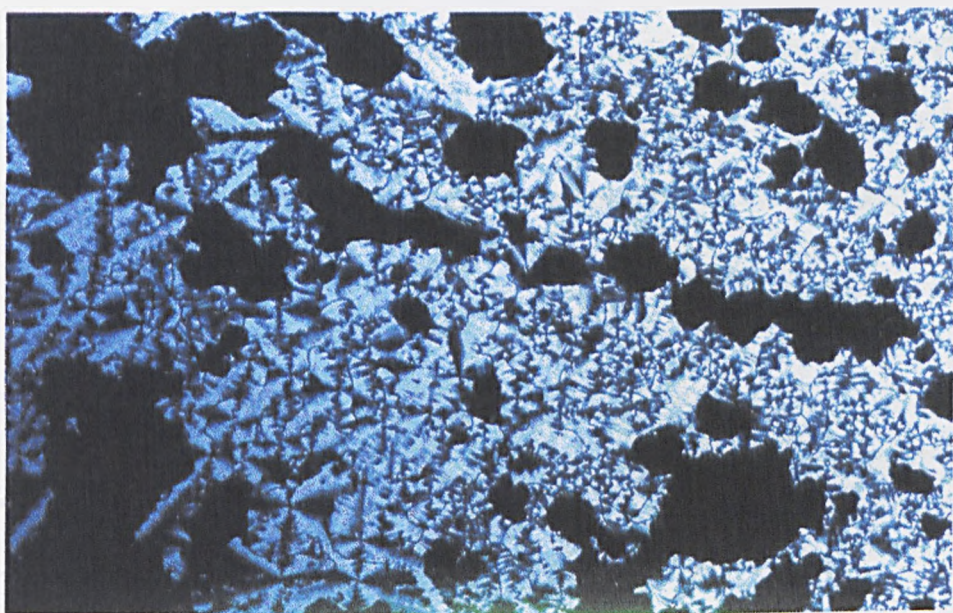
The textures of the "SmY" phase in both *thin* and *thick* cells bears a little resemblance to a phase with short-range hexatic-ordering, although this does not itself preclude that the phase is an ordered phase.

A related material, 1Bu7POBC (compound **9b**, *figure 91*), was reported to possess a phase which exhibited an optical texture, which bears some resemblance to the "SmY" phase [70]. X-ray investigations of this material suggested that the phase possesses an increased degree of order within the smectic layers in comparison with the SmC$_{alt}$ phase and was consequently designated SmI. This phase was found to be miscible with the "SmY" phase of compound **2c** (*graph 29*). However, the enthalpy change for the transition to this phase, from the SmC$_{alt}$ phase, was reported to be too small to be calculated from DSC. This somewhat contradicts the idea that this phase, in **9e**, is an ordered phase since for a transition from a relatively disordered smectic phase (such as a SmC$_{alt}$) to a more-ordered phase (such as a SmI), we would certainly expect to observe a much larger enthalpy change. *Figures 92a* and *b* show the complete and expanded DSC plots obtained for compound **2c**. The very small change in enthalpy for the first-order transition between the SmC$_{alt}$ and the "SmY" phases (noticeably smaller than the SmA to SmC$_{alt}$ transition) does not support the idea that an ordered phase is formed.
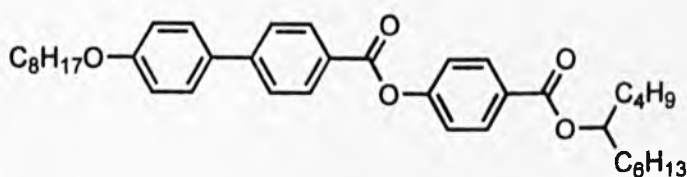
Figure 91:- Structure of compound **9b** (1Bu7POBC).
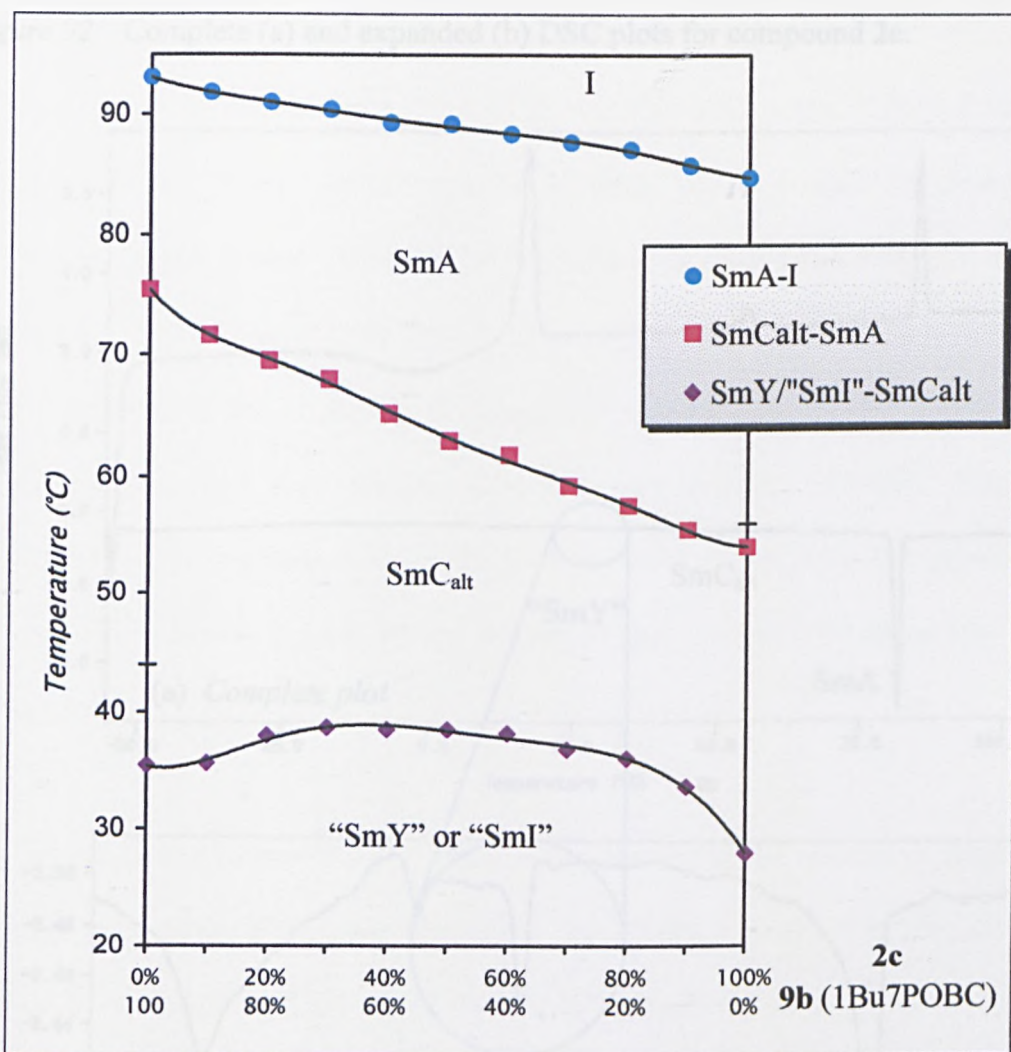
Graph 29:- Miscibility diagram between compounds **2c** and **9b** (1Bu7OPBC).

Figure 92:- Complete (a) and expanded (b) DSC plots for compound **2c**.

(a) *Complete plot*

(b) *Expanded plot*
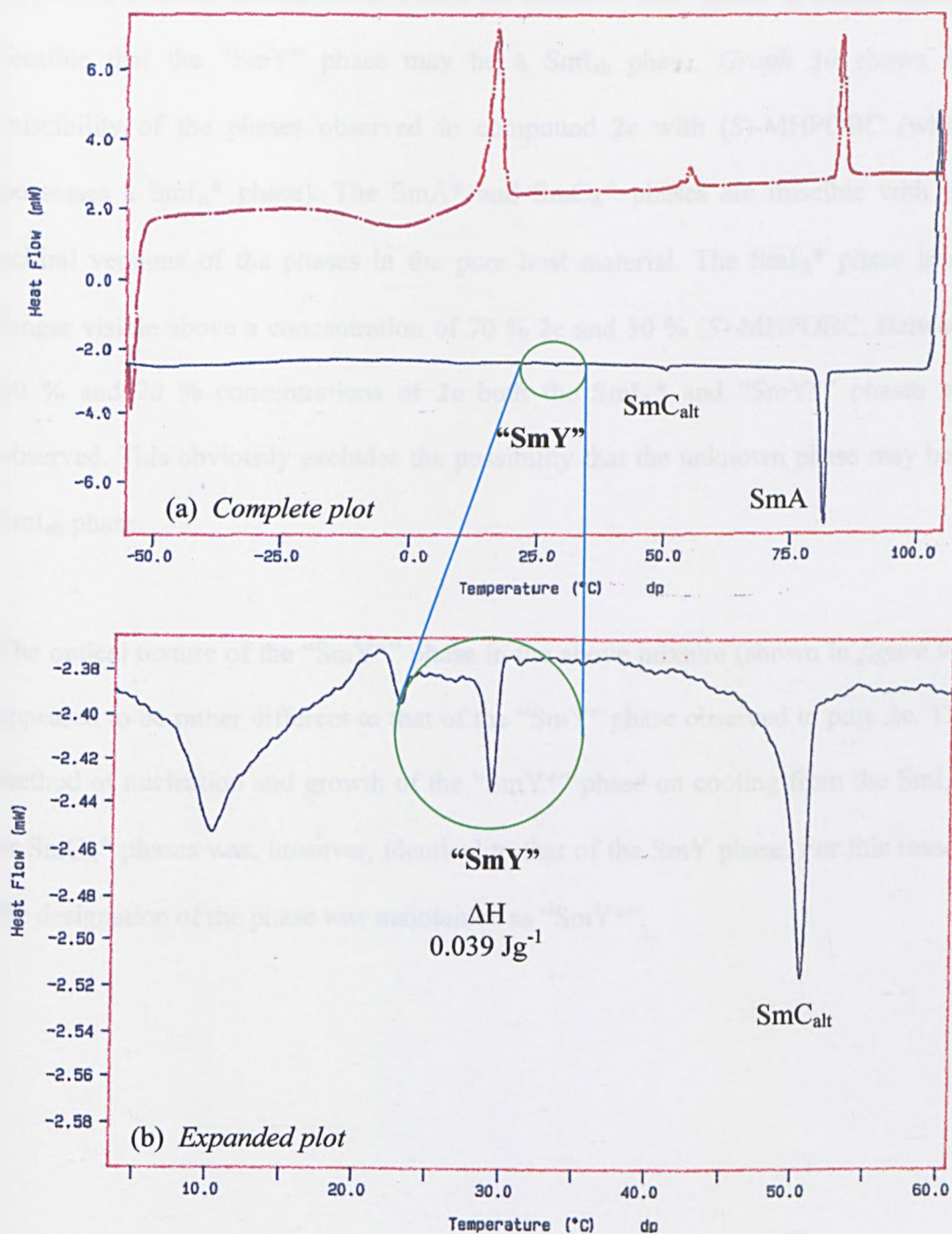
It has been suggested that an anticlinic SmI phase (SmI_{alt} or SmI_A^*) is formed on cooling from the SmC_{alt} or SmC_A^* phase when the strong interactions, which lead to the formation of the anticlinic ordering in the first instance, can be maintained in the

ordered phase [128]. As we have shown swallow-tailed materials of this type appear to possess a strong driving force to form the anticlinic SmC phase. It should then be feasible that the "SmY" phase may be a SmI$_{alt}$ phase. *Graph 30* shows the miscibility of the phases observed in compound **2c** with (*S*)-MHPOBC (which possesses a SmI$_A$* phase). The SmA* and SmC$_A$* phases are miscible with the achiral versions of the phases in the pure host material. The SmI$_A$* phase is no longer visible above a concentration of 70 % **2c** and 30 % (*S*)-MHPOBC. Between 60 % and 70 % concentrations of **2c** both the SmI$_A$* and "SmY*" phases are observed. This obviously excludes the possibility that the unknown phase may be a SmI$_{alt}$ phase.

The optical texture of the "SmY*" phase in the above mixture (shown in *figure 93*) appeared to be rather different to that of the "SmY" phase observed in pure **2c**. The method of nucleation and growth of the "SmY*" phase on cooling from the SmI$_A$* or SmC$_A$* phases was, however, identical to that of the SmY phase. For this reason the designation of the phase was maintained as "SmY*".
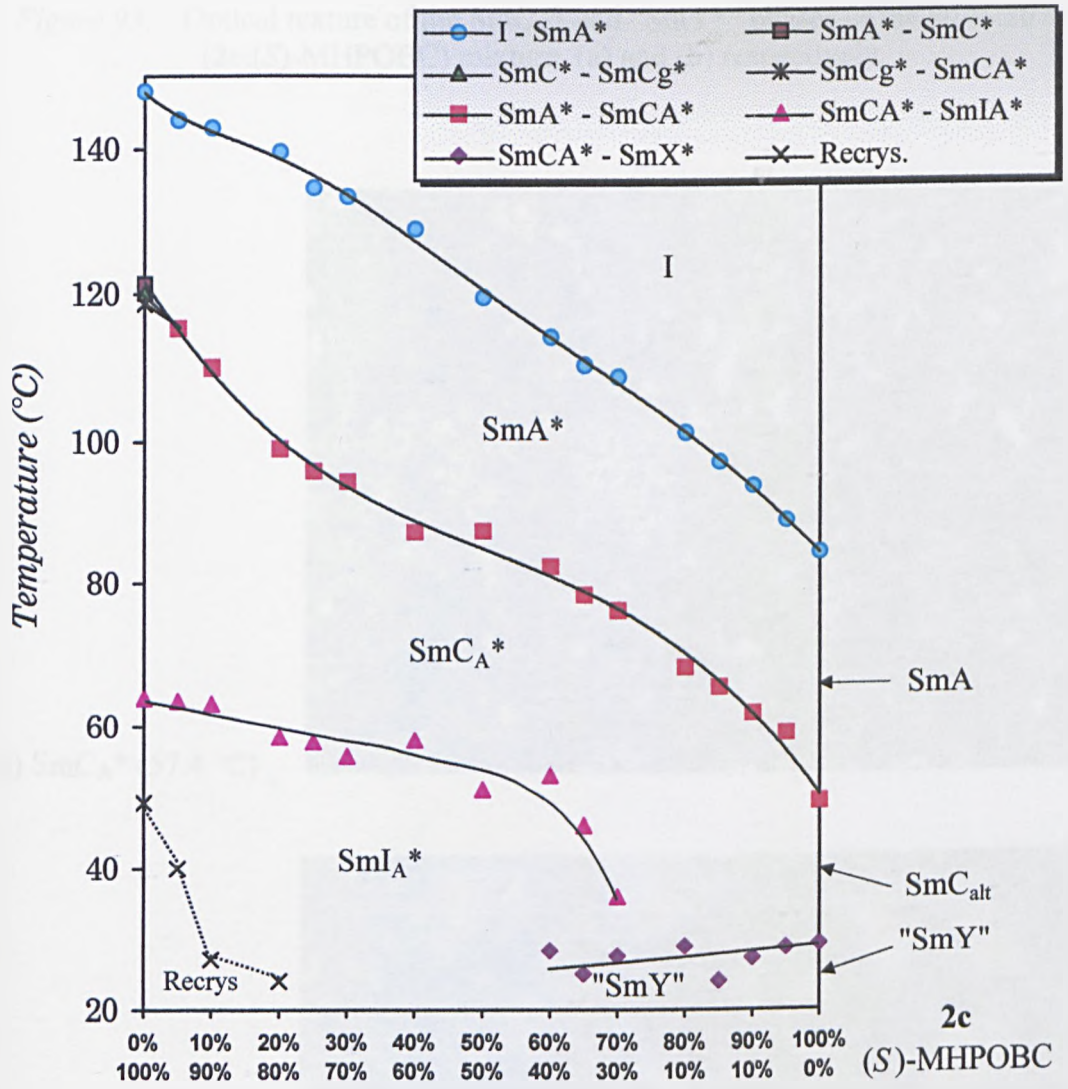
Graph 30:- Phase diagram between **2c** and (S)-MHPOBC.

Figure 93:- Optical texture of the SmC$_A$* and "SmY*" phases of the 80 %:20 %
(2c:(S)-MHPOBC) mixture, (a) and (b) respectively.
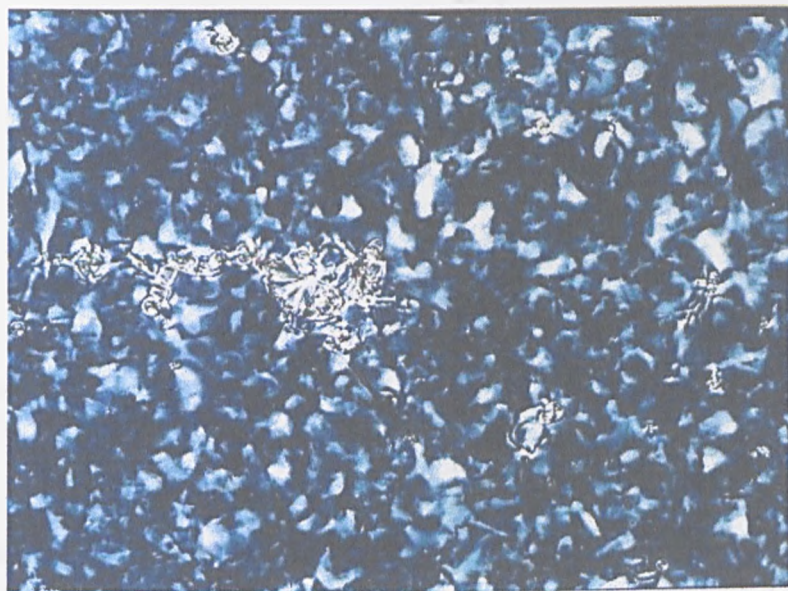
(a) SmC$_A$* (57.4 °C)
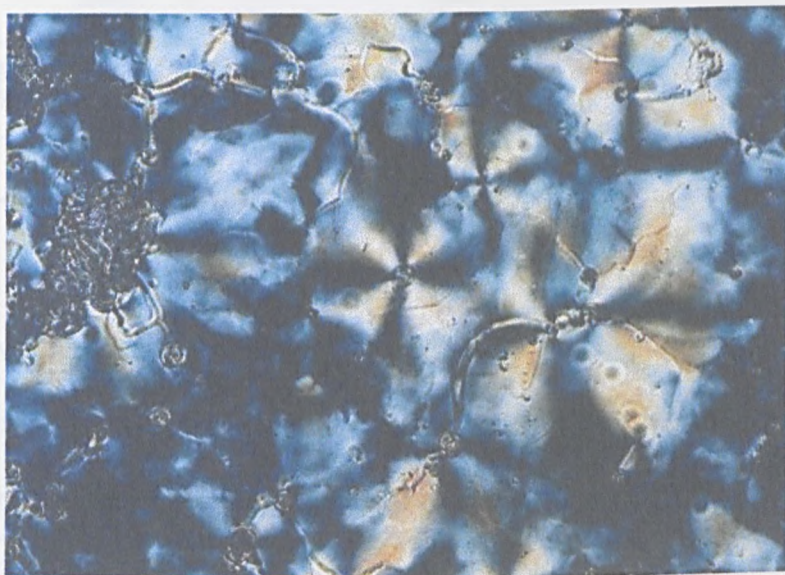
(b) "SmY*" (26.4 °C)

In order to confirm that the unknown phase observed in a related material, compound 2a, is also a "SmY" a phase diagram was prepared between this material and 2c (graph 31). The SmA, SmC$_{alt}$ and "SmY" phases are miscible across the entire phase diagram.
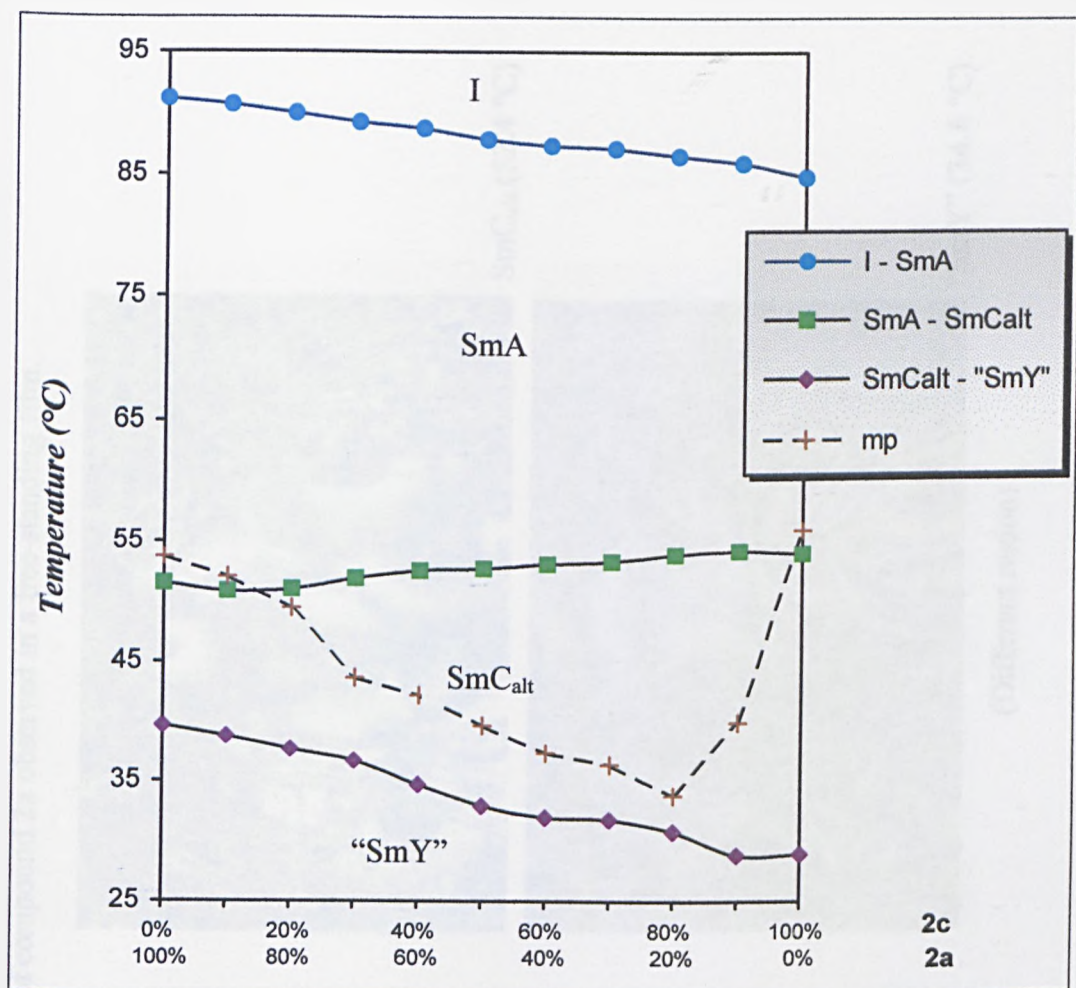
Graph 31:- Phase diagram between compounds **2c** and **2a**.

The SmX_2 phase observed in compound **7e** showed a similar optical texture to that of the "SmY" phase. The textures of the respective phases observed in free-standing films, however, bear little resemblance with each other (*Figures 94* and *95*). In order to compare the miscibility of the SmX_2 phase with the "SmY", a phase diagram between compound **2a** and compound **7e** was prepared (*graph 32*). Compound **2a** was selected for this study since the transition temperature of the "SmY" phase is close to that of the SmX_2 phase of **7e**. At a concentration of 3:7 (**7e:2a**) the transition to the SmC_{alt} phase drops in termperature by almost 20 °C and neither the "SmY" or SmX_2 phases are observed. The phase diagram appears to suggest that the "SmY" and SmX_2 phases are not miscible with each other.

Figure 94:- Optical textures of the phases of compound **2a** observed in a free-standing film.
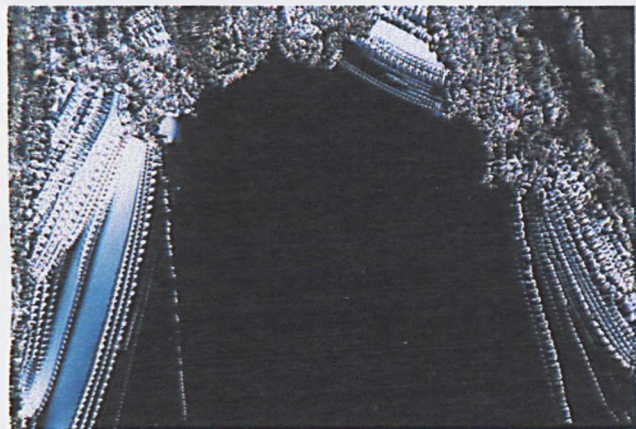
SmA (82.7 °C)

SmC$_{alt}$ (52.4 °C)

"SmY" (34.6 °C)
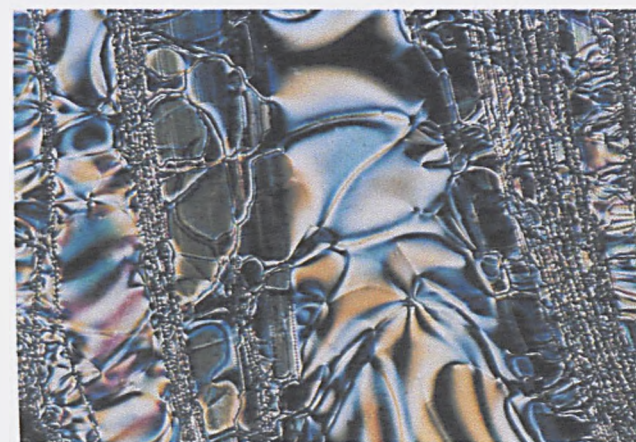
"SmY" (34.6 °C)

(Different region)

Figure 95:- Free-standing film textures of the phases observed in compound **7e**.

SmA (90.0 °C)

SmC$_{alt}$ (49.0 °C)

SmX$_2$ (39.0 °C)

SmX$_2$ (39.0 °C)
(Different region)
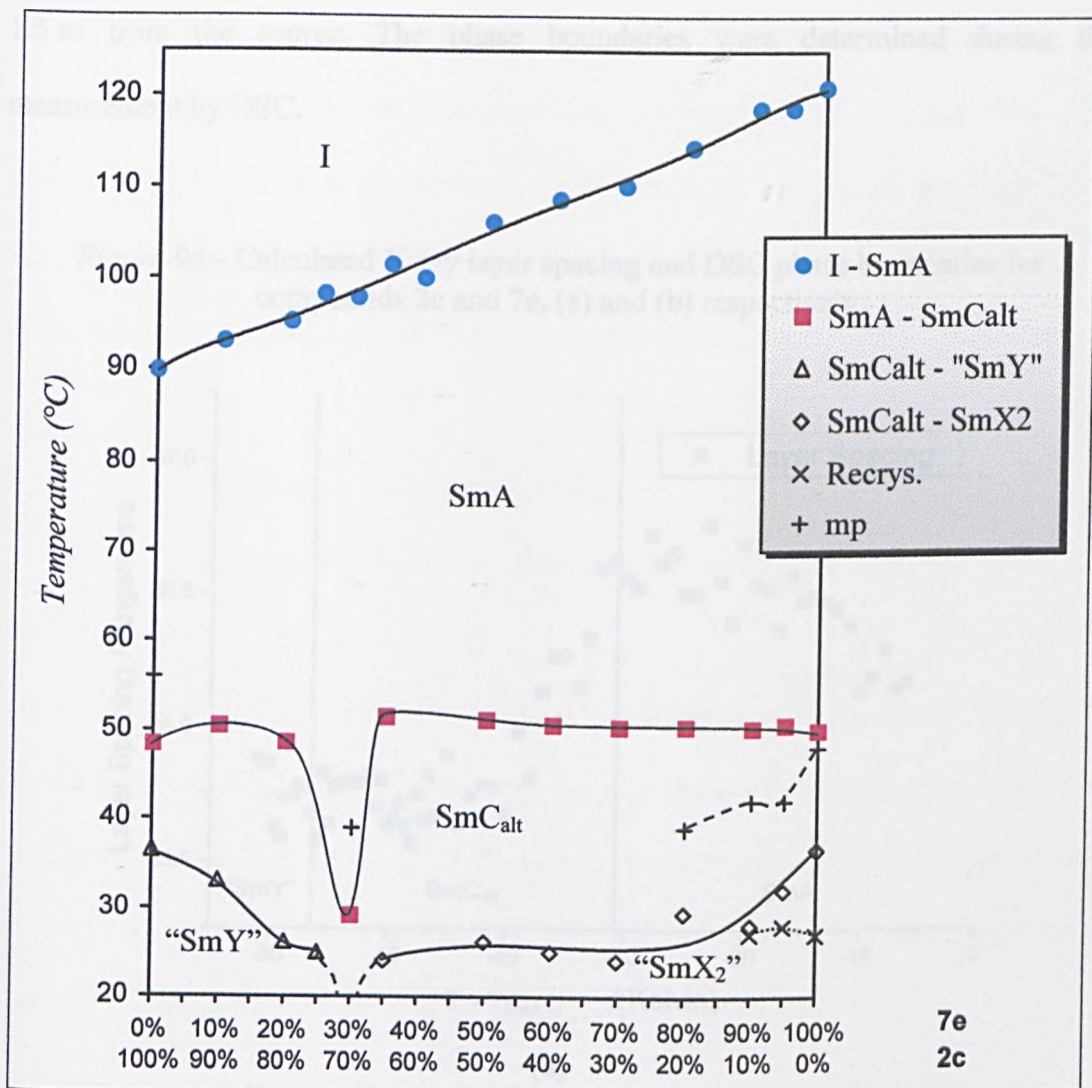
Graph 32:- Phase diagram between compounds 7e and 2c.

X-Ray Investigations

In order to investigate the changes in layer spacing of the "SmY" and SmX_2 phases preliminery X-ray diffraction measurements were carried out on the two materials (by Mr L. Baylis *et al.* at station 8.2, SRS Daresebury). The calculated smectic layer spacings on cooling from the isotropic liquid are shown in *figures 96a* and *b* for compounds **2c** and **7e**, respectively. The powdered samples were held in the beam in transparent DSC pans and the diffraction rings were recorded on an area detector

1.5 m from the source. The phase boundaries were determined during the measurement by DSC.

Figure 96:- Calculated X-ray layer spacing and DSC phase boundaries for compounds **2c** and **7e,** (a) and (b) respectively.
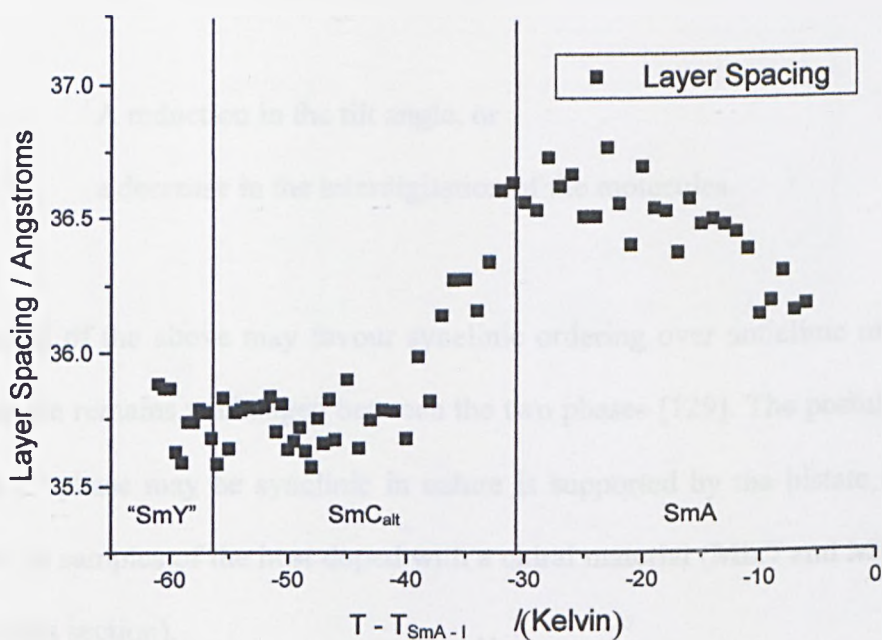
(a)
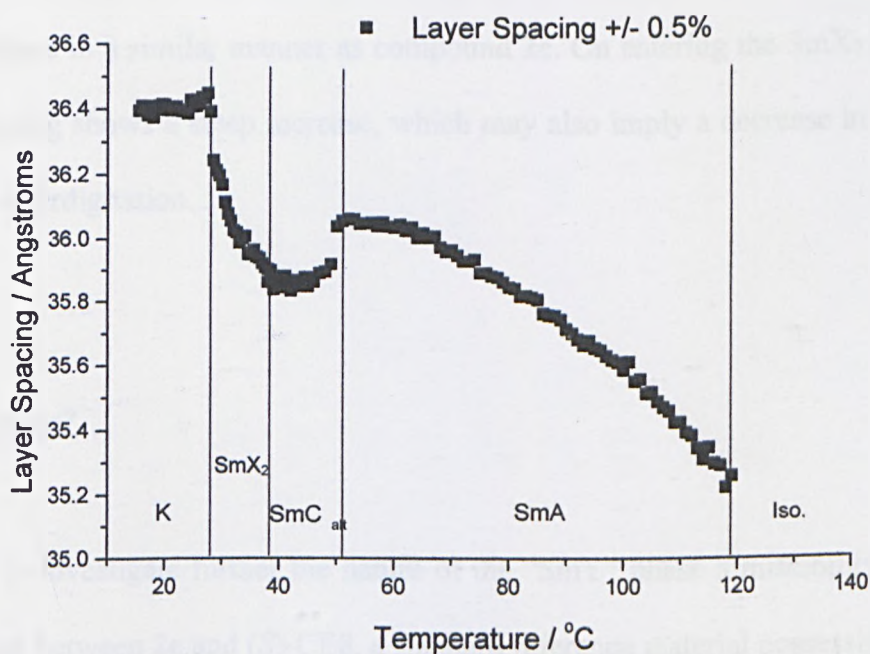
(b)

The layer spacing of compound **2c** increases on cooling in the SmA phase. A decrease in the layer spacing is observed on entering the SmC_{alt} phase. This is no doubt due to the tilting of the molecules with respect to the smectic layer normal in the SmC_{alt} phase. On entering the "SmY" phase a slight increase in layer spacing is observed. Two explanations may account for this behaviour:

    i.   A reduction in the tilt angle, or

    ii.   a decrease in the interdigitation of the molecules.

The second of the above may favour synclinic ordering over anticlinic ordering, if the tilt angle remains unchanged between the two phases [129]. The postulation that the "SmY" phase may be synclinic in nature is supported by the bistate switching observed in samples of the host doped with a chiral material (**Mix7** and **Mix17** from the previous section).

The layer spacing of compound **7e** increases in the SmA phase and decreases in the SmC_{alt} phase in a similar manner as compound **2c**. On entering the SmX_2 phase the layer spacing shows a steep increase, which may also imply a decrease in either tilt angle or interdigitation.

A SmC phase?

In order to investigate further the nature of the "SmY" phase a miscibility test was carried out between **2c** and (*S*)-CE8, a standard reference material possessing SmA*,

SmC*, SmI*, SmF*, SmJ* and SmG* phases (*graph 33*). The phase diagram shows rather complex behaviour. The "SmY*" phase is not observed below the 90 %:10 % (**2c**:(*S*)-CE8) mixture and consequently does not appear to be miscible with any of the phases observed in (*S*)-CE8.
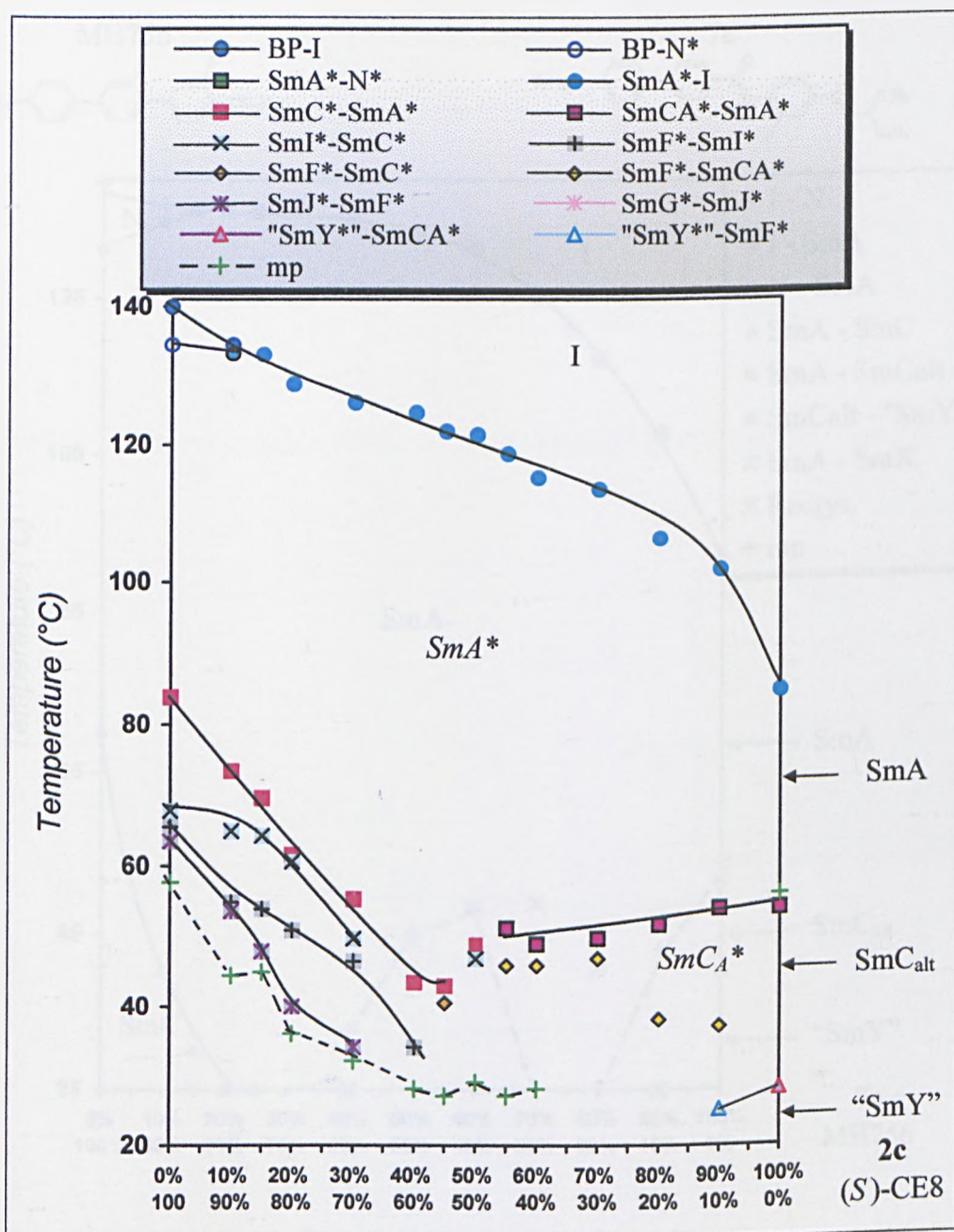
Graph 33:- Miscibility diagram between **2c** and (*S*)-CE8.

A miscibility test was also carried out between compound **7e** and a material possessing an achiral SmC phase, MH756 (*graph 34*). The "SmY" phase does not appear to be miscible with the SmC phase above room temperature although the possibility that the phases could "meet" below room temperature should not be discounted.
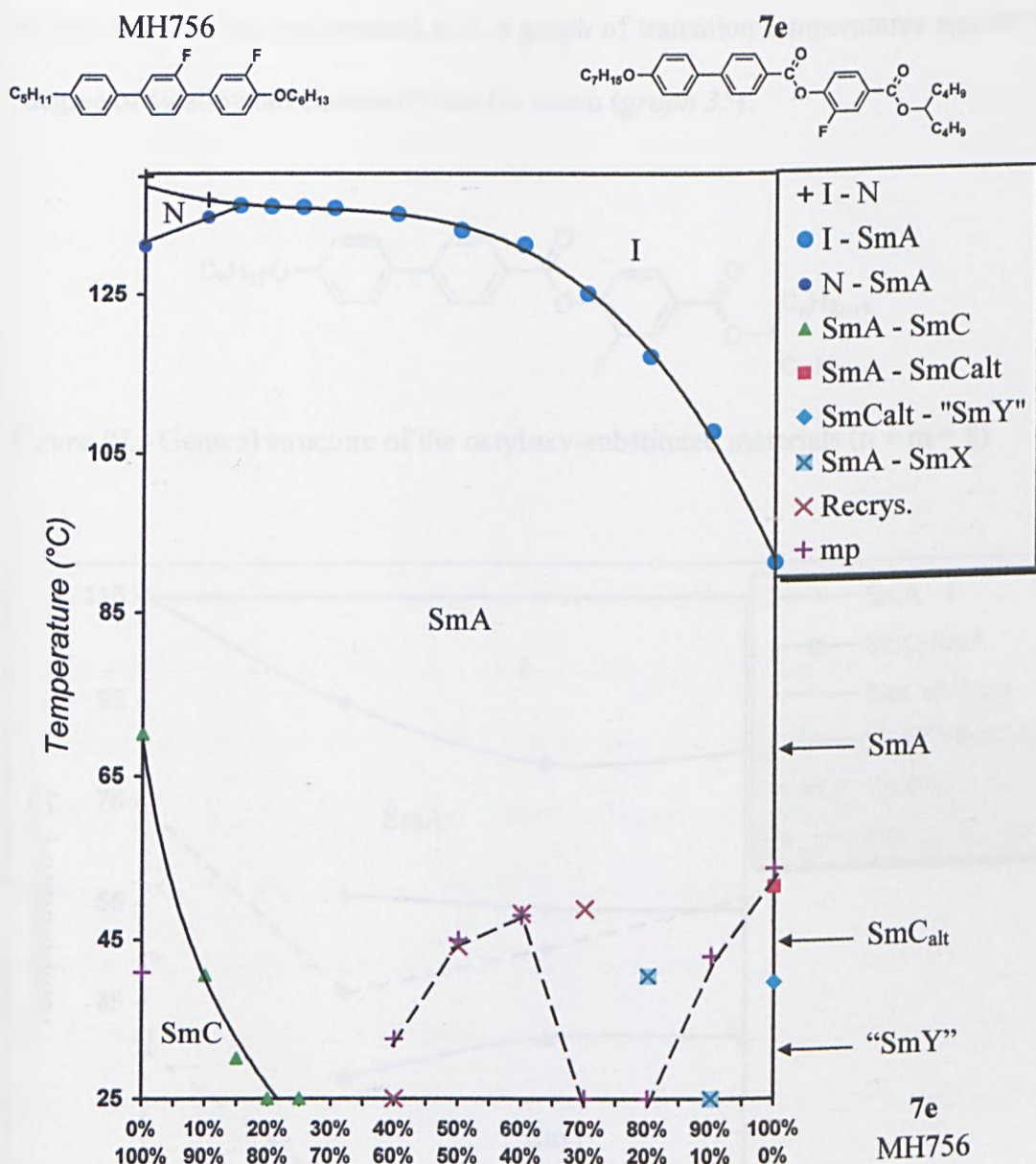
Graph 34:- Miscibility diagram between **7e** and MH756.

The "SmY" phase appears to occur principally in the octyloxy-susbtituted materials prepared in this thesis (*figure 97*). By maintaining the value of the unbranched terminal chain at x = 8, and varying the "point of attachment" of the branched chain so that n + m is also maintained at 8, a graph of transition temperatures against the "degree of swallowtail character" can be drawn (*graph 35*).
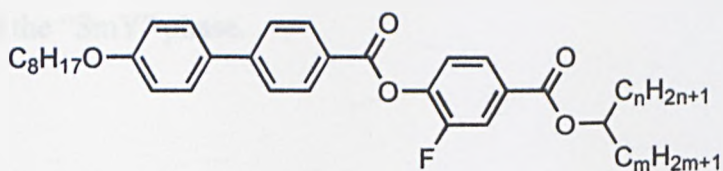
Figure 97:- General structure of the octyloxy-substituted materials (n + m = 8)
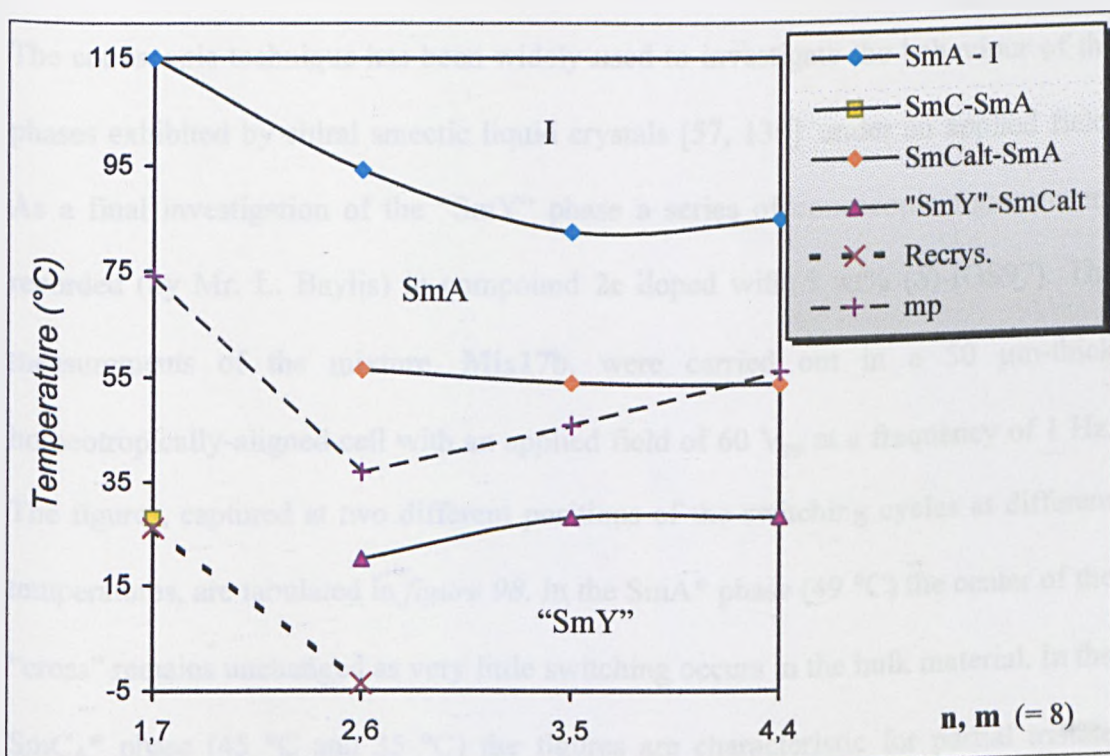
Graph 35:- Transition temperatures of the octyloxy-substituted materials against "swallowtail character" (n, m)

The SmC$_{alt}$ and "SmY" phases are not observed in the n = 1; m = 7 material. This component is a member of the homologous series of materials discussed earlier (*Table 18*) which shows a very strong odd-even effect (marked by the observation of alternate SmC and SmC$_{alt}$ phases). An increase in the "swallowtail character" appears to decrease the SmA - I transition temperature between n = 1; m = 7 to n = 4; m = 4. There is only a small difference in the transition temperatures for the SmA, SmC$_{alt}$ and "SmY" phases between the n = 3; m = 5 and n = 4; m = 4 materials. Consequently the degree of swallowtail character has limited effect on the stabilisation of the "SmY" phase.

Conoscopic Investigations

The conoscopic technique has been widely used to investigate the behaviour of the phases exhibited by chiral smectic liquid crystals [57, 130] under an applied field. As a final investigation of the "SmY" phase a series of conoscopic figures were recorded (by Mr. L. Baylis) in compound **2c** doped with 5 wt% (*S*)-IGS97). The measurements of the mixture, **Mix17b**, were carried out in a 50 μm-thick homeotropically-aligned cell with an applied field of 60 V$_{pp}$ at a frequency of 1 Hz. The figures, captured at two different positions of the switching cycles at different temperatures, are tabulated in *figure 98*. In the SmA* phase (49 °C) the center of the "cross" remains unchanged as very little switching occurs in the bulk material. In the SmC$_A$* phase (45 °C and 35 °C) the figures are characteristic for partial tristate (antiferroelectric) switching [130]. At the border between the SmC$_A$* and "SmY*" phases (32 °C) the mode of switching changes as a contribution from bistate

(ferroelectric) switching occurs. The figures bear some resemblance to the ferrielectric SmC_γ^* phase(s) observed in related materials [86] although the appearance of this sample is more-than-likely a consequence of the combined effects of the presence of both phases at the transition border. On cooling into the "SmY*" phase the switching becomes completely bistate (ferroelectric) in character as two tilted states can be clearly observed. On removal of the applied field the circular figure centralises slowly implying a return to a helical bulk structure.

Figure 98:- Conoscopic figures recorded for **Mix17b**.

49 °C (SmA*)   45 °C (SmC$_A$*)   35 °C (SmC$_A$*)   32 °C (SmC$_A$*/"SmY*")   30 °C ("SmY*")
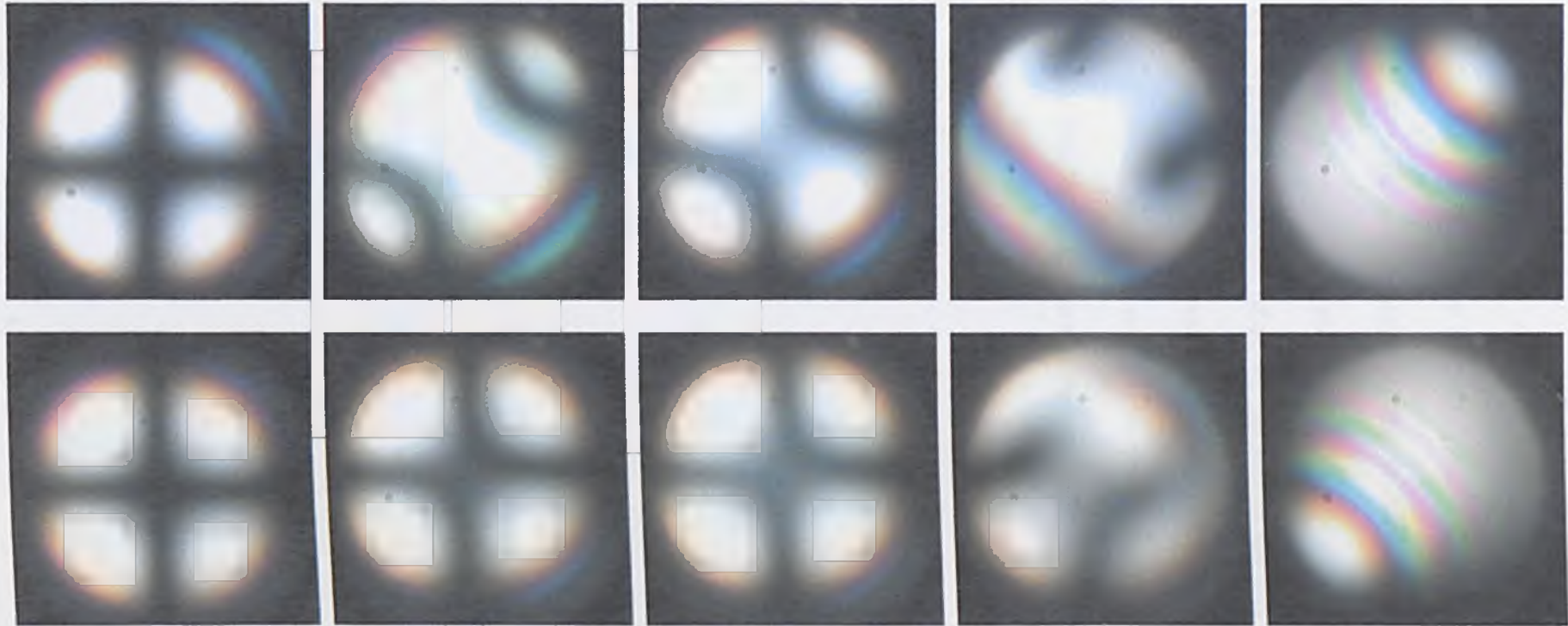
Summary of this Section

In this section of the thesis the nature of two unidentified phases, in particular the "SmY" phase, observed in a series of structurally-related materials was investigated by a combination of miscibility tests, X-ray analysis and conoscopy. Together with the observations of the switching behaviour of doped samples of the first material to exhibit this phase, compound **2c**, the evidence thus far suggests that the phase is ferroelectric in character. There is, however, no clear evidence that could allow the phase to be categorised as a SmC or SmI phase. Consequently the actual identity of the phase is, as yet, unresolved.

Conclusions / Further Work

CONCLUSIONS

The aims of this thesis were initially two-fold:

(i)   to investigate the structural factors necessary for the formation of the SmC_{alt}

phase in a series of related achiral and racemic materials, and

(ii)   to evaluate the use of the materials as hosts for chiral-dopant

antiferroelectric liquid-crystalline mixtures.

The goals of the thesis, with regards to the above aims, were achieved systematically. A thorough investigation into the formation of the SmC_{alt} phase was carried out for a series of unsymmetrically and symmetrically-substituted liquid crystals synthesised during the course of this work. The relationship between structure, occurrence and type of smectic phases, and transition temperatures in both series of materials were discussed. A series of chiral antiferroelectric materials was also prepared and their physical properties were measured. The most suitable host materials were selected and combined with the most suitable liquid-crystalline and non liquid-crystalline chiral dopant materials. The physical properties of the model binary chiral-dopant mixtures were investigated and their behaviour was discussed. A number of materials with apparently unusual mesomorphic properties were observed and preliminary physical investigations were carried out on one of the materials.

A number of conclusions can be drawn with regards to the host materials, dopants, binary chiral dopant-mixtures, and materials with unusual mesomorphic properties investigated in this thesis. These are summarised below for each category.

1.   *Host materials*

(i)   The criteria identified for the most suitable host materials are: a wide SmC_{alt} phase range with high thermal stability, low melting point and low recrystallization temperature.

(ii)   The size and type of the branched terminal chain of the molecule plays a greater role in the formation of the SmC_{alt} phase than the length of the unbranched chain (labelled in *figure 99*) in alkoxy-substituted materials. The ether linkage in the unbranched chain plays an important role in the stabilisation of the SmC_{alt} phase.
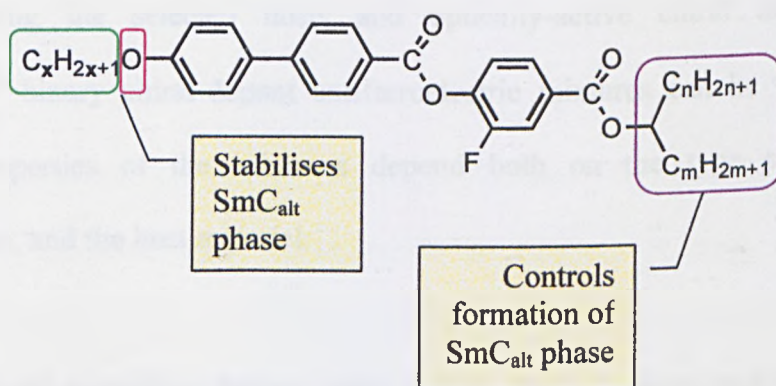
Figure 99:- General structure of the molecules studied.

(iii)   The presence of the lateral fluoro substituent lowers the transition temperatures of the observed phases in comparison with the non-fluorinated analogues (both chiral and racemic).

(iv)   Steric interactions, between the branched and unbranched terminal alkyl chains of molecules in adjacent smectic layers, play a crucial role in the formation and stabilisation of anticlinic smectic phases.

2.   *Dopant materials*

Both liquid-crystalline and non liquid-crystalline chiral materials can be used as dopants for chiral-dopant antiferroelectric mixtures.

3.   *Binary Chiral-Dopant Mixtures*

By combining the selected hosts and optically-active chiral dopants model "switchable" binary chiral-dopant antiferroelectric mixtures can be prepared. The physical properties of the mixtures depend both on the type of dopant, its concentration, and the host material:

(i)   A liquid-crystalline dopant with a high SmC_A^* phase stability and high threshold to switching confers similar properties on the mixture. A non liquid-crystalline dopant destabilises all the observed phases, confers a lower threshold for switching on the induced SmC_A^* phase than that observed for

the liquid-crystalline dopants.

(ii)   A mixture composed of a host material in which the anticlinic phase is strongly favoured (such as the ethylheptyl-substituted or "swallow-tailed" materials) exhibits a high threshold voltage for switching.

(iii)   In certain mixtures that possess both SmC* and SmC_A* phases the destabilisation of the smectic phases, particularly the SmC_A* phase results in a type of coexistence between both phases across a broad temperature range in aligned test cells.

4.   Unusual Mesomorphic Properties

An as-yet unclassified smectic phase was observed in some of the materials prepared. The exact nature of this phase is unclear, although the phase is found to be ferroelectric in character when doped with a chiral material.

In conclusion, the work presented in this thesis has shown that the behaviour of binary chiral-dopant antiferroelectric liquid-crystalline mixtures is more complex than initially supposed. Further investigations of the mixtures would be required in order to provide a clear understanding of the mesomorphic and electrooptic behaviour of chiral dopant antiferroelectric mixtures before the concept can be successfully applied to practical multi-component mixtures for commercial applications.

FURTHER WORK

The work that could be carried out in order to both develop and explore further the use of the chiral-dopant technique with respect to antiferroelectric liquid crystals can be divided into three general categories;

i. Synthesis of new materials

ii. Further physical investigations

iii. Preparation and evaluation of further mixtures

These suggestions are expanded upon below;

i.   Synthesis of New Materials

The materials prepared in this thesis were based on the structure of MHPOBC, the earliest reported antiferroelectric liquid crystal [52, 131]. The majority of chiral antiferroelectric liquid crystals share common structural features with this molecule (three-ring aromatic core, ester linking group, and ether-linked unbranched alkyl chains). Many recent examples of chiral materials, which deviate slightly from this structure "template", have none-the-less been found to exhibit antiferroelectric properties [132-134] [68]. In some cases very promising antiferroelectric properties have been achieved (eg. wide SmC_A^* phase range, large tilt angles, etc.). The synthesis and evaluation of new chiral, racemic, and "swallow-tailed" materials, should be carried out in order to gain a better understanding of the structural

requirements for the formation of anticlinic smectic phases. *Table 41* shows a modular concept for some potentially anticlinic structures which could be prepared and investigated using a general structure for liquid crystals similar to that shown in the **Introduction** [12]. For comparison with previously prepared materials (both published and reported in this thesis) the structure "template" of the materials is maintained as that of MHPOBC. A large number of combinations of components may be prepared using this concept. Two examples of potential structures are shown in *figure 100*.

$$(x = 6 - 10)$$

$$(x = 8 - 12)$$
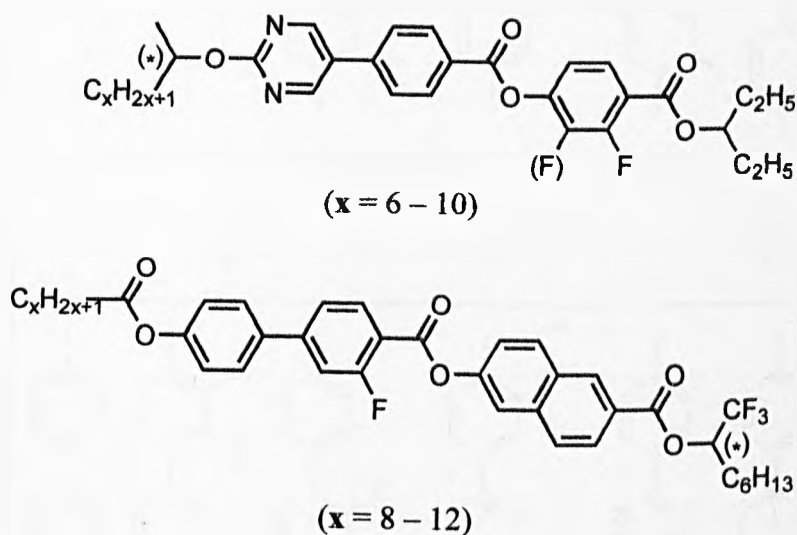
Figure 100:- Examples of *potentially anticlinic* structures derived by combining different components from *Table 41*.

Table 41:- Modular concept for some potentially SmC_A^* or SmC_{alt}-forming liquid crystal structures.

Substituent	Linkage	Aromatic group	Linkage	Aromatic group	Linkage	Substituent
C_xH_{2x+1} (x = 8 – 12) (∗) $C_xH_{2x+1}(CH_3)CH -$ (x = 6 – 10)	-O- -S- -CHO- -COO-	(biphenyl); (biphenyl with (F), F); (biphenyl with F, (F)); (pyridyl-phenyl, N); (pyrimidinyl-phenyl, N, N); (cyclohexyl-phenyl)	-COO- -CO- -O-	(phenyl); (phenyl with F); (phenyl with (F), F); (tetrafluorophenyl, F, F, F, F); (naphthyl)	-COO- -CO- -O-	CH_3/(∗)/C_6H_{13}; CF_3/(∗)/C_6H_{13}; C_3H_7/(∗)/C_5H_{11}; C_2H_5/C_2H_5; C_4H_9/C_4H_9; (ester with C_2H_5, C_2H_5)

The introduction of a narrow nematic or chiral nematic phase above the SmA / SmA*
phase is known to greatly aid the monodomain alignment of SmC* materials both in
test cells and in actual devices. The fact that the overwhelming majority of liquid
crystals, that form SmC_{alt} and SmC_A* phases, do not possess a nematic phase suggests
that their structure is generally incompatible with the formation of nematic phases.
However, by introducing a degree of disorder into the structure a nematic phase may,
in principle, be "injected" above the anticlinic phase. Several strategies may be
employed in order to attempt this. For example, the inclusion of double bonds at
certain positions in the terminal alkyl chains of certain SmC or SmC*-forming
materials is known to support, and even promote, the formation of nematic phases by
introducing a degree of disorder not present in the materials with saturated-alkyl
chains [135]. Therefore, by attaching a terminal chain incorporating a carbon-carbon
double bond to the core of a SmC_{alt} or SmC_A*-forming material it may be possible to
induce a N or N* phase above the SmA or SmA* phase (*figure 101*).
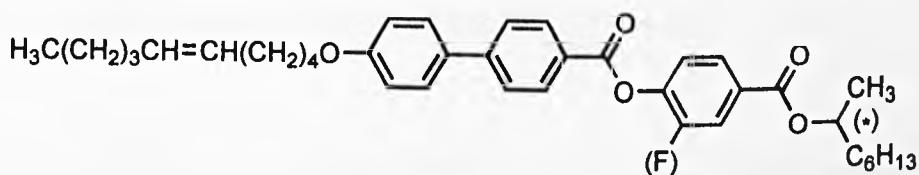
Figure 101:- An example of a molecule possessing a double-bond in the unbranched
terminal alkyl chain.

ii. Further Physical Investigations

Certain binary chiral dopant mixtures prepared during the course of this work (with compound **8a** as the host) exhibited switching which could not be described as tristate in character in the temperature region of the antiferroelectric phase. This was principally due to the absence, during switching, of a clearly observable third (antiferroelectric) state between the two ferroelectric states. The electrooptic behaviour of these mixtures should be investigated at different frequencies, and field strengths, in cells of different thickness and surface treatment. This may provide more information about the actual nature of the switching that takes place in a cell containing the mixture and also the influences that control the observed behaviour.

Dielectric spectroscopy is a powerful tool in probing the behaviour of chiral smectic liquid crystals at the microscopic level [119, 136-138]. Consequently it may also be a very useful technique for investigating changes in the dielectric properties of the mixtures, particularly between the SmC^* and SmC_A^* phases.

Measurement of the helical pitch of the binary mixtures would provide precise information on the effects of different dopants on the pitch length of the mixtures. The pitch length of the chiral versions of the (unsymmetrically-substituted) hosts should also be measured as a comparison.

iii.   Preparation and Evaluation of Further Mixtures

In achieving the ultimate goal of this work, ie. the development of antiferroelectric mixtures based on the chiral-dopant concept and their successful use in test devices, the next logical step for this work would be the preparation of multi-component chiral-dopant mixtures. By combining selected racemic or achiral materials prepared during the course of this work, either with a chiral dopant or a combination of chiral dopant and chiral antiferroelectric materials, prototype mixtures with reasonably wide SmC_A^* phases may be obtained. Developing these mixtures, principally by replacing and substituting individual components with alternative components should provide the means to understand how the mesomorphic and physical properties of the mixtures can be enhanced for use in practical devices.

The unusual mesomorphic properties discussed in the final section of the **Results and Discussion** chapter should be investigated further in order to ascertain the identity of the "SmY" phase. Further physical measurements, such as more detailed X-ray studies, electrooptic and dielectric investigations, together with miscibility tests below room temperature, should assist in characterising the phase.

Experimental

EXPERIMENTAL

Overview

All reactions were carried out under anhydrous conditions unless stated otherwise. Reactions were monitored by thin layer chromatography using silica on aluminium plates and observation under a UV lamp (254 and 365 nm). Column chromatography was carried out on silica gel using light petroleum (bp. 40-60 °C) and dichloromethane or ethyl acetate mixtures as eluents. Magnesium turnings used in Grignard reactions were dried in an oven for two hours before use.

All chemical reagents and solvents were obtained from commercial sources. All solvents were dried unless water was present as a reagent or co-solvent.

The analyses of the intermediate and final products were carried out on the following instruments:

^{1}H-NMR: Jeol JNM-GX270 FT-NMR Spectrometer (400 MHz);

IR: Perkin Elmer 9836 Spectrophotometer;

MS: Finnigan Mat 1020 GC/MS;

HPLC: Kontron 420 Pump, Spectroflow 757 Absorbance Detector, Chromapack MUST Streamswitch, Perkin Elmer ISS-100 Autosampler, PL Data Collection Unit;

DSC: Perkin Elmer DSC7, TAC 7/3 Instrument Controller;

Microscopy: Olympus Microscope, Mettler FP52 Hot-Stage and FP5 Control Unit

Experimental

i. General Intermediates

1-Benzyloxy-4-bromo-2-fluorobenzene

4-bromo-2-fluorophenol (5.0 g, 26.18 mmol) was added to a suspension of potassium carbonate (18.0 g, 130.90 mmol) in 80 ml butanone. Benzyl bromide (3.12 ml, 26.18 mmol) was added and the mixture was heated to reflux overnight. The inorganic material was filtered off and the filtrate washed with water (2 x 80 ml). The aqueous layers were then washed with ether (2 x 80 ml). The combined organic phases were dried over magnesium sulphate and the solvents were removed *in vacuo*. The product was recrystallized from ethanol to yield colourless crystals.

Yield: 4.28 g (60.7 %). *MS:* 282/280 (M$^+$, 2 %/2 %), 91 (100 %), 81 (3 %). *^{1}H-NMR (CDCl$_3$)* δ: 7.44-7.30 - Bz-H (5H, m); 7.25 - Ar-H (1H, t); 7.15 - Ar-H (1H, m); 6.86 – Ar-H (1H, t); 5.10 - -OCH$_2$- (2H, s). *IR (KBr)* v_{max}/cm^{-1}: 3025, 2875, 1490, 1385, 1260, 1200, 1130, 1005, 865, 805. *Mp:* 66 - 68°C.

4-Benzyloxy-3-fluorobenzoic acid

A solution of the Grignard reagent formed in the usual way from 1-benzyloxy-4-bromo-2-fluorobenzene (20.0 g, 71.17 mmol) and magnesium turnings (2.6 g, 107 mmol) in 100 ml THF was added to a slurry of solid carbon dioxide (very large excess) in 200 ml THF. The mixture was allowed to warm to room temperature, then acidified with cold dilute hydrochloric acid (pH1). The precipitated product was filtered off, washed repeatedly with cold DCM, then dried *in vacuo* (P$_2$O$_5$).

Yield: 10.95 g (62.8 %) *MS:* 246 (M$^+$, 13 %), 91 (100 %), 65 (13 %). *^{1}H-NMR (CDCl$_3$)* δ: 7.72 - Ar-H (1H, t); 7.66 - Ar-H (1H, m); 7.31 - Bz-H (5H, m); 6.96 - Ar-H (1H, t); 5.25 - -CH$_2$- (2H, s). *IR (KBr)* v_{max}/cm^{-1}: 2925, 2870, 1700, 1610, 1510, 1445, 1385, 1210, 985, 765, 690, 645. *Mp:* 187 -189 °C.

4-(Methoxycarbonyloxy)benzoic acid

4-Hydroxybenzoic acid (5.0 g, 36.2 mmol) was added to a solution of NaOH (4.34 g, 108.5 mmol) in distilled water at 0 °C. Methylchloroformate (4.2 g, 44.4 mmol) was added to the mixture dropwise. The mixture was allowed to stir at 0 °C for four hours then excess dilute HCl (10 %) was added (to pH 5). The resulting precipitate was separated by filtration, washed with water, and dried. The colourless product was recrystallized from glacial acetic acid, washed with water, and dried again *in vacuo* (P_2O_5).

Yield: 4.42 g (76.2 %) *MS:* 196 (M^+, 36 %), 152 (39 %), 135 (100 %), 107 (25 %). *^{1}H-NMR (CDCl$_3$/DMSO) δ:* 8.10 (2H, d) 7.24 (2H, d) 3.94 (3H, s). *IR (KBr) v_{max}/cm^{-1}:* 3415, 2960, 1765, 1755, 1680, 1425, 1260, 1160, 1070, 935, 770, 725, 655. *Mp:* 175 - 177 °C.

1-Methylheptyl 4-benzyloxy-3-fluorobenzoate

A mixture of 4-benzyloxy-3-fluorobenzoic acid (2.0 g, 8.13 mmol) in 70 ml THF, 2-octanol (1.29 ml, 8.13 mmol), DEAD (1.28 ml, 8.13 mmol), and triphenylphosphine (2.13 g, 8.13 mmol) was stirred for 72 hours. The solvent was removed *in vacuo* to yield a yellow oil and the crude product was purified by column chromatography (1:1 DCM/Petrol 40-60 °C).

Yield: 1.08 g (37.2 %). *MS:* 358 (M^+, 5 %), 247 (8 %), 229 (9 %), 91 (100 %). *^{1}H-NMR (CDCl$_3$) δ:* 7.78 - Ar-H (1H, t); 7.74 - Ar-H (1H, m); 7.38 - Bz-H (5H, m); 5.17 - -OCH$_2$- (2H, s); 5.24 - -C-H (1H, sx); 1.80-1.20 - -CH$_2$- (10H, m); 0.87 - CH$_3$ (6H, m). *IR (KBr) v_{max}/cm^{-1}:* 2935, 2835, 1695, 1585, 1505, 1260, 1185, 945, 750, 695.

1-Methylethyl 4-benzyloxy-3-fluorobenzoate

The experimental procedure was as described for the preparation of 1-methylheptyl 4-benzyloxy-3-fluorobenzoate above.

Quantities: 4-benzyloxy-3-fluorobenzoic acid (3.0 g, 12.2 mmol), 2-propanol (0.66 g, 11.0 mmol), DEAD (1.9 g, 11.0 mmol), triphenylphosphine (2.88 g, 11.0 mmol).

Yield: 1.31 g (41.4 %). *MS:* 288 (M^+, 4 %), 247 (7 %), 91 (100 %), 229 (11 %). *^{1}H-NMR (CDCl$_3$) δ:* 7.78 - Ar-H (1H, t), 7.74 - Ar-H (1H, m), 7.50-7.35 - Bz-H (5H, m),

7.00 - Ar-H (1H, t), 5.21 - -CH$_2$- (2H, s), 1.57 - -C-H (1H, sp), 1.35 - -CH$_3$ (6H, d). *IR (KBr)* v_{max}/cm^{-1}: 3040, 2880, 1710, 1600, 1280, 1190, 760.

1-Methylpropyl 4-benzyloxy-3-fluorobenzoate

The experimental procedure was as described for the preparation of 1-methylheptyl 4-benzyloxy-3-fluorobenzoate above.

Quantities: 4-benzyloxy-3-fluorobenzoic acid (1.5 g, 6.15 mmol), 2-butanol (0.45 g, 6.1 mmol), DEAD (1.06g 6.1 mmol), triphenylphosphine (1.60 g, 6.1 mmol).

Yield: 1.28 g (70.1 %). *MS:* 302 (M$^+$, 3 %), 247 (8 %), 229 (10 %), 91 (100 %). *^{1}H-NMR (CDCl$_3$)* δ: 7.78 - Ar-H (1H, t), 7.75 - Ar-H (1H, m), 7.45-7.30 – Bz-H (5H, m), 7.00 – Ar-H (1H, t), 5.20 - -CH$_2$- (2H, s), 5.05 - -CH (1H, sx), 1.70 - -CH$_2$- (2H, p), 1.30 - -CH$_3$ (3H, d), 0.95 - -CH$_3$ (3H, t). *IR (KBr)* v_{max}/cm^{-1}: 2960, 2900, 1705, 1605, 1280, 1195, 1120, 755.

1-Methylbutyl 4-benzyloxy-3-fluorobenzoate

The experimental procedure was as described for the preparation of 1-methylheptyl 4-benzyloxy-3-fluorobenzoate above.

Quantities: 4-benzyloxy-3-fluorobenzoic acid (1.7 g, 7 mmol), 2-pentanol (0.54 g, 6.15 mmol), DEAD (1.07 g, 6.15 mmol), triphenylphosphine (1.61 g, 6.15 mmol).

Yield: 0.85 g (44.3 %). *MS:* 316 (M$^+$, trace), 247 (8 %), 229 (10 %), 91 (100 %). *^{1}H-NMR (CDCl$_3$)* δ: 7.77 – Ar-H (1H, t), 7.75 – Ar-H (1H, m), 7.45-7.3 - Bz-H (5H, m), 7.00 Ar-H (1H, t), 5.21 - -CH$_2$- (2H, s), 5.00 – -CH (1H, sx), 1.70-1.60 - -CH$_2$- (4H, m), 1.30 – -CH$_3$ (3H, d), 0.94 - -CH$_3$ (3H, t). *IR (KBr)* v_{max}/cm^{-1}: 3020, 2860, 1705, 2610, 1505, 1280, 1120, 755.

1-Methylpentyl 4-benzyloxy-3-fluorobenzoate

The experimental procedure was as described for the preparation of 1-methylheptyl 4-benzyloxy-3-fluorobenzoate above.

Quantities: 4-benzyloxy-3-fluorobenzoic acid (1.7 g, 7 mmol), 2-hexanol (0.63 g, 6.15 mmol), DEAD (1.07 g, 6.15 mmol), triphenylphosphine (1.61 g, 6.15 mmol).

Yield: 0.94 g (44.3 %). *MS:* 330 (M$^+$, 4 %), 247 (7 %), 229 (9 %), 91 (100 %),. *^{1}H-NMR (CDCl$_3$)* δ: 7.77 – Ar-H (1H, t), 7.72 – Ar-H (1H, m), 7.45-7.30 – Bz-H (5H, m), 7.00 – Ar-H (1H, t), 5.20 - -CH$_2$- (2H, s), 5.00 - -CH (1H, sx), 1.70-1.58 - -CH$_2$- (4H, m), 1.45-1.25 - -CH$_2$-/-CH$_3$ (5H, m), 0.90 - -CH$_3$ (3H, t). *IR (KBr)* v_{max}/cm^{-1}: 3000, 2880, 1705, 1605, 1505, 1277, 1120, 1000, 760.

1-Methylhexyl 4-benzyloxy-3-fluorobenzoate

The experimental procedure was as described for the preparation of 1-methylheptyl 4-benzyloxy-3-fluorobenzoate above.

Quantities: 4-benzyloxy-3-fluorobenzoic acid (1.7 g, 7 mmol), 2-heptanol (0.71 g, 6.15 mmol), DEAD (1.07 g, 6.15 mmol), triphenylphosphine (1.61 g, 6.15 mmol).

Yield: 1.16 g (57.9 %). *MS:* 344 (M$^+$, 3 %), 247 (6 %), 229 (8 %), 91 (100 %). *^{1}H-NMR (CDCl$_3$)* δ: 7.77 – Ar-H (1H, t), 7.72 – Ar-H (1H, m), 7.45 – 7.30 – Bz-H (5H, m), 7.00 – Ar-H (1H, t), 5.2 - -CH$_2$- (2H, s), 5.00 - -CH (1H, sx), 1.70-1.57 – -CH$_2$- (2H, m), 1.43–1.23 - -CH$_2$-/-CH$_3$ (9H, m), 0.87 - -CH$_3$ (3H, t). *IR (KBr)* v_{max}/cm^{-1}: 3020, 2850, 1705, 1610, 1510, 1275, 1190, 1120, 100, 755.

1-Methyloctyl 4-benzyloxy-3-fluorobenzoate

The experimental procedure was as described for the preparation of 1-methylheptyl 4-benzyloxy-3-fluorobenzoate above.

Quantities: 4-benzyloxy-3-fluorobenzoic acid (2.0 g, 8.12 mmol), 2-nonanol (1.08 g, 7.50 mmol), DEAD (1.30 g, 7.50 mmol), triphenylphosphine (1.97 g, 7.50 mmol).

Yield: 1.07 g (38.3 %). *MS:* 372 (M$^+$, 2%), 247 (6%), 91 (100%), 229 (9%). *^{1}H-NMR (CDCl$_3$)* δ: 7.79 – Ar-H (1H, t), 7.75 – Ar-H (1H, m), 7. 45-7.33 – Bz-H (5H, m), 7.01 – Ar-H (1H, t), 5.25 - -CH$_2$- (2H, s), 5.18 - -CH (1H, sx), 1.79-1.21 - -CH$_2$- (12H, m), 0.88 - -CH$_3$ (6H, t). *IR (KBr)* v_{max}/cm^{-1}: 2940, 2840, 1700, 1585, 1500, 1265, 1185, 1000, 755, 695.

1-Ethylheptyl 4-benzyloxy-3-fluorobenzoate

The experimental procedure was as described for the preparation of 1-methylheptyl 4-benzyloxy-3-fluorobenzoate above.

Quantities: 4-benzyloxy-3-fluorobenzoic acid (10.0 g, 40.65 mmol), 3-nonanol (5.78 g, 40.65 mmol), DEAD (6.53g 40.65 mmol), triphenylphosphine (10.5 g, 40.65 mmol).

Yield: 4.47 g (29.6 %). *MS:* 372 (M^+, 4 %), 247 (7 %), 229 (9 %), 91 (100 %). *^{1}H-NMR (CDCl$_3$)* δ: 7.80 - Ar-H (1H, t); 7.76 - Ar-H (1H, m); 7.44 - 7.23 Bz-H (5H, m); 7.00 - Ar-H (1H, t); 5.34 - -CH$_2$- (2H, s); 5.15 - -C-H (1H, p); 1.55 - 1.13 - -CH$_2$- (12H, m); 0.80 - -CH$_3$ (6H, m). *IR (KBr)* v_{max}/cm^{-1}: 2980, 2855, 1710, 1615, 1510, 1280, 955, 765, 695.

1-Propylhexyl 4-benzyloxy-3-fluorobenzoate

The experimental procedure was as described for the preparation of 1-methylheptyl 4-benzyloxy-3-fluorobenzoate.

Quantities: 4-benzyloxy-3-fluorobenzoic acid (4.42 g, 17.97 mmol), 4-nonanol (2.65 g, 17.97 mmol), DEAD (2.88 g, 17.97 mmol), triphenylphosphine (4.64 g, 17.97 mmol).

Yield: 2.10 g (31.4 %). *MS:* 372 (M^+, 5 %), 247 (7 %), 229 (8 %), 91 (100 %). *^{1}H-NMR (CDCl$_3$)* δ: 7.79 - Ar-H (1H, t); 7.75 - Ar-H (m); 7.47-7.31 - Bz-H (5H, m); 7.02 - Ar-H (1H, t); 5.21 - -CH$_2$- (2H, s); 5.11 - -C-H (1H, p); 1.55-1.06 - -CH$_2$- (12H, m); 0.80 - -CH$_3$ (6H, m). *IR (KBr)* v_{max}/cm^{-1}: 2950, 2870, 1705, 1610, 1510, 1275, 1000, 765, 695.

1-Ethylpropyl 4-benzyloxy-3-fluorobenzoate

The experimental procedure was as described for the preparation of 1-methylheptyl 4-benzyloxy-3-fluorobenzoate above.

Quantities: 4-benzyloxy-3-fluorobenzoic acid (3.28 g, 13.33 mmol), 3-pentanol (1.18 g, 13.33 mmol), DEAD (2.32 g, 13.33 mmol), triphenylphosphine (3.5 g, 13.33 mmol).

Yield: 1.47 g (35.57 %). *MS:* 316 (M^+, trace), 247 (6 %), 229 (8 %), 91 (100 %). *^{1}H-

NMR (CDCl₃) δ: 7.78 - -AR-H (1H, t), 7.74 – Ar-H (1H, m), 7.46-7.3 – Bz-H (5H, m), 7.00 – Ar-H (1H, t), 5.19 - -CH$_2$- (2H, s), 5.11 - -CH (1H, m), 1.35 - -CH$_3$ (6H, d). *IR (KBr)* v_{max}/cm^{-1}: 2972, 2880, 1705, 1610, 1510, 1275, 1195, 1050, 760.

1-Propylbutyl 4-benzyloxy-3-fluorobenzoate

The experimental procedure was as described for the preparation of 1-methylheptyl 4-benzyloxy-3-fluorobenzoate above.

Quantities: 4-benzyloxy-3-fluorobenzoic acid (3.0 g, 12.2 mmol), 4-heptanol (1.41 g, 12.2 mmol), DEAD (2.11 g, 12.2 mmol), triphenylphosphine (3.2 g, 12.2 mmol).

Yield: 1.39 g (33.09 %). *MS:* 344 (M$^+$, 5 %), 247 (7 %), 229 (9 %), 91 (100 %). *^{1}H-NMR (CDCl₃) δ:* 7.79 – Ar-H (1H, t), 7.75 – Ar-H (1H, m), 7.47-7.34 – Bz-H (5H, m), 7.01 – Ar-H (1H, t), 5.22 - -CH$_2$- (2H, s), 5.12 - -CH (1H, p), 1.61-1.29 - -CH$_2$- (8H, m), 0.93 - -CH$_3$ (6H, t). *IR (KBr)* v_{max}/cm^{-1}: 3040, 2875, 1710, 1610, 1510, 1280, 1200, 1125, 765, 695.

1-Butylpentyl 4-benzyloxy-3-fluorobenzoate

The experimental procedure was as described for the preparation of 1-methylheptyl 4-benzyloxy-3-fluorobenzoate above.

Quantities: 4-benzyloxy-3-fluorobenzoic acid (2.9 g, 11.78 mmol), 5-nonanol (1.68 g, 11.63 mmol), DEAD (2.04g 11.63 mmol), triphenylphosphine (3.05 g, 11.63 mmol).

Yield: 1.81 g (41.8%). *MS:* 372 (M$^+$, 3 %), 246 (7 %), 229 (9 %), 91 (100 %). *^{1}H-NMR (CDCl₃) δ:* 7.79 - -Ar-H (1H, t), 7.74 – Ar-H (1H, m), 7.47-7.34 – Bz-H (5H, m), 7.01 – Ar-H (1H, t), 5.22 - -CH$_2$- (2H, s), 5.08 - -CH (1H, p), 1.80-1.33 - -CH$_2$- (12H, m), 0.87 - -CH$_3$ (6H, t). *IR (KBr)* v_{max}/cm^{-1}: 2960, 2860, 1715, 1610, 1500, 1280, 1200, 1040, 745, 695.

1-Butylpentyl 4-benzyloxy-3-fluorobenzoate *(alternative method)*

DCC (2.48 g, 12.0 mmol) was added to a mixture of 4-benzyloxy-3-fluorobenzoic acid (3.1 g, 12.6 mmol), 5-nonanol (1.73 g, 12.0 mmol), and a catalytic quantity of DMAP in 70 ml DCM. The reaction was allowed to stir at room temperature for 72

hours then the solvent was removed *in vacuo*. The crude oily product was purified by column chromatography (1:1 DCM/Petrol 40-60 °C).

Yield: 3.14 g (66.90 %). *MS:* 372 (M^+, 4 %), 247 (7 %), 229 (9 %), 91 (100 %). *^{1}H-NMR (CDCl$_3$)* δ: 7.79 – Ar-H (1H, t), 7.75 – Ar-H (1H, m), 7.46-7.33 – Bz-H (5H, m), 7.02 – Ar-H (1H, t), 5.21 - -CH$_2$- (2H, s), 5.09 - -CH (1H, p), 1.65 - -CH$_2$- (4H, m), 1.35 - -CH$_2$- (8H, m), 0.90 - -CH$_3$ (6H, t). *IR (KBr)* v_{max}/cm^{-1}: 2965, 2865, 1710, 1605,1510, 1280, 1195, 1035, 760, 760, 695.

1-Pentylhexyl 4-benzyloxy-3-fluorobenzoate

The experimental procedure was as described for the preparation of 1-methylheptyl 4-benzyloxy-3-fluorobenzoate above.

Quantities: 4-benzyloxy-3-fluorobenzoic acid (3.0 g, 12.2 mmol), 6-undecanol (2.11 g, 12.2 mmol), DEAD (2.11g 12.2 mmol), triphenylphosphine (3.2 g, 12.2 mmol).

Yield: 2.30 g (47.09 %). *MS:* 400 (M^+, 3 %), 247 (7 %), 229 (9 %), 91 (100 %). *^{1}H-NMR (CDCl$_3$)* δ: 7.79 – Ar-H (1H, t), 7.75 – Ar-H (1H, m), 7.48-7.32 – Bz-H (5H, m), 7.01 – Ar-H (1H, t), 5.21 - -CH$_2$- (2H, p), 5.11 - -CH (1H, p), 1.60 - -CH$_2$- (4H, m), 1.30 - -CH$_2$- (12H, m), 0.85 - -CH$_3$ (6H, t). *IR (KBr)* v_{max}/cm^{-1}: 3030, 2880, 1710, 1610, 1505, 1280, 1195, 1000, 760, 735, 695.

1-Butylpentyl 4-(methoxycarbonyloxy)benzoate

The experimental procedure was as described for the preparation of 1-methylheptyl 4-benzyloxy-3-fluorobenzoate above.

Quantities: 4-(methoxycarbonyloxy)-benzoic acid (3.0 g, 15.3 mmol), 5-nonanol (2.2 g, 15.3 mmol), DEAD (2.66 g, 15.3 mmol), triphenylphosphine (4.0 g, 15.3 mmol).

Yield: 1.94 g (27.7 %). *MS:* 322 (M^+, trace), 197 (35 %), 179 (100 %), 152 (40 %). *^{1}H-NMR (CDCl$_3$)* δ: 8.01 – Ar-H (2H, d), 7.25, -Ar-H (2H, d), 5.13 - -CH (1H, p), 3.90 - -CH$_3$ (3H, s), 1.70 - -CH$_2$- (2H, m), 1.33 - -CH$_2$- (8H, m), 0.90 - -CH$_3$ (6H, m). *IR (KBr)* v_{max}/cm^{-1}: 2960, 2860, 1770, 1715, 1610, 1260, 1220, 115, 775.

1-Butylheptyl 4-(methoxycarbonyloxy)benzoate

The experimental procedure was as described for the preparation of 1-methylheptyl 4-benzyloxy-3-fluorobenzoate above.

Quantities: 4-(methoxycarbonyloxy)-benzoic acid (2.5 g, 14.04 mmol), 5-undecanol (2.41 g, 14.04 mmol), DEAD (2.40 g, 14.04 mmol), triphenylphosphine (3.68 g, 14.04 mmol).

Yield: 1.72 g (38.96 %). *MS:* 350 (M^+, trace), 197 (30 %), 179 (100 %), 152 (39 %). *^{1}H-NMR (CDCl$_3$)* δ: 8.10 – Ar-H (2H, d), 7.25 – Ar-H (2H, d), 5.14 - -CH (1H, p), 3.25 - -CH$_3$ (3H, s), 1.65 - -CH$_2$- (4H, m), 1.30 - -CH$_2$- (12H, m), 0.88 - -CH$_3$ (6H, m). *IR (KBr)* v_{max}/cm^{-1}: 2960, 2860, 1770, 1610, 1445, 1310, 1220, 1115, 775.

(S)-1-Methylheptyl 4-(methoxycarbonyloxy)benzoate

The experimental procedure was as described for the preparation of 1-methylheptyl 4-benzyloxy-3-fluorobenzoate above.

Quantities: 4-(methoxycarbonyloxy)-benzoic acid (1.0 g, 5.56 mmol), (*R*)-2-octanol (0.72 g, 5.56 mmol), DEAD (0.96 g, 5.56 mmol), triphenylphosphine (1.46 g, 5.56 mmol).

Yield: 1.07 g (68.06 %). *MS:* 308 (M^+, 2 %), 197 (29 %), 179 (100 %), 152 (37 %). *^{1}H-NMR (CDCl$_3$)* δ: 8.10 – Ar-H (2H, d), 7.25 – Ar-H (2H, d), 5.17 – CH (1H, sx), 3.89 - -CH$_3$ (3H, s), 1.85-1.23 - -CH$_2$/CH$_3$ (13H, m), 0.85 - -CH$_3$ (3H, t). *IR (KBr)* v_{max}/cm^{-1}: 2960, 2860, 1760, 1715, 1260, 1220, 1115, 775.

(S)-1-Methylheptyl 4-benzyloxy-3-fluorobenzoate

The experimental procedure was as described for the preparation of 1-methylheptyl 4-benzyloxy-3-fluorobenzoate above.

Quantities: 4-benzyloxy-3-fluorobenzoic acid (4.0 g, 16.26 mmol), (*R*)-2-octanol (2.08 g, 16.0 mmol), DEAD (2.78 g, 16.0 mmol), triphenylphosphine (4.2 g, 16.0 mmol).

Yield: 3.77 g (65.8 %). *MS:* 358 (M^+, 2 %), 247 (8 %), 229 (11 %), 139 (100 %). *^{1}H-NMR (CDCl$_3$)* δ: 7.79 – Ar-H (1H, t), 7.74 – Ar-H, (1H, m), 7.47-7.31 – Bz-H (5H, m), 7.01 – Ar-H (1H, t), 5.21 –CH$_2$- (2H, s), 5.12 – -CH (1H, sx), 1.73-1.26 - -CH$_2$-/-

CH$_3$ (13H, m), 0.87 - -CH$_3$ (3H, t). *IR (KBr)* v_{max}/cm^{-1}: 3020, 2860, 1710, 1615, 1515, 1275, 1200, 1125, 765, 700.

(R)-1-Ethylheptyl 4-benzyloxy-3-fluorobenzoate

The experimental procedure was as described for the preparation of 1-methylheptyl 4-benzyloxy-3-fluorobenzoate above.

Quantities: 4-benzyloxy-3-fluorobenzoic acid (2.2 g, 9.01 mmol), (*S*)-3-nonanol (1.18 g, 8.2 mmol), DEAD (1.43 g, 8.2 mmol), triphenylphosphine (2.15 g, 8.2 mmol).

Yield: 1.37 g (45.2 %). *MS:* 372 (M$^+$, 2 %), 247 (7 %), 229 (12 %), 91 (100 %). ^{1}H-NMR *(CDCl$_3$)* δ: 7.78 – Ar-H (1H, t), 7.76 – Ar-H, (1H, m), 7.45 – 7.32 – Bz-H (5H, m), 7.02 – Ar-H (1H, t), 5.21 - -CH$_2$- (2H, s), 5.03 – CH (1H, p), 1.71-1.60 - -CH$_2$- (4H, m), 1.27 - -CH$_2$- (8H, m), 0.93 - -CH$_3$ (3H, t), 0.87 - -CH$_3$ (3H, t). *IR (KBr)* v_{max}/cm^{-1}: 3000, 2830, 1700, 1610, 1500, 1185, 1110, 745.

1-Methylheptyl 3-fluoro-4-hydroxybenzoate

A small spatula-tip of 10 % palladium-on-charcoal catalyst was added to a solution of 1-methylheptyl 4-benzyloxy-3-fluorobenzoate (1.08 g, 3.0 mmol) in 80 ml of a mixture of ethanol and ethyl acetate (1:1). After degassing under vacuum, the mixture was stirred under hydrogen for 72 hours at room temperature, filtered, and the filtrate evaporated down to a brown oil *in vacuo*. The raw product was used without further purification.

Yield: 0.73 g (90.9 %). *MS:* 268 (M$^+$, 2 %), 156 (20 %), 139 (100 %), 126 (32 %). ^{1}H-NMR *(CDCl$_3$)* δ: 9.83 - -OH (1H, broad s), 7.70 - Ar-H (2H, m), 7.00 - Ar-H (1H, t), 5.05 - -C-H (1H, sx), 1.75-1.15 - -CH$_2$-/-CH$_3$ (13H, m), 0.75 - -CH$_3$ (3H, broad s). *IR (KBr)* v_{max}/cm^{-1}: 3320, 2950, 2830, 1770, 1610, 1290, 1115, 765.

(S)-1-Methylheptyl 3-fluoro-4-hydroxybenzoate

The experimental procedure was as described for the preparation of 1-methylheptyl 3-fluoro-4-hydroxybenzoate above. The quantity of (*S*)-1-methylheptyl 4-benzyloxy-3-fluorobenzoate used was 1.31 g (4.54 mmol).

Yield: 0.74 g (74.5 %). *MS:* 268 (M$^+$, trace), 156 (20 %), 139 (100 %), 126 (15 %). *^{1}H-NMR (CDCl$_3$)* δ: 9.60 - -OH (1H, broad s), 7.71 – Ar-H (2H, m), 7.00 – Ar-H, (1H, t), 5.06 - -CH (1H, sx), 1.74–1.17 - -CH$_2$-/-CH$_3$ (13H, m), 0.76 - -CH$_3$ (3H, t). *IR (KBr)* v_{max}/cm^{-1}: 3350, 2960, 1860, 1690, 1620, 1300, 1220, 115, 765.

(R)-1-Ethylheptyl 3-fluoro-4-hydroxybenzoate

The experimental procedure was as described for the preparation of 1-methylheptyl 3-fluoro-4-hydroxybenzoate above. The quantity of (*R*)-1-ethylheptyl 4-benzyloxy-3-fluorobenzoate used was 1.37 g (3.68 mmol).

Yield: 1.00 g (96.2 %). *MS:* 282 (M$^+$, trace), 156 (16 %), 139 (100 %), 126 (21 %). *^{1}H-NMR (CDCl$_3$)* δ: 7.79 – Ar-H (1H, t), 7.76 – Ar-H (1H, m), 7.03 – Ar-H, (1H, t), 5.04 – -CH (1H, p), 1.66 - -CH$_2$- (4H, m), 1.24 - -CH$_2$- (8H, m), 0.93 - -CH$_3$ (3H, t), 0.87 - -CH$_3$ (3H, t). *IR (KBr)* v_{max}/cm^{-1}: 3340, 2955, 2855, 1700, 1615, 1300, 1215, 1120, 765.

1-Methylethyl 3-fluoro-4-hydroxybenzoate

The experimental procedure was as described for the preparation of 1-methylheptyl 3-fluoro-4-hydroxybenzoate above. The quantity of 1-methylethyl 4-benzyloxy-3-fluorobenzoate used was 1.31 g (4.54 mmol).

Yield: 0.69 g (76.9 %). *MS:* 198 (M$^+$, 2 %), 156 (40 %), 139 (100 %), 126 (21 %). *^{1}H-NMR (CDCl$_3$)* δ: 7.79 – Ar-H (1H, t), 7.75 – Ar-H (1H, m), 7.3 – Ar-H (1H, t), 5.22 - -CH (1H, sp), 1.37 - -CH$_3$ (6H, d), {-OH not observed}. *IR (KBr)* v_{max}/cm^{-1}: 3275, 2980, 2860, 1760, 1620, 1300, 1105, 915.

1-Methylpropyl 3-fluoro-4-hydroxybenzoate

The experimental procedure was as described for the preparation of 1-methylheptyl 3-fluoro-4-hydroxybenzoate above. The quantity of 1-methylpropyl 4-benzyloxy-3-fluorobenzoate used was 1.28 g (4.23 mmol).

Yield: 0.65 g (72.20 %). *MS:* 212 (M$^+$, 2 %), 156 (20 %), 139 (100 %), 126 (25 %). *^{1}H-NMR (CDCl$_3$)* δ: 7.79 – Ar-H (1H, t), 7.75 – Ar-H (1H, m), 7.03 – Ar-H (1H, t),

5.56 - -OH (1H, broad s), 5.06 - -CH (1H, sx), 1.68 - -CH$_2$- (2H, p), 1.33 - -CH$_3$ (3H, d), 0.97 - -CH$_3$ (3H, t). *IR (KBr)* v_{max}/cm^{-1}: 3340, 2960, 2860, 1680, 1610, 1510, 1105, 760.

1-Methylbutyl 3-fluoro-4-hydroxybenzoate

The experimental procedure was as described for the preparation of 1-methylheptyl 3-fluoro-4-hydroxybenzoate above. The quantity of 1-methylbutyl 4-benzyloxy-3-fluorobenzoate used was 0.85 g (2.69 mmol).

Yield: 0.58 g (95.4 %). *MS:* 226 (M$^+$, trace), 156 (16 %), 139 (100 %), 126 (24 %). *^{1}H-NMR (CDCl$_3$)* δ: 7.78 – Ar-H (2H, d), 7.02 – Ar-H (1H, t), 5.58 - -OH (1H, broad s), 5.10 - -CH (1H, sx), 1.67 - -CH$_2$- (2H, m), 1.34 - -CH$_2$-/-CH$_3$ (5H, m), 0.92 - -CH$_3$ (3H, t). *IR (KBr)* v_{max}/cm^{-1}: 3320, 2950, 2850, 1680, 1610, 1510, 1300, 1210, 1110, 755.

1-Methylpentyl 3-fluoro-4-hydroxybenzoate

The experimental procedure was as described for the preparation of 1-methylheptyl 3-fluoro-4-hydroxybenzoate above. The quantity of 1-methylpentyl 4-benzyloxy-3-fluorobenzoate used was 0.94 g (2.85 mmol).

Yield: 0.67 g (98.0 %). *MS:* 240 (M$^+$, trace), 156 (30 %), 139 (100 %), 126 (24 %). *^{1}H-NMR (CDCl$_3$)* δ: 7.78 – AR-H (2H, m), 7.03 – Ar-H (1H, t), 5.60 - -OH (1H, broad s), 5.12 - -CH (1H, sx), 1.66 - -CH$_2$- (2H, m), 1.35 - -CH$_2$-/-CH$_3$ (7H, m), 0.89 - -CH$_3$ (3H, t). *IR (KBr)* v_{max}/cm^{-1}: 3340, 3010, 2855, 1690, 1610, 1510, 1295, 1210, 1110, 750.

1-Methylhexyl 3-fluoro-4-hydroxybenzoate

The experimental procedure was as described for the preparation of 1-methylheptyl 3-fluoro-4-hydroxybenzoate above. The quantity of 1-methylhexyl 4-benzyloxy-3-fluorobenzoate used was 1.16 g (3.37 mmol).

Yield: 0.85 g (99.2 %). *MS:* 254 (M$^+$, 2 %), 156 (20 %), 139 (100 %), 126 (28 %). *^{1}H-NMR (CDCl$_3$)* δ: 7.76 – Ar-H (2H, m), 7.03 – Ar-H (1H, t), 5.5 - -OH (1H, broad

s), 5.12 - -CH (1H, sx), 1.65 - -CH$_2$- (2H, m), 1.30 - -CH$_2$-/-CH$_3$ (9H, m), 0.88 - -CH$_3$ (3H, t). *IR (KBr)* v_{max}/cm^{-1}: 3320, 2950, 2880, 1685, 1615, 1515, 1290, 1215, 1110, 760.

1-Methyloctyl 3-fluoro-4-hydroxybenzoate

The experimental procedure was as described for the preparation of 1-methylheptyl 3-fluoro-4-hydroxybenzoate above. The quantity of 1-methyloctyl 4-benzyloxy-3-fluorobenzoate used was 1.07 g (2.87 mmol).

Yield: 0.66 g (81.7 %). *MS:* 282 (M$^+$, 2 %), 156 (20 %), 139 (100 %), 126 (26 %).
^{1}*H-NMR (CDCl$_3$)* δ: 7.67 – Ar-H (2H, m), 6.95 - -Ar-H (1H, t), 5.5 - -CH (1H, sx), 1.71 – 1.15 - -CH$_2$/-CH$_3$ (15H, m), 0.78 - -CH$_3$ (3H, t) {-OH not observed}. *IR (KBr)* v_{max}/cm^{-1}: 3350, 2960, 2860, 1685, 1615, 1515, 1300, 1215, 1115, 765.

1-Ethylpropyl 3-fluoro-4-hydroxybenzoate

The experimental procedure was as described for the preparation of 1-methylheptyl 3-fluoro-4-hydroxybenzoate above. The quantity of 1-ethylpropyl 4-benzyloxy-3-fluorobenzoate used was 1.47 g (4.65 mmol).

Yield: 1.02 g (97.5 %). *MS:* 226 (M$^+$, trace), 156 (18 %), 139 (100 %), 126 (24 %).
^{1}*H-NMR (CDCl$_3$)* δ: 7.79 - -Ar-H (2H, m), 7.04 – Ar-H (1H, t), 5.80 - -OH (1H, broad s), 4.99 - -CH (1H, p), 1.69 - -CH$_2$- (4H, p), 0. 94 - -CH$_3$ (6H, t). *IR (KBr)* v_{max}/cm^{-1}: 3340, 2975, 2880, 1770, 1615, 1290, 1215, 1110, 950, 765.

1-Propylbutyl 3-fluoro-4-hydroxybenzoate

The experimental procedure was as described for the preparation of 1-methylheptyl 3-fluoro-4-hydroxybenzoate above. The quantity of 1-propylbutyl 4-benzyloxy-3-fluorobenzoate used was 1.39 g (4.04 mmol).

Yield: 0.97 g (94.5 %). *MS:* 254 (M$^+$, 2 %), 156 (26 %), 139 (100 %), 126 (31 %).
^{1}*H-NMR (CDCl$_3$)* δ: 7.65 – Ar-H (2H, m), 7.10 – Ar-H (1H, t), 6.05 - -OH (1H, broad s), 5.10 - -CH (1H, p), 1.60 - -CH$_2$- (8H, m), 0.86 - -CH$_3$ (6H, t). *IR (KBr)* v_{max}/cm^{-1}: 3380, 2960, 2860, 1685, 1610, 1510, 1280, 1215, 1115, 765.

1-Butylpentyl 3-fluoro-4-hydroxybenzoate

The experimental procedure was as described for 1-methylheptyl 3-fluoro-4-hydroxybenzoate above. The quantity of 1-butylpentyl 4-benzyloxy-3-fluorobenzoate used was 1.07 g (1.87 mmol).

Yield: 0.77 g (95.1 %). *MS:* 282 (M^+, trace), 156 (19 %), 139 (100 %), 126 (27 %). ^{1}*H-NMR (CDCl$_3$)* δ: 7.56-7.54 Ar-H (2H, m); 7.14 - Ar-H (1H, t); 6.55 - -O-H (1H, broad s); 5.19 - -C-H (1H, p); 1.54 - 0.9 - -CH$_2$- (12H, m); 0.78 - -CH$_3$ (6H, t). *IR (KBr)* v_{max}/cm^{-1}: 3340, 2960, 2860, 1685, 1615, 1515, 1295, 1215, 1115, 765.

1-Pentylhexyl 3-fluoro-4-hydroxybenzoate

The experimental procedure was as described for 1-methylheptyl 3-fluoro-4-hydroxybenzoate above. The quantity of 1-pentylhexyl 4-benzyloxy-3-fluorobenzoate used was 2.3 g (5.74 mmol).

Yield: 1.77 g (99.3 %). *MS:* 310 (M^+, trace), 156 (22 %), 139 (100 %), 126 (32 %). ^{1}*H-NMR (CDCl$_3$)* δ: 7.79 – Ar-H (1H, t), 7.75 – Ar-H (1H, m), 7.04 – Ar-H (1H, t), 5.09 - -CH (1H, p), 1.65 - -CH$_2$- (4H, m), 1.27 - -CH$_2$- (12H, m), 0.87 - -CH$_3$ (3H, t). *IR (KBr)* v_{max}/cm^{-1}: 3350, 2955, 2860, 1685, 1615, 1510, 1280, 1215, 1115, 765.

1-Ethylheptyl 3-fluoro-4-hydroxybenzoate

The experimental procedure was as described for 1-methylheptyl 3-fluoro-4-hydroxybenzoate above. The quantity of 1-ethylheptyl 4-benzyloxy-3-fluorobenzoate used was 4.47 g (12.0 mmol).

Yield: 3.13 g (92.4 %). *MS:* 282 (M^+, 2 %), 156 (17 %), 139 (100 %), 126 (22 %). ^{1}*H-NMR (CDCl$_3$)* δ: 7.78-7.72 - Ar-H (2H, m); 7.3 - Ar-H (1H, t); 6.51 - -O-H (1H, broad s); 5.54 - -C-H (1H, p); 1.55-0.92 -CH$_2$- (12H, m); 0.86 - CH$_3$ (6H, t). *IR (KBr)* v_{max}/cm^{-1}: 3340, 2955, 2855, 1685, 1610, 1510, 1295, 1115, 980, 765.

1-Propylhexyl 3-fluoro-4-hydroxybenzoate

The experimental procedure was as described for 1-methylheptyl 3-fluoro-4-hydroxybenzoate above. The quantity of 1-propylhexyl 4-benzyloxy-3-fluorobenzoate

used was 2.1 g (5.64 mmol).

Yield: 1.41 g (88.7 %). *MS:* 282 (M$^+$, trace), 156 (19 %), 139 (100 %), 126 (25 %). *^{1}H-NMR (CDCl$_3$)* δ: 7.79-7.73 (2H, m); 7.30 - (1H, t); 6.40 - -O-H (1H, broad s); 5.11 - -C-H (1H, p); 1.54-0.90 - -CH$_2$- (12H,m); 0.75 - -CH$_3$ (6H, t). *IR (KBr)* v_{max}/cm^{-1}: 3340, 2960, 2855, 1685, 1615, 1515, 1290, 1215, 1115, 955, 765.

1-Butylpentyl 4-hydroxybenzoate

To a stirred solution of the protected ester (1-butylpentyl 4-methylformate-benzoate) (1.94 g, 5.47 mmol) in 30 ml ethanol was added 30 ml ammonia solution (35 %). The mixture was allowed to stir at room temperature until the starting material had disappeared (monitored by TLC). The reaction mixture was poured onto excess cold water and the solvents were removed *in vacuo*.

Yield: 1.43 g (89.9 %). *MS:* 264 (M$^+$, trace), 168 (11 %), 138 (55 %), 121 (100 %). *^{1}H-NMR (CDCl$_3$)* δ: 7.97 – Ar-H (2H, d), 6.90 – Ar-H (2H, d), 5.95 - -OH (1H, broad s), 5.10 - -CH (1H, p), 1.72 - -CH$_2$ (4H. M), 1.35 - -CH$_2$- (8H, m), 0.90 - -CH$_3$ (6H, t). *IR (KBr)* v_{max}/cm^{-1}: 3355, 2960, 2860, 2755, 2620, 2525, 2380, 2265, 2225, 950, 775.

1-Butylheptyl 4-hydroxybenzoate

The experimental procedure was as described 1-butylpentyl 4-hydroxybenzoate above. The quantity of 1-butylheptyl 4-methylformate-benzoate used was 1.72 g (4.91 mmol).

Yield: 1.23 g (85.7 %). *MS:* 292 (M$^+$, trace), 168 (10 %), 138 (58 %), 121 (100 %). *^{1}H-NMR (CDCl$_3$)* δ: 7.96 – Ar-H (2H, d), 6.87 – Ar-H (2H, d), 5.71 - -OH (1H, broad s), 5.10 - -CH (1H, p), 1.65 - -CH$_2$- (4H, m), 1.60 - -CH$_2$- (12H, m), 0.88 - -CH$_3$ (6H, t). *IR (KBr)* v_{max}/cm^{-1}: 3350, 2960, 2860, 1675, 1610, 1510, 1450, 1280, 1165, 1115, 950, 775.

(S)-2-Methylheptyl 4-hydroxybenzoate

The experimental procedure was as described 1-butylpentyl 4-hydroxybenzoate above. The quantity of (S)-1-methylheptyl 4-methylformate-benzoate used was 4.00 g (12.97 mmol).

Yield: 2.35 g (70.4. %). *MS:* 250 (M^+, 2 %), 168 (14 %), 138 (50 %), 121 (100%). *^{1}H-NMR (CDCl$_3$)* δ: 7.96 – Ar-H (2H, d), 6.86 – Ar-H (2H, d), 5.64 - -OH (1H, broad s), 5.12 - -CH (1H, p), 1.64 - -CH$_2$- (2H, m), 1.30 - -CH$_2$-/-CH$_3$ (11H, m), 0.88 - -CH$_3$ (3H, t). *IR (KBr) v_{max}/cm^{-1}:* 3350, 2955, 2855, 1670, 1610, 1510, 1440, 1280, 1165, 1110, 850, 770.

4-Bromo-4'-decyloxybiphenyl

A mixture of 1-bromodecane (4.5 g, 221 mmol) potassium carbonate (13.85 g, 1 mol), 4-bromo-4'-hydroxybiphenyl (5.0 g, 201 mmol) and 80 ml butanone was refluxed overnight. The cooled reaction mixture was added to water and the product was extracted into dichloromethane. The combined organic layers were washed with water (3 x 100 ml), and dried over anhydrous magnesium sulphate. The solvents were removed *in vacuo* and the product was recrystallized from ethanol.

Yield: 6.96 g (89.1 %). *MS:* 386/388 (M^+, 12/12 %), 246/248 (100 %/99 %), 232/234 (8 %/9 %), 151 (5 %). *^{1}H-NMR (CDCl$_3$)* δ: 7.55-7.38 Ar-H (6H,m); 6.96 - Ar-H (2H, d); 3.85 - -CH$_2$-O (2H); 1.85-1.25 - -CH$_2$- (16H); 0.88 - -CH$_3$ (3H, t). The material was used without further analysis. *Mp:* 123 °C.

4-Bromo-4'-octyloxybiphenyl

The experimental procedure was as described for the alternative preparation of 4-bromo-4'-decyloxybiphenyl above.

Quantities: 4-bromo-4'-hydroxybiphenyl (10.0 g, 401.42 mmol), potassium carbonate (28.0 g, 2.01 mol); 1-bromooctane (7.0 ml, 445.0 mmol).

Yield: 13.39 g (92.1 %). *MS:* 360/362 (M^+, 14 %/14 %), 246/248 (98 %/100 %), 232/234 (10 %/10 %), 151 (4 %). *^{1}H-NMR (CDCl$_3$)* δ: 7.55-7.38 - Ar-H (6H, m); 6.96 - Ar-H (2H, d); 3.99 - -CH$_2$-O- (2H, t); 1.85-1.25 - -CH$_2$- (14H, m); 0.89 - -CH$_3$ (3H, t). The material was used without further analysis.

4-Cyano-4'-octyloxybiphenyl

A mixture of 4-cyano-4'-hydroxybiphenyl (10.0 g, 50 mmol), potassium carbonate (22.0 g, 150 mmol), butanone (200 ml), and 1-bromooctane (9.65 g, 60 mmol) was refluxed overnight. The product mixture was filtered and washed with water (2 x 100 ml) and the aqueous layers were extracted with ether (2 x 100 ml). The combined organic phases were dried over magnesium sulphate and the solvents were removed *in vacuo*. The product was recrystallized from ethanol to yield white crystals.

Yield: 15.55 g (77.6 %). *MS*: 307 (M^+, 20 %), 195 (100 %), 178 (2 %), 166 (4 %). *^{1}H-NMR (CDCl$_3$)* δ: 7.75-7.50 Ar-H (6H, m); 7.00 - Ar-H (2H, d); 4.03 - -CH$_2$-O (2H, t); 1.88-1.25 (12H, m); 0.90 - -CH$_3$ (3H, t). *IR (KBr)* v_{max}/cm^{-1}: 2950, 2850, 2215, 1600, 1490, 1250, 1180, 825.

TT (°C): Cr 54 SmA 65.3 N 79.6 I (Recryst. 27.4).

4-Cyano-4'-heptyloxybiphenyl

The experimental procedure was as described for the preparation of 4-cyano-4'-octyloxybiphenyl above.

Quantities: 4-cyano-4'-hydroxybiphenyl (10.0 g, 50.0 mmol), potassium carbonate (22.0 g, 150 mmol), 1-bromoheptane (10.7 g, 59.7 mmol).

Yield: 10.87 g (72.4 %). *MS*: 293 (M^+, 4 %), 195 (100 %), 177 (4 %), 166 (12 %). *^{1}H-NMR (CDCl$_3$)* δ: 7.75 – 7.60 – Ar-H (6H, m), 7.00 – Ar-H (2H, d), 4.03 - -CH$_2$-O (2H, t), 1.85 - -CH$_2$- (2H, p), 1.40 - -CH$_2$- (8H, m), 0.80 - -CH$_3$ (3H, t). *IR (KBr)* v_{max}/cm^{-1}: 2955, 2855, 2215, 1600, 1490, 1250, 1180, 830.

TT (°C): Cr 52 N 73.4 I (Recryst. 30.5).

4-Cyano-4'-nonyloxybiphenyl

The experimental procedure was as described for the preparation of 4-cyano-4'-octyloxybiphenyl above.

Quantities: 4-cyano-4'-hydroxybiphenyl (10.0 g, 50.0 mmol), potassium carbonate (22.0 g, 150 mmol), 1-bromononane (12.5 g, 60.3 mmol).

Yield: 13.83 (67.2 %). *MS*: 321 (M^+, 28 %), 195 (100 %), 166 (10 %), 140 (14 %). *^{1}H-NMR (CDCl$_3$)* δ: 7.72-7.49 – Ar-H (6H, m), 6.99 – Ar-H (2H, d), 4.01 - -CH$_2$-O

(2H, t), 1.85 - -CH$_2$- (2H, p), 1.40 - -CH$_2$- (12H, m), 0.80 - -CH$_3$ (3H, t). *IR (KBr)* v$_{max}$/cm^{-1}: 2955, 2855, 2215, 1600, 1485, 1250, 1180, 825.

TT (°C): Cr 55 SmA 77.4 N 79.7 I (Recryst. 30.5).

4-Cyano-4'-decyloxybiphenyl

The experimental procedure was as described for the preparation of 4-cyano-4'-octyloxybiphenyl above.

Quantities: 4-cyano-4'-hydroxybiphenyl (30.0 g, 153.85 mmol), potassium carbonate (64.0 g, 461.53 mmol), 1-bromodecane (34.03 g, 153.85 mmol).

Yield: 45.38 g (87.79 %). *MS:* 335 (M$^+$, 10 %), 195 (100 %), 178 (3 %), 166 (7 %).

^{1}H-NMR (CDCl$_3$) δ: 7.70-7.47 - Ar-H (6H, m); 6.96 - Ar-H (2H, d); 4.00 - -CH$_2$-O (2H, t); 1.86-1.25 (16H, m); 0.87 - -CH$_3$ (3H, t). *IR (KBr)* v$_{max}$/cm^{-1}: 2955, 2850, 2235, 1600, 1490, 1250, 1180, 825.

TT (°C): Cr 58 SmA 84.1 I (Recryst. 41).

4-Cyano-4'-undecyloxybiphenyl

The experimental procedure was as described for the preparation of 4-cyano-4'-octyloxybiphenyl.

Quantities: 4-cyano-4'-hydroxybiphenyl (10.0 g, 50.0 mmol), potassium carbonate (22.0 g, 150 mmol), 1-bromoundecane (14.5 g, 61.6 mmol).

Yield: 12.67 g (70.8 %). *MS:* 349 (M$^+$, 59 %), 195 (100 %), 177 (7 %), 166 (25 %).

^{1}H-NMR (CDCl$_3$) δ: 7.74-7.48 – Ar-H (6H, m), 6.99 – Ar-H (2H, d), 4.02 - -CH$_2$-O (2H, t), 1.85 - -CH$_2$- (2H, p), 1.35 - -CH$_2$- (16H, m), 0.90 - -CH$_3$ (3H, t). *IR (KBr)* v$_{max}$/cm^{-1}: 2955, 2855, 2235, 1600, 1490, 1250, 1180, 825.

TT (°C): Cr 70 SmA 85.8 I (Recryst. 45).

4-Cyano-4'-dodecyloxybiphenyl

The experimental procedure was as described for the preparation of 4-octyloxy-4'-cyanobiphenyl above.

Quantities: 4-cyano-4'-hydroxybiphenyl (10.0 g, 51.28 mmol), potassium carbonate

(21.3 g, 153.85 mmol), 1-bromododecane (12.7 g, 76.9 mmol).

Yield: 10.23 (54.8 %). *MS:* 363 (M$^+$, 41 %), 195 (100 %), 178 (7 %), 166 (16 %). *^{1}H-NMR (CDCl$_3$)* δ: 7.66 - Ar-H (4H, m), 7.55 - Ar-H (2H, d), 6.98 - Ar-H (2H, d), 4.00 - -CH$_2$-O (2H, t), 1.85 - -CH$_2$- (20H, m), 0.85 - -CH$_3$ (3H, t). *IR (KBr)* v_{max}/cm^{-1}: 2955, 2850, 2235, 1605, 1490, 1250, 1180, 825.

TT (°C): Cr 69 SmA 89 I (Recryst. 48).

4-Cyano-4'-tetradecyloxybiphenyl

The experimental procedure was as described for the preparation of 4-octyloxy-4'-cyanobiphenyl above.

Quantities: 4-cyano-4'-hydroxybiphenyl (10.0 g, 51.3 mmol), potassium carbonate (21.3 g, 153.9 mmol), 1-bromotetradecane (17.0 g, 76.9 mmol).

Yield: 11.1 g (55.1 %). *MS:* 391 (M$^+$, 8 %), 195 (100 %), 178 (3 %), 166 (9 %). *^{1}H-NMR (CDCl$_3$)* δ: 7.67 - Ar-H (4H, m), 7.54 - Ar-H (2H, d), 6.96 - Ar-H (2H, d), 4.02 - -CH$_2$-O (2H, t), 1.86 - -CH$_2$- (24H, m), 0.86 - -CH$_3$ (3H, t). *IR (KBr)* v_{max}/cm^{-1}: 2950, 2850, 2240, 1600, 1255, 1185, 820.

TT (°C): Cr 76 SmA 91 (Recryst. 58.3).

4-Octyloxybiphenyl-4'-carboxylic acid

18M sulphuric acid (20 ml) and water (20 ml) were added dropwise to a solution of 4-cyano-4'-octyloxybiphenyl (5.0 g, 16.2 mmol) in glacial acetic acid (100 ml). After refluxing the mixture overnight the reaction was allowed to cool to room temperature. The precipitate was filtered off, washed repeatedly with water and cold DCM (3 x 50 ml), then dried.

Yield: 4.17 g (78.6 %). *MS:* 326 (M$^+$, 31 %), 214 (100 %), 197 (25 %), 139 (18 %). *^{1}H-NMR (d-DMSO/CDCl$_3$)* δ: 8.08 - Ar-H (2H, ddd); 7.67-7.53 - Ar-H (4H, m); 9.96 - Ar-H (2H, d); 4.07 - -CH$_2$-O (2H ,t); 1.88-1.24 - -CH$_2$- (14H, m); 0.87 - -CH$_3$ (3H, t) {-COOH not observed}. *IR (KBr)* v_{max}/cm^{-1}: 3000, 2950, 2850, 1680, 1430, 1290, 1200, 835, 770.

TT (°C): Cr 185 SmC 257 N 266 I (Recryst. 158).

4-Heptyloxybiphenyl-4'-carboxylic acid

The experimental procedure was as described for the preparation of 4-octyloxy-biphenyl-4'-carboxylic acid above.

Quantities: 4-Cyano-4'-heptyloxybiphenyl (5.0 g, 17.04 mmol), glacial acetic acid (100 ml), 18M sulphuric acid (20 ml), water (20 ml).

Yield: 4.55 g (85.5 %). *MS:* 312 (M$^+$, 36 %), 214 (100 %), 197 (30 %), 139 (21 %). ^{1}H-NMR *(d-DMSO/CDCl$_3$)* δ: 12.18 - -COOH (1H, broad s), 8.09 – Ar-H (2H, d), 7.58 – Ar-H (4H, m), 6.99 – Ar-H (2H, d), 4.05 - -CH$_2$-O (2H, t), 1.85 - -CH$_2$- (2H, p), 1.40 - -CH$_2$- (8H, m), 0.80 - -CH$_3$ (3H, t). *IR (KBr)* v_{max}/cm^{-1}: 3000, 2950, 2850, 1680, 1600, 1430, 1290, 1250, 1200, 835, 760.

TT (°C): Cr 190 SmX$_{ii}$ 237 SmX$_i$ 250 N 261 I (Recryst. 175).

4-Nonyloxybiphenyl-4'-carboxylic acid

The experimental procedure was as described for the preparation of 4-octyloxy-biphenyl-4'-carboxylic acid above.

Quantities: 4-Cyano-4'-nonyloxybiphenyl (7.0 g, 21.78 mmol), glacial acetic acid (120 ml), 18M sulphuric acid (25 ml), water (25 ml).

Yield: 5.91 g (79.8 %). *MS:* 340 (M$^+$, 38 %), 214 (100 %), 197 (20 %), 185 (13 %). ^{1}H-NMR *(d-DMSO/CDCl$_3$)* δ: 8.10 – Ar-H (2H, d), 7.60 – Ar-H (4H, m), 7.02 – Ar-H (2H, m), 4.03 - -CH$_2$-O (2H, t), 1.83 - -CH$_2$- (2H, p), 1.40 - -CH$_2$- (14H, m), 0.90 - -CH$_3$ (3H, t) {-COOH not observed}. *IR (KBr)* v_{max}/cm^{-1}: 3000, 2950, 2845, 1680, 1600, 1430, 1290, 1200, 835, 770.

TT (°C): Cr 176 SmX$_{iii}$ 193.6 SmX$_{ii}$ 249.9 SmX$_i$ 253.4 N 260 I (Recryst. 172.5).

4-Decyloxybiphenyl-4'-carboxylic acid

The experimental procedure was as described for the preparation of 4-octyloxy-biphenyl-4'-carboxylic acid above.

Quantities: 4-Cyano-4'-decyloxybiphenyl (10.0 g, 29.8 mmol), glacial acetic acid (150 ml), 18M sulphuric acid (35 ml), water (35 ml).

Yield: 9.94 g (94.1 %). *MS:* 354 (M$^+$, 22 %), 214 (100 %), 197 (35 %), 168 (30 %). ^{1}H-NMR *(d-DMSO/CDCl$_3$)* δ: 12.15 - -COOH (1H, broad s), 8.08 - Ar-H (2H, d),

7.40 - Ar-H (4H, m), 6.96 - Ar-H (2H, d), 4.00 - -CH$_2$-O (2H, t), 1.87-1.22 -CH$_2$-(16H, m), 0.87 - -CH$_3$ (3H, t). *IR (KBr)* v_{max}/cm^{-1}: 3000, 2950, 2950, 1680, 1600, 1435, 1290, 1200, 835, 765.

TT (°C): Cr 175 SmC 258 N 259 I (Recryst. 164).

4-Undecyloxybiphenyl-4'-carboxylic acid

The experimental procedure was as described for the preparation of 4-octyloxy-biphenyl-4'-carboxylic acid above.

Quantities: 4-Cyano-4'-undecyloxybiphenyl (7.0 g, 20.03 mmol), glacial acetic acid (120 ml), 18M sulphuric acid (25 ml), water (25 ml).

Yield: 5.7 g (77.3 %). *MS:* 368 (M$^+$, 12 %), 214 (100 %), 197 (52 %), 168 (14 %).

^{1}H-NMR (d-DMSO/CDCl$_3$) δ: 12.12 - -COOH (1H, broad s), 8.09 – Ar-H (2H, d), 7.50 – Ar-H (4H, m), 7.00 – Ar-H (2H, m), 4.03 - -CH$_2$-O (2H, t), 1.85-1.24 - -CH$_2$-(18H, m), 0.89 - -CH$_3$ (3H, t). *IR (KBr)* v_{max}/cm^{-1}: 3000, 2955, 2855, 1680, 1600, 1440, 1285, 1200, 830, 765.

TT (°C): Cr 206 SmX$_{ii}$ 168.9 SmX$_i$ 231.8 N 239.7 (Recryst. 147.5).

4-Dodecyloxybiphenyl-4'-carboxylic acid

The experimental procedure was as described for the preparation of 4-octyloxy-biphenyl-4'-carboxylic acid above.

Quantities: 4-Cyano-4'-dodecyloxy-biphenyl (5.0 g, 13.74 mmol), glacial acetic acid (100 ml), 18M sulphuric acid (20 ml), water (20 ml).

Yield: 3.90 g (74.2 %). *MS:* 382 (M$^+$, 18 %), 214 (100 %), 197 (40 %), 150 (11 %).

^{1}H-NMR (d-DMSO/CDCl$_3$) δ: 12.10 - -COOH (1H, broad s); 8.10 - Ar-H (2H, d); 7.58 - Ar-H (4H, m); 6.97 - Ar-H (2H, d); 4.03 - -CH$_2$-O (2H, t); 1.85-1.20 - -CH$_2$-(20H, m); 0.90 - -CH$_3$ (3H, t). *IR (KBr)* v_{max}/cm^{-1}: 3010, 2950, 2850, 1685, 1600, 1435, 1290, 1200, 835, 765.

TT (°C): Cr 168 SmC 254 I (Recryst. 153).

4-Tetradecyloxybiphenyl-4'-carboxylic acid

The experimental procedure was the same as for the preparation of 4-octyloxy-4'-biphenyl-4'-carboxylic acid above, the quantities of reagents used were as follows;-

Quantities: 4-Cyano-4'-tetradecyloxy-biphenyl (5.47 g, 13.96 mmol), glacial acetic acid (100 ml), 18M sulphuric acid (20 ml), water (20 ml).

Yield: 6.19 g (84.3 %). *MS:* 410 (M^+, 10 %), 214 (100 %), 197 (43 %), 168 (15 %). ^{1}H-NMR *(d-DMSO/CDCl$_3$)* δ: 12.25 - -COOH (1H, broad s); 8.07- Ar-H (2H, d); 7.15-7.00 - Ar-H (4H, m); 6.96 - Ar-H (2H, d); 4.00 - -CH$_2$-O (2H, t); 1.86-1.20 - -CH$_2$- (24H, m); 0.86 - -CH$_3$ (3H, t). *IR (KBr)* v_{max}/cm^{-1}: 3020, 2955, 2840, 1680, 1600, 1430, 1290, 1200, 835, 770.

TT (°C): Cr 159 SmC 246 I (Recryst. 143).

4-Decyloxybiphenyl-4'-carboxylic acid *(alternative preparation)*

A solution of the Grignard reagent formed in the usual way from 4-bromo-4'-decyloxybiphenyl (5.59 g, 14.99 mmol) and magnesium turnings (1.0 g, 37.47 mmol) in 80 ml THF was added to a slurry of solid carbon dioxide (very large excess) in 200 ml THF. The mixture was allowed to warm to room temperature, then acidified with cold dilute hydrochloric acid (pH1). The precipitated product was filtered, washed repeatedly with cold DCM and then dried.

Yield: 2.67 g (52.3 %). *MS:* 354 (M^+, 34%), 214 (100%), 197 (34%), 168 (12%). ^{1}H-NMR *(d-DMSO)* δ: 8.07 - Ar-H (2H, ddd); 7.65-7.52 - Ar-H (4H, m); 6.98 - Ar-H (2H, d); 4.05 - -CH$_2$-O (2H, t); 1.87-1.22 - -CH$_2$- (16H, m); 4.10 - -CH$_3$- (3H, t). *IR (KBr)* v_{max}/cm^{-1}: 3200, 2955, 2855, 1685, 1435, 1285, 1200, 835, 765.

TT (°C): Cr 173 SmC 256 N 252 I (Recryst. 162).

4-Octyloxybiphenyl-4'-carboxylic acid *(alternative preparation)*

The experimental procedure was as described for the preparation of 4-decyloxy-biphenyl-4'-carboxylic acid.

Quantities: 4-Bromo-4'-octyloxybiphenyl (6.0 g, 16.57 mmol), magnesium turnings (1.0 g, 41.43 mmol).

Yield: 3.52 g (58.6 %). ***MS:*** 326 (M$^+$, 26 %), 214 (100 %), 197 (21 %), 168 (12 %).

^{1}H-NMR (d-DMSO) δ: 8.07 - Ar-H (2H, d); 7.65-7.52 - Ar-H (4H, m); 7.98 - Ar-H (2H, d); 4.10 - -CH$_2$-O (2H, t); 1.86-1.24 - -CH$_2$- (14H, m); 0.88 - -CH$_3$ (3H, t). ***IR (KBr)*** v_{max}/cm^{-1}: 3300, 2955, 2850, 1690, 1435, 1290, 1200, 1200, 840, 765.

TT (°C): Cr 184 SmC 257 N 265 I (Recryst. 173).

Compound 11a {(S)-MHPOBC}

(S)-4-(1-methylheptyloxycarbonyl)phenyl 4'-octyloxybiphenyl-4-carboxylate.

DCC (0.83 g, 4 mmol) was added to a mixture of 4-octyloxybiphenyl-4'-carboxylic acid (1.34 g, 4.11 mmol), (S)-1-methylheptyl 4-hydroxybenzoate (1.0 g, 4 mmol), and a catalytic quantity of DMAP in DCM. The mixture was stirred at room temperature for two days, then the mixture was filtered and the filtrate washed with potassium hydroxide. The solvent was removed *in vacuo* and the product was purified by column chromatography using 1:1 petrol:dichloromethane, and recrystallization from ethanol to yield a colourless solid.

Yield: 0.46 g (20.6 %); *MS:* 558 (M^+, trace), 309 (100 %), 197 (18 %), 169 (8 %) (M^+ not observed). *^{1}H-NMR (CDCl$_3$) δ:* 8.19 - Ar-H (2H, dd); 7.66 - Ar-H (2H, dd); 7.32 - Ar-H (2H, d); 7.05 - Ar-H (2H, d); 5.16 - -C-H (1H, sx); 4.02 - -CH$_2$-O (2H, t); 1.85 - 1.3 - -CH$_2$-/-CH$_3$ (29H, m); 0.9 - -CH$_3$ (3H, t). *IR (KBr) v_{max}/cm^{-1}:* 2940, 2850, 1715, 1705, 1600, 1270, 1240, 1190, 1060, 825, 765. *HPLC (90 % acetonitrile, 10 % chloroform):* 99.5 %.

TT (°C): Cr 65 (SmI$_A$*) 62 SmC$_A$* 117.8 SmC$_\gamma$* 118.8 SmC* 119.9 SmA* 145.2 I (Recryst. 30).

Compound 1a

1-Methylheptyl 4-(4'-decylbiphenyl-4-carbonyloxy)-3-fluorobenzoate

4-Decylbiphenyl-4'-carboxylic acid (1.29 g, 3.73 mmol) was added to a solution of 1-methylheptyl 3-fluoro-4-hydroxybenzoate (1.0 g, 3.73 mmol) and a catalytic quantity of DMAP in molecular sieve-dried dichloromethane. DCC (0.77 g, 3.73 mmol) was slowly added to the mixture and the reaction was stirred overnight. The reaction mixture was filtered and the filtrate was washed with potassium hydroxide solution and the solvent was removed *in vacuo*. The product was purified by column chromatography using 1:1 petrol:dichloromethane, and recrystallization from ethanol to yield a colourless solid.

Yield: 1.26 g (59.4 %); *MS:* 588 (M^+, trace) 321 (100 %), 194 (11 %), 167 (22 %).

^{1}H-NMR (CDCl$_3$) δ: 8.25 - Ar-H (2H, d); 7.90 - Ar-H (2H, m); 7.74 - Ar-H (2H, d); 7.58 - Ar-H (2H, d), 7.39-7.25 - (3H, m); 5.16 - -C-H (1H, sx); 2.67 - -CH$_2$-Ar (2H, t); 1.58-1.20 -CH$_2$-/-CH$_3$ (29H, m); 0.80 - -CH$_3$ (6H, t). IR (KBr) v_{max}/cm^{-1}: 2950, 2850, 1740, 1710, 1590, 1505, 1260, 825, 760. HPLC (90 % acetonitrile, 10 % chloroform): 96 %.

TT (°C): Cr 51 SmA 76 I (Recryst. 39)

Compound 1b

1-Ethylheptyl 4-(4'-decylbiphenyl-4-carbonyloxy)-3-fluorobenzoate

The procedure was as described for the preparation of compound 1a (dev22) above.

Quantities: 4-Decylbiphenyl-4'-carboxylic acid (1.5 g, 4.42 mmol), 1-ethylheptyl 3-fluoro-4-hydroxybenzoate (1.25 g, 4.42 mmol), DCC (0.91 g, 4.42 mmol).

Yield: 0.58 g (22.4 %); *MS:* 602 (M$^+$, trace), 366 (83 %), 321 (20 %), 239 (100 %).

^{1}H-NMR (CDCl$_3$) δ: 8.25 - Ar-H (2H, d); 7.91 - Ar-H (2H, m); 7.73 - Ar-H (2H, d); 7.57 - Ar-H (2H, d); 7.40-7.27 - Ar-H (3H, m); 5.80 - -C-H (1H, p); 2.66 - -CH$_2$- (2H, t); 1.55-1.14 - -CH$_2$- (28H); 0.87 - -CH$_3$ (9H, m). IR (KBr) v_{max}/cm^{-1}: 2970, 2850, 1745, 1715, 1605, 1500, 1255, 1155, 825, 760. HPLC (90 % acetonitrile, 10 % chloroform): 99.9 %.

TT (°C): Cr <25 (SmC$_{alt}$ 9) SmA 43 I (Recryst. <0).

Compound 1c

1-Butylpentyl 4-(4'-decylbiphenyl-4-carbonyloxy)-3-fluorobenzoate.

The procedure was as described for the preparation of compound 1 (dev22).

Quantities: 4-Decylbiphenyl-4'-carboxylic acid (2.4 g, 7.09 mmol), 1-butylpentyl 3-fluoro-4-hydroxybenzoate (2.0 g, 7.09 mmol), DCC (1.47 g, 7.09 mmol).

Yield: 0.59 g (14.3 %). *MS:* 603 (M$^+$, trace), 321 (100 %), 166 (23 %). ^{1}H-NMR (CDCl$_3$) δ: 8.26 - Ar-H (2H, d); 7.94 - Ar-H (2H, m); 7.72 - Ar-H (2H, d); 7.58 - Ar-H (2H, d); 7.40-7.20 - Ar-H (3H, m); 5.14 - Ar-H (1H, p); 2.66 - Ar-H (2H, t); 1.54-1.04 - -CH$_2$- (28H, m); 0.80 - -CH$_3$ (9H, m). IR (KBr) v_{max}/cm^{-1}: 2950, 2850, 1745, 1715, 1600, 1500, 1290, 1255, 1180, 825, 760. HPLC (90 % acetonitrile, 10 %

chloroform): 99.4 %.

TT (°C): Cr <0 SmC$_{alt}$ 0 SmA 28 I (Recryst. <0).

Compound 7g

1-Ethylhexyl 4-(4'-octyloxybiphenyl-4-carbonyloxy)-3-fluorobenzoate

The procedure was as described for the preparation of compound **1** (dev22).

Quantities: 4-Octyloxybiphenyl-4'-carboxylic acid (1.22 g, 3.73 mmol), 1-methylpentyl 3-fluoro-4-hydroxybenzoate (1.0 g, 3.73 mmol), DCC (0.76 g, 3.73 mmol).

Yield: 0.76 g (18.5 %). *MS:* 576 (M$^+$, trace), 309 (100 %), 197 (20%), 169 (12 %). ^{1}*H-NMR (CDCl$_3$)* δ: 8.24 - Ar-H (2H, d); 7.91 - Ar-H (2H, m); 7.71 - Ar-H (2H, d); 7.60 - Ar-H (2H, d); 7.26 - Ar-H (1H, dd); 7.05 - Ar-H (2H, d); 5.08 - -C-H (1H, m); 4.04 - -CH$_2$-O (2H, t); 1.85-1.20 - -CH$_2$- (22H, m); 0.90 - -CH$_3$ (9H, m). *IR (KBr)* v_{max}/cm^{-1}: 2950, 2750, 1740, 1705, 1599, 1285, 1265, 1060, 825, 760. *HPLC (90 % acetonitrile, 10 % chloroform):* 98.4 %.

TT (°C): Cr 34 ("SmX$_2$" 22) SmC$_{alt}$ 53.5 SmA 93.5 I (Recryst. <0).

Compound 7f

1-Methyloctyl 4-(4'-octyloxybiphenyl-4-carbonyloxy)-3-fluorobenzoate.

The procedure was the same as for the preparation of compound **1** (dev22).

Quantities: 4-Octyloxybiphenyl-4'-carboxylic (5.88 g, 1.8 mmol), 1-methyoctyl 3-fluoro-4-hydroxybenzoate (5.65 g, 1.8 mmol), DCC (3.72 g, 1.8 mmol).

Yield: 6.83 g (68.0 %). *MS:* 590 (M$^+$, trace), 309 (100 %), 197 (22 %), 169 (10 %). ^{1}*H-NMR (CDCl$_3$)* δ: 8.25 - Ar-H (2H, d); 7.90 - Ar-H (2H, m); 7.72 - Ar-H (2H, ddd); 7.60 - Ar-H (2H, ddd); 7.37 - Ar-H (1H, dd); 7.02 - Ar-H (2H, ddd); 5.32 - -C-H (1H, p); 4.02 - -CH$_2$-O (2H, t); 1.80-1.25 - -CH$_2$- (24H, m); 0.90 - -CH$_3$ (9H, m). *IR (KBr)* v_{max}/cm^{-1}: 2940, 2850, 1740, 1710, 1600, 1295, 1260, 1185, 1060, 825, 760. *HPLC (90 % acetonitrile, 10 % chloroform):* 100 %.

TT (°C): Cr 74 (SmC 28) SmA 115 I (Recryst. 26).

Compound 8c

1-Methylheptyl 4-(4'-dodecyloxybiphenyl-4-carbonyloxy)-3-fluorobenzoate.

The procedure was the same as for the preparation of compound 1 (dev22).

Quantities: 4-Dodecyloxybiphenyl-4'-carboxylic acid (1.42 g, 3.73 mmol), 1-methylheptyl 3-fluoro-4-hydroxybenzoate (1.0 g, 3.73 mmol), DCC (0.77 g, 3.73 mmol).

Yield: 0.39 g (16.4 %). *MS:* 632 (M^+, trace), 365 (100 %), 214 (22 %), 197 (51 %), 133 (45 %). ^{1}*H-NMR (CDCl$_3$)* δ: 8.24 - Ar-H (2H,d); 7.90 - Ar-H (2H, m); 7.71 - Ar-H (2H, d); 7.60 - Ar-H (2H, d); 7.36 - Ar-H (1H, dd); 7.01 - Ar-H (2H, d); 5.16 - -C-H (1H, sx); 4.02 - -CH$_2$-O (2H, t); 1.57-1.04 - -CH$_2$- (30H, m); 0.88 - -CH$_3$ (9H, t). *IR (KBr) v_{max}/cm^{-1}:* 2950, 2840, 1745, 1715, 1600, 1505, 1295, 1260, 1185, 1060, 825, 760. *HPLC (90 % acetonitrile, 10 % chloroform):* 99.7 %.

TT (°C): Cr 52 SmC$_{alt}$ 75 SmC 88.6 SmA 105 I (Recryst. <25).

Compound 8d

1-Ethylheptyl 4-(4'-dodecyloxybiphenyl-4-carbonyloxy)-3-fluorobenzoate.

The procedure was as described for the preparation of compound 1 (dev22).

Quantities: 4-Dodecyloxybiphenyl-4'-carboxylic acid (1.35 g, 3.55 mmol), 1-ethylheptyl 3-fluoro-4-hydroxybenzoate (1.0 g, 3.55 mmol), DCC (0.74 g, 3.55 mmol).

Yield: 0.77 g (33.3 %). *MS:* 646 (M^+, trace), 365 (100 %), 197 (16 %), 139 (60 %), 41 (100 %). ^{1}*H-NMR (CDCl$_3$)* δ: 8.25 - Ar-H (2H, d); 7.92 - Ar-H (2H, m); 7.71 - Ar-H (2H, d); 7.60 - Ar-H (2H, d);7.37 - Ar-H (1H, dd); 7.01 - Ar-H (2H, d); 5.09 - -C-H (1H, p); 4.02 - -CH$_2$-O (2H, t); 1.87-1.22 - -CH$_2$- (30H, m); 1.00-0.85 - -CH$_3$- (9H, m). *IR (KBr) v_{max}/cm^{-1}:* 2950, 2842, 1745, 1715, 1600, 1505, 1295, 1260, 1185, 1165, 825, 760. *HPLC (90 % acetonitrile, 10 % chloroform):* 99.6 %.

TT (°C): Cr 34 SmC$_{alt}$ 60 SmA 75.4 I (Recryst. <25)

Compound 6c

1-Propylhexyl 4-(4'-dodecyloxybiphenyl-4-carbonyloxy)-3-fluorobenzoate.

The procedure was as described for the preparation of compound **1** (dev22) above.

Quantities: 4-Dodecyloxybiphenyl-4'-carboxylic acid (0.9 g, 2.35 mmol), 1-propylhexyl 3-fluoro-4-hydroxybenzoate (0.5 g, 2.35 mmol), DCC (0.48 g, 2.35 mmol).

Yield: 0.93 g (60.2 %). *MS:* 646 (M^+, 2 %), 365 (100 %), 196 (20 %). ^{1}*H-NMR (CDCl$_3$)* δ: 8.25 - Ar-H (2H, d); 7.91 - Ar-H (2H, m); 7.71 - Ar-H (2H, d); 7.60 - Ar-H (2H, d); 7.37 - Ar-H (1H, m); 7.01 - Ar-H (2H, d); 5.17 - -C-H (1H, p); 4.02 - -CH$_2$-O (2H, t); 1.87-1.24 - -CH$_2$- (30H); 0.98-0.85 - -CH$_3$ (9H, m). *IR (KBr)* v_{max}/cm^{-1}: 2955, 2850, 1740, 1715, 1600, 1500, 1290, 1255, 1180, 1055, 765. *HPLC (90 % acetonitrile, 10 % chloroform):* 99.6 %.

TT (°C): Cr 39 SmC 45 SmA 61 I (Recryst. <25).

Compound 2a

1-Butylpentyl 4-(4'-hexybiphenyl-4-carbonyloxy)-3-fluorobenzoate.

The procedure was as described for the preparation of compound **1** (dev22).

Quantities: 4-Hexyloxybiphenyl-4'-carboxylic acid (0.7 g, 2.88 mmol), 1-butylpentyl 3-fluoro-4-hydroxybenzoate (0.68 g, 2.88 mmol), DCC (0.5 g, 2.88 mmol).

Yield: 0.69 g (44.0 %). *MS:* 562 (M^+, 2 %), 365 (10 %), 323 (78 %), 281 (100 %), 197 (55 %). ^{1}*H-NMR (CDCl$_3$)* δ: 8.23 - Ar-H (2H, d); 7.90 - Ar-H (2H, m); 7.71 - Ar-H (2H, d); 7.60 - AR-H (2H, d); 7.34 - Ar-H (1H, dd); 7.05 - Ar-H (2H, d); 5.20 - -C-H (1H, p); 4.05 - -CH$_2$-O (2H, t); 1.89-1.25 - -CH$_2$- (22H, m); 0.90 - -CH$_3$ (9H, t). *IR (KBr)* v_{max}/cm^{-1}: 2955, 2850, 1745, 1718, 1601, 1500, 1292, 1254, 1184, 1055, 762. *HPLC (90 % acetonitrile, 10 % chloroform):* 99.5 %.

TT (°C): Cr 46 (SmC$_{alt}$ 43) SmA 88.2 I (Recryst. 31)

Compound 2c

1-Butylpentyl 4-(4'-octyloxybiphenyl-4-carbonyloxy)-3-fluorobenzoate.

The procedure was as described for the preparation of compound 1 (dev22).

Quantities: 4-Octyloxybiphenyl-4'-carboxylic acid (0.7 g, 2.14 mmol), 1-butylpentyl 3-fluoro-4-hydroxybenzoate (0.6 g, 2.128 mmol), DCC (0.44 g, 2.128 mmol).

Yield: 0.69 g (54.8 %). *MS:* 590 (M$^+$, 16 %), 308 (100 %), 197 (40 %), 139 (46 %). ^{1}*H-NMR (CDCl$_3$)* δ: 8.25 - Ar-H (2H, d); 7.91 - Ar-H (2H, m); 7.71 - Ar-H (2H, d); 7.60 - Ar-H (2H, d); 7.37 - Ar-H (1H, dd); 7.01 - Ar-H (2H, d); 5.14 - -C-H (1H, p); 4.02 - -CH$_2$-O (2H, t); 1.85-1.25 - -CH$_2$- (24H, m); 0.90 - -CH$_3$ (9H, m). *IR (KBr)* v_{max}/cm^{-1}: 2945, 2850, 1735, 1705, 1600, 1425, 1285, 1250, 1175, 1060, 825, 760. *HPLC (90 % acetonitrile, 10 % chloroform):* 99.8 %.

TT (°C): Cr 56 ("SmY" 28 SmC$_{alt}$ 54) SmA 85 I (Recryst. <25)

Compound 2e

1-Butylpentyl 4-(4'-decyloxybiphenyl-4-carbonyloxy)-3-fluorobenzoate.

The procedure was as described for the preparation of compound 1 (dev22).

Quantities: 4-Decyloxybiphenyl-4'-carboxylic acid (2.1 g, 5.93 mmol), 1-butylpentyl 3-fluoro-4-hydroxybenzoate (1.62 g, 5.72 mmol), DCC (1.18 g, 5.72 mmol).

Yield: 2.2 g (62.2 %). *MS:* 618 (M$^+$, 7 %), 337 (100 %), 197 (16 %), 139 (15 %). ^{1}*H-NMR (CDCl$_3$)* δ: 8.31 - Ar-H (2H, d); 7.98 - Ar-H (2H, m); 7.78 - Ar-H (2H, d); 7.66 - Ar-H (2H, d); 7.43 - Ar-H (1H, dd); 7.07 - Ar-H (2H, d); 5.21 - -C-H (1H, p); 4.08 - -CH$_2$-O (2H, t); 1.95-1.25 - -CH$_2$- (28H, m); 0.95 - -CH$_3$ (9H, m). *IR (KBr)* v_{max}/cm^{-1}: 2950, 2855, 1740, 1710, 1600, 1500, 1290, 1250, 1180, 1055, 825, 760. *HPLC (90 % acetonitrile, 10 % chloroform):* 100 %.

TT (°C): Cr 73 (SmC$_{alt}$ 46.1 SmA 64.6) I (Recryst. <25).

Compound 2f

1-Butylpentyl 4-(4'-dodecyloxybiphenyl-4-carbonyloxy)-3-fluorobenzoate.

The procedure was as described for the preparation of compound 1 (dev22).

Quantities: 4-Dodecyloxybiphenyl-4'-carboxylic acid (2.17 g, 5.67 mmol), 1-

butylpentyl 3-fluoro-4-hydroxybenzoate (1.6 g, 5.67 mmol), DCC (1.17 g, 5.67 mmol).

Yield: 1.00 g (28.1 %). *MS:* 646 (M$^+$, 11 %), 367 (100 %), 197 (76 %), 169 (51 %), 140 (75 %). ^{1}*H-NMR (CDCl$_3$)* δ: 8.25 - Ar-H (2H, d); 7.91 - Ar-H (2H, m); 7.71 - Ar-H (2H, d); 7.60 - Ar-H (2H, d); 7.37 - Ar-H (1H, dd); 7.01 - Ar-H (2H, d); 5.14 - -C-H (1H, p); 4.02 - -CH$_2$-O (2H, d); 1.87-1.24 - -CH$_2$- (30H, m); 0.90 - -CH$_3$ (9H, m). *IR (KBr)* v_{max}/cm^{-1}: 2945, 2860, 1735, 1710, 1600, 1500, 1280, 1250, 1175, 1060, 820, 760. *HPLC (90 % acetonitrile, 10 % chloroform):* 100 %.

TT (°C): Cr 49 (SmC$_{alt}$ 45.7) SmA 58.1 I (Recryst. 40).

Compound 2g

1-Butylpentyl 4-(4'-tetradecyloxybiphenyl-4-carbonyloxy)-3-fluorobenzoate.

The procedure was as described for the preparation of compound 1 (dev22) above.

Quantities: 4-Tetradecyloxybiphenyl-4'-carboxylic acid (0.88 g, 2.13 mmol), 1-butylpentyl 3-fluoro-4-hydroxybenzoate (0.6 g, 2.13 mmol), DCC (0.44 g, 2.13 mmol).

Yield: 0.79 g (56.2 %). *MS:* 674 (M$^+$, 46 %), 651 (4 %), 531 (12 %), 476 (37 %), 406 (100 %). ^{1}*H-NMR (CDCl$_3$)* δ: 8.25 - Ar-H (2H, d); 7.91 - Ar-H (2H, m); 7.71 - Ar-H (2H, d); 7.60 - Ar-H (2H, d); 7.36 - Ar-H (1H, dd); 7.01 - Ar-H (2H, d); 5.14 - -C-H (1H, p); 4.02 - -CH$_2$-O (2H, t); 1.88-1.23 - -CH$_2$- (38H, m); 0.91 - -CH$_3$ (9H, t). *IR (KBr)* v_{max}/cm^{-1}: 2955, 2840, 1740, 1705, 1600, 1285, 1260, 1190, 1065, 830, 760. *HPLC (90 % acetonitrile, 10 % chloroform):* 98.9 %.

TT (°C): Cr 56 (SmC$_{alt}$ 41 SmA 54) I (Recryst. <25).

Compound 2b

1-Butylpentyl 4-(4'-heptyloxybiphenyl-4-carbonyloxy)-3-fluorobenzoate.

The procedure was as described for the preparation of compound 1 (dev22).

Quantities: 4-Heptyloxybiphenyl-4'-carboxylic acid (0.56 g, 1.92 mmol), 1-butylpentyl 3-fluoro-4-hydroxybenzoate (0.4 g, 1.68 mmol), DCC (0.35 g, 1.68 mmol).

Yield: 0.3 g (20.9 %). *MS:* 576 (M⁺, trace), 295 (100 %), 196 (38 %). *¹H-NMR (CDCl₃)* δ: 8.25 - Ar-H (2H, d); 7.91 - Ar-H (2H, m); 7.71 - Ar-H (2H, d); 7.60 - Ar-H (2H, d); 7.37 - Ar-H (1H, dd); 7.01 - Ar-H (2H, d); 5.14 - -C-H (1H, p); 4.02 - -CH₂-O (2H, t); 1.77-1.40 - -CH₂- (22H, m), 0.85 - -CH₃ (9H, m). *IR (KBr)* v_{max}/cm^{-1}: 2955, 2855, 1740, 1708, 1600, 1285, 1260, 1185, 1060, 825, 760. *HPLC (90 % acetonitrile, 10 % chloroform):* 99.3 %.

TT (°C): Cr 52 ("SmY" 36.6) 55 SmA 91.1 (Recryst. 26).

Compound 8b

1-Ethylheptyl 4-(4'-decyloxybiphenyl-4-carbonyloxy)-3-fluorobenzoate.

The procedure was as described for the preparation of compound 1 (dev22) above.

Quantities: 4-Decyloxybiphenyl-4'-carboxylic acid (2.42 g, 6.84 mmol), 1-butylpentyl 3-fluoro-4-hydroxybenzoate (1.89 g, 6.7 mmol), DCC (1.39 g, 6.7 mmol).

Yield: 1.33 g (32.1 %). *MS:* 618 (M⁺, 2 %), 337 (100 %), 196 (14 %), 138 (13 %). *¹H-NMR (CDCl₃)* δ: 8.25 - - Ar-H (2H, d); 7.92 - Ar-H (2H, m); 7.71- Ar-H (2H, d); 7.60 - Ar-H (2H, d); 7.37 - Ar-H (1H, dd); 7.01 - Ar-H (2H, d); 5.09 - -C-H (1H, p); 4.02 - -CH₂-O (2H, t); 1.80-1.40 - -CH₂- (28H, m), 0.85 - -CH₃ (9H, m). *IR (KBr)* v_{max}/cm^{-1}: 2920, 2850, 1740, 1710, 1600, 1280, 1255, 1180, 1055, 825. *HPLC (90 % acetonitrile, 10 % chloroform):* 99.3 %.

TT (°C): Cr 34 SmC_alt 57 SmA 79 I (Recryst. <25).

Compound 2d

1-Butylpentyl 4-(4'-nonyloxybiphenyl-4-carbonyloxy)-3-fluorobenzoate.

The procedure was as described for the preparation of compound 1 (dev22) above.

Quantities: 4-Nonyloxybiphenyl-4'-carboxylic acid (0.6 g, 1.76 mmol), 1-butylpentyl 3-fluoro-4-hydroxybenzoate (0.4 g, 1.68 mmol), DCC (0.35 g, 1.68 mmol).

Yield: 0.53 g (52.1 %). *MS:* 604 (M⁺, 13 %), 323 (100 %), 197 (67 %), 168 (53 %). *¹H-NMR (CDCl₃)* δ: 8.25 – Ar-H (2H, d), 7.91 – Ar-H (2H, m), 7.72 – Ar-H (2H, d), 7.60 – Ar-H (2H, d), 7.37 – Ar-H (1H, dd), 7.01 – Ar-H (2H, d), 5.14 - -C-H (1H, p), 4.02 - -CH₂-O (2H, t), 1.85-1.30 - -CH₂- (26H, m), 0.90 - -CH₃ (9H, m). *IR (KBr)*

v_{max}/cm^{-1}: 2920, 2850, 1740, 1715, 1600, 1280, 1255, 1170, 1055, 825, 765. **HPLC** *(90 % acetonitrile, 10 % chloroform):* 100 %.

TT *(°C):* Cr 77 (SmC$_{alt}$ 46.6 SmA 70.3) I (Recryst. 24).

Compound 3d

1-Pentylhexyl 4-(4'-octyloxybiphenyl-4-carbonyloxy)-3-fluorobenzoate.

The procedure was as described for the preparation of compound **1** (dev22) above.

Quantities: 4-Octyloxybiphenyl-4'-carboxylic acid (0.54 g, 16.56 mmol), 1-pentylhexyl 3-fluoro-4-hydroxybenzoate (0.5 g, 16.13 mmol), DCC (0.34 g, 16.14 mmol).

Yield: 0.26 (26.1 %). **MS:** 618 (M$^+$, 2 %), 323 (100 %), 196 (10 %). ^{1}**H-NMR** *(CDCl$_3$)* δ: 8.25 – Ar-H (2H, d), 7.91 – Ar-H (2H, m), 7.71 – Ar-H (2H, d), 7.60 – Ar-H (2H, d), 7.37 – Ar-H (1H, dd), 7.01 – Ar-H (2H, d), 5.10 - -C-H (1H, p), 4.02 - -CH$_2$-O (2H, t), 1.80-1.35 - -CH$_2$- (28H, m), 0.85 - -CH$_3$ (9H, m). **IR** *(KBr)* v_{max}/cm^{-1}: 2930, 2845, 1740, 1710, 1600, 1275, 1250, 1175, 1060, 820, 760. **HPLC** *(90 % acetonitrile, 10 % chloroform):* 99.8 %.

TT *(°C):* Cr 42 (SmC$_{alt}$ 38.8) SmA 71.5 I (Recryst. <25).

Compound 3c

1-Propylbutyl 4-(4'-octyloxybiphenyl-4-carbonyloxy)-3-fluorobenzoate.

The procedure was as described for the preparation of compound **1** (dev22) above.

Quantities: 4-Octyloxybiphenyl-4'-carboxylic acid (0.46 g, 14.11 mmol), 1-propylbutyl 3-fluoro-4-hydroxybenzoate (0.35 g, 13.78 mmol), DCC (0.28 g, 13.78 mmol).

Yield: 0.08 g (10.3 %). **MS:** 562 (M$^+$, trace), 309 (100 %), 197 (9 %). ^{1}**H-NMR** *(CDCl$_3$)* δ: 8.25 – Ar-H (2H, d), 7.90 – Ar-H (2H, m), 7.71 – Ar-H (2H, d), 7.60 – Ar-H (2H, d), 7.36 – Ar-H (1H, dd), 7.01 – Ar-H (2H, d), 5.18 - -C-H (1H, p), 4.02 - -CH$_2$-O (2H, t), 1.85-1.40 - -CH$_2$- (20H, m), 0.85 - -CH$_3$ (9H, m). **IR** *(KBr)* v_{max}/cm^{-1}: 2960, 2860, 1735, 1710, 1600, 1285, 1250, 1175, 1060, 825, 760. **HPLC** *(90 % acetonitrile, 10 % chloroform):* 99.3 %.

TT (°C): Cr 86 (SmC$_{alt}$ 67.4) SmA 96.7 I (Recryst. 39).

Compound 8a

1-Methylheptyl 4-(4'-decyloxybiphenyl-4-carbonyloxy)-3-fluorobenzoate.

The procedure was as described for the preparation of compound **1** (dev22) above.

Quantities: 4-decyloxybiphenyl-4'-carboxylic acid (1.06 g, 3.0 mmol), 1-methylheptyl 3-fluoro-4-hydroxybenzoate (0.78 g, 2.91 mmol), DCC (0.62 g, 2.91 mmol).

Yield: 0.89 g (50.7 %). *MS:* 604 (M$^+$, 1 %), 337 (100 %), 197 (10 %). ^{1}*H-NMR (CDCl$_3$)* δ: 8.22 – Ar-H (2H, d), 7.89 – Ar-H (2H, m), 7.70 – Ar-H (2H, d), 7.59 – Ar-H (2H, d), 7.35 – Ar-H (1H, dd), 5.15 - -C-H (1H, sx), 4.01 - -CH$_2$-O (2H, t), 1.80-1.35 - -CH$_2$-/-CH$_3$ (29H, m), 0.88 - -CH$_3$ (6H, t). *IR (KBr)* v$_{max}$/cm^{-1}: 2920, 2850, 1745, 1715, 1600, 1295, 1260, 1180, 1065, 825, 760. *HPLC (90 % acetonitrile, 10 % chloroform):* 99.3 %.

TT (°C): Cr 38 SmC$_{alt}$ 79.5 SmC 83 SmA 111 I (Recryst. <25).

Compound 7h

1-Ethylheptyl 4-(4'-octyloxybiphenyl-4-carbonyloxy)-3-fluorobenzoate.

The procedure was as described for the preparation of compound **1** (dev22) above.

Quantities: 4-octyloxybiphenyl-4'-carboxylic acid (1.1 g, 2.71 mmol), 1-ethylheptyl 3-fluoro-4-hydroxybenzoate (0.7g, 2.47 mmol), DCC (0.51 g, 2.47 mmol).

Yield: 0.93 g (51.3 %). *MS:* 590 (M$^+$, trace), 309 (100 %), 196 (11 %). ^{1}*H-NMR (CDCl$_3$)* δ: 8.25 – Ar-H (2H, d), 7.92 – Ar-H (2H, m), 7.71 – Ar-H (2H, d), 7.60 – Ar-H (2H, d), 7.37 – Ar-H (2H, d), 5.09 - -C-H (1H, p), 4.02 - -CH$_2$-O (2H, t), 1.8-1.35 (24H, m), 0.93 - -CH$_3$ (9H, m). *IR (KBr)* v$_{max}$/cm^{-1}: 2920, 2850, 1740, 1710, 1600, 1290, 1255, 1180, 1055, 825, 765. *HPLC (90 % acetonitrile, 10 % chloroform):* 99.8 %. *TT (°C):* Cr 37 ("SmX$_2$" 20) SmC$_{alt}$ 56.5 SmA 94 I (Recryst. <25).

Compound 3b

1-Ethylpropyl 4-(4'-octyloxybiphenyl-4-carbonyloxy)-3-fluorobenzoate.

The procedure was as described for the preparation of compound **1** (dev22) above, the quantities of reagents used were as follows;

Quantities: 4-octyloxybiphenyl-4'-carboxylic acid (1.08 g, 3.32 mmol), 1-ethylpropyl 3-fluoro-4-hydroxybenzoate (0.75 g, 3.32 mmol), DCC (0.68 g, 3.32 mmol).

Yield: 1.61 (91 %). *MS:* 534 (M$^+$, 4 %), 309 (100 %), 197 (10 %), 168 (5 %). *^{1}H-NMR (CDCl$_3$)* δ: 8.26 – Ar-H (2H, d), 7.93 – Ar-H (2H, m), 7.71 – Ar-H (2H, d), 7.61 – Ar-H (2H, d), 7.38 – Ar-H (1H, dd), 7.01 – Ar-H (2H, d), 5.03 - -C-H (1H, p), 4.04 - -CH$_2$-O (2H, t), 1.80-1.35 - -CH$_2$- (16H, m), 0.96 - -CH$_3$ (9H, m). *HPLC (90 % acetonitrile, 10 % chloroform):* 100 %.

TT (°C): Cr 77 (SmC$_{alt}$ 74.2) SmA 119.6 I (Recryst. 43).

Compound 4c

1-Pentylhexyl 4-(4'-dodecyloxybiphenyl-4-carbonyloxy)-3-fluorobenzoate.

The procedure was as described for the preparation of compound **1** (dev22) above, the quantities of reagents used were as follows;

Quantities: 4-Decyloxybiphenyl-4'-carboxylic acid (0.4 g, 1.05 mmol), 1-pentylhexyl-3 fluoro-4-hydroxybenzoate (0.28 g, 0.92 mmol), DCC (0.19 g, 0.92 mmol).

Yield: 0.4 g (59.9 %). *MS:* 674 (M$^+$, 3 %), 365 (100 %), 197 (9 %). *^{1}H-NMR (CDCl$_3$)* δ: 8.25 – Ar-H (2H, d), 7.91 – Ar-H (2H, m), 7.71 – Ar-H (2H, d), 7.60 – Ar-H (2H, d), 7.37 (1H, dd), 7.01 – Ar-H (2H, d), 5.14 - -C-H (1H, p), 4.02 - -CH$_2$- (2H, t), 1.80-1.35 - -CH$_2$- (36H, m), 0.89 - -CH$_3$ (9H). *IR (KBr) v_{max}/cm^{-1}:* 2915, 2845, 1735, 1710, 1595, 1285, 1255, 1055, 825, 760. *HPLC (90 % acetonitrile, 10 % chloroform):* 100 %. *TT (°C):* Cr 49 (SmC$_{alt}$ 45.7) SmA 58.1 (Recryst. 40).

Compound 7e

1-Methylheptyl 4-(4'-octyloxybiphenyl-4-carbonyloxy)-3-fluorobenzoate.

The procedure was the same as for the preparation of compound **1** (dev22) above, the quantities of reagents used were as follows;

Quantities: 4-Octyloxybiphenyl-4'-carboxylic acid (0.9 g, 2.76 mmol), 1-methylheptyl 3-fluoro-4-hydroxybenzoate (0.62 g, 2.31 mmol), DCC (0.48 g, 2.31 mmol).

Yield: 0.3g (22.6 %). *MS:* 574 (M^+, trace), 309 (100 %), 196 (10 %). ^{1}*H-NMR (CDCl$_3$)* δ: 8.24 – Ar-H (2H, d), 7.91 – Ar-H (2H, m), 7.71 – Ar-H (2H, d), 7.60 – Ar-H (2H, d), 7.37 – Ar-H (1H, dd), 7.01 – Ar-H (2H, d), 5.17 - -C-H (1H, sx), 4.02 - -CH$_2$- (2H, t), 1.77-1.29 - -CH$_2$-/-CH$_3$ (25H, m), 0.88 - -CH$_3$ (6H, m). *IR (KBr)* v_{max}/cm^{-1}: 2935, 2840, 1740, 1715, 1595, 1290, 1260, 1175, 1060, 830, 765. *HPLC (90 % acetonitrile, 10 % chloroform):* 99.9 %.

TT (°C): Cr 48 ("SmX$_2$" 38) SmC$_{alt}$ 49 SmA 117 I (Recryst. 27).

Compound 9a

4-(1-Butylpentyloxycarbonyl)phenyl 4'-octyloxybiphenyl-4-carboxylate.

Triphenylphosphine (0.7 g, 2.65 mmol) was slowly added to a stirred mixture of 4-ocyloxybiphenyl-4'-carboxylic acid (1.0 g, 3.07 mmol), 1-butylpentyl 4-hydroxybenzoate (0.7 g, 2.65 mmol) and DEAD (0.46 g, 2.65 mmol) in 70 ml THF. The reaction mixture was stirred at room temperature for 72 hours then the solvent was removed *in vacuo*. The crude product was purified by column chromatography (50 %/50 % DCM/Petrol 40-60 °C) to yield a white crystalline solid.

Yield: 0.6 g (39.6 %). *MS:* 572 (M^+, 4 %), 309 (100 %) 196 (12 %). ^{1}*H-NMR (CDCl$_3$)* δ: 8.24 – Ar-H (2H, d), 8.14 – Ar-H (2H, d), 7.70 – Ar-H (2H, d), 7.60 – Ar-H (2H, d), 7.32 – Ar-H (2H, d), 7.01 – Ar-H (2H, d), 5.14 - -C-H (1H, p), 4.03 - -CH$_2$-O (2H, t), 1.82-1.34 - -CH$_2$-/-CH$_3$ (27H, m), 0.90 - -CH$_3$ (6H, m). *IR (KBr)* v_{max}/cm^{-1}: 2960, 2935, 2860, 1735, 1715, 1615, 1470, 1275, 1195, 1180, 1070, 830, 770. *HPLC (90 % acetonitrile, 10 % chloroform):* 100%.

TT (°C): Cr 53 ("SmY" 47.5) SmC$_{alt}$ 91.5 SmA 107.9 I (Recryst. <25).

Compound 9b

4-(1-Butylheptyloxycarbonyl)phenyl 4'-octyloxybiphenyl-4-carboxylate.

The procedure was the same as for the preparation of compound **25** (dev98) above, the quantities of reagents used were as follows;

Quantities: 4-ocyloxybiphenyl-4'-carboxylic acid (0.95 g, 2.91 mmol), 1-butylheptyl 4-hydroxybenzoate (0.7 g, 2.4 mmol) and DEAD (0.42 g, 2.4 mmol), Triphenylphosphine (0.63 g, 2.4 mmol).

Yield: 0.52 g (36.9 %). *MS:* 600 (M^+, 2 %), 309 (100 %), 196 (15 %). ^{1}*H-NMR (CDCl$_3$)* δ: 8.25 – Ar-H (2H, d), 8.14 – Ar-H (2H, d), 7.71 – Ar-H (2H, d), 7.61 – Ar-H (2H, d), 7.31 – Ar-H (2H, d), 7.01 – Ar-H (2H, d), 5.14 - -C-H (1H, p), 4.02 - -CH$_2$-O (2H, t), 1.84-1.33 - -CH$_2$-/-CH$_3$ (23H, m), 0.89 – CH$_3$ (6H, m). *IR (KBr)* v_{max}/cm^{-1}: 2950, 2855, 1740, 1710, 1610, 1475, 1270, 1190, 1185, 1065, 825, 765. *HPLC (90 % acetonitrile, 10 % chloroform):* 99.8 %.

TT (°C): Cr 44 ("SmY" 35.4) SmC$_{alt}$ 75.4 93.1 I (Recryst. <25).

Compound 5b

4-(1-Butylpentyloxycarbonyl)-phenyl 4'-nonyl-(2,5-dioxanylphenyl)-4-carboxylate.

The procedure was the same as for the preparation of compound **25** (dev98) above, the quantities of reagents used were as follows;

Quantities: 4-nonyl phenyl-2,5-dioxanyl-4'-carboxylic acid (1.05 g, 3.14 mmol), 1-butylpentyl 4-hydroxybenzoate (0.8 g, 3.03 mmol) and DEAD (0.53 g, 3.03 mmol), triphenylphosphine (0.69g, 3.03 mmol).

Yield: 0.09g (5.0 %). *MS:* 580 (M^+, trace), 317 (100 %), 104 (20 %). ^{1}*H-NMR (CDCl$_3$)* δ: 8.20 – Ar-H (2H, d), 8.12 – Ar-H (2H, d), 7.64 – Ar-H (2H, d), 7.24 – Ar-H (2H, d), 5.48 - -O-C-H (1H, s), 5.14 - -C-H (1H, p), 4.27 - -CH$_2$- (2H, dd), 3.56 - -CH$_2$- (2H, t), 2.15 - -C-H (1H, p), 1.67-1.13 - -CH$_2$- (28H, m), 0.88 - -CH$_3$ (9H, m). *IR (KBr)* v_{max}/cm^{-1}: 2915, 2850, 1745, 1705, 1600, 1510, 1255, 1195, 1055, 1010, 755. *HPLC (90 % acetonitrile, 10 % chloroform):* 99.5 %.

TT (°C): Cr 83 (SmA 71.1) I (Recryst. 70).

Compound 3a

4-(1-Methylethyloxycarbonyl)phenyl 4'-octyloxybiphenyl-4-carboxylate.

The procedure was the same as for the preparation of compound **25** (dev98) above, the quantities of reagents used were as follows;

Quantities: 4-octyloxybiphenyl-4'-carboxylic acid (0.9 g, 2.76 mmol), 1-methylethyl 4-hydroxybenzoate (0.51 g, 2.58 mmol) and DEAD (0.45 g, 2.58 mmol), Triphenylphosphine (0.68 g, 2.58 mmol).

Yield: 0.81 g (62 %). *MS:* 506 (M^+, 3 %), 309 (100 %), 197 (20 %), 168 (10 %). ^1H-*NMR (CDCl$_3$)* δ: 8.25 – Ar-H (2H, d), 7.88 – Ar-H (2H, m), 7.70 – Ar-H (2H, d), 7.37 – Ar-H (1H, dd), 7.01 – Ar-H (2H, d), 5.27 - -C-H (1H, sp), 4.01 - -CH$_2$-O (2H, t), 1.85-1.30 - -CH$_2$-/-CH$_3$ (15H, m), 0.90 - -CH$_3$ (6H, t). *IR (KBr)* v_{max}/cm^{-1}: 2925, 2845, 1750, 1710, 1600, 1505, 1415, 1255, 1170, 1110, 1060, 825, 760. *HPLC (90 % acetonitrile, 10 % chloroform):* 100 %.

TT (°C): Cr 83 (SmC 81.3) SmA 157.2 (Recryst. 75).

Compound 6b

1-Propylhexyl 4-(4'-octyloxybiphenyl-4-carbonyloxy)-3-fluorobenzoate.

The procedure was the same as for the preparation of compound **25** (dev98) above, the quantities of reagents used were as follows;

Quantities: 4-octyloxybiphenyl-4'-carboxylic acid (1.25 g, 3.83 mmol), 1-propylhexyl 3-fluoro-4-hydroxybenzoate (1.0 g, 3.55 mmol) and DEAD (0.62 g, 3.55 mmol), Triphenylphosphine (0.93 g, 3.55 mmol).

Yield: 1.05 g (50.1 %). *MS:* 590 (M^+, 4%), 309 (100 %), 197 (16 %), 168 (12 %). ^1H-*NMR (CDCl$_3$)* δ: 8.26 - Ar-H (2H, d); 7.90 - Ar-H (2H, m); 7.70 - Ar-H (2H, d); 7.61 - Ar-H (2H, d); 7.36 - Ar-H (1H, dd); 7.00 - Ar-H (2H, d); 5.15 - -C-H (1H, p); 4.01 - -CH$_2$-O (2H, t); 1.86-1.24 - -CH$_2$- (24H, m); 0.89 - -CH$_3$ (9H, m). *IR (KBr)* v_{max}/cm^{-1}: 2940, 2845, 1740, 1710, 1595, 1420, 1280, 1255, 1170, 1055, 830, 755. *HPLC (90 % acetonitrile, 10 % chloroform):* 100 %.

TT (°C): Cr 46 ("SmY" 28) SmC$_{alt}$ 54.6 SmA 82.4 I (Recryst. 28).

Compound 5a

1-Butylpentyl 4-(4'-octyloxyphenyl-4-benzoyl)-3-fluorobenzoate.

The procedure was the same as for the preparation of compound **25** (dev98) above, the quantities of reagents used were as follows;

Quantities: 4-octyloxybenzoyloxy-4'-benzoic acid (0.85 g, 2.3 mmol), 1-butylheptyl 3-fluoro-4-hydroxybenzoate (0.61 g, 2.16 mmol) and DEAD (0.38 g, 2.16 mmol), triphenylphosphine (0.57 g, 2.16 mmol).

Yield: 0.59 g (43.1 %). *MS:* 634 (M^+, 3 %), 353 (7 %), 120 (100 %). *^{1}H-NMR (CDCl$_3$) δ:* 8.29 – Ar-H (2H, d), 8.15 – Ar-H (2H, d), 7.91 – Ar-H (2H, m), 7.37 – Ar-H (3H, m), 6.99 – Ar-H (2H, d), 5.14 - -C-H (1H, p), 4.06 - -CH$_2$-O (2H, t), 1.83-1.34 - -CH$_2$- (m, 24H), 0.90 - -CH$_3$ (9H, m).*IR (KBr) v_{max}/cm^{-1}:* 2930, 2850, 1750, 1730, 1600, 1510, 1290, 1255, 1160, 1045, 755. *HPLC (90 % acetonitrile, 10 % chloroform):* 100 %.

TT (°C): Cr 71 (SmC$_{alt}$ 47.7) SmA 86.7 I (Recryst. 44).

Compound 6a

1-Propylhexyl 4-(4'-heptyloxybiphenyl-4-carbonyloxy)-3-fluorobenzoate.

The procedure was the same as for the preparation of compound **25** (dev98) above, the quantities of reagents used were as follows;

Quantities: 4-heptyloxybiphenyl-4'-carboxylic acid (1.2 g, 3.85 mmol), 1-propylhexyl-3 fluoro-4-hydroxybenzoate (0.90 g, 3.2 mmol) and DEAD (0.56 g, 3.2 mmol), triphenylphosphine (0.84 g, 3.2 mmol).

Yield: 0.54 g (29.3 %). *MS:* 576 (M^+, 7 %), 295 (100 %), 196 (14 %). *^{1}H-NMR (CDCl$_3$) δ:* 8.24 – Ar-H (2H, d), 7.90 – Ar-H (2H, m), 7.70 – Ar-H (2H, d), 7.61 – Ar-H (2H, d), 7.37 – Ar-H (1H, dd), 7.01 – Ar-H (2H, d), 5.14 - -C-H (1H, p), 4.02 - -CH$_2$-O (2H, t), 1.86-1.24 - -CH$_2$- (22H, m), 0.89 - -CH$_3$ (9H, m). *IR (KBr) v_{max}/cm^{-1}:* 2950, 2850, 1740, 1710, 1600, 1425, 1285, 145, 1170, 1055, 820, 755. *HPLC (90 % acetonitrile, 10 % chloroform):* 99.9 %.

TT (°C): Cr 40 ("SmX" 32) SmC 44.6 SmA 88.2 I (Recryst. 27).

Compound 5d

1-Butylpentyl 4-(4'-octyloxy-3-fluorobiphenyl-4-carbonyloxy)-3-fluorobenzoate.

The procedure was the same as for the preparation of compound **25** (dev98) above, the quantities of reagents used were as follows;

Quantities: 4-octyloxy-3'-fluorobiphenyl-4'-carboxylic acid (0.31 g, 0.9 mmol), 1-

butylpentyl-4 hydroxybenzoate (0.2 g, 0.77 mmol) and DEAD (0.13 g, 0.77 mmol), triphenylphosphine (0.2 g, 0.77 mmol).

Yield: 0.21 g (44.3 %). *MS:* 608 (M$^+$, 2 %), 328 (100 %), 215 (17 %), 198 (1 %). ^{1}*H-NMR (CDCl$_3$)* δ: 8.13 – Ar-H (3H, m), 7.58 – Ar-H (2H, d), 7.47 – Ar-H (1H, dd), 7.40 – Ar-H (1H, dd), 7.33 – Ar-H (2H, d), 7.01 – Ar-H (2H, d), 5.14 – Ar-H (1H, p), 4.02 – -CH$_2$-O (2H, t), 1.82-1.35 - -CH$_2$- (24H, m), 0.90 - -CH$_3$ (9H, m). *IR (KBr)* v_{max}/cm^{-1}: 2930, 2860, 1720, 1605, 1505, 1275, 1205, 1160, 1110, 825, 765. *HPLC (90 % acetonitrile, 10 % chloroform):* 95.6 %.

TT (°C): Cr 31 SmC$_{alt}$ 68.4 SmA 87.9 I (Recryst. <25).

Compound 4a

1-Methylethyl 4-(4'-dodecyloxybiphenyl-4-carbonyloxy)-3-fluorobenzoate.

The procedure was the same as for the preparation of compound **25** (dev98) above, the quantities of reagents used were as follows;

Quantities: 4-dodecyloxy biphenyl-4'-carboxylic acid (2.0 g, 5.24 mmol), 1-methyethyl 3-fluoro-4-hydroxybenzoate (1.0 g, 5.05 mmol) and DEAD (0.88 g, 5.05 mmol), triphenylphosphine (1.32 g, 5.05 mmol).

Yield: 0.87 g (30.7 %). *MS:* 562 (M$^+$, 3 %), 365 (100 %), 196 (14 %). ^{1}*H-NMR (CDCl$_3$)* δ: 8.24 – Ar-H (2H, d), 7.89 – Ar-H (m, 2H), 7.70 – Ar-H (2H, d), 7.59 – Ar-H (2H, d), 7.36 – Ar-H (1H, dd), 7.00 – Ar-H (2H, d), 5.27 - -C-H (1H, sp), 4.01 - -CH$_2$-O (2H, t), 1.81 - -CH$_2$- (2H, p), 1.55-1.27 - -CH$_2$-/-CH$_3$ (m, 21H), 0.88 - -CH$_3$ (6H, t). *IR (KBr)* v_{max}/cm^{-1}: 2920, 2840, 1745, 1715, 1600, 1500, 1420, 1250, 1175, 1105, 1055, 830, 755. *HPLC (90 % acetonitrile, 10 % chloroform):* 99.9 %.

TT (°C): Cr 69 SmC 89.7 SmA 146.2 I (Recryst. 45).

Compound 5c

4-(1-Butylylpentyloxycarbonyl)phenyl 4'-octyloxy-3'-bromobiphenyl-4-carboxylate.

The procedure was the same as for the preparation of compound **25** (dev98) above, the quantities of reagents used were as follows;

Quantities: 4-octyloxy-3-bromobiphenphenyl-4'-carboxylic acid (0.44 g, 1.17 mmol), 1-butylpentyl 4-hydroxybenzoate (0.3 g, 1.13 mmol) and DEAD (0.2 g, 1.13 mmol), triphenylphosphine (0.3 g, 1.13 mmol).

Yield: 0.26 g (38.1 %). *MS:* 650/652 (M$^+$, 2 %/2 %), 387/389 (100/100 %), 274/276 (12 %/13 %). *H-NMR (CDCl$_3$)* δ: 8.24 – Ar-H (2H, d), 8.14 – Ar-H (2H, d), 7.86 – Ar-H (1H, d), 7.67 – Ar-H (2H, d), 7.55 – Ar-H (1H, dd), 7.37 – Ar-H (d, 2H), 6.98 – Ar-H (1H, d), 5.14 - -C-H (1H, p), 4.08 - -CH$_2$-O (2H, t), 1.87 - -CH$_2$- (2H, p), 1.67-1.32 - -CH$_2$- (22H, m), 0.89 - -CH$_3$ (9H, t). *IR (KBr)* v_{max}/cm^{-1}: 2920, 2850, 1735, 1705, 1595, 1495, 1460, 1265, 1190, 1060, 755, 685. *HPLC (90 % acetonitrile, 10 % chloroform):* 98.9 %.

TT (°C): Cr 49 (SmA 40) I (Recryst. <25).

Compound 7b

1-Methylbutyl 4-(4'-octyloxybiphenyl-4-carbonyloxy)-3-fluorobenzoate.

The procedure was the same as for the preparation of compound **25** (dev98) above, the quantities of reagents used were as follows;

Quantities: 4-octyloxybiphenyl-4'-carboxylic acid (1.15 g, 3.53 mmol), 1-methylbutyl 3-fluoro-4-hydroxybenzoate (0.6 g, 3.3 mmol) and DEAD (0.51 g, 3.3 mmol), triphenylphosphine (0.77 g, 3.3 mmol).

Yield: 0.26 g (14 %). *MS:* 534 (M$^+$, 3 %), 309 (100 %), 196 (20 %). *H-NMR (CDCl$_3$)* δ: 8.24 – Ar-H (2H, d), 7.90 – Ar-H (2H, m), 7.71 – Ar-H (2H, d), 7.59 – Ar-H (2H, d), 7.37 – Ar-H (1H, dd), 7.01 – Ar-H (2H, d), 5.17 - -C-H (1H, sx), 4.02 - -CH$_2$- (2H, t), 1.82 - -CH$_2$- (2H, p), 1.60 - -CH$_2$-/-CH$_3$ (14H, m), 0.96 – -CH$_3$ (3H, t), 0.90 - -CH$_3$ (3H, t). *IR (KBr)* v_{max}/cm^{-1}: 2930, 2855, 1745, 1715, 1605, 1510, 1430, 1290, 1265, 1190, 1120, 1060, 825, 765. *HPLC (90 % acetonitrile, 10 % chloroform):* 100 %.

TT (°C): Cr 60 ("SmX$_2$" 58.3) SmC$_{alt}$ 78.8 SmA 132.6 I (Recryst. 47).

Compound 7d

1-Methylhexyl 4-(4'-octyloxybiphenyl-4-carbonyloxy)-3-fluorobenzoate.

The procedure was as described for the preparation of compound **25** (dev98) above,

the quantities of reagents used were as follows;

Quantities: 4-octyloxybiphenyl-4'-carboxylic acid (1.2 g, 3.68 mmol), 1-methylhexyl 3-fluoro-4-hydroxybenzoate (0.85 g, 3.35 mmol) and DEAD (0.58 g, 3.35 mmol), triphenylphosphine (0.88 g, 3.35 mmol).

Yield: 0.19 g (10.1 %). *MS:* 562 (M^+, 2 %), 311 (100 %), 197 (60 %), 139 (20 %). ^{1}H-NMR *(CDCl$_3$)* δ: 8.25 – Ar-H (2H, d), 7.90 – Ar-H (2H, m), 7.70 – Ar-H (2H, d), 7.59 – Ar-H (2H, d), 7.36 – Ar-H (1H, m), 7.00 – Ar-H (2H, d), 5.15 - -C-H (1H, sx), 4.02 - -CH$_2$-O (2H, t), 1.80-1.30 - -CH$_2$- (20H, m), 0.80 - -CH$_3$ (9H, m). *IR (KBr)* v_{max}/cm^{-1}: 2925, 2850, 1740, 1710, 1600, 1505, 1425, 1285, 1260, 1185, 1115, 1055, 760.

HPLC (90 % acetonitrile, 10 % chloroform): 99.9 %.

TT (°C): Cr 51 ("SmX$_3$" 34.8) SmC 63.1 SmA 123.2 I (Recryst. 33.7).

Compound 7c

1-Methylpentyl 4-(4'-octyloxybiphenyl-4-carbonyloxy)-3-fluorobenzoate

The procedure was as described for the preparation of compound **25** (dev98) above, the quantities of reagents used were as follows;

Quantities: 4-octyloxybiphenyl-4'-carboxylic acid (1.25 g, 3.83 mmol), 1-methylpentyl 3-fluoro-4-hydroxybenzoate (0.69 g, 3.52 mmol) and DEAD (0.61 g, 3.52 mmol), triphenylphosphine (0.92 g, 3.52 mmol).

Yield: 0.3 g (15.5 %). *MS:* 548 (M^+, trace), 311 (100 %), 197 (40 %), 169 (24 %). ^{1}H-NMR *(CDCl$_3$)* δ: 8.24 – Ar-H (2H, d), 7.91 – Ar-H (2H, m), 7.71 – Ar-H (2H, d), 7.60 – Ar-H (2H, d), 7.37 – Ar-H (1H, dd), 7.01 – Ar-H (2H, d), 5.17 – -C-H (1H, sx), 4.03 – -CH$_2$-O (2H, t), 1.82-1.30 – -CH$_2$-/-CH$_3$ (21H, m), 0.91 – -CH$_3$ (6H, m). *IR (KBr)* v_{max}/cm^{-1}: 2930, 2855, 1745, 1715, 1600, 1510, 1430, 1290, 1190, 1115, 1060, 830, 765. *HPLC (90 % acetonitrile, 10 % chloroform):* 99.9 %.

TT (°C): Cr 52 ("SmX$_2$" 36) SmC$_{alt}$ 64.5 SmA 127.9 I (Recryst. 28).

Compound 7a

1-Methylpropyl 4-(4'-octyloxybiphenyl-4-carbonyloxy)-3-fluorobenzoate.

The procedure was as described for the preparation of compound **25** (dev98) above, the quantities of reagents used were as follows;

Quantities: 4-octyloxybiphenyl-4'-carboxylic acid (1.45 g, 4.45 mmol), 1-methylpropyl 3-fluoro-4-hydroxybenzoate (0.87 g, 4.1 mmol) and DEAD (0.71 g, 4.1 mmol), triphenylphosphine (1.08 g, 4.1 mmol).

Yield: 0.32 g (15 %). *MS:* 520 (M$^+$, 3%), 311 (100 %), 197 (70 %), 169 (55 %), 140 (68 %). ^{1}*H-NMR (CDCl$_3$)* δ: 8.25 – Ar-H (2H, d), 7.91 – Ar-H (2H, m), 7.70 – Ar-H (2H, d), 7.60 – Ar-H (2H, d), 7.36 – Ar-H (1H, dd), 7.00 – Ar-H (2H, d), 5.16 - -C-H (1H, sx), 4.02 - -CH$_2$- (2H, t), 1.82 - -CH$_2$- (2H, p), 1.60 - -CH$_2$-/-CH$_3$ (12H, m), 0.95 – -CH$_3$ (3H, t), 0.90 - -CH$_3$ (3H, t). *IR (KBr)* v_{max}/cm^{-1}: 2940, 2850, 1740, 1710, 1600, 1505, 1435, 1285, 1260, 1185, 1115, 1055, 830, 760. *HPLC (90 % acetonitrile, 10 % chloroform):* 99.9 %.

TT (°C): Cr 72 (SmC 68.3) SmA 144 I (Recryst. 47).

Compound 10c

(S)-1-Methylheptyl 4-(4'-decyloxybiphenyl-4-carbonyloxy)-3-fluorobenzoate.

The procedure was as described for the preparation of compound **25** (dev98) above, the quantities of reagents used were as follows;

Quantities: 4-decyloxybiphenyl-4'-carboxylic acid (1.1 g, 3.1 mmol), (S)-1-methylheptyl 3-fluoro-4-hydroxybenzoate (0.8 g, 2.96 mmol) and DEAD (0.51 g, 2.96 mmol), triphenylphosphine (0.78 g, 2.96 mmol).

Yield: 0.93g (51.9 %). *MS:* 604 (M$^+$, 1 %), 337 (100 %), 197 (32 %), 168 (9 %), 139 (10 %). ^{1}*H-NMR (CDCl$_3$)* δ: 8.25 – Ar-H (2H, d), 7.89 – Ar-H (2H, t), 7.71 – Ar-H (2H, d), 7.70 – Ar-H (2H, d), 7.37 – Ar-H (t), 7.00 – Ar-H (2H, d), 5.16 - -C-H (1H, sx), 4.01 - -CH$_2$-O (2H, t), 1.82-1.29 - -CH$_2$-/-CH$_3$ (29H, m), 0.89 - -CH$_3$ (6H, t). *IR (KBr)* v_{max}/cm^{-1}: 2915, 2760, 1750, 1725, 1605, 1510, 1300, 1255, 1190, 1115, 1045, 830, 715. *HPLC (90 % acetonitrile, 10 % chloroform):* 100 %.

TT (°C): Cr 45 SmC$_A$* 78.8 SmC$_\gamma$* 80.3 SmC* 82.3 SmA* 109.2 I (Recryst. 24).

Compound 10a

(S)-1-Methylheptyl 4-(4'-octyloxybiphenyl-4-carbonyloxy)-3-fluorobenzoate

The procedure was as described for the preparation of compound **25** (dev98) above, the quantities of reagents used were as follows;

Quantities: 4-octyloxybiphenyl-4'-carboxylic acid (1.42 g, 4.36 mmol), (S)-1-methylheptyl 3-fluoro-4-hydroxybenzoate (1.0 g, 3.55 mmol) and DEAD (0.62 g, 3.55 mmol), triphenylphosphine (0.93 g, 3.55 mmol).

Yield: 0.92 g (42.9 %). *MS:* 604 (M^+, 2 %), 337 (100 %), 197 (32 %), 168 (9 %), 139 (10 %). ^{1}*H-NMR (CDCl$_3$)* δ: 8.24 – Ar-H (2H, d), 7.89 – Ar-H (2H, dd), 7.71 – Ar-H (2H, d), 7.59 – Ar-H (2H, d), 7.37 – Ar-H (1H, dd), 7.01 – Ar-H (2H, d), 5.17 – -C-H (1H, sx), 4.02 – -CH$_2$-O (2H, t), 1.82-1.30 - -CH$_2$-/-CH$_3$ (25H), 0.88 - -CH$_3$ (m, 6H).
IR (KBr) v_{max}/cm^{-1}: 2920, 2850, 1745, 1710, 1595, 1415, 1285, 1185, 1055, 825, 760.
HPLC (90 % acetonitrile, 10 % chloroform): 99.8 %.
TT (°C): Cr 55 (SmC$_A$* 47.5) SmA* 118.4 I (Recryst. 39).

Compound 10b

(S)-1-Methylheptyl 4-(4'-nonyloxybiphenyl-4-carbonyloxy)-3-fluorobenzoate.

The procedure was as described for the preparation of compound **25** (dev98) above, the quantities of reagents used were as follows;

Quantities: 4-nonyloxybiphenyl-4'-carboxylic acid (2.4 g, 6.7 mmol), (S)-1-methylheptyl 3-fluoro-4-hydroxybenzoate (1.58 g, 5.88 mmol) and DEAD (1.02 g, 5.88 mmol), triphenylphosphine (1.54 g, 5.88 mmol).

Yield: 0.97 g (26.5 %). *MS:* 590 (M^+, 2 %), 323 (100 %), 197 (15 %), 168 (11 %).
^{1}*H-NMR (CDCl$_3$)* δ: 8.24 – Ar-H (2H, d), 7.9 – Ar-H (2H, d), 7.71 – Ar-H (2H, d), 7.60 – Ar-H (2H, d), 7.37 – Ar-H (1H, dd), 7.01 – Ar-H (2H, d), 5.16 - -C(*)-H (1H, sx), 4.02 - -CH$_2$-O (2H, t), 1.82-1.30 – -CH$_2$-/-CH$_3$ (27H, m), 0.88 - -CH$_3$ (6H, m). *IR (KBr)* v_{max}/cm^{-1}: 2950, 2830, 1735, 1710, 1595, 1495, 1285, 1255, 1175, 1105, 1055, 815, 750. *HPLC (90 % acetonitrile, 10 % chloroform):* 100 %.
TT (°C): Cr 56 SmC$_A$* 67.2 SmC$_\gamma$* 70.8 SmC* 73.4 SmA* 112.4 I (Recryst. 30).

Compound 10d

(S)-1-Methylheptyl 4-(4'-undecyloxybiphenyl-4-carbonyloxy)-3-fluorobenzoate.

The procedure was as described for the preparation of compound **25** (dev98) above, the quantities of reagents used were as follows;

Quantities: 4-undecyloxybiphenyl-4'-carboxylic acid (1.45 g, 3.94 mmol), (*S*)-1-methylheptyl 3-fluoro-4-hydroxybenzoate (1.0 g, 3.73 mmol) and DEAD (0.65 g, 3.73 mmol), triphenylphosphine (0.98 g, 3.73 mmol).

Yield: 0.38 g (16.5 %). *MS:* 618 (M^+, 5 %), 351 (100 %), 197 (20 %), 168 (12 %).

^{1}*H-NMR (CDCl$_3$)* δ: 8.24 – Ar-H (2H, d), 7.89 – Ar-H (2H, t), 7.70 – Ar-H (2H, d), 7.69 – Ar-H (2H, d), 7.36 – Ar-H (t), 7.01 – Ar-H (2H, d), 5.17 - -C-H (1H, sx), 4.02 - -CH$_2$-O (2H, t), 1.81-1.28 - -CH$_2$-/-CH$_3$ (31H, m), 0.88 - -CH$_3$ (6H, t). *IR (KBr)* v_{max}/cm^{-1}: 2920, 2850, 1735, 1710, 1600, 1510, 1465, 1295, 1195, 1110, 1070, 815, 760. *HPLC (90 % acetonitrile, 10 % chloroform):* 100 %.

TT (°C): Cr 56 SmC$_A$* 67.6 SmC$_\gamma$* 69.2 SmC* 76.1 SmC$_\alpha$* 84 SmA* 107.5 I (Recryst. 28).

Compound 11b

(R)-1-Ethylheptyl 4-(4'-octyloxybiphenyl-4-carbonyloxy)-3-fluorobenzoate.

The procedure was as described for the preparation of compound **25** (dev98) above, the quantities of reagents used were as follows;

Quantities: 4-octyloxybiphenyl-4'-carboxylic acid (1.25 g, 3.83 mmol), (*R*)-1-ethylheptyl 3-fluoro-4-hydroxybenzoate (1.0 g, 3.55 mmol) and DEAD (0.62 g, 3.55 mmol), triphenylphosphine (0.93 g, 3.55 mmol).

Yield: 1.58 g (71.5 %). *MS:* 590 (M^+, 2 %), 309 (100 %), 197 (30 %), 169 (12 %).

^{1}*H-NMR (CDCl$_3$)* δ: 8.25 – Ar-H (2H, d), 7.92 – Ar-H (2H, t), 7.71 – Ar-H (2H, d), 7.60 – Ar-H (2H, d), 7.37 – Ar-H (1H, t), 7.01 – Ar-H (2H, d), 5.08 – -C-H (1H, p), 4.02 - -CH$_2$-O (2H, t), 1.82-1.27 - -CH$_2$- (24H, m), 0.95 - -CH$_3$ (3H, t), 0.88 - -CH$_3$ (6H, m). *IR (KBr)* v_{max}/cm^{-1}: 2920, 2850, 1745, 1710, 1600, 1510, 1410, 1285, 1260, 1185, 1055, 950, 825, 755. *HPLC (90 % acetonitrile, 10 % chloroform):* 99.9 %.

TT (°C): Cr 52 SmC$_A$* 52.2 SmA* 93.6 I (Recryst. <25).

Compound 11c

(R)-1-Fluoromethylheptyl 4-(4'-nonyloxybiphenyl-4-carbonyloxy)-3-fluorobenzoate.
The procedure was as described for the preparation of compound **25** (dev98) above,
the quantities of reagents used were as follows;

Quantities: 4-decyloxybiphenyl-4'-carboxylic acid (2.5 g, 7.06 mmol), (*R*)-1-
(fluoromethyl)heptyl 3-fluoro-4-hydroxybenzoate (1.92 g, 6.71 mmol) and DEAD
(1.17 g, 6.71 mmol), triphenylphosphine (1.76 g, 6.71 mmol).

Yield: 2.83 g (67.8 %). *MS:* 622 (M^+, 2 %), 337 (100 %), 197 (28 %), 168 (8 %). ^1H-
NMR (CDCl₃) δ: 8.17 – Ar-H (2H, d), 7.83 – Ar-H (2H, m), 7.64 – Ar-H (2H, d),
7.53 – Ar-H (2H, d), 7.27 – Ar-H (1H, dd), 6.94 – Ar-H (2H, d), 5.24 - -C-H (1H, m),
4.50 - -CH₂-F (2H, m), 3.96 - -CH₂- (2H, t), 1.74-1.23 – -CH₂- (26H, m), 0.82 - -CH₃
(6H, t). *IR (KBr) v_{max}/cm^{-1}:* 2900, 2825, 1765, 1710, 1585, 1495, 1450, 1410, 1280,
1245, 1210, 1170, 1100, 1055, 1005, 875, 810, 745. *HPLC (90 % acetonitrile, 10 %*
chloroform): 100 %.

TT (°C): Cr 59.8 SmC* 68.7 SmA* 101.3 I (Recryst. 30).

References

REFERENCES

[1]   Goodby, J. W., *Science*, 1986, p. 231.

[2]   Templer, R. and Attard, G., *New Scientist*, 4th May 1991: p. 25-29.

[3]   Reinitzer, F., *Monatsch. Chem.*, 1888, **9**, p. 421.

[4]   Lehmann, O. H., *Z. Phys. Chem.*, 1889, **4**, p. 462.

[5]   Kelker, H., *Mol. Cryst. Liq. Cryst.*, 1973, **21**, p. 1.

[6]   Nehring, J. and Osman, M. A., *Z. Naturforsch.*, 1976, **31A**, p. 76.

[7]   Schadt, M., *Liq. Cryst.*, 1989, **5**, p. 57.

[8]   Schaetzing, R. and Lister, J. D., "Advances in Liquid Crystals"
        ed. Brown, G. H. 1983 (Academic Press). **4**.

[9]   Chandrasekhar, S., *Liq. Cryst.*, 1993, **14**, p. 3.

[10]   Ed. Collyer, A. A., "Liquid Crystal Polymers: From Structures to
        Applications", 1993, Oxford University Press (Oxford).

[11]   Fréedericksz, V. and Zwetkoff, V., *Acta. Physiochim.*, 1935, **3**, p. 895.

[12]   Priestley, E. B., "Introduction to Liquid Crystals", 1975, Plenum Press
        (New York).

[13]   Goodby, J. W. Nishiyama, I., Slaney, A. J., Booth, C. J., Toyne, K. J.,
        Liq. Cryst., 1993, **14**, p. 37.

[14]   Bhatt, J. H., Fung, B. M., and Nicholas, K. M. 1993, *J. Organomet. Chem.*,
        413, p. 263.

[15]   Hird, M. Styring. P., Hindmarsh. P., Goodby, J. W., 1993, *J. Mater. Chem.*, **3**,
        p. 1117.

[16]   See for example: Banks, L., Alvelda, P., Artigliere, A., *et al.*, 1999,
        Proceedings of EID'99 (Sandown, UK). **3**.

[17]   Kelly, S. M. and Takatsu, T., "Liquid Crystals for Electrooptic Applications"
        Ed. Gray, G. W., Goodby, J. W., Taylor and Francis (London), in press.

[18]   Kelly, S. M., "Advanced Organic Materials for Flat Panel Displays",
        RSC monograph ed. Connor, A. C., in press.

[19]   Jutamulia, S. and Yu, F., 1997, *SPIE OE Reports*:
        http://www.spie.org/web/oer/may/may97/slm.html.

[20] Grindlay, J., "An Introduction to The Phenomenological Theory of Ferroelectricity", 1970, Pergamon Press (Oxford).

[21] Jona, F. and Shirane, G., 1993, "Ferroelectric Crystals", Dover Publications Inc. (New York).

[22] Burfoot, F. C., 1967, "Ferroelectrics: An Introduction to the Physical Principles", D. Van Nostrand Company Ltd. (London).

[23] Lines, M. E. and Glass, A. M., 1977, "Principles and Applications of Ferroelectrics and Related Materials", Clarendon Press (Oxford).

[24] Meyer, R. B., presented at the 5th International Liquid Crystal Conference (ILCC '74), Stockholm, 1974.

[25] Meyer, R. B., Liebert, L., Strzole., L., Keller, P., *J. Phys. (Lett.)*, 1975, **36**, p. L69.

[26] Goodby, J. W. and Leslie, T. M., *Mol. Cryst. Liq. Cryst.*, 1984, **110**, p. 175.

[27] Goodby, J. W. Slaney, A. J., Booth, C. J., Nishiyama, I., Vuijk, J. D., Styring, P., Toyne, K. J., *Mol. Cryst. Liq. Cryst.*, 1994, **243**, p. 231.

[28] Goodby, J. W., *Mol. Cryst. Liq. Cryst.*, 1997, **292**, p. 245.

[29] Bone, M. F., Bradshaw, M. J., Chan, L. K. M., Coates, D., Constant, J., Gemmell, P. A., Gray, G. W., Lacey, D., Toyne, K. J., *Mol. Cryst. Liq. Cryst.*, 1988, **164**, p. 117.

[30] Parghi, D. D., Gough, N., Lewis, R. A., Hird, M., *Mol. Cryst. Liq. Cryst.*, 1998, **332**, p. 347.

[31] Liu, H. and Nohira, H., *Liq. Cryst.*, 1998, **24**, p. 719.

[32] Kasthuraiah, N. Sadashiva, B. K., Krishnaprasad, S., Nair, G., *J. Mater. Chem.*, 1996, **6**, p. 1619.

[33] Doucet, J. *et al.*, *J. Phys.*, **39**, 1978, p. 548.

[34] Clark, N. A. and Lagerwall, S. T., *Appl. Phys. Lett.*, 1980, **36**, p. 899.

[35] Lagerwall, S. T. Clark, N. A., Dijon, J., Clerc, J. F., *Ferroelectrics*, 1989, **94**, p. 3.

[36] Surguy, P., *Displays Focus (DTA Newsletter)*, 1997, **1**.

[37] *http://www.displaytech.com/*.

[38] Wakita, N., Uemura, T., Ohnishi, H., Mizuno, H., Yamazoe, H., *Ferroelectrics*, 1993, **149**, p. 229.

[39] Itoh, K., Johno, M., Takanishi, Y., Ouchi, Y., Takezoe, H., Fukuda, H., *Jpn. J. Appl. Phys.*, 1991, **30**, p. 735.

[40]   Fuenfschilling, J. and Schadt, M, *Proc. SID.*, 1990, **31**, p. 119.

[41]   Fuenfschilling, J. and Schadt, M., *Jpn. J. Appl. Phys.*, 1996, **35**, p. 5765.

[42]   Verhulst, A. G. H. and Cnossen, G., *Ferroelectrics,* 1996, **179**, p. 141.

[43]   Fuenfschilling, J. and Schadt, M., *SID Digest*, 1990, p. 106.

[44]   Fuenfschilling, J. and Schadt, M., *Jap. J. Appl. Phys.*, 1991, **30**: p. 741.

[45]   Pertuis, V. and Patel, J. S., *Ferroelectrics*, 1993, **149**, p. 193.

[46]   Goodby, J. W. and Patel, J. S., *SPIE (Liquid Crystals & Spatial Light Modulator Materials)*, 1986, **684**, p. 52.

[47]   Walba, D. M. and Clark, N. A., *Ferroelectrics*, 1988, **84**, p. 65.

[48]   Wand, M. D. Vohra, R., Walba, D. M., Clark, N. A., Shao, R., *Mol. Cryst. Liq. Cryst.*, 1991, **202,** p. 183.

[49]   Koden, M., *Ferroelectrics*, 1996, **179**, p. 121.

[50]   Michelson, A., Cabib, D., and Benguigui, L., *J. Physique*, 1977, **8**, p. 961.

[51]   Chandani, A. D. L., Ouchi, Y., Takezoe, H., Fukuda, A., *Jpn. J. Appl. Phys.*, 1988, **27**, p. L276.

[52]   Chandani, A. D. L., Hagiwara, T., Suzuki, Y-I., Ouchi, Y., Takezoe, H., Fukuda, A., *Jpn. J. Appl. Phys.*, 1988, **27**, p. L729.

[53]   Miyasato, K., Abe, S., Takezoe, H., Fukuda, A., Kuze, E., *Jpn. J. Appl. Phys.*, 1983, **22**, p. L661.

[54]   Johno, M. Chandani, A. D. L., Ouchi, Y., Takezoe, H., Fukuda, A., Ichihashi, M., Furukawa, K., *Jpn. J. Appl. Phys.*, 1989, **28**, p. L119.

[55]   Furukawa, K., Terashima, K., Ichihashi, M., Saitoh, S., Miyazawa, K., Inukai, T., *Ferroelectrics*, 1988, **85**, p. 63.

[56]   Fukui, M., Orihara, H., Yamamda, Y., Yamamoto, N., Ishibashi, Y., *Jpn. J. Appl. Phys.*, 1989, **28**, p. L849.

[57]   Chandani, A. D. L., Gorecka, E., Ouchi, Y., Takezoe, H., Fukuda, A., *Jpn. J. Appl. Phys.*, 1989, **28**, p. L1265.

[58]   Chandani, A. D. L., Ouchi, Y., Takezoe, H., Fukuda, A., Terashima, K., Furukawa, K., Kishi, A., *Jpn. J. Appl. Phys.*, 1989, **28**, p. L1261.

[59]   Suzuki, Y., Nonaka, O., Koide, Y., Okabe, N., Hagiwara, T., Kawamura, I., Yamamoto, N., Yamada, Y., Kitazume, T., *Ferroelectrics*, 1993, **147**, p. 109.

[60]   Okabe, N., Suzuki, Y., Kawamura, I., Isozaki, T., Takezoe, H., Fukuda, A., *Jpn. J. Appl. Phys.*, 1992, **31**, p. L793.

[61] Isozaki, T., Suzuki, Y., Kawamura, I., Mori, K., Yamamoto, N., Yamada, Y., Orihara, H., Ishibashi, Y., *Jpn. J. Appl. Phys.*, 1991, **30**, p. L1573.

[62] Yamada, Y., Yamamoto, N., Mori, K., Nakamura, K., Hagiwara, T., Suzuki, Y., Kanamura, I., Orihara, H., Ishibashi, Y., *Jpn. J. Appl. Phys.*, 1990, **29**, p. 1757.

[63] Yamada, Y., Yamamoto, N., Mori, K., Koshoubu, N., Nakamura, K., Kawamura, I., Suzuki, Y., *J. SID*, 1993, **1**, p. 289.

[64] Tajima, E., Kondoh, S., and Suzuki, Y., *Ferroelectrics*, 1993, **149**, p. 255.

[65] Miyachi, K. and Fukuda, A., *Antiferroelectric Liquid Crystals* in "Handbook of Liquid Crystals", ed. D. Demus *et al.*, 2B: Low Molecular Weight Liquid Crystals II, p. 684, 1998, Wiley-VCH (Weinheim).

[66] Suzuki, Y., Hagiwara, T., Kawamura, I., Okamura, N., Kitazume, T., Kakimoto, M., Imai, Y., Ouchi, Y., Yakezoe, H., Fukuda, A., *Liq. Cryst.*,1989, **6**, p. 167.

[67] Inui, S., Suzuki, t., Ilmura, N., Iwane, H., Nohira, H., *Mol. Cryst. Liq. Cryst.*, 1994, **239**, p. 1.

[68] Aoki, Y. and Nohira, H., *Liq. Cryst.*, 1995 **19**, p. 15.

[69] Faye, V., Barbeau, A., Placin, F., Nguyen, H. T., Barois, P., Laux, V., Isaert, N., *Liq. Cryst.*, 1996, **21**, p. 485.

[70] Ouchi, Y., Yoshioka, Y., Ishii, H. Seki, K., Kitamura, M., Noyori, R., Takanishi, Y., Nishiyama, I., *J. Mater. Chem.*, 1995, **5**, p. 2297.

[71] Neundorf, M., Takanishi, Y., Fukuda, A., Saito, S., Murashiro, K., Inukai, T., Demus, D., *J. Mater. Chem.*, 1995, **5**, p. 2221.

[72] Yoshizawa, A., Nishiyama, I., Kikuzaki, H., Ise, N., *Jpn. J. Appl. Phys.*, 1992, **31**, p. L860.

[73] Goodby, J. W., Gray, G. W., and McDonnell, D. G., *Mol. Cryst. Liq. Cryst.*, 1977, **34**, p. 183.

[74] Takezoe, H., Fukuda, A., Ikeda, A., Takanishi, Y., Umemoto, T., Watanabe, J., Iwane, H., Hara, M., Itoh, K., *Ferroelectrics*, 1991, **122**, p. 167.

[75] Glaser, M., *presented at ECLC'99*, 1999 (Crete, Greece).

[76] Dahl, I., *Ferroelectrics*, 1993, **122**, p. 311.

[77] Goodby, J. W., Patel, J. S., and Chin, E., *J. Mater. Chem.*, 1992, **2**, p. 197.

[78] Fukuda, A., Takanishi, Y., Isozaki, T., Ishikawa, K., Takezoe, H., *J. Mater. Chem.*, 1994, **4**, p. 997.

[79]   Booth, C. J., Dunmur, D. A., Goodby, J. W., Haley, J., Toyne, K. J.,
         Liq. Cryst., 1996, **20**, p. 387.

[80]   Tuffin, R. P., Goodby, J. W., Bennemann, D., Heppke, G., Loetzsch,
         Scherowsky, G., *Mol. Cryst. Liq. Cryst.*, 1995, **260**, p. 51.

[81]   Hird, M., Lock, S. J., Toyne, K. J., Goodby, J. W., *Ferroelectrics*, 1996, **180**,
         p. 355.

[82]   Nakauchi, J., Uematsu, M., Sakashita, K., Kageyama, Y., Hayashi, S.,
         Ikemoto, T., Mori, K., *Jpn. J,. Appl. Phys.*, 1989, **28**, p. L1258.

[83]   Weissflog, W., Rogunova, M., Leitko, I., Diele, S., Pelzl, G., *Liq. Cryst.*,
         1996, **21**, p. 13.

[84]   Lose, D., Diele, S., Pelzl, G., Dietzmann, E., Weissflog, W., *Liq. Cryst.*, 1998,
         24, p. 707.

[85]   S-L.Wu, Yen, P.-C., and Hsieh, W.-J., *Liq. Cryst.*, 1998, **24**, p. 741.

[86]   Isozaki, T., Fijukawa, T., Takezoe, H., Fukuda, A., *Phys. Rev. B.*, 1993, **48**,
         p. 13,439.

[87]   Isozaki, T., Hiraoka, K., Takanishi, Y., Takezoe, H., Fukuda, A., Suzuki, Y.,
         Kawamura, I., *Liq. Cryst.*, 1992, **12**, p. 59.

[88]   Hiraoka, K., Uematsu, Y., Takezoe, H., Fukuda, A., *Jpn. J. Appl. Phys.*, 1996,
         35, p. 6157.

[89]   Hiraoka, K., Takanishi, Y., Takezoe, H., Fukuda, A., Isozaki, T., Suzuki, Y.,
         Kawamura, I., *Jpn. J. Appl. Phys.*, 1992, **31**, p. 3394.

[90]   Takanishi, Y., Hiraoka, K., Agrawal, V., Takezoe, H., Fukuda, A.,
         Matsushita, M., *Jpn. J. Appl. Phys.*, 1991, **30**, p. 2023.

[91]   Hiraoka, K., Tsumita, T., Sugiyama, Y., Monzen, K., Uematsu, Y., Suzuki, Y.,
         Jpn. J. Appl. Phys., 1997, **36**, p. 6847.

[92]   Isozaki, T., Ishikawa, K., takezoe, H., Fukuda, A., *Ferroelectrics*, 1993, **147**,
         p. 121.

[93]   Panarin, Y. P., Xu, H., MacLughadha, S. T., Vij, J. K., Seed, A. J., Hird, M.,
         Goodby, J. W., *J. Phys.: Condens. Matter.*, 1995, **7**, p. L351.

[94]   Yamamoto, N., Koshoubu, N., Mori, K., Nakamura, K., Yamada, Y.,
         Ferroelectrics, 1993, **149**, p. 295.

[95]   Sabater, J. and Oton, J. M., *Liq. Cryst.*, 1996, **21**, p. 175.

[96]   Ouchi, Y., Takezoe, H, and Fukuda, A., *SID Digest '91*, 1991 p. 385.

[97]   Heimrath, M., *Proceedings of ITG'98*, 1998 (Garmisch-Partenkirchen, Germany).

[98]   Li, M.-H., Detre, L., Cluzeau, P., Isaert, N., Nguyen, H-T., *Liq. Cryst.*, 1998, **24**, p. 347.

[99]   Geelhaar, T., *Ferroelectrics*, 1988, **85**, p. 329.

[100] Bömelberg, J., *PhD Thesis*, 1993, **Berlin**.

[101] Zaschke, H., Isenberg, A., Schubert, H., J. prakt. Chem., 1979, **321**, p. 629.

[102] Collings, P. J. and Hird, M., "Introduction to Liquid Crystals", 1997, Taylor & Francis (UK).

[103] Chan, L. K. M., Gray, G. W., Lacey, D., Scrowston, R. M., Shenouda, I. G., Toyne, K. J., *Mol. Cryst. Liq. Cryst.*, 1989, **172,** p. 125.

[104] Mitsonubu, O., 1981, *Synthesis*, p. 1.

[105] Hassner, A. and Alexanian, V., *Tetrahedron Lett.*, 1978, p. 4475.

[106] Fukuda, A., "Future Liquid Crystal Display and Its Materials": CMC, 1992, Tokyo.

[107] Heppke, G., Kleinberg, P., and Loetsch, D., *Liq. Cryst.*, 1993, **14,** p. 67.

[108] Nishiyama, I. and Goodby, J. W., *J. Mater. Chem.*, 1993, **3**, p. 149.

[109] Nishiyama, I. and Goodby, J. W., *J. Mater. Chem.*, 1992, **2**, p. 1015.

[110] Yamada, Y., Mori, K., Yamamoto, N., Hayashi,H., Nakamura, K., Yamawaki, M., orihara, H., Ishibashi, Y., *Jpn. J. Appl. Phys.*, 1989, **28**, p. 1606.

[111] Nishiyama, I., Chin, E., and Goodby, J. W., *J. Mater. Chem.*, 1993, **3**, p. 161.

[112] Cluzeau, P., Nguyen, H. T., Destrade, C., Isaert, N., Barois, P., Babeau, A., *Mol. Cryst. Liq. Cryst.*, 1995, **260**, p. 69.

[113] Nishiyama, I., Yoshizawa, M. Fukumasa, M., Hirai, T., *Jpn. J. Appl. Phys.*, 1989, **28**, p. 2248.

[114] Aoki, Y. and Nohira, H., *Ferroelectrics*, 1996, **178**, p. 213.

[115] Gough, N., Hird, M., Newsome, C. J., O'Neill, M., Samra, A. K., *Ferroelectrics*, 1998, **212**, p. 293.

[116] Takanishi, Y., Takezoe, H., Fukuda, A., Komura, H., Watanabe, J., *J. Mater. Chem.*, 1992, **2**, p. 71.

[117] Gray, G. W. and Goodby, J. W., "Smectic Liquid Crystals: Textures and Structures", 1984, Leonard Hill (Glasgow).

[118] Yamamoto, N., Yamada, Y., Mori, K., Nakamura, K., Orihara, H.,

Ishibashi, Y., Suzuki, Y., Negi, Y., Kawamura, I., *Jpn. J. Appl. Phys.*, 1991, **30**, p. 2380.

[119] Gouda, F., Skarp, K., Lagerwall, S.T., *Ferroelectrics*, 1991, **113**, p. 165; Moritake, H., Shigeno, N., Ozaki, M., Yoshino, K., *Liq. Cryst.* 1993, **14**, p. 1283.

[120] Hatano, J., Hanakai, Y., Furue, H., Uehara, H., Saito, S., Murashiro, K., *Ferroelectrics*, 1995, **19**, p. 377.

[121] Robinson, W. K., Gleeson, H. F., Hird, M., Seed, A. J., Styring, P., *Ferroelectrics*, 1996, **178**, p. 249.

[122] Bourhis, L. L. and Dupont, L., *Ferroelectrics*, 1993, **149**, p. 69.

[123] Matsui, E., Nito, K., and Yasuda, A., *Ferroelectrics*, 1993, **149**, p. 97.

[124] Carvalho, P. S., Cluzeau, P., Destrade, C., Nguyen, H. T., Chaves, M. R., *Ferroelectrics*, 1996, **178**, p. 195.

[125] Chandani, A. D. L., Cui, Y., Seomun, S. S., Takanishi, Y., Ishikawa, K., Takezoe, H., Fukuda, A., *Liq. Cryst.*, 1999, **26**, p. 167.

[126] Parghi, D. D., Lagerwall, J. P. F., and Heppke, G., Mo*l. Cryst. Liq. Cryst.*, in press.

[127] Lagerwall, J. P. F., Parghi, D. D., and Heppke, G., *Ferroelectrics*, in press.

[128] Takanishi, Y., Takezoe, H., and Fukuda, A., *Ferroelectrics*, 1993, **147**, p. 135.

[129] Morse, A. and Gleeson, H. F., *Liq. Cryst.*, 1997, **23**, p. 531.

[130] Gorecka, E., Chandani, A. D. L., Ouchi, Y., Takezoe, H., Fukuda, A., *Jpn. J. Appl. Phys.*, 1990, **29**, p. 131.

[131] Hiji, N., Chandani, A. D. L., Nishiyama, S-I., Ouchi, Y., Takezoe, H., Fukuda, A., *Ferroelectrics*, 1988, **85**, p. 99.

[132] Wu, S.-L. and Hsieh, W.-J., *Chem. Mater.*, 1999.

[133] Suzuki, Y., Isozaki, T., Hashimoto, S. S., Kusumoto, T., Hiyama, T., Takanishi, Y., Takezoe, H., Fukuda, A., *J. Mater. Chem.*, 1996, **6**, p. 753.

[134] Kusumoto, T., Ogino, K., Hiyama, T., Isozaki, T., Suzuki, Y., *Chem. Lett.*, 1996, p. 865.

[135] Kelly, S. M., *Liq. Cryst.*, 1996, **20**, p. 493.

[136] Orihara, H. and Ishibashi, Y., *Ferroelectrics*, 1991, **122**, p. 177.

[137] Gisse, P., Pavel, J., Nguyen, H. T., Lorman, V. L., *Ferroelectrics*, 1993, **147**, p. 27.

[138] Hou, J., Schacht, J., Giesselmann, F., Zugenmaier, P., *Liq. Cryst.*, 1997, **22**, p. 409.

[139] Levelut, A-M., Germain, C., Keller, P., Liebert, L., Billard, J., *J. Physique*, 1983, **44**, p. 623.

[140] Galerne, Y. and Liebert, L., *Phys. Rev. Lett.*, 1990, **64**, p. 906.

[141] Galerne, Y. and Liebert, L., *Phys. Rev. Lett.*, 1991, **66**, p. 2891.

[142] Cladis, P. E. and Brand, H. R., *Liq. Cryst.*, 1993, **14**, p. 1327.

[143] Heppke, G., Kleineberg, P., and Loetsch, D., *presented at the 21st Freiburger Arbeitagung Fluessigkristalle*, 1992 (Freiburg, Germany).

[144] Heppke, G., Kleineberg, P., Loetzsch, D., Mery, S., Shashidhar, R., *Mol. Cryst. Liq. Cryst.*, 1993, **231**, p. 257.

[145] Takanishi, Y., Takezoe, H., Johno, M., Yui, T., Fukuda, A., *Jpn. J. Appl. Phys.*, 1993, **32**, p. 4605.

[146] Musevic, I., Blinc, R., Zeks, B., Copic, M., Whitebrood, M. M., Rasing, Th., Orihara, H., Ishibashi, Y., *Phys. Rev. Lett.*, 1993, **71**, p. 1180.

[147] Blinc, R. and Musevic, I., *Mol. Cryst. Liq. Cryst.*, 1997, **292**, p. 311.

[148] Mach, P., Pindak, R., Levelut, A-M., Barois, P., Nguyen, H. T., Huang, C. C., Furenlid, L., *Phys. Rev. Lett.,* 1998, **81**, p. 1015.

Appendix

A P P E N D I X

Appendix A

Care should be taken not to confuse the direction of the polarisation in the SmC* layers,
"+P" and "-P", with the spontaneous polarisation direction, "$P_s(+)$" and "$P_s(-)$". The
latter of these is a specific term used to describe the direction the spontaneous
polarisation of a ferroelectric liquid crystal molecule based on the following convention
(*figure 102*). If the molecule is tilted back "into" the page the direction of the
spontaneous polarisation to the right of the molecule is described as *positive* ("$P_s(+)$")
and *negative* if it lies to the left ("$P_s(-)$").
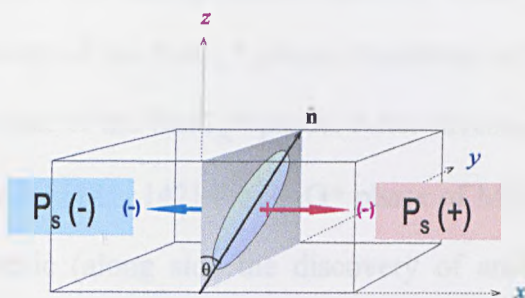

Figure 102:- Convention used to describe the direction of the spontaneous
polarisation, P_s, in FLCs and AFLCs.

The direction of the spontaneous polarisation is a specific property and is related to
the spatial configuration of the chiral material ((R) and (S)). The arbitrary terms "+P"
and "-P" are used in this thesis simply to distinguish between the two ferroelectric
states in which the spontaneous polarisation faces in opposite directions.

Although the phenomenon of antiferroelectricity in liquid crystals was first recognised in (R)-MHPOBC [52], the antiferroelectric smectic phase itself was initially observed some years earlier in the enantiomers of a cinnamate derivative (MHTAC, *figure 103*) by Levelut *et al.* [139].
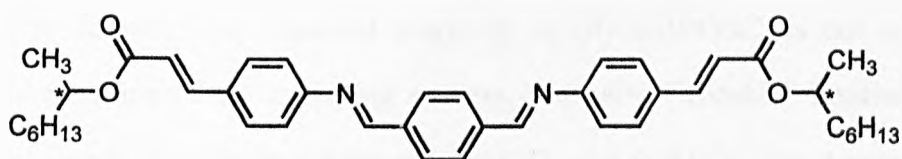

Figure 103:- Structure of MHTAC

The material possessed a new mesophase, designated "SmO*", the structure of which was (before the discovery of the SmC_A^* phase) elucidated as being of a "herringbone" type [140] similar to that of the SmC_A^* phase. After investigation of the electrooptic properties of the material [141, 142] the SmO* phase of MHTAC was also classified as being antiferroelectric (along side the discovery of antiferroelectricity in chiral MHPOBC). Further electrooptic and miscibility studies lead to the conclusion that the SmO* phase and the SmC_A^* phase of MHPOBC were in fact identical [143-145]. The SmC_A^* phase was also observed in materials similar in structure to MHPOBC at approximately the same time as the discovery of the phase in (R)-MHPOBC; the postulations as to the nature of the phase were however different [250].

As "tristate switching" (hence antiferroelectricity) was first detected experimentally by observation of the switching behaviour in an external electric field of (R)-MHPOBC [52, 57], it is generally accepted as being the first formal antiferroelectric liquid crystal. The SmC_A^* phase is therefore more often referred to than the SmO* phase. The work carried out in the exploration of the SmO* phase was, never the less,

not an inconsequential contribution to the wider study of liquid crystals, and it is fitting that it should be mentioned here.

Appendix C

The expression "tristable switching", used to describe surface-stabilised antiferroelectric switching observed originally in (R)-MHPOBC, is not an entirely accurate description of the switching process. The term "tristable" implies that the three states involved in the switching process (FO-, AF and FO+) are degenerate, and therefore equally stable. However, unlike the "bistable switching" in surface-stabilised ferroelectric liquid crystals, on removal of the external electric field only one "stable" state, the antiferroelectric state, can exist. A field is required to maintain the orientation of the molecules in one of the two ferroelectric states. For this reason the expression "tristate switching" is used in place of "tristable switching" to describe the switching process in surface-stabilised antiferroelectric liquid crystals.

Appendix D

An alternative model to the "Devil's Staircase", to account for the occurrence of the SmC* subphases, is the "Clock" model [146-148]. The model is based on the postulation that the molecules are arranged at equidistant positions around the helical cone of the SmC* phase (from layer to layer) to produce the so-called "frustrated" ferrielectric subphases. As the model is a relatively recent development in the study of the SmC* subphases few publications exist which describe the "Clock" model in detail. For this reason it is beyond the scope of this thesis to offer a detailed description of the model.

The spontaneous polarisation (P_s) of the materials and mixtures under test were measured using the current-pulse technique [53]. The basic set-up of the equipment is shown below (*figure 104*).
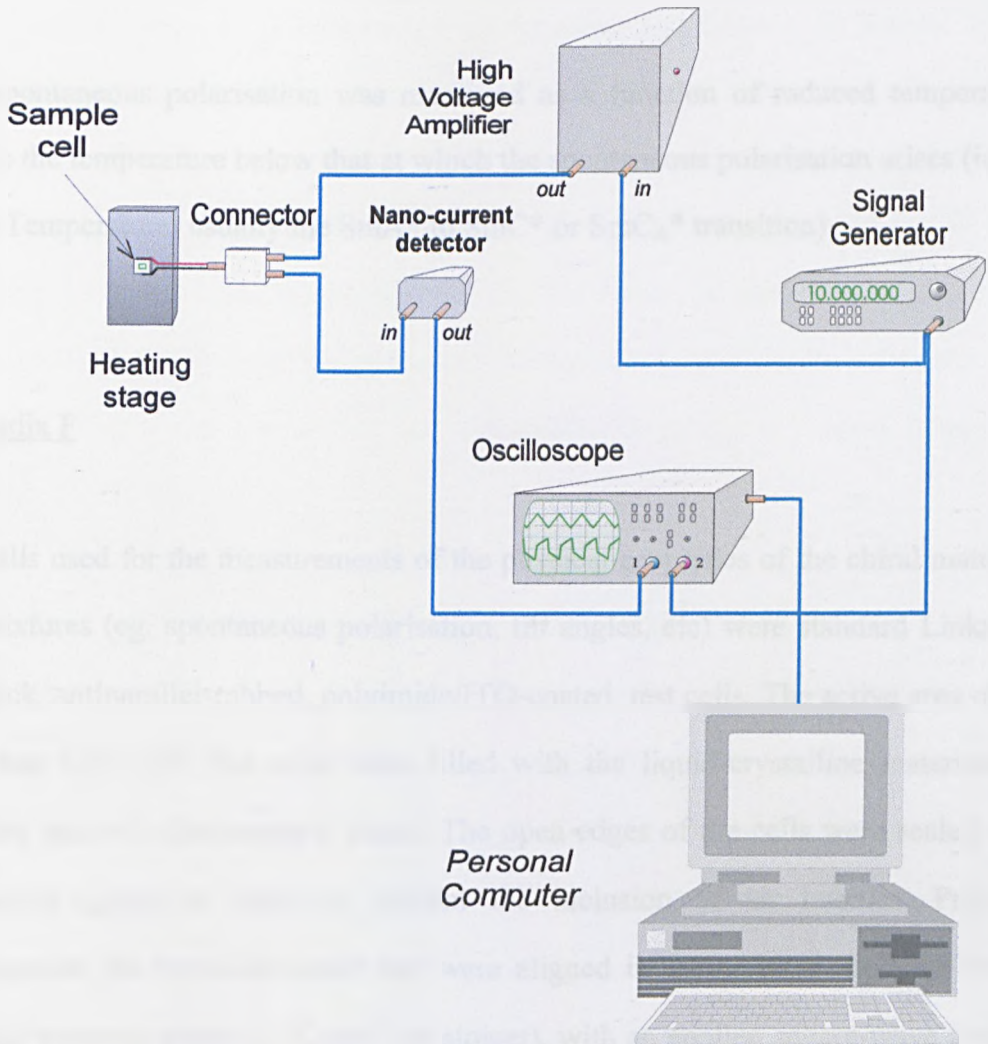

Figure 104:- The spontaneous polarisation measurement set-up

An HP-54600B oscilloscope was used to display the input and output signals, from the HP-33120A signal generator and Linkam cell, respectively. The Linkam THM600 hotstage was controlled by a Linkam TP91 temperature controller and LNP1 cooling pump. Data was captured onto a 486 personal computer fitted with an HP-DAS1600 board using "BenchLink/Scope"; the program used to calculate the spontaneous polarisation values ("OptResp") was written by Dr. Marcus Watson.

The spontaneous polarisation was measured as a function of reduced temperature. This is the temperature below that at which the spontaneous polarisation arises (ie. the Curie Temperature, usually the SmA* to SmC* or SmC$_A$* transition).

Appendix F

The cells used for the measurements of the physical properties of the chiral materials and mixtures (eg. spontaneous polarisation, tilt angles, etc) were standard Linkam 5 μm-thick, antiparallel-rubbed, polyimide/ITO-coated, test cells. The active area of the cells was 0.81 cm^2. The cells were filled with the liquid-crystalline materials by capillary action in the isotropic phase. The open edges of the cells were sealed with conductive epoxy in order to prevent the inclusion of air bubbles. Prior to measurement the materials under test were aligned in the cells, by cooling slowly from the isotropic phase (1 °C min^{-1} or slower), with an applied square-wave field of 180 V$_{pp}$ (±18 V$_{ac}$ μm^{-1}) at a frequency of 100 Hz.

The observed tilt angles were calculated as one-half of the angle, obtained by rotation of the heating stage between two "dark states" (positions of extinction of light), on application of a low-frequency square-wave field (0.1 Hz, 100 V_{pp}). The use of low frequencies for these measurements also accounts for the measurable tilt angles despite the absence of a measurable spontaneous polarisation in several of the physical investigations described in the **Results and Discussion** section. The strength of the observed optical response in ALFCs and FLCs usually decreases on increasing the frequency (at constant field strength). The threshold to switching is as a consequence higher at higher frequencies. For this reason an applied frequency of 0.1 Hz could allow switching in the mixtures to take place in order for the tilt angles to be measured despite the absence of any observable switching at higher frequencies (upwards of 20 Hz).

The contrast ratios and response times for the materials measured were calculated using a set-up similar to that described in **Appendix E**. A filled cell switching at a frequency of 20 Hz (square wave) with an applied field of 100 V_{pp} (Feedback FG600 function generator) was placed in the path of a red laser beam (λ = 632.8 nm). An active photodiode was used to compare the differences in transmission, through the cell between the "light" and "dark" states, at 90 % and 10 % transmission respectively (*figure 105*). The response times were calculated as the time taken for the material to switch between these two transmission states (Tektronix TDS220 digital oscilloscope).
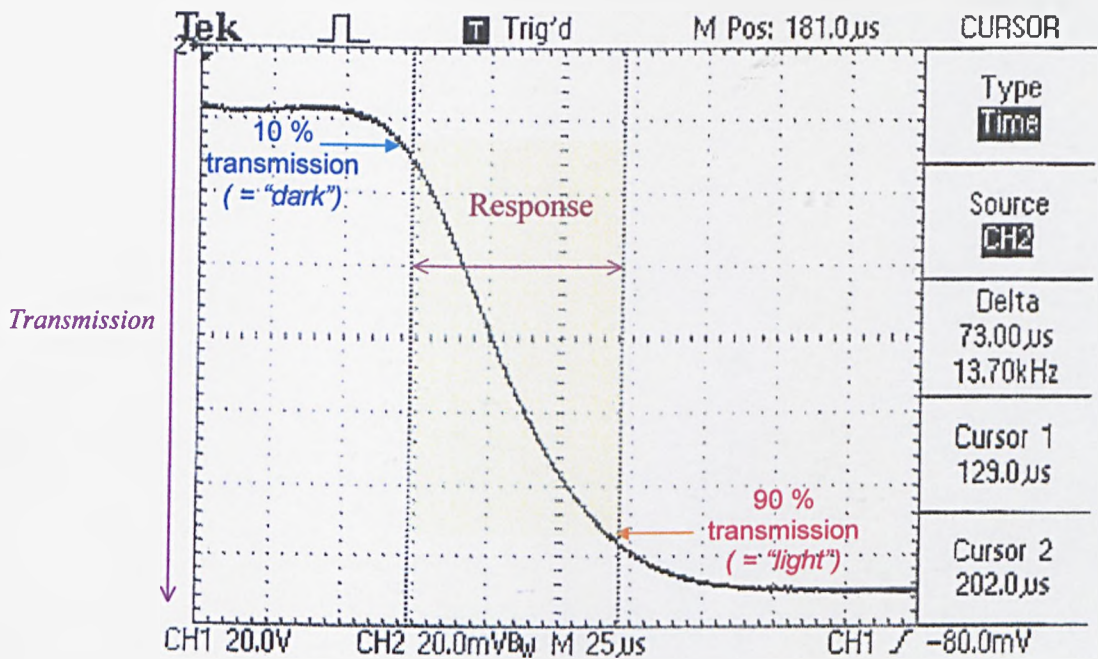
Figure 105:- Transmission vs. time response of the standard antiferroelectric liquid crystal (*S*)-MHPOBC (10 % to 90 % transmission; 100 V_{pp}, 20 Hz square-wave field applied).

Due to the limitations of the available equipment, and also as a consequence of being unable to directly view the quality of alignment of the liquid crystal in the cell, the contrast ratios are reported to the nearest multiple of 10.

It should also be noted that the techniques employed to measure the physical parameters, described above, are purely qualitative. In evaluating antiferroelectric materials, for use in potential SS-AFLCDs, the antiferroelectric (SmC$_A$*) state is usually selected as the "dark" state with the two ferroelectric (SmC*) states as the "light" states. Since the cell gap required to enforce surface-stabilisation (unwinding of the helix) in the SmC$_A$* phase is usually of the order of 1.5 to 2 μm, the 5 μm-thick cells used for this work could not be considered to effectively surface-stabilise the materials for study in the usual manner. In order to avoid complications, arising principally from the formation of a helix in the relaxed antiferroelectric phase, the two ferroelectric states were chosen as the "light" and "dark" states for the switching experiments.